Technische Universität München
TUM Campus Straubing für Biotechnologie und Nachhaltigkeit

Development of a Cyanobacterial Biorefinery -

From Biomass Analysis and Enzymatic Hydrolysis to Yeast Fermentation Strategy and LCSA

Korbinian Benedikt Sinzinger

Vollständiger Abdruck der von dem TUM Campus Straubing für Biotechnologie und Nachhaltigkeit der Technischen Universität München zur Erlangung eines

Doktors der Naturwissenschaften (Dr. rer. nat.)

genehmigten Dissertation.

Vorsitz: Prof. Dr. Marc Ledendecker

Prüfende der Dissertation:

1. Prof. Dr. Volker Sieber
2. Prof. Dr. Herbert Riepl

Die Dissertation wurde am 25.04.2025 bei der Technischen Universität München eingereicht und durch den TUM Campus Straubing für Biotechnologie und Nachhaltigkeit am 25.08.2025 angenommen.

“The magic you are looking for is in the work you are avoiding.”

— Dipen Parmar

“It is better to be a warrior in a garden, than a gardener in a war.”

— Miyamoto Musashi,

“You should be a monster, an absolute monster, ruthlessly ambitious, and then you should learn how to control it.”

— Jordan Peterson

Acknowledgments

First and foremost, a big thank you to my “Doktorvater” Prof. Dr. Volker Sieber. I’m deeply thankful, I could conduct my doctorate research at your chair. The constant scientific exchange and discussions are exactly what is needed. The close collaboration between the working groups allowed me to acquire a deep understanding in the field. Also, I highly appreciate the freedom that I was given to bring in my own ideas, creative thinking and pursue my own path. It made the project my own and assured my commitment.

A special, and I mean a very special thanks to Dr. Doris Schieder as my direct supervisor. Doris thank you so much for the trust you have put in me during my almost four and a half years with you at CBR. Likewise, I want to express my gratitude to Dr. Broder Rühmann. Broder and Doris thank you for your guidance and mentorship. Broder say hi to Ludwig and Chantalle for me.

Also, thank you Prof. Dr. Jochen Schmidt for being my mentor. As well as thank you board of examination.

Furthermore, I am truly thankful to Anja Schmidt, Petra Lommes, and André Pick. Anja and Petra taught me a lot in the lab and helped out whenever they could. Special thanks for the help with the DASGIP system and the GC. André actually deserves a medal for being there for everyone on the weekends or after seven p.m. in the lab. That’s what I call gold standard of mentorship.

Thanks to all my office buddies Tatjana Laudage, Samed Güner, Torben Hüsing, Robert Genth, Tobias Gmelch, Mathilde Steinmaßl and Dennis Romeis. Our discussions were often but not always about science but always a lot of fun. How could we forget Elisabeth shout for one of us, Doris's shoes clicking down the hall, or Broder’s laughter from across the hall.

Also, thanks to those who made my doctoral work exciting, a hell lot of fun and of course more prosperous. I would like to name Tristan Rath, Samuel Sutiono, Christoph Schilling, Alex Fuchs, Alex Benson, Moritz Gansbiller, Scott Bottoms, Mariko Tashima, Vivian Willers, Edilberto Medina Cabrera, Paul Stockmann, Sumanth Ranganathan, Johanna Radomski, Dhananjai Pangotra, and Mahdi Siadat. Not to forget, thanks to the other great people in our lab Irmgard Urban, Magdalena Haslbeck, Lena Würstl, and Janine Huber who were always helpful and made the time in the lab worthwhile.

Special thanks to Sumanth Ranganathan and Christoph Schilling for proofreading my work repeatedly and making great suggestions.

Thanks to my family Ludwig (and his family), Andrea, Michaela, and Erwin as well as Jakob and Claudia, and their support during frustrating times and writing.

Last but most importantly, thanks to my wife, Eva. Thank you for your support, especially for pushing me to finish my thesis. You are truly the best and my everything.

Summary

The global shift away from fossil resources, driven by climate change and the pursuit of sustainability, has significantly altered resource maps and supply chains. As a result, the demand for renewable raw materials to replace fossil-based fuels, chemicals, and plastics has surged. A key political and scientific response to these challenges is the promotion of a circular bioeconomy, which relies on renewable resources. While renewable energy addresses the energy demand, biomass has emerged as a primary resource for the chemical industry, giving rise to the interdisciplinary field of multiproduct biorefineries. Lignocellulosic biomass from agriculture and forestry has been extensively researched, but microalgal and cyanobacterial biomass present a highly promising, yet underutilized, alternative due to high cultivation and investment costs.

This thesis contributes to the development of biorefinery concepts through the investigation of biomass composition, fermentative processes, multiproduct extraction strategies, and life cycle sustainability assessment (LCSA). Specifically, the biomass of seven *Nostoc* strains was examined, with a detailed analysis of their complex heteroglycan saccharide profiles. These profiles revealed a range of components, including neutral sugars, uronic acids, amino sugars, and various methylated sugars. In addition, the biocomposition of three key *Nostoc* strains — *Nostoc* sp. De1, *Nostoc* sp. Cc3, and *Nostoc* muscorum I—was assessed, quantifying moisture, ash, lipids, starch, structural saccharides, and protein content. Industrial enzymes were tested for their ability to saccharify and solubilize the biomass, highlighting both the complexity of *Nostoc* heteroglycans and the challenges of their industrial utilization. Nonetheless, sufficient biomass solubilization was achieved, paving the way for potential biorefinery applications.

Further, this work addressed the challenge of optimizing enzyme production strains and determining favorable conditions for enzyme expression. The production of enzymes itself presents difficulties, such as the need to use secondary feedstocks. By employing a holistic and integrative bioprocess development approach, this research rapidly identified improved conditions for enzyme expression and secretion, using cyanobacterial waste biomass to support *Pichia pastoris* fermentation. This was demonstrated through the production of phytase, secreted by *P. pastoris* grown on cyanobacterium hydrolysate and buffered glycerol-complex (BMGY) medium, with genetic expression conditions optimized via high-throughput screening of a randomized secretion library.

In addition, a multiproduct biorefinery concept was developed, centered on the cyanobacterial strain *Cylindrospermum alatosporum* CCALA 988, known for producing high-value cyclic lipopeptides such as puwainaphycins (PUWs) and minutisamides (MINs). A sequential extraction strategy was explored, followed by enzymatic hydrolysis of residual biomass for its use as a medium supplement in *P. pastoris* fermentations expressing *E. coli*

phytase. A bench-scale mass balance was conducted, and key products including PUWs, MINs, phycobiliproteins, and pigments were proposed. The results from a 1L fermentation system supported the further development of this biorefinery concept.

Finally, an LCSA was performed for the proposed biorefinery using *C. alatosporum* CCALA 988, involving four key steps: gathering assumptions from literature data, synthesizing an industrial-scale process, evaluating environmental impacts, and assessing economic feasibility.

Future research should focus on scaling up the biorefinery concept and enhancing the solubilization of residual biomass. Additionally, optimization of the *P. pastoris* fermentation process in larger-scale systems will be essential for commercial application.

List of Publications

Sinzinger, Korbinian; Schieder, Doris; Rühmann, Broder; Sieber, Volker (2022): Towards a cyanobacterial biorefinery: Carbohydrate fingerprint, biocomposition and enzymatic hydrolysis of Nostoc biomass. In: *Algal Research* 65, S. 102744. DOI: 10.1016/j.algal.2022.102744.

Sinzinger, Korbinian; Bieringer, Sebastian; Schieder, Doris; Riepl, Herbert; Sieber, Volker (2023): Biorefinery concept for Cylindrospermum alatosporum CCALA 988 extracting multiple high-value compounds and residue utilization by P. pastoris fermentation producing phytase. In: *Algal Research* 76, S. 103302. DOI: 10.1016/j.algal.2023.103302.

Sinzinger, Korbinian; Obst, Ulrike; Güner, Samed; Döring, Manuel; Haslbeck, Magdalena; Schieder, Doris; Sieber, Volker (2024): The Pichia pastoris enzyme production platform: From combinatorial library screening to bench-top fermentation on residual cyanobacterial biomass. In: *Journal of Bioresources and Bioproducts* 9 (1), S. In: *2369-9698* 9 (1), S. 43–57. DOI: 10.1016/j.jobab.2023.12.005.

Sinzinger, Korbinian; Schieder, Doris; Sieber, Volker (2025): LCSA for the biorefinery concept for *Cylindrospermum* alatosporum CCALA 988 extracting multiple high-value compounds and residue utilization by *P. pastoris* fermentation producing phytase. In: *Algal Research* (submitted manuscript)

Not part of this thesis:

Eckel, Felix; **Sinzinger, Korbinian**; van Opdenbosch, Daniel; Schieder, Doris; Sieber, Volker; Zollfrank, Cordt (2024): Influence of microbial biomass content on biodegradation and mechanical properties of poly(3-hydroxybutyrate) composites. In: *Biodegradation* 35 (2), S. 209–224. DOI: 10.1007/s10532-023-10038-1.

Table of Content

1. Introduction

1.1. Towards UN's sustainable development goals

1.1.1. A paradigm-shift – the circular bioeconomy

Our global society has seen tremendous growth in wealth and prosperity in the last century[1,2]. Especially in the emerging economies in the last 30 - 40 years, gross national incomes have grown tremendously, bringing hundreds of millions of people out of poverty but also resulting in a dangerous worsening of the world's ecosphere[3,4]. Unprecedented environmental pollution and a global increase in greenhouse gas (GHG) emissions have been seen as the root causes[5,6]. In the last decades, warning voices have become louder for governments to take imminent action. In 2015, the world's governments have thus committed to two core sets of goals for the future: the Sustainable Development Goals (SDG's) and the Paris Agreement on Climate Change, which essentially aims to phase out fossil fuels by 2100 and 80 % by 2050[7–9]. These sets of goals were lined out to be reached by a paradigm shift of transforming our linear fossil fuel driven economy, society and biosphere (**Figure 1**)[10].

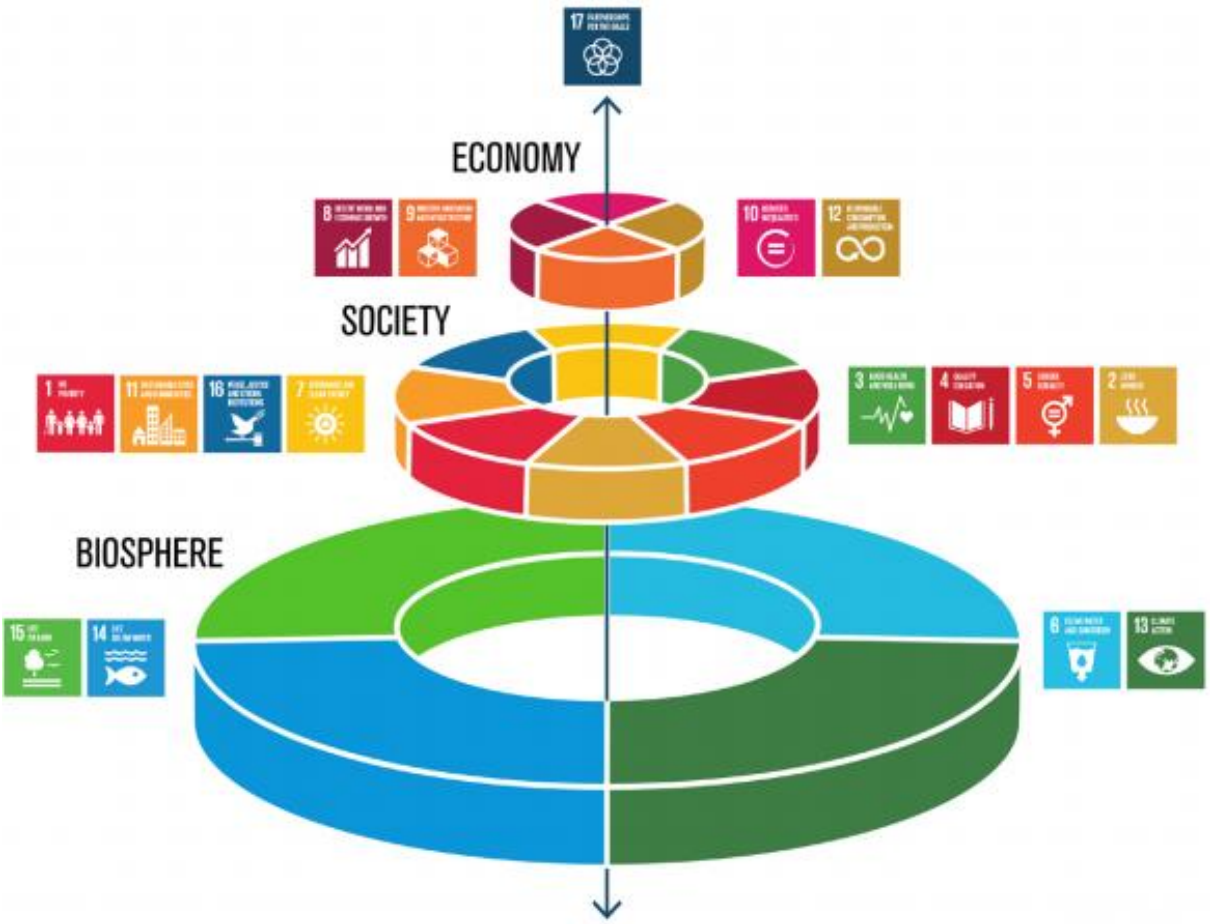

Figure 1: The layers of the Sustainable Development Goals and their impact levels (Hetemäki *et al.*[10]).

This transformation of our European and global economy poses a challenge to all fibers of our society[11–14]. It requires the merging of two novel concepts equally – to renew the old value chains and replace fossil industry feedstocks. The 2012 put out concept by the European Commision for a "bioeconomy" and the concept for a "circular economy", the second appearing first a few years later[15]. The merging of these two concepts has led to the term "circular bioeconomy", which appeared increasingly in scientific publications since 2016. The circular bioeconomy can be separated into two cycles: the technical cycle and the biological cycle (**Figure 2**). The biological cycle relys on the switch to renewable energy sources and focuses on the sustainable, resource-efficient valorization of biomass in integrated, multi-output production chains (e.g. biorefineries) while also making use of residues and waste streams[16]. Additionaly, the value of biomass is increased over time via cascading. The technical cycle relies on recycling, maintenace, reusing, remanufacturing, and sharing[11]. Both cycles are closely connected, as the bio-based products also enter the technical cycle[13,14].

"European Bioeconomy needs to have sustainability and circularity at its heart."

European Commission[17].

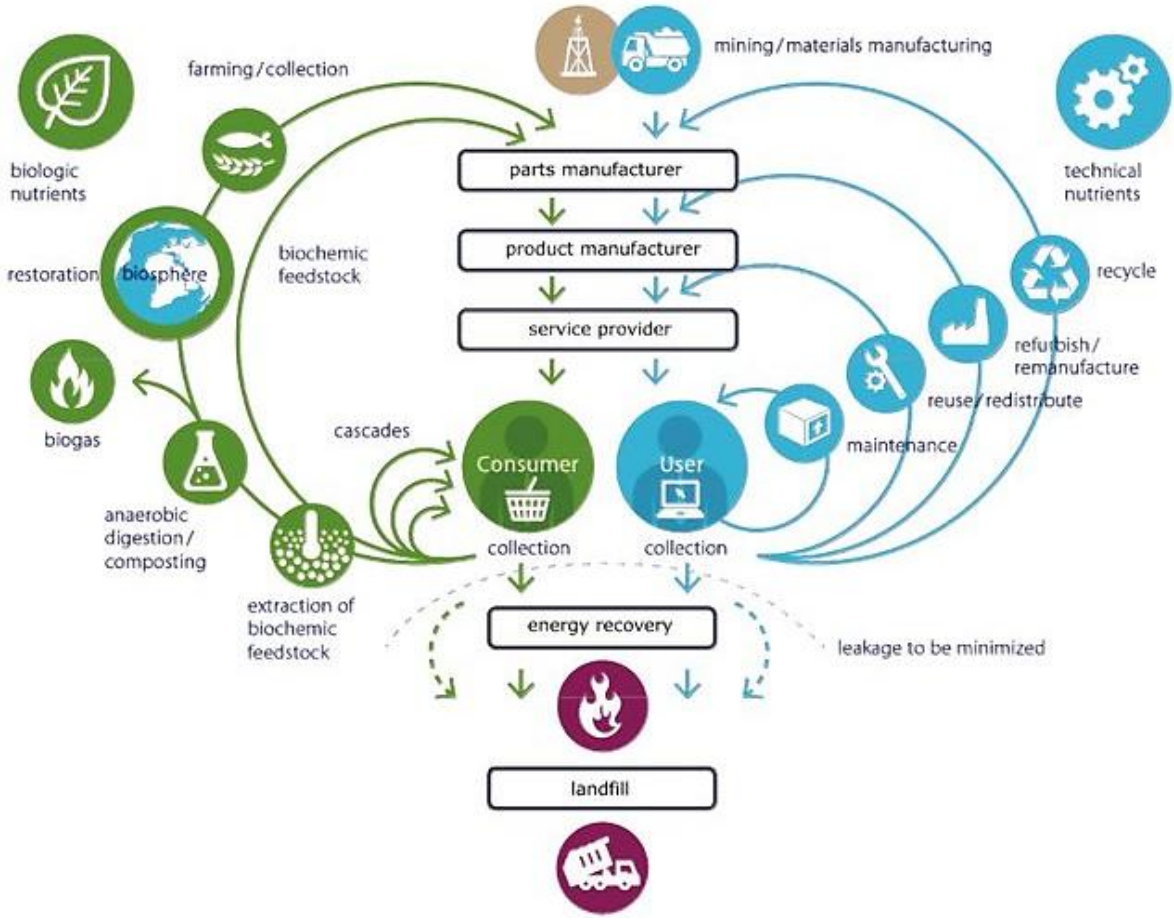

Figure 2: Flowchart of the Circular Bioeconomy (Soldal[13]).

New concepts have developed within the circular bioeconomy in recent years. Yet, some limitations still need to be overcome. Cascading use usually increases the efficient use of resources, thereby reducing GHG emission[18]. But net emissions only decrease if the emissions for collection, separation, and processing of waste streams are lower than for sourcing and producing a competitor product. So, to comprehensively assess the sustainability of a cascade, a full life cycle assessment is crucial. One element to improving the life cycle assessment is the implementation of renewable energy sources. Using renewable energy, including bioenergy from biomass, has the potential to make more cascading steps justifiable from a GHG footprint perspective. This highlights the importance of the energy transition, away from fossil sources to renewable sources, as we have seen historically inversely before.

1.1.2. The next energy transition

Fossil fuels have allowed our global society to grow and prosper tremendously. The hydrocarbons have given us a feedstock for products in all industry segments. A society without fossil hydrocarbons is hardly imaginable. Yet, the need for the next transition from our current global energy system is of paramount importance[19]. Adverse effects are causing our climate to change by frightening pace. Global warming cannot be stopped or inversed, only limiting the combustion of fossil fuels can keep us away from 20 % to 65 % adverse effects. The International Renewable Energy Agency (IRENA), which is an intergovernmental organization that supports countries in their transition to a sustainable energy future, regularly publishes new outlooks for the world to achieve the Paris agreement goals. Key findings are that net zero energy technologies already exist today, a combination of technologies is needed to keep us on a 1.5 °C pathway, fossil fuel investments are already diverted into sustainable sources, and energy transition investments will have to increase by 30 % over planned investment to a total of 131 trillion € between now and 2050, corresponding to 4.4 trillion € on average every year[20].

A next energy transition from mainly fossil fuels to renewable energy does not arise from depletion of fossil fuels[21]. Despite increasing demand and many parties claiming peak oil and the world running out of oil soon, oil reserves have risen from 2003 to 2013 by 27 %[22]. Fossil fuels use have increased tremendously in the last 70 years and supply 80 % of our 13.7 giga tons of oil equivalent or over 160 Petawatt hours energy demand (**Figure 2**). Yet, proven oil reserves are rather to double by 2050. The numbers show the complete dependency of our society on these resources. Nevertheless, no more than 33 % of proven fossil fuel reserves may be used before 2050, if we are to achieve a 2 °C climate goal.

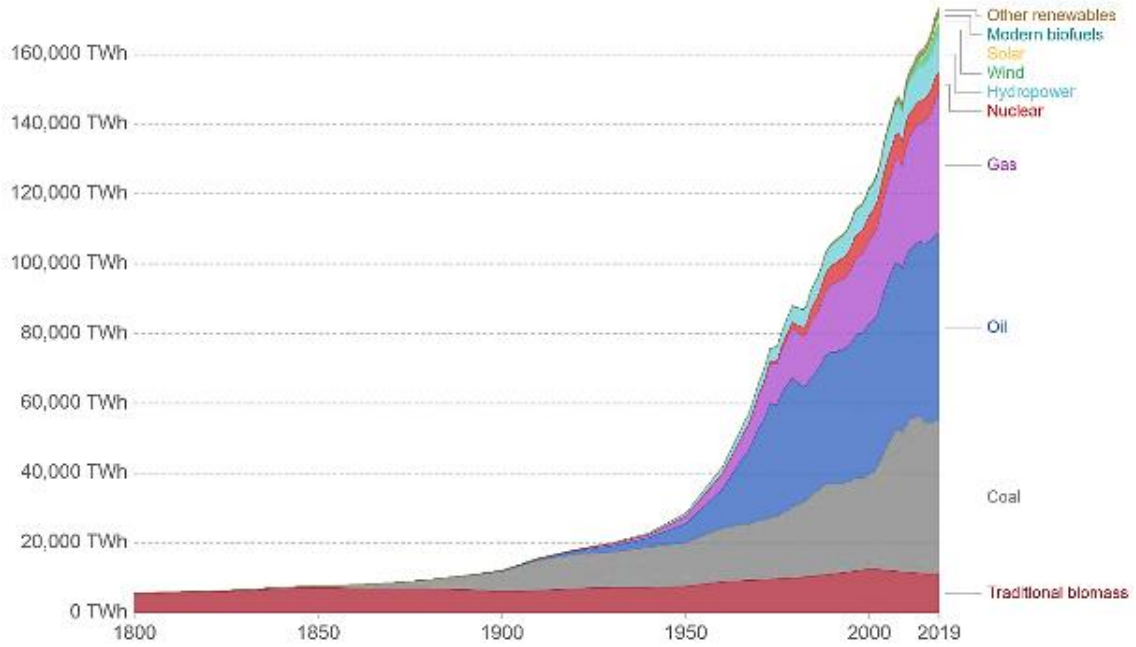

Figure 3: Global energy consumption from 1800 to 2008 differentiated by source (World Energy Transition Outlook[20]).

Taking from history, energy transitions take time. It has usually taken from 50 to 70 years for a new energy source to take a large share overall (**Figure 3**)[19]. For coal as an energy source, it took 70 years from 1830 to 1900 to go from 5 % to over 50 %. It took oil the time span from 1900 to 1970 to reach almost 50 % of the global energy supply. For around the last 85 years, gas rose to replace wood as a traditional energy source even further but took only a small share below 25 %[19]. It was similar with other sources such as nuclear, hydro, or solar. So, it seems impossible to replace our global fossil fuel system in a short time but rather it might take decades. Nevertheless, there is no need for one system to replace it but rather we will see a sustainable energy mix of different sources, which might in the future power a global hydrogen economy[23].

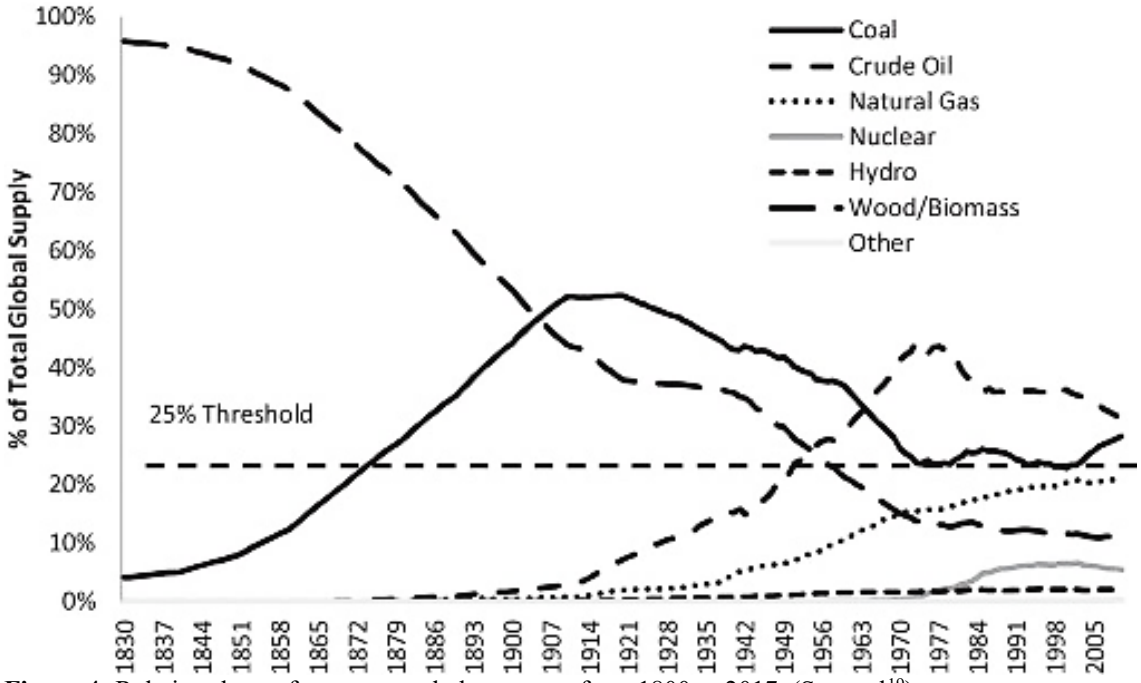

Figure 4: Relative share of energy supply by sources from 1800 to 2017 (Sovacol[19]).

The next energy transition will require a holistic innovation approach tailored to the needs of each renewable energy and energy efficiency technology since a wide range of approaches will be required across all sectors of the energy system[20]. While aiming at increasing investment in R&D for low-carbon technologies benefits the energy transition, more attention can be paid to monitoring and verifying that those investments have the desired impact and that R&D budgets, and priorities are impact-driven[24]. Among all sources, biomass needs to fulfill more than just the role of an energy feedstock. It also needs to fulfill the important purpose of replacing oil as feedstock for the chemical industry[25].

1.1.3. Biomass – Phasing out oil

Biomass offers a source of carbon from the biosphere as an alternative to fossilized carbon laid down tens of millions of years ago[26]. The range of possible biomass feedstocks available is very wide, it only needs to be refined. Projections show that by 2050 biofuels could satisfy around one-third of worldwide primary energy demand[27]. Therefore, refining biomass solely for biofuels as a future strategy, has been found to be a dead end. This becomes clearer when looking at a barrel of crude oil. The distribution of a whole barrel of crude oil is shown in **Figure 4.** About 15 % - 20 % of crude oil yields in chemicals, whereas 80 % - 85 % are converted into liquid fuels. The around 80 % - 85 % liquid fuels from 1 kg of crude oil have a caloric content of 32 MJ[28]. In contrast, if biomass is diverted to liquid fuels, yields from 1 kg reach no higher than 6 MJ. But when diverting biomass to chemicals, a yield of up to 80 % can be reached. This fact and the

strongly growing case for a hydrogen economy with a clean energy mix allows biomass being used more towards feedstock for chemicals[29,30].

For the United States alone, the biomass feedstock potential is one billion tons, global potentials are at least four times higher coming from aquatic and green terrestrial sources[24]. Biomass will play an important role in shaping the future of the chemical industry like crude oil and shale gas, as synthetic catalytic chemistry matures, and synthetic biology emerges further[26]. However, unlike biorefining, wherein it is treated as a renewable surrogate for crude oil, biomass should be viewed as a complement to crude oil and shale gas and advocate its thermochemical, chemical, or biological conversion to chemicals and materials, not fuels. Yet, until the whole barrel of oil can be replaced, biomass should also be used as feedstock for biofuels. This has not been achieved until now. Many specialty chemicals or pharmaceuticals still need to be made from fossil sources[31]. An additional approach is to find new natural compounds from natural sources such as fungi or microalgae and cyanobacteria[32]

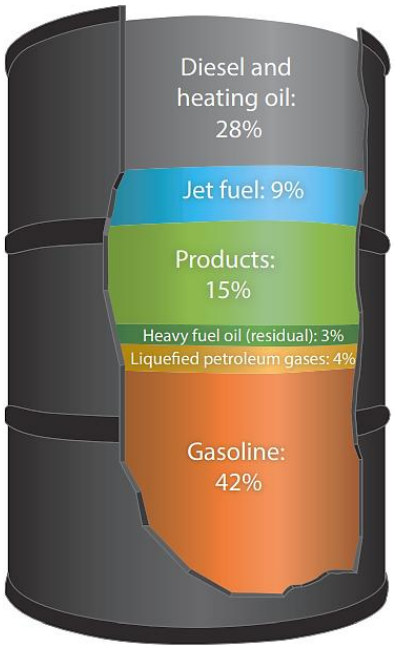

Figure 5: Use of a barrel of crude oil (percentage) (U.S. Department of Energy[1]).

1.2. The biorefinery concept

1.2.1. Generations of biomass

There are several routes to create clean energy from wind, sun, and water. Yet, the use of biomass is highly important because unlike the other energy sources, it provides liquid fuels and chemicals[33]. Based on feedstocks and method of production, biofuels and other bioproducts are classified in different groups named after their generation of feedstock, namely first, second, third, and fourth generation biomass or biofuels[34,35]. The four generations of biomass including their sources are depicted in **Figure 5**. The first-generation biomass uses edible crops as source for starch and sugar[36]. The use of crops for biofuel harms the environment more than petrol, the cost of production and causes inefficient utilization of resources and energy spent in cultivating crops. Yet, it has helped to articulate sustainability issues and challenges that need to be considered in implementing the utilization for the second generation of biomass. The second generation of biomass is based on more sustainable renewable feedstocks[37]. It includes utilizing inedible lignocellulosic biomass such as switchgrass, sawdust, low-priced woods, crop wastes, and

municipal wastes. Even though this generation of biomass allowed to overcome the drawbacks of the first generation, more steps are required to produce adequate biofuels and bioproducts at competitive pricing[38]. The recent years have seen tremendous progress in overcoming these obstacles for commercialization of the utilization of the second-generation biomass[39].

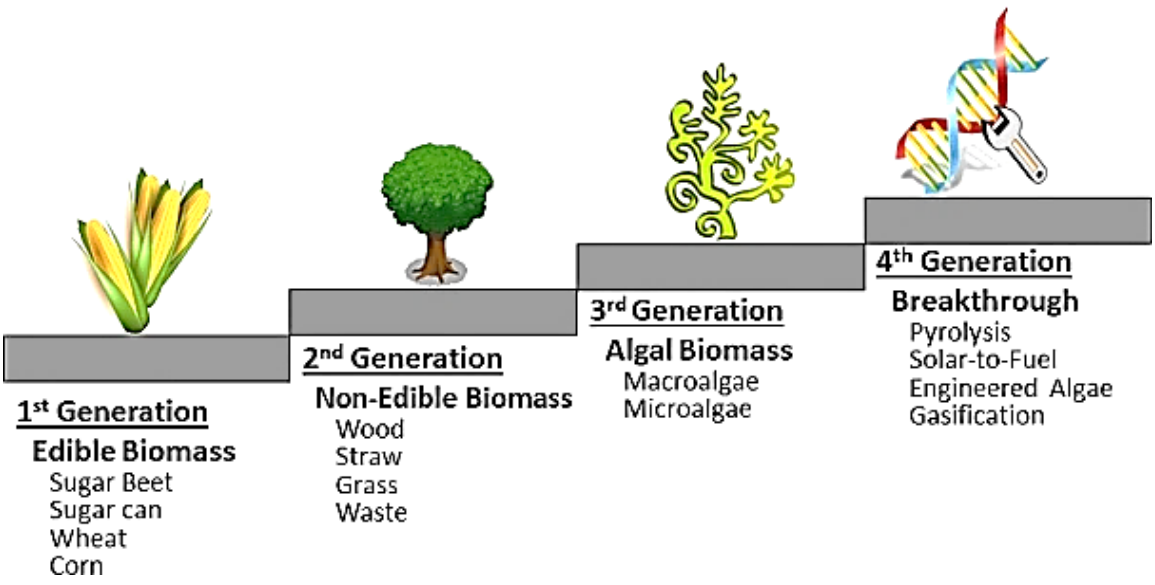

Figure 6: Overview of the four generations of biomass (Hyder et al.[34]).

Aquatic feedstocks such as algae and cyanobacteria are used as the third-generation biomass[40–42]. Algae such as seaweed or microalgae and cyanobacteria, which are unicellular phytoplankton and bacteria, capture high quantities of CO_2 and generate O_2 as well as high amounts of biomass[43–46]. This generation of biomass is promising due to its high biomass formation rate and low need of arable land. Until now, this generation of biomass has had some disadvantages such as its high costs[45]. The fourth-generation biomass, which is still in an early developmental stage, uses bioengineered microorganisms such as algae or cyanobacteria to consume more CO_2 from the environment than they emit when they are consumed (burning) or secrete valuable products[47]. Yet, the price pressure makes it difficult for biomass to compete with fossil fuels and their economy of scale. This urges the importance of integrating different feed streams coupled to generating multiple products in biorefinery concepts. Thus, in the future development to obtain bioproducts in a bioeconomy, the biorefinery concept plays an important role[33,36,48,49].

1.2.2. First and second-generation biorefinery

Biorefineries can be classified according to the implementation status of applied technology such as conventional and advanced, or first- and second-generation[35,38,50]. The classifications of a biorefinery, its technological implementation status, and type of feedstock are related. Types of biomass feedstock for first and second generation biorefineries are crops and lignocellulosic residues[35]. Platforms can be syngas or sugar. Products are fuels and chemicals, and conversion processes are thermochemical and biotechnological. First-generation feedstocks comprise oil and high-sugar crops, such as sugar beet and sugarcane, which are generally edible (**Figure 6**). As of 2020, 224 working biorefineries are registered in Europe, and a significant number is based on sugar/starch (63) and oil/fat (64). Twenty-four are wood-based biorefineries, and food waste is processed in 13 biorefineries. Five use non-wood lignocellulose. As such, a vast potential exists for second-generation biorefineries processing food waste and agricultural residues[18,51]. Cumulatively, biobased products account for more than 2 trillion € annual turnover in Europe, and market demand in the EU is expected to double by 2030[52].

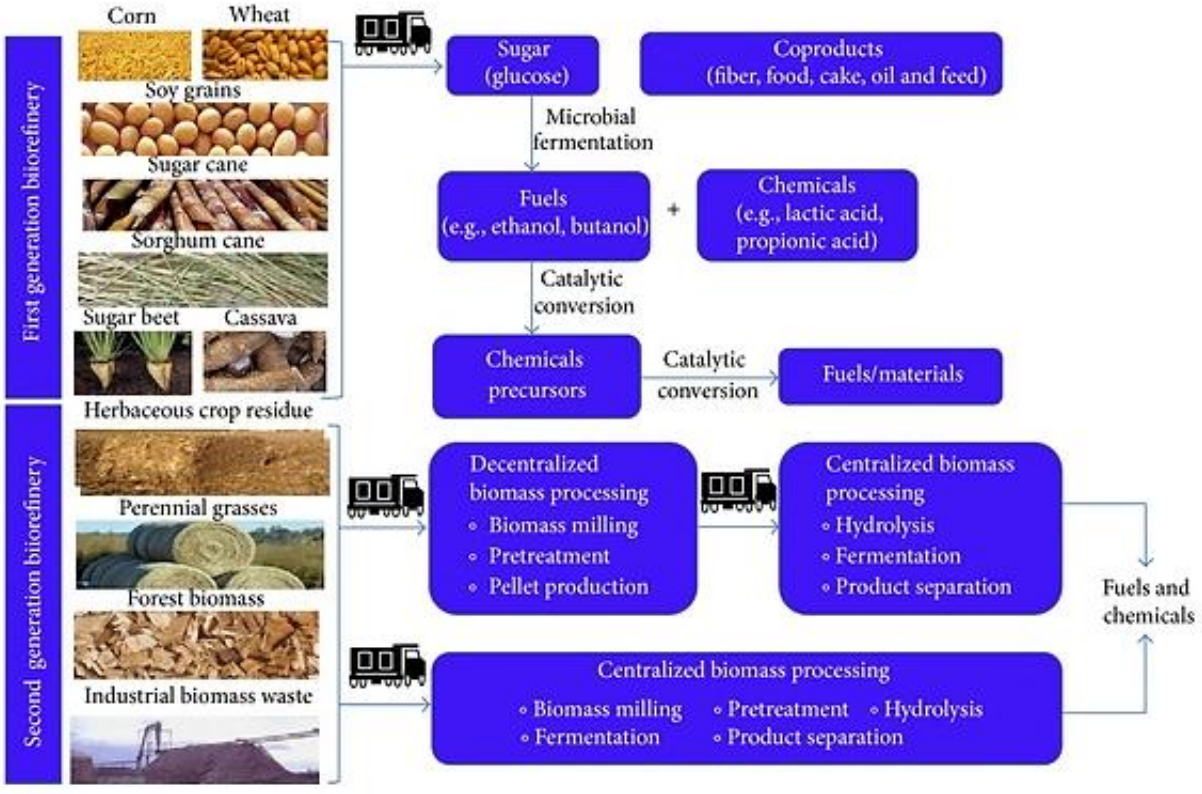

Figure 7: Overview of first- and second-generation biomass biorefinery concepts adapted from Balan et al.[52].

The S2Biom project has estimated that under sustainable practices 1,049 - 1,372 million tons of biomass can be made available within Europe by 2030[53]. The market for bio-based products was expected to be worth 40 million € by 2020, increasing to about 50 billion € by 2030.

Research in industry and academia have been galvanized to address the twin challenges of lignocellulosic breakdown and conversion into viable products: between 130–150 patents are filed annually in the lignocellulosic biofuel area, and this is expected to reach 200 annual filings[54]. Such indigestible biological wastes are the most promising source of biomass for producing bulk chemicals and fuels. It is an abundantly available lignocellulosic byproduct from agricultural and forestry industries. Lignocellulose is present as microfibrils in the cell walls of plants and trees. It consists mainly of the two polysaccharides hemicellulose (ca. 20 – 30 %) and cellulose (35 – 50 %) and lignin (ca. 10 – 25 %). Lignin is a highly cross-linked polymer made up of substituted phenols. These components can be used to produce several platform chemicals, which are essential for our industry (**Figure 7**)[54].

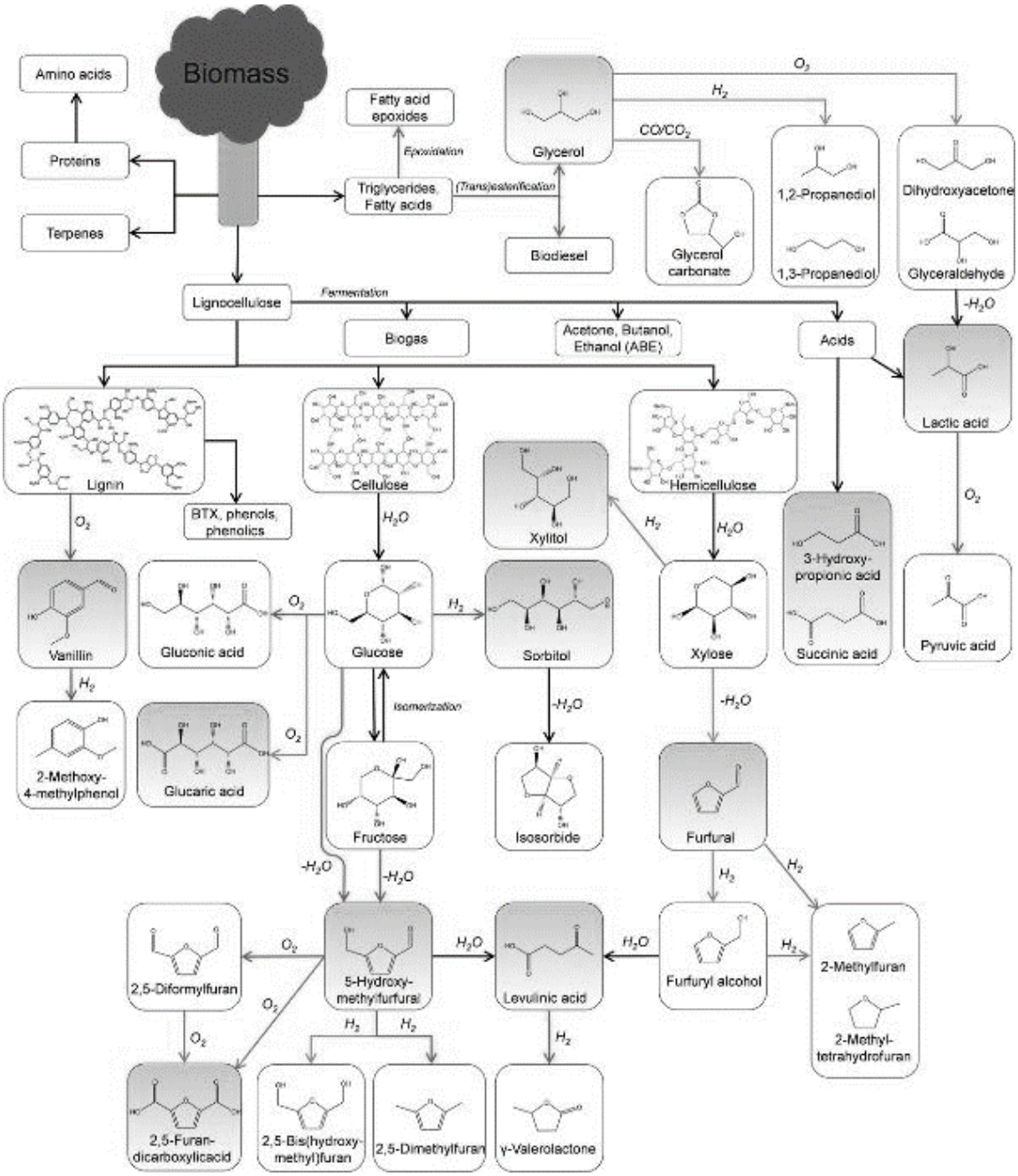

Figure 8: Overview of platform chemicals derived from biomass with selected reaction pathways, adapted from Hommes et al[54]. Grey boxes indicate the most promising biobased platform chemicals.

1.2.3. Microalgae and Cyanobacteria biorefineries

The third generation of biorefineries, which is based on the biomass of macroalgae, microlage and cyanobacteria, is technologocially not as advanced as the first and second generation biorefineries[55–57]. The big advantages of third generation biorefineries are the GHG reduction potential, due to the high CO_2 absorption rate and a high biomass production rate resulting in a high areal productivity[58]. This and the controled cultivation make especially microalgae and cyanobacteria a promising renewable feedstock for future bulk commodities. A

flow scheme of a microalgae or cyanobacteria biorefinery concept can be seen in **Figure 8**. However, the production of microalgae for low-value products, such as proteins for food/feed applications, bulk chemicals, or even biofuels, is economically not yet feasible[59–62].

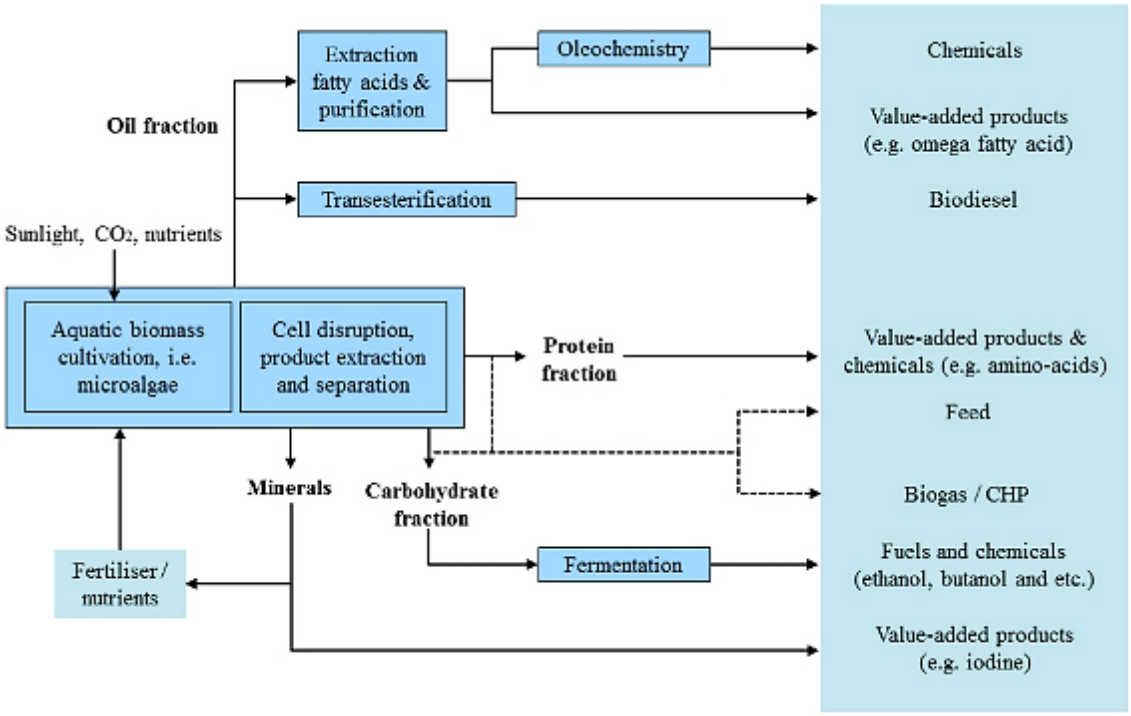

Figure 9: Flow scheme of a microalgae & cyanobacteria biomass biorefinery concept adapted from Kit Wayne et al.[60].

A systematic approach for integrated biorefineries need to be developed for the design and evaluation of cyanobacteria biorefineries[63]. Specifically, a superstructure model that includes supply, production, and purification subsystems[64]. Such a superstructure approach can be found in **Figure 10.** The supply subsystem includes flue/exhaust gases from industrial processes generally consisting of NO_x, CO, CO_2, and SO_x, which can be won for the cultivation of microalgae or cyanobacteria. Also, water and nutrient supply from a wastewater treatment plant should be considered. The production subsystem receives CO_2, water, and nutrients from the supply subsystem and grows cyanobacteria to produce biomass. In the production subsystem, two strain specific properties, productivity and residence time allow to determine a continuous flow from production subsystem to the purification subsystem. A system-wide optimization to dentify the optimal biorefinery configuration requires a holisitc life cycle sustaibility assessment[64].

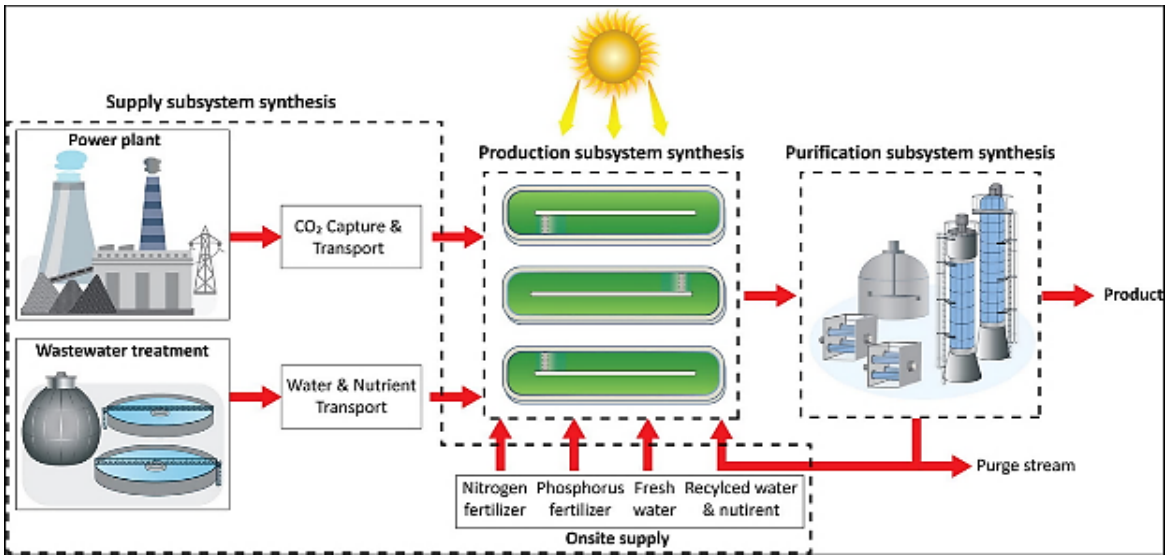

Figure 10: Superstructure approach of an integrated microalgae biorefinery concept divided into three subsystems adopted from Fasahati et al.[64].

1.2.4. Cyanobacterial products

Cyanobacteria (blue-green-algae) belong to an ancient group of photosynthetic prokaryotes that present a very wide range of cellular strategies, physiological capacities, and adaptations that support their colonization of very diverse microenvironments worldwide[43,65–67]. Therefore, cyanobacteria occur in varied and often extreme habitats and are then able to settle in diverse biotopes (e.g., marine, terrestrial, freshwater, thermal springs). Cyanobacteria have gained considerable attention in recent years for their possible use in many fields like agriculture, nutraceuticals, effluent treatment, food products, and the production of biofuels, various secondary metabolites including vitamins, toxins, and enzymes (**Figure 10**)[68–71]. They are also well known to produce a wide variety of bioactive natural products, including some potent toxins (e.g., microcystins, anatoxins, and saxitoxins). Due to the remarkable capability of cyanobacteria to proliferate and form toxic blooms that induce potential human health consequences, numerous studies have been conducted to develop tools for the monitoring of such blooms or effective strategies for the mitigation of their overgrowth. On the contrary, certain cyanotoxins could also constitute a promising opportunity for drug development such as certain cancer therapies[66,69,71,72].

Figure 11: Overview of potential products from cyanobacterial biomass[73].

The bioactive compounds from cyanobacteria have been identified as high-value products, which could make cyanobacteria biorefineries possible. 260 families of compounds were classified by their chemical classes, and 10 different classes were listed: alkaloids, depsipeptides, lipopeptides, macrolides/lactones, peptides, terpenes, polysaccharides, lipids, polyketides, and others[69]. This is not surprising, regarding the diversity of biosynthetic pathways described in cyanobacteria: NRPS (non-ribosomal peptide synthase), PKS (polyketide synthase), and RiPPs (ribosomally synthesized and post-translationally modified peptides) with the ability to produce a wide range of metabolites and notable peptides. Fourteen major activities have been listed from the literature: lethality, neurotoxicity, hepatotoxicity, dermal toxicity and cytotoxicity, anti-inflammatory, antioxidant, antiviral, anti-microalgal, antibacterial, antifungal, and antiprotozoal activities as well as protease and enzyme inhibition activities (**Figure 11**)[69]. Cytotoxic activity against various cell lines is the most frequently detected type of bioactivity with up to 110 families of the 260 listed. On the other hand, lethality and the antibacterial activities have been detected for 54 and 43 compound families, respectively.

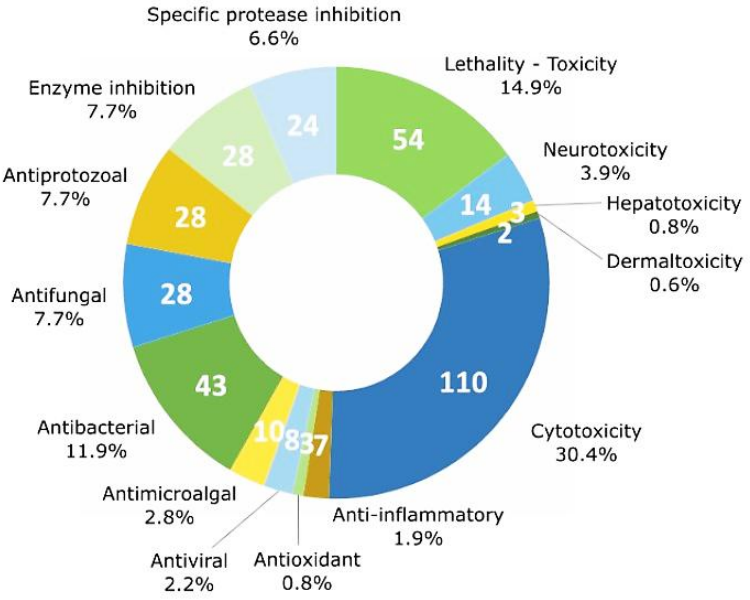

Figure 12: The reported 14 types of compounds and their bioactivities as products from cyanobacterial biomass adapted, Demay et al.[69].

These high-value compounds are reportedly the lever to make cyanobacteria biorefinery concepts economically feasible[65,74]. The global market for microalgae and cyanobacteria based products was estimated at 32.60 billion USD and is projected to reach approximately 53.43 billion USD by 2026[75]. Currently, more than 75 % of the production of microalgae-derived products is dedicated to food, feed, or nutraceutical applications. But other potential markets have emerged. As such, it is estimated that in 2020, dyeing agents were still the leading microalgae product on the market (800 million USD), closely followed by pharmaceuticals/ chemicals (500 million USD), nutraceuticals (300 million USD) and finally cosmetics (30 million USD). Yet, after the extraction of high value compounds, the residual biomass often is left as waste. The valorization of such residual biomass is economically also important[75].

1.2.5. Residual biomass utilization

Extracted high value compounds from cyanobacterial biomass makes up only minor fractions of the total biomass but give the main products for economic viabilty. Yet, the residual biomass can also be valorized and can serve as an alternative feedstock for biofuels or bioproducts employing different methods depending on the targeted products. The residual biomass needs adequate pre-treatment before valorization is possible. These different methods include thermochemical (combustion, torrefaction, pyrolysis, gasification, hydrothermal liquefaction, etc.), mechanical/physicochemical (ball milling, microwave, ultrasound, electric pulse, etc.) and biochemical (acid, alkali, enzymatic, etc.) processes (**Figure 12**). The methods need to be chosen depending on the subsequent valorization concept.

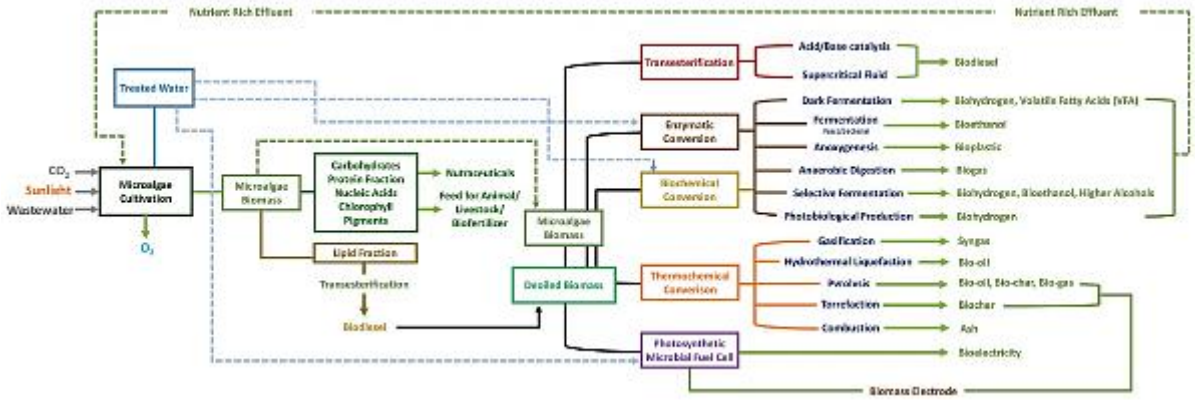

Figure 13: Flow chart of a microalgae biorefinery illustrating possible biomass treatment methods for relevant products adapted from Venkata *et al.*[76] .

Thermochemical conversion

Thermochemical conversion is employed to produce liquid/gaseous fuels and biocharcoal. Pyrolysis operated at a temperature between 200 and 750 °C in absence of oxygen produces solids (bio-char), liquids (bio-oil) and gaseous (bio-gas) products of interest. In slow pyrolysis, biomass is heated stepwise (10 °C/min) to the desired final temperature. Fast pyrolysis is used when the output required is liquid or gas (heating rate, 1–200 °C/s; particle size < 1 mm). For the production of only liquids, flash pyrolysis is used with rapid heating (temperature > 1000 °C/s; particle size < 0.2 mm) for few seconds. Hydrothermal liquefaction (HTL), which is suitable for treating wet algal biomass is usually performed at a temperature (250–450 °C) and pressures (100–350 bar) to facilitate depolymerization reactions (hydrolysis, dehydration and decarboxylation) and re-polymerization reactions (condensation) to form both water-soluble intermediates (HTL-AW) and water-insoluble products including bio-oil, biocrude and biochar along with gas rich in CO_2. HTL yields in bio-oil composed of furan, phenol, acid, and ester

derivatives with high percentage of aliphatic, phenolic, alcoholic, carboxylic and hydroxyl groups. The effect of pH modifiers, water medium, catalyst, temperature and heating rate regulate the product profile and efficiency of HTL process. Alkaline assisted HTL generates NH_3 and nitrogenous compounds during hydrolysis and deamination of microalgal protein wherein 80 % can be recovered as struvite.

Physicochemical conversion

Mechanical, microwave, ultrasound, electric pulse, osmotic shock, etc were used in different combinations to enhance the efficiency of cell wall disruption, sugar recovery and fermentation. Mechanical pretreatment processes such as bead milling were used for cellular disruption. Freezing and thawing method generates ice crystals that mechanically break the cell wall to release water-soluble intracellular compounds. Low frequency ultrasound with different solvents was used to extract carbohydrates, lipids, proteins and pigments. Ultrasound treatment is additionally reported to enhance enzymatic hydrolysis of the carbohydrates for fermentation by structural modification of the crystalline regions for which water uptake of the starch granules improved. Microwave pretreatment is considered to be a rapid process to carry out 80 % of cell lysis. Pulse electric field pretreatment for the extraction of different compounds can be applied in a broad range of pH. High pressure homogenization (HPH) of microalgal cell suspension showed higher yields of intracellular compounds. HPH can effectively function with slurries (~20 % solids) with higher cell disruption efficiency than mechanical methods.

Biochemical conversion

The cell wall of microalgae or cyanobacteria is composed of complex and structurally robust low biodegradable substances (e. g. algaenan and sporopollenin) that complicate the biological transformation into feedstock. Cell wall hydrolysis using acid and base due to harsh conditions is not regularly applied. Usually, enzymatic treatment is utilized to release fermentable sugars for the use in a secondary process such as fermentation. Enzymes such as serine proteases, trypsin and chymotrypsin were applied to release amino acid from algal protein by cell lysis. Additionally, endo-β-(1,4)- D-glucanase, exo-β-(1,4)- D-glucanase and β - glucosidase enzymes were combined to break cellulose to glucose and maltose. Different enzymatic cocktails for the hydrolysis (e.g., cellulases, amyloglucosidases, amylases, proteases and alkaline proteases) were found to be most effective compared to hydrothermal pretreatment. Multiple steps such as enzymatic hydrolysis with other mechanical treatment methods can be integrated for maximizing sugar and amino acid yield.

1.3. Pichia pastoris fermentation

1.3.1. *Pichia pastoris* bioprocess development

In the last years, the demand for protein in a broad range of industrial applications has increased strongly. The global biopharmaceutical market was expected to hit 400 billion € in 2020 with an annual growth rate (CAGR) of over 10 %. Industrial enzymes were estimated to accumulate to 6.3 billion € in 2021 with a CAGR of 4.7 %[77]. Further increasing demand and evolving production platforms allow for further reduction in costs and development of novel proteins. The quest for the development of new or improved bioprocess designs begins with the choice of a suitable cell factory. Production parameters such as yield, productivity, scale up capacity and downstream processes are here the dictating parameters. Product requirements also play a role in host considerations. In this regards, bacteria, yeast, or mammalian cells are chosen as cell factories. Yeasts as intermediate host with the best from both worlds have gotten more interest lately. Especially the yeast *Pichia pastoris* (*Komagataella phaffi*) with its many advantages has not only been used in lab scale more often but also in industry. The many advantages of *P. pastoris* in genetic, protein, and bioprocess engineering that make this organism so interesting can be found in **Table 1**. Yet, so far the fermentation technology has not reached the same maturity as for other organisms such as *E. coli*[77].

Table 1: Summary of the main advantages of *P. pastoris* as a recombinant protein expression platform adapted from Garcia-Ortega et al.[77]. (GRAS: generally recognized as safe, DCW: dry cell weight).

Genetic engineering	Protein processing	Bioprocess engineering
Simple and stable genetic manipulation	Eukaryotic capacity for folding, assembling, and performing post-translational modifications	GRAS organism lacks detectable endotoxins
Numerous tools available for genetic manipulation including CRISPR/Cas9 system	Protein processing and secreting pathway similar to higher eukaryotes	Non-fermentative growth on glucose
Different strong and efficient promoters	Ability to efficiently secrete target proteins combined with low levels of secretion for native proteins	Growth in chemically defined medium up to 120 g/L (DCW)
Reported high yield and stable producing strains	Reduced hyper glycosylation and reported human-like glycoengineered strains	Well-established large-scale production and downstream processing

The development of a bioprocess with *P. pastoris* is a multi-step process. On the way towards industrial implementation, there are several critical factors that can cost bioprocess efficiency. The two tasks of strain development and process strategy need to collaboratively determine the specific production rate of a producer strain. Going back and forth to improve the strain once an optimized bioprocess was designed. Yet, scaling up from lab scale to pilot or industrial scale holds many challenges as process parameters are difficult to be maintained[78].

Based on volumetric productivity, the space time yield (STY) and product yield optimization criteria need to be identified and regulated to improve the bioprocess efficiency. Improving the efficiency for a bioprocess means identifying optimum conditions for biomass growth and product formation, including pH, temperature, oxygen, and nutrient supply. Essential to identifying the physiological constraints of *P. pastoris* is the development of a suitable mode of adding carbon, which means developing an energy substrate feed profile or feeding strategy. Culture conditions and feeding strategies vary but can be determined for each individual product. Succeeding in doing so will allow to bring a bioprocess towards industrial production[79].

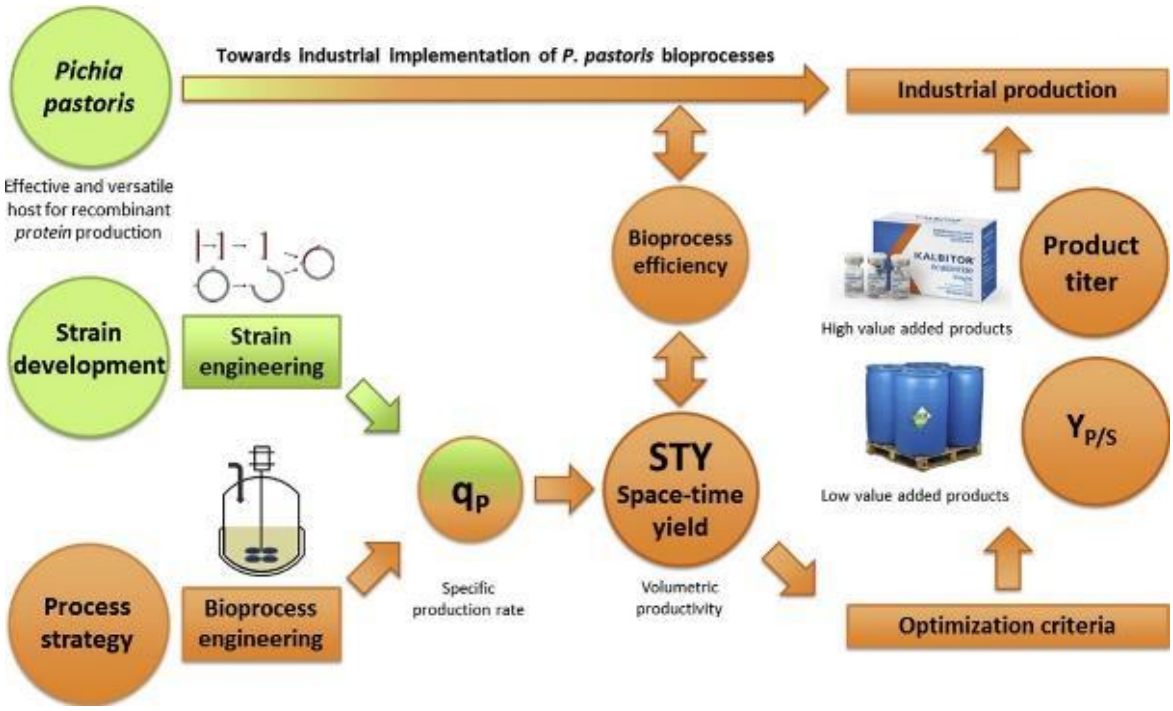

Figure 14: Overview of a *Pichia pastoris* bioprocess development towards industrial implementation adapted from Garcia-Ortega et al.[77].

There are different commercial protocols available (e. g. Invitrogen) for recombinant protein production with *P. pastoris* but recent developments have gone a different direction[80]. Concepts that allow for the development of a specific process strategy, which are tailored to both a particular product/genetic construct combination and the characteristics and limitations of a specific bioreactor equipment[81]. Originally there were two operational strategies for *P. pastoris* processes derived from the most widely used promoters: inducible AOX1 (alcohol oxidase 1) or constitutive GAP (glyceraldehyde-3- phosphate dehydrogenase)[82]. The major disadvantage of the mostly favored AOX1 over GAP is that methanol is required[83]. Methanol, added as a carbon and energy source is principally required for AOX1 induction for product formation. In a co-feeding

strategy, some sugars such as sorbitol can be added for biomass growth. Different other promotor variants have recently been developed but they are mostly derived or similar to the named two. For obvious disadvantages including having to deal with methanol on industrial scale and heavily increased oxidative stress, constitutive promoters seem advantages. Yet, it always depends on the enzyme if growth kinetics and product formation are strong for certain constructs. This has to be determined.

1.3.2. Growth kinetics and product formation

During batch cultivation, in which substrate is available in excess, biomass growth is unrestricted, and growth characteristics can be determined directly. The choice of carbon-substrate and, therefore, the feasible operational range with respect to specific growth rate (μ) and optimum productivity (q_p in mg product built per g cell dry weight and per hour) is dependent on the chosen promoter. With glycerol or glucose, *P. pastoris* grows significantly faster (e. g., 1.7–8.5 times faster) than with methanol. Values of the growth characteristics are crucial since they give a direct indication of whether the strain is physiologically impaired due to the introduction and expression of a foreign gene. Decreased maximum specific growth rates are most probably related to genetic burdens introduced by strain engineering and/or metabolic burdens of recombinant protein production. During batch growth with glucose, μ_{max} varied from 0.28 h^{-1} to 0.16 h^{-1} for strains differing with respect to productivity, whereas the best-producer strains grew slower. Hence, μ is a critical factor in enhancing product formation.

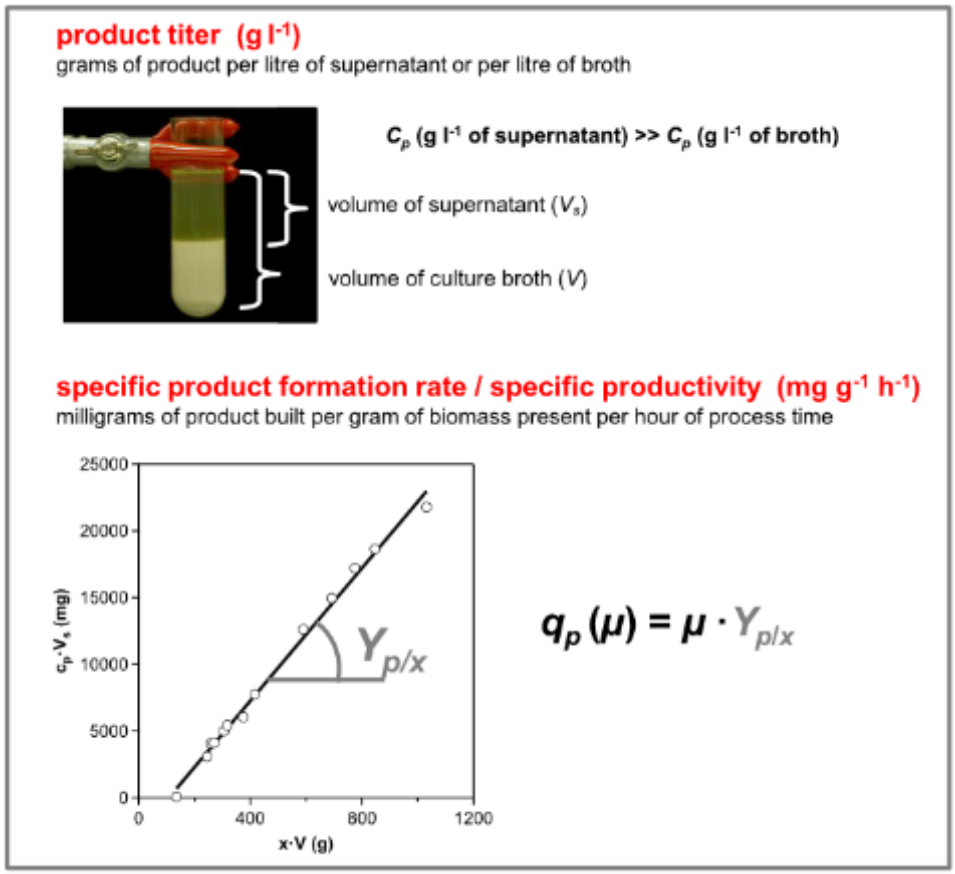

Figure 15: Calculation of growth titer and specific productivity adapted from Looser et al[81] .

The relationship between q_p and μ reflects the equilibrium between various processes in a cell until the product is secreted (i.e., induction of gene expression, translation, protein folding and degradation in the endoplasmic reticulum, flux of folded protein out of the ER, and trafficking through the secretory machinery). This relationship, also termed 'production kinetics' is essential for the design of production strategies in which growth is retained at a certain optimum μ-value by the controlled addition of carbon-substrate in fed batch mode. For AOX1-controlled production, methanol is typically pulsed repeatedly after complete depletion of the pulsed glucose substrate in order to maintain a residual substrate concentration within predetermined upper and lower concentration limits. During phases of substrate excess (which occur immediately after pulsing of the substrate), biomass grows with a specific growth rate close to its maximum (μ_{max}). Between subsequent pulses, i.e., after substrate depletion, biomass growth typically declines to 0 h^{-1} and biomass concentration stagnates. Unlike pulsed strategies applied in screening, in a bioreactor, the specific growth rate is controlled by the rate of substrate addition at a defined value lower than or equal to its maximum (μ_{max}). The optimum for AOX1-controlled product formation, according to current literature on kinetics, is often considerably below μ_{max}. However, for GAP-controlled product formation, the optimum specific growth rate is often near to μ_{max}, which is also reached during screening. The consequence may be a serious failure to identify clones that will become true 'top producers' under large-scale cultivation conditions. However, identifying a clone able to express large amounts of the desired product does not merely entail selecting the 'best producer' that is appropriate for the final production/ manufacturing scale.

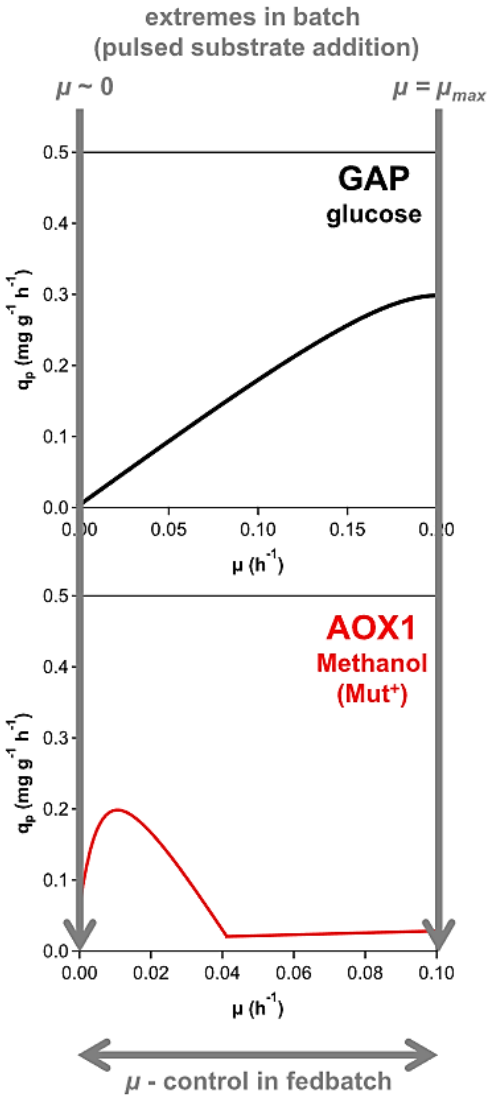

Figure 16: Relation of specific growth rate and specific productivity adapted from Looser et al[81].

1.3.3. Strategy development – feed profile

Historically, the strong and tightly regulated AOX1-promoter (pAOX1) has been mainly used for recombinant protein expression in *P. pastoris*. Using the AOX1-promoter, methanol acts as an inducer for recombinant protein production and, at the same time, as a carbon and energy source. Thus, induction and production of heterologous protein are interconnected with substrate utilization and biomass growth. Moreover, purpose-engineered AOX1-phenotypes that relate to the efficiency of methanol utilization represent an additional opportunity in strain/process design. In this respect, the *P. pastoris* expression system can be differentiated from, for example, *E. coli*, in which promoters can be induced by an independent, non-metabolizable agent. Consequently, *P. pastoris* production processes are more complex to control as oxidative stress is quite high for AOX1 systems. The typical *P. pastoris* cultivation process, therefore, follows a three-stage strategy: 1) a batch phase for biomass growth with glycerol or glucose, 2) a fed-batch phase for further biomass enhancement with glycerol or glucose and 3) an optional methanol-induced adaptation (transition) phase, which is followed by a production phase in fed-batch mode. Generally, numerous laborious and time-consuming fed-batch or continuous cultivations are performed at several different pre-set μ-values to establish the desired $q_p(\mu)$-relationship. Fed-batch strategies for continuous addition of an organic carbon and energy source are usually based on mathematical functions describing time dependency on the rate of substrate addition. In such strategies, substrate is added at predefined rates that increase or decrease following linear or exponential functions, or by equivalent stepwise approximations as shown in **Figure 16**. Unlike pulsed strategies the specific growth rate is controlled by the rate of substrate addition at a defined value lower than or equal to its maximum (μ_{max}). The added substrate is immediately utilized and therefore cells can only grow as fast as the rate of substrate supply. In order to maintain a constant specific growth rate over the entire course of a fed-batch process, the feed rate must be increased exponentially (the biomass also grows exponentially) providing a constant amount of substrate $CDW^{-1}\ h^{-1}$. Establishing production kinetics with fed-batch cultivations at several different pre-set μ-values is laborious and time-consuming, and, therefore, alternative approaches are being sought.

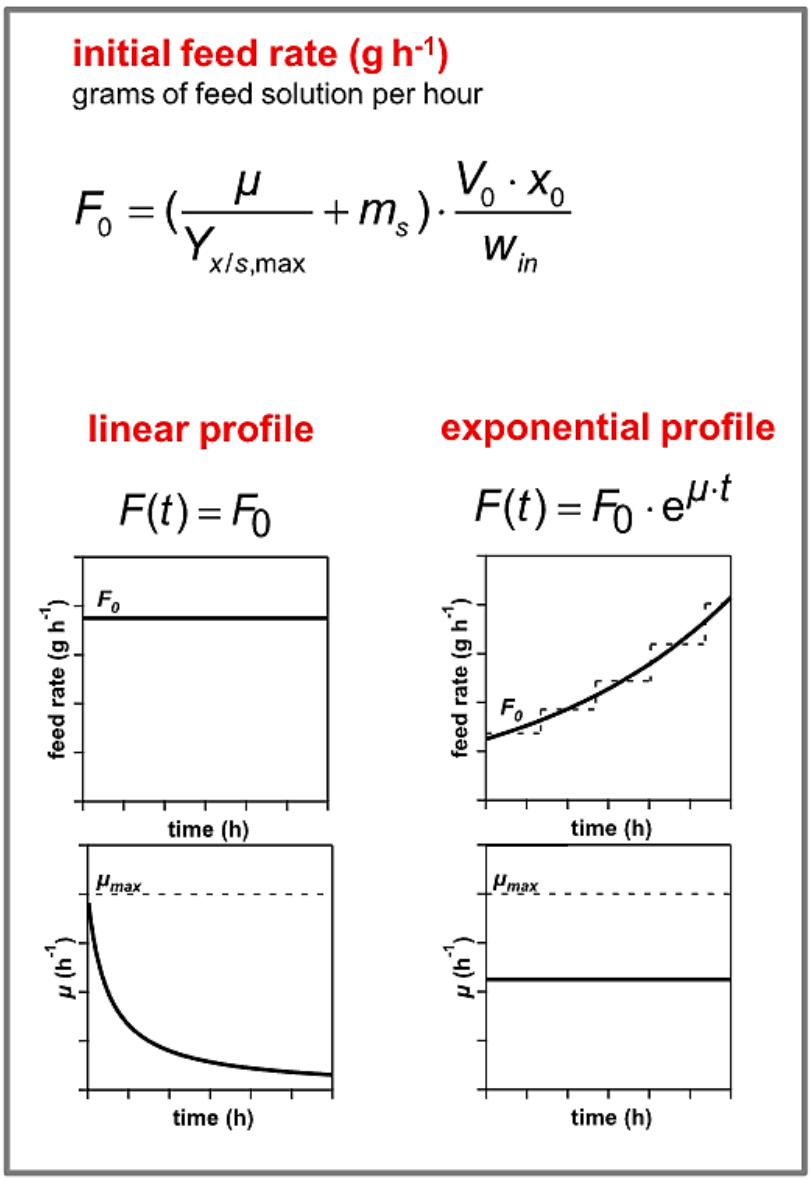

Figure 17: Calculations for initial feed rate and linear and exponential feed profiles adapted from Looser et al[81].

In recent years, protocol design has shifted from classical 'recipes' to more conceptual attempts. Considering the maximum specific growth rate (μ_{max}) as the upper limit and the production kinetics $q_p(\mu)$ as an indicator of the optimum production range of μ, design of a customized fed-batch feed profile to maximize product titer is possible. A thorough characterization is needed in every fermentation system before production can start as shown in the flow chart in **Figure 17**. For first characterization batch and pulsed batch fermentation are fundamental to find μ_{max}. Although, dynamic fed-batch approaches are reported support finding μ_{opt} or $q_p(\mu)_{max}$. Yet, for all systems oxygen and/or heat transfer are most often the limiting factors in high cell density *P. pastoris* cultivations irrespective of the substrate used. However, heat

evolution and oxygen uptake strongly depend on specific growth rates and, therefore, the process must be designed within the technical limitations of the available equipment.

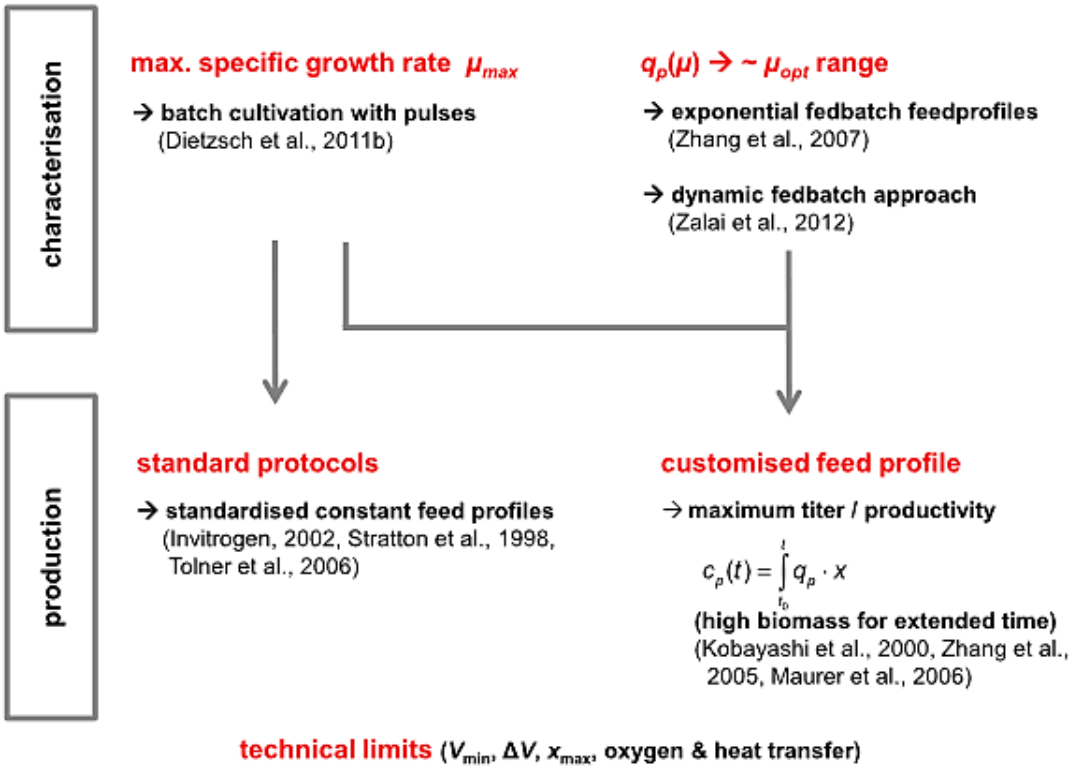

Figure 18: Flow chart for the development of a *Pichia pastoris* bioprocess strategy, adapted from Looser et al[81].

1.3.4. Industry enzyme – Phytase

Phytate (myo-inositol hexakisphosphate) is the main storage form of phosphorus in plant-derived feed[84–87]. It is an inositol ring with one phosphate group attached to each carbon atom. It mainly accumulates in protein storage vacuoles in grains (e.g., rape, wheat, maize, or sesame) and plant seeds. It can account for up to 80 % of the total phosphorus in seeds[88]. The phosphate groups in phytate are negatively charged and strongly bind to positively charged species like metallic cations or charged proteins. Especially divalent cations like calcium, iron, and zinc are chelated reducing their bioavailability. Phytate is stable but phytases (myo-inositol hexakisphosphate phosphohydrolases) can hydrolyze the phosphoester bonds and release the phosphate groups and therefore the chelated ions (**Figure 18**). Monogastric animals, such as pigs, poultry, and fish are lacking enzymes with phytase activity in their gastrointestinal tracts, therefore they utilize dietary phosphorus inefficiently. Hence, phytases have significant value as animal feed additives[87].

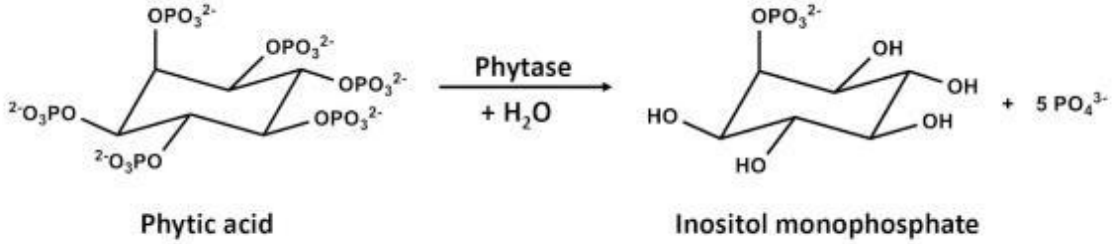

Figure 19: Reaction scheme of phytate conversion to inositol and free phosphate by phytase[89].

Phytases can be classified based on their optimal pH, the catalytic mechanism, or the initiation site of dephosphorylation. Considering the reaction mechanism, three groups can be defined: (1) histidine acid phosphatases or acid phosphatases (EC 3.1.3.2), (2) β-propeller phytases (EC 3.1.3.8), and (3) purple acid phosphatases or cysteine phytases (EC 3.1.3.2). The phytase market has exceeded 300 million €, growing about 10 % per year. Besides in the animal feed industry, there have been many new discoveries for phytase applications lately[90]. Different applications in food processing for human nutrition and industrial non-food products are emerging[89]. Therefore, there is tremendous interest in improving catalytic efficiency, substrate specificity, thermostability, modification of the pH profile, and reduction in production cost. Despite the many applications and market interest, it is not trivial to compare published activities. Different assays for the determination of phytase activity are out there and different reaction conditions are used for each assay. So, one must be cautious comparing reported values. Yet, it has become apparent that the appA *E. coli* phytase is regarded as the one with the highest specific activity[85].

1.4. Scope of this work

The general aim of this thesis is the development of a biorefinery concept for cyanobacterial biomass with the focus on the fermentative utilization of the residual biomass after the extraction of multiple high-value compounds. Biomass from the promising genera *Nostoc* and *Cylindrospermum* were investigated throughout this thesis.

In order to accomplish the realization of such a concept, analytical methods for primary metabolites of cyanobacterial biomass need to be utilized for biocompositional analysis. The saccharide, protein, and lipids content of *Nostoc* biomass need to be quantified. Moreover, the divers saccharide fingerprint needs to be elucidated to be able to evaluate the potential utilization of the storage or structural sugars fermentatively. Especially substituted saccharides such as deoxy, methyl-, amino-, and sulfated sugars, or uronic acids pose difficulties to enzymatically

hydrolyze such biomass. The HT-PMP method for fingerprinting algal carbohydrates that is available for this work allows to investigate the broad range of saccharides present in promising strains[91]. Furthermore, different industrial enzymes have to be investigated on their hydrolysis efficiency on cyanobacterial biomass.

Enzymatically produced hydrolysate from cyanobacterial biomass needs to be investigated as growth medium and it needs to be decided, which product ought to be aimed for fermentatively. After identifying a producer strain, a proof of concept in a bench scale reactor system needs to be conducted. In a multi-field research approach, we can use the *P. pastoris* enzyme production platform and use cyanobacterial biomass as feedstock. Developing a fed-batch strategy for AppA *E. coli* phytase expression and demonstrating the utilization of *Nostoc* sp. De1 biomass hydrolysate. Show a relevant producer strain can emerge from the extended *P. pastoris* toolkit and the enzyme expression with cyanobacterial biomass as feedstock may be an industrially relevant and more sustainable alternative to currently used sources.

Once the proof of concept for the fermentative utilization with the identified producer strain of the cyanobacterial biomass hydrolysate has been done, a fermentation strategy can be developed. The development of such a bioprocess should focus on the specific process mode as at this point the producer strain and the biomass hydrolysate as medium supplement are already identified.

The most vital point for the development of a biorefinery concept is the identification of specific cyanobacterial strains, which produce high-value compounds from the genus *Nostoc* or *Cylindrospermum*. The Cylindrospermum strain *C. alatosporum* CCALA988 had shown promising with several interesting compounds such as cyclic lipopeptides[92]. A sequential extraction of multiple high-value compounds needs to be verified as feasible before the residual biomass ought to be utilized in a determined way. The residual biomass should be converted into a hydrolysate and utilized as fermentation medium again. Such a multi high-value product biorefinery concept should also be evaluated by a techno-economic analysis or a life cycle sustainability assessment (LCSA), which will allow to draw sophisticated conclusions about potential social, environmental, and economic impacts.

2. Material

The material employed was either available at the chair or bought from listed manufacturers.

2.1.1. Equipment

Table 2: Overview of used devices.

Device	Model	Manufacturer
1 L parallel bioreactor	DASGIP SSL 1000	DASGIP GmbH, Jülich, Germany
Gas mixing	MX4/4	DASGIP GmbH, Jülich, Germany
Off-gas analysis	GA4	DASGIP GmbH, Jülich, Germany
Pumps	MP8	DASGIP GmbH, Jülich, Germany
Sensors	PH4PO4RD4	DASGIP GmbH, Jülich, Germany
Temperature, agitation	TC4SC4B	DASGIP GmbH, Jülich, Germany
Analytical balance	Entris	Sartorius AG, Göttingen, Germany
Analytical balance	AW320	Shimadzu Deutschland GmbH, Duisburg, Germany
Autoclave	Varioclav S135 with S2 filter	Thermo Fisher Scientific, Waltham, USA
Balance	TE 1502, TE6101	Sartorius AG, Göttingen, Germany
Centrifuge	Sorvall RC6+	Thermo Fisher Scientific, Waltham, USA
Rotors	SS-34, SH-3000 and F9-4x 1000y	Thermo Fisher Scientific, Waltham, USA
Centrifuge	Heraeus Pico 17	Thermo Fisher Scientific, Waltham, USA
Rotors	Bioflex HC, A27-8x 50	Thermo Fisher Scientific, Waltham, USA
Clean bench	MSC Advantage	Thermo Fisher Scientific, Waltham, USA
Drying oven	Heraeus Function Line T12	Thermo Fisher Scientific, Waltham, USA
Elemental Analyser	Euro EA	Hekatech GmbH, Wegberg, Germany
Freezer -20 °C	Mediline Lgex 3410	Liebherr-Hausgeräte GmbH, Ochsenhausen, Germany
Freezer -80 °C	Forma 906 -86 °C ULT	Thermo Fisher Scientific, Waltham, USA
Gas chromatograph	Trace GC 2000 with Ultra Trace	Thermo Fisher Scientific, Waltham, USA
Autosampler	TriPlus Autosampler	Thermo Fisher Scientific, Waltham, USA
Column	Rxi®-5Sil-MS column (30 m by 0.53 mm, 20 µm film)	Restek GmbH, Bad Homburg, Germany
Mass-spectrometer	Ultra-Trace DSQ II	Thermo Fisher Scientific, Waltham, USA
Gel electrophoresis	Mini-PROTEAN®-Tetra Cell, Mini-Protean®3Multi-Casting Chamber	Bio-Rad Laboratories, Munich, Germany
Power supply	PowerPAC Basic	Bio-Rad Laboratories, Munich, Germany
Documentation (camera)	Gel iX imager	Intas Science Imaging Instruments GmbH, Göttingen, Germany
Documentation (Transilluminator)	Transiluminator DR-46B	MoBiTec GmbH, Göttingen, Germany
Heating block	Tmix	Jenaanalytik GmbH, Jena, Germany
Heating block	EC-1V-210	VLM GmbH, Bielefeld, Germany
Heating block	Starfish plate	Heidolph Instruments GmbH & Co. KG, Schwabach, Germany
Ice machine	Flockeneisbereiter AF 80	Scotsman, Milano, Italy
Incubator	HAT Minitron	Infors AG, Basel, Switzerland
Lyophylle	Alpha2-4 LD plus	Martin Christ Gefriertrocknungsanlagen GmbH, Osterode am Harz, Germany
Magnetic stirrer	Variomag Telesystem	Thermo Fisher Scientific, Waltham, USA
Microwave	MH 25 ED	ECG, Prague, Czech Republic

Mixer Mill	MM400	Retch GmbH, Haan, Germany
Muffle furnace	LM 312.27	Linn High Term GmbH, Eschenfelden, Germany
Multichannel pipette	S-8, adjustable, CE-IVD, DE-M	Brand GmbH & Co. KG, Wertheim, Germany
pH meter, electrode	Five Easy and InLab Epert Pro	Mettler-Toledo GmbH, Giessen, Germany
Pipettes	Transferpettes	Brand GmbH & Co. KG, Wertheim, Germany
Repetitive pipette	HandyStep	Brand GmbH & Co. KG, Wertheim, Germany
Rotary vacuum evaporator	Büchi Rotavapor R-210	Thermo Fisher Scientific, Waltham, USA
Pump	Membranpump V-700	Thermo Fisher Scientific, Waltham, USA
Vacuum controller	Vakuumcontroller V-850	Thermo Fisher Scientific, Waltham, USA
Scanning electron microscope	DSM 940A	Carl Zeiss AG, Overkochem, Germany
Shakers	MaxQ 2000	Thermo Fisher Scientific, Waltham, USA
Sonotrode	UIS250L with LS24d3	Hielscher Ultrasonics GmbH, Teltow, Germany
Special clamping device	In-house development	K. Rühmann, Goltoft, Germany
Spectrophotometer	Varioscan Flash	Thermo Fisher Scientific, Waltham, USA
Spectrophotometer	M200 Infinite	Tecan Group AG, Männedorf, Switzerland
Spectrophotometer	Ultrospec 10	Amersham Biosciences Corp., Little Chalfont, England
Table centrifuge	Heraeus Fresco 21	Thermo Fisher Scientific, Waltham, USA
Thermocycler	Mycycler	Bio-Rad Laboratories, Munich, Germany
UHPLC	Ultimate 3000RS	Dionex Corporation, Sunnyvale, USA
Degasser	SRD 3400	Dionex Corporation, Sunnyvale, USA
Pump module	HPG 3400RS	Dionex Corporation, Sunnyvale, USA
Autosampler	WPS 3000TRS	Dionex Corporation, Sunnyvale, USA
Colum compartment	TCC 3000RS	Dionex Corporation, Sunnyvale, USA
Diode array detector	DAD 3000RS	Dionex Corporation, Sunnyvale, USA
RI detector	RI 101	Shodex, Tokyo, Japan
High-capacity ion trap	APCI, ESI, HCT	Bruker Daltonics, Billerica, USA
Ultrapure water system	Milli-Q Reference	Merck KGaA, Darmstadt, Germany
Ultrapure water system	PURELAB classic	ELGA LabWater, Celle, Germany
Ultrasonic bath	USC200-2600	VWR International GmbH, Darmstadt, Germany
Vacuum drying oven	VDL 53	Binder, Tuttlingen, Germany
Vacuum pump	PC 2004 VARIO	VACUUBRAND GmbH & Co. KG, Wertheim, Germany
Vortexer	Vortex Genie 2	Scientific Indutries, Bohemia, USA
Water bath	CC1	Peter Huber Kältemschinen AG, Offenburg, Germany

2.1.2. Software and databases

Table 3: Overview of software and databases used.

Product	Application	Manufacturer
Microsoft Office 2010	text processing, calculations, visualization	Microsoft Corporation, Redmond, USA
Bacterial Carbohydrate Structural Database	Identifying of polysaccharides	Toukach et al. 2007
ChemDraw 18.0	Drawing chemical structures	Cambridge Soft, Cambridge, England
Chromeleon	Data analyzing HPLC	Dionex Corporation, Sunnyvale, USA

Citavi 5	Reference management	Swiss Academics Software GmbH, Wädenswil, Switzerland
DataAnalysis	MS-data analysing	Bruker Daltonics, Billerica, USA
HyStar	System control	Bruker Daltonics, Billerica, USA
LibraryEditor	Spectra database	Bruker Daltonics, Billerica, USA
Magellan	MTP-reader control software	Tecan Group Ltd., Männedorf, Switzerland
OriginPro 2020	Scientific graphing	OriginLab Corporation, Northampton, USA
QuantAnalysis	Quantification of MS-data	Bruker Daltonics, Billerica, USA
SkanIt	MTP-reader control software	Thermo Fisher Scientific, Waltham, USA
Xcalibur	Data analyzing GC	Thermo Fisher Scientific, Waltham, USA
Web of knowledge	Literature research	Thomson Reuters
DASware control	Controlling bioprocesses	DASGIP GmbH, Jülich, Germany

2.1.3. Special consumables

Table 4: Overview of used special consumables.

Product	**Specification/Catalog Nr.**	**Manufacturer**
96-silicon cap mat	7704-0105	Whatmann, Little Chalfont, England
96-well deep well plate 2.0 mL	655101	Greiner Bio-One GmbH, Frickenhausen, Germany
96-well micro titer plate F-bottom (UV)	781614	Greiner Bio-One GmbH, Frickenhausen, Germany
96-well SpinColumn G-25 (25-100 µL)	74-5612	Harvard Apparatus, Holliston, USA
96-well-PCR-plate	781350	Brand GmbH & Co. KG, Wertheim, Germany
Bottletop filters	Nalgene RapidFlow 0.2 µm	Thermo Fisher Scientific, Waltham, USA
Centrifugal filters	516-0230	VWR International GmbH, Darmstadt, Germany
Cryo pure tube	1.5 white	Sarstedt AG & Co. KG, Nümbrecht, Germany
Cuvettes	759015, PS, 10 mm	Sartorius Stedim Biotech GmbH, Göttingen
Filter plate 0.2 µm Supor	PN 8031	Pall Corporation, Port Wahsington, USA
Filtration membrane	18407–47——N	Sartorius Stedim Biotech GmbH, Göttingen
HPLC C18 column	NUCLEODUR C18 Gravity, 1.8 µm, 100 mm, ID: 2 mm	Macherey, Nagel GmbH & Co. KG, Düren Germany
HPLC IEX column	Rezex ROA-Organic Acid H+ (8%); 300 x 7.8 mm; 00H-0138-K0	Phenomenex Duetschland Ltd., Aschafenburg, Germany
Nunc 96-Well MicroWell	249944	Greiner Bio-One GmbH, Frickenhausen, Germany
Pasteur pipettes	612-1681	VWR International GmbH, Darmstadt, Germany
Petri dishes	-	Sarstedt AG & Co. KG, Nümbrecht, Germany
Pipette tips	various	Brand GmbH & Co. KG, Wertheim, Germany
Reaction tubes (PP)	1.5, 2.0, 15, and 50 mL	Sarstedt AG & Co. KG, Nümbrecht, Germany

Syringe filters 0.2 µm	various	VWR International GmbH, Darmstadt, Germany
Syringes	various	B. Braun Melsungen AG, Melsungen, Germany
Thermoplastic elastomer cap mat (TPE)	781405	Brand GmbH & Co. KG, Wertheim, Germany

2.1.4. Chemicals and reagents

Table 5: Overview of used chemicals and reagents.

Product	Catalog Nr.	Manufacturer
1-Phenyl-3-Methyl-5-pyrazolone	M70800	Sigma-Aldrich, Deisenhofen, Germany
ABTS	A1888	Sigma-Aldrich, Deisenhofen, Germany
Acetic acid	338826	Sigma-Aldrich, Deisenhofen, Germany
Acetone	7328	Carl-Roth GmbH & Co. KG, Karlsruhe Germany
Acetonitrile LC-MS grade	83.040.320	VWR International GmbH, Darmstadt, Germany
Acrylamid-Bisacrylamids Rotiphorese Gel 30	3029	Carl-Roth GmbH & Co. KG, Karlsruhe Germany
Agar-agar	5210.2	Carl-Roth GmbH & Co. KG, Karlsruhe Germany
Ammonium persulfate	1012010500	Merck KGaA, Darmstadt, Germany
Ammonium solution 32 %	P093.1	Carl-Roth GmbH & Co. KG, Karlsruhe Germany
Ammonium sulfate	A5132	Sigma-Aldrich, Deisenhofen, Germany
Antifoam B	A5757	Avantor Performance Materials B.V., Deventer, Netherlands
Biotin	B4639	Sigma-Aldrich, Deisenhofen, Germany
Boric acid	B7901	Sigma-Aldrich, Deisenhofen, Germany
Bovine serum albumin	A2153	Sigma-Aldrich, Deisenhofen, Germany
C4 - C24 FAMEs	49454-U	Sigma-Aldrich, Deisenhofen, Germany
Calcium chloride	5239.1	Carl-Roth GmbH & Co. KG, Karlsruhe Germany
Calibration buffer pH 10	10.00 ± 0.02	VWR International GmbH, Darmstadt, Germany
Calibration buffer pH 4	4.00 ± 0.02	VWR International GmbH, Darmstadt, Germany
Calibration buffer pH 7	7.00 ± 0.02	VWR International GmbH, Darmstadt, Germany
Chloroform	AE59.1	Carl-Roth GmbH & Co. KG, Karlsruhe Germany
Citric acid	251.275	Sigma-Aldrich, Deisenhofen, Germany
Cobalt (II) chloride hexahydrate	A16346	Alfa Aesar GmbH + Co. KG, Karlsruhe, Germany
Coomassie Brilliant Blue G250	27815	Sigma-Aldrich, Deisenhofen, Germany
Copper (II) sulfate pentahydrate	61245	Sigma-Aldrich, Deisenhofen, Germany
Ethanol absolute	20.821.321	VWR International GmbH, Darmstadt, Germany
Glucose	6887.5	Carl-Roth GmbH & Co. KG, Karlsruhe Germany
Glycerol (99.5 % p.a.)	3783.2	Carl-Roth GmbH & Co. KG, Karlsruhe Germany
Hydrochloric acid, 37 %	4625.1	Carl-Roth GmbH & Co. KG, Karlsruhe Germany
Iron (II) sulfate heptahydrate	31236	Sigma-Aldrich, Deisenhofen, Germany
Magnesium sulfate heptahydrate	1.058.861.000	Merck KGaA, Darmstadt, Germany
Manganese (II) chloride tetrahydrate	63535	Sigma-Aldrich, Deisenhofen, Germany
Methanol LC-MS	83.638.320	VWR International GmbH, Darmstadt, Germany

N,N,N′,N′-Tetramethylethylendiamine	M146	VWR International GmbH, Darmstadt, Germany
Natriumcitrat-dihydrat	W302600	Sigma-Aldrich, Deisenhofen, Germany
Peptone from casein	8952.5	Carl-Roth GmbH & Co. KG, Karlsruhe Germany
Phenol red	B21710	Alfa Aesar GmbH + Co. KG, Karlsruhe, Germany
Potassium phosphate dibasic	P749.3	Carl-Roth GmbH & Co. KG, Karlsruhe Germany
Potassium phosphate monobasic	1.048.731.000	Merck KGaA, Darmstadt, Germany
Potassium sulfate	221368	Merck KGaA, Darmstadt, Germany
Rubidium chloride	12892	Alfa Aesar GmbH + Co. KG, Karlsruhe, Germany
Sodium chloride	P029.3	Carl-Roth GmbH & Co. KG, Karlsruhe Germany
Sodium hydroxide	6771.2	Carl-Roth GmbH & Co. KG, Karlsruhe Germany
Sodium molybdate dehydrate	CN-62	Carl-Roth GmbH & Co. KG, Karlsruhe Germany
Sodium-azide	71290	Sigma-Aldrich, Deisenhofen, Germany
Sulphuric acid	4363.1	Carl-Roth GmbH & Co. KG, Karlsruhe Germany
Trifluoroacetic acid	T6508	Sigma-Aldrich, Deisenhofen, Germany
Tris	AE15.2	Carl-Roth GmbH & Co. KG, Karlsruhe Germany
Yeast extract	2363	Carl-Roth GmbH & Co. KG, Karlsruhe Germany
Yeast nitrogen base without amino acids	Y0626	Sigma-Aldrich, Deisenhofen, Germany
Zeocin	R25001	Thermo Fisher Scientific, Waltham, USA
Zinc chloride	1.088.160.250	Merck KGaA, Darmstadt, Germany

2.1.5. Kits

Table 6: Overview of used kits.

Product	Specification/Catalog Nr.	Manufacturer
Total Starch Assay Kit	K-TSTA-100A	Megazyme Ltd, Bray, Ireland
Protein quantification (Bradford)	Roti Quant Universal	Carl-Roth GmbH & Co. KG, Karlsruhe Germany

2.1.6. Enzymes

Table 7: Overview of used enzymes.

Product	Specification/Catalog Nr.	Manufacturer
Horseradish peroxidase	P6782	VWR International GmbH, Darmstadt, Germany
Celluclast®	Viscosity reduction of fibrous plant tissue	Novozymes A/S, Bagsværd, Denmark
DISTILLASE® CS	Saccharifying Enzyme for Ethanol Production	DuPont Inc, Wilmington, USA
FERMGEN™	Acid Fungal Protease Enzyme for Ethanol Production	DuPont Inc, Wilmington, USA
Glucose oxidase	G2133	Sigma-Aldrich, Deisenhofen, Germany
OPTIMASH™ BG	Beta Glucanase/Xylanase for Barley and Wheat Ethanol Manufacturing	DuPont Inc, Wilmington, USA

ROHAPECT® B1L	Pectinase preparation with high hemicellulolytic side activities	AB Enzymes GmbH, Darmstadt, Germany
ROHAPECT® UF	Decomposition of „residual pectic substances“ in fruit juices	AB Enzymes GmbH, Darmstadt, Germany
Viscozyme® L	V2010, cellulolytic enzyme mixture	Sigma-Aldrich, Deisenhofen, Germany

2.1.7. Organisms

Table 8: Overview of used organisms.

Strain	Growth Medium	Cultivation Conditions	CBR Reference
S. cerevisiae BY4741	YPD	30 °C, pH 4-5	CBR_S_168
C. necator	Medium 1 (Nutrient rich)	37 °C, pH 7	CBR_S_73
E. coli BL21 (DE3)	LB	37 °C, pH 7	CBR_S_1
P. pastoris attP	YPD, BMGY/Glc	30 °C, pH 5	CBR_S_127 (pUO_pL963)
Y. lipolytica H222	YPD	30 °C, pH 5	CBR_S_67

2.1.8. Cyanobacterial biomass

Table 9: Overview of used cyanobacterial biomass.

Strain	Growth Medium	Producer
Nostoc sp. De1	BG 11	Centre Algatech, Třeboň, Czech Republic
Nostoc sp. Cc3	BG 11	Centre Algatech, Třeboň, Czech Republic
Nostoc muscorum I	BG 11	Centre Algatech, Třeboň, Czech Republic
Nostoc piscinale	BG 11	Centre Algatech, Třeboň, Czech Republic
Nostoc viola	BG 11	Centre Algatech, Třeboň, Czech Republic
Nostoc sp. F 15c	BG 11	Centre Algatech, Třeboň, Czech Republic
Nostoc linckia VT - 15	Alen Arnon	Centre Algatech, Třeboň, Czech Republic
Cylindrospermum alatosporum CCALA988	BG 11	Centre Algatech, Třeboň, Czech Republic

2.1.9. Sugar standards

Table 10: Overview of used sugar standards.

Name of the Sugar	Company	Catalog No.	Batch
2-Deoxy-D-(-)-ribose	Sigma-Aldrich, Deisenhofen, Germany	31170	BCBB5360V
2-Deoxy-D-(+)-glucose	Carl-Roth GmbH & Co. KG, Karlsruhe Germany	CN96.2	160152839
2-O-Methyl-D-glucose	Carbosynth Ltd., Compton, England	MM28994	MM289941601
3-Deoxy-D-glucose	Carbosynth Ltd., Compton, England	MD03580	MD035801301
3-O-Methyl-D-glucose	Carbosynth Ltd., Compton, England	MM159606	170320
4-Deoxy-D-glucose	Carbosynth Ltd., Compton, England	MD06660	MD066601501
4-O-Methyl-D-glucose	Carbosynth Ltd., Compton, England	MM153283	MM1532831701
6-Deoxy-D-glucose	Carbosynth Ltd., Compton, England	MD04994	MD049940701
6-Deoxy-L-talose	Carbosynth Ltd., Compton, England	MD44533	MD445331501
6-O-Methyl-D-glucose	Carbosynth Ltd., Compton, England	MM153284	MM1532841701
D-(-)-Ribose	Sigma-Aldrich, Deisenhofen, Germany	R7500	078K0668

D-(+)-Cellobiose (Glc β-(1-4) Glc)	Honeywell Fluka, Charlotte, USA	22150	1428928
D-(+)-Galactosamine	Carl-Roth GmbH & Co. KG, Karlsruhe Germany	7411.1	51167784
D-(+)-Galactose	Serva Electrophoresis GmbH, Heidelberg	22020	81143
D-(+)-Galacturonic acid	Sigma-Aldrich, Deisenhofen, Germany	48280	1350875
D-(+)-Gentiobiose (Glc β-(1-6) Glc)	Carl-Roth GmbH & Co. KG, Karlsruhe Germany	4123.2	150156002
D-(+)-Glucosamine	Merck KGaA, Darmstadt, Germany	346299	D00081856
D-(+)-Glucose monohydrate	Carl-Roth GmbH & Co. KG, Karlsruhe Germany	6887.5	87767633
D-(+)-Glucuronic acid	Molekula GmbH, Munich, Germany	M24989192	52529
D-(+)-Isomaltose (Glc α-(1-6) Glc)	Carbosynth Ltd., Compton, England	MI04560	MI045601201
D-(+)-Lactose monohydrate (Gal β-(1-4) Glc)	Carl-Roth GmbH & Co. KG, Karlsruhe Germany	6868.1	429108510
D-(+)-Maltose monohydrate (Glc α-(1-4) Glc)	Carl-Roth GmbH & Co. KG, Karlsruhe Germany	8951	61167504
D-(+)-Mannose	Serva Electrophoresis GmbH, Heidelberg	28460	90079
D-(+)-Xylose	Alfa Aesar GmbH + Co. KG, Karlsruhe, Germany	95731	1342345
L-(-)-Fucose	Carl-Roth GmbH & Co. KG, Karlsruhe Germany	KK10.2	391174839
L-(+)-Arabinose	Carl-Roth GmbH & Co. KG, Karlsruhe Germany	5118.1	32898814
L-(+)-Rhamnose monohydrate	Honeywell Fluka, Charlotte, USA	83650	BCBC6943
L-Iduronic acid	Carbosynth Ltd., Compton, England	MI08102	MI081021201
L-Mannuronic acid	Carbosynth Ltd., Compton, England	MM00711	
N-Acetyl-D-(+)-glucosamine	Carl-Roth GmbH & Co. KG, Karlsruhe Germany	8993	490162510
N-Acetyl-D-galactosamine	Sigma-Aldrich, Deisenhofen, Germany	A2795	BCBC7483V

2.1.10. Media and Buffer

All growth media were sterilized by autoclaving at 121 °C for 20 min. To prevent maillard reactions, sugars and other media compounds were sterilized separately. Temperature instable or labile compounds and trace element solution were filter-sterilized and added after temperature treatment. To prepare agar plates, 1.5 % (w/v) agar was added to liquid media prior to autoclaving.

LB medium

10 g/L tryptone, 5 g/L yeast extract, 10 g/L sodium chloride.

YPD medium

10 g/L yeast extract, 20 g/L peptone, 20 g/L dextrose. To make 100 mL YPD: 50 mL 2X YP, 4 mL 50 % (w/v) dextrose, and filled up with sterile water.

Medium 1 (Nutrient rich, NR)

5 g/L peptone and 3 g/L meat extract.

Buffered complex medium

Buffered complex medium was either prepared with glycerol (BMGY) or glucose (BMGlc). Clarifying nomenclature, the abbreviation is often followed by the respective concentrations of the C source. The buffered complex medium was prepared for shake flask with 10 g/L yeast extract, 20 g/L peptone, 13.4 g/L yeast nitrogen base, 4 x 10^{-4} g/L biotin, and dextrose or glycerol from stock solutions (**Table 10**). The pre-culture (from stock solutions) and the medium for the DASGIP fermentations were prepared as described in **Table 11** and **Table 12**.

Table 11: Stock solutions for buffered complex medium preparation.

Solution	Composition
2x YP	20 g/L yeast extract, 40 g/L peptone dissolved in water
10x YNB	13.4 % (w/v) yeast nitrogen base with ammonium sulfate without amino acids 100 g/L ammonium sulfate, 34 g/L yeast nitrogen base The solution was heated to dissolve completely in water, filter sterilized (0.2 µm filter) and stored at 4 °C.
500x B	0.02 % (w/v) biotin The solution was filter sterilized (0.2 µm filter) and stored at 4 °C.
50% (w/v) Dextrose/Glycerol	500 g/L D-glucose or glycerol dissolved in water

Table 12: *P. pastoris* DASGIP fermentation pre-culture medium preparation.

Stock	Final conc.	For 250 mL
2xYP	1 % (w/v) yeast extract 2 % (w/v) peptone	125 mL
10x YNB	1.34 % (w/v) YNB	25 mL
500x B	4 x 10^{-5} % (w/v) biotin	0.5 mL
50x Glycerol	1 % (w/v) glycerol	5 mL
ddH_2O	-	94.5 mL

Table 13: *P. pastoris* DASGIP fermentation BMGY medium preparation.

Component	Final conc.	For 4x 450 mL
Pepton	2 % (w/v) peptone	40 g
Yeast extract	1 % (w/v) yeast extract	20 g
Glycerol	4 % (w/v) glycerol	80 g
ddH_2O	-	fill to 1816.4 mL
10x YNB	1.34 % (w/v) YNB	45 mL to each vessel
500x B	4 x 10^{-5} % (w/v) biotin	0.9 mL to each vessel

Pichia trace salt solution

The *Pichia* trace salt solution (PTM) was composed of 8.0 mg/L $CuSO_4 \cdot 5H_2O$, 1.2 mg/L KI, 28.0 mg/L $MnSO_4 \cdot H_2O$, 5.2 mg/L $Na_2MoO_4 \cdot 2H_2O$, 8.0 mg/L H_3BO_3, 44.0 mg/L $ZnSO_4 \cdot 7H_2O$, 75.0 mg/L $FeCl_3 \cdot 6H_2O$, 8.0 mg/L $CoCl_2 \cdot 6H_2O$ and 1.74 mg/L biotin. 1 L stock solution was prepared as stock of which 50 mL were sterile filtered (0.2 µm) when needed.

D'Anjou medium

The D'Anjou medium was composed of 20.0 g/L $(NH_4)_2SO_4$, 12 g/L KH_2PO_4, 0.36 g/L $CaCl_2 \cdot 2H_2O$, 4.7 g/L $MgSO_4 \cdot 7H_2O$, and 40 g/L glycerol. 2 mL sterile PTM solution was added after autoclaving.

Minimal salt medium

The MSM medium was composed of 18.84 g/L $(NH_4)_2SO_4$, 5.62 g/L KH_2PO_4, 0.11 g/L $CaCl_2 \cdot 2H_2O$, 1.18 g/L $MgSO_4 \cdot 7H_2O$, and 40 g/L glycerol. 2 mL sterile PTM solution was added after autoclaving.

Ammonium-acetate buffer pH 5.6

572 µL acetic acid (MS-grade) was added in 1,900 mL ddH_2O in a 2 L volumetric flask. Then the pH was adjusted to 5.6 with ammonia solution (three drops of 32 % (v/v) solution and then with 3.2 % (v/v) solution) and filled up. Finally, the buffer was filtered with a 0.2 µm regenerated cellulose filter membrane. The buffer is only stable for one week.

Eluent A

1,700 mL ammonium-acetate buffer (pH 5.6) was added to 300 mL acetonitrile. The eluent is only stable for two weeks.

3. Methods

The methods were taken from the standard operating procedures of the Chair of Chemistry of Biogenic Resources (TUM Campus Straubing).

3.1. Microbiological methods

3.1.1. Cryo-conservation

Cryo-cultures were prepared by mixing 250 µL liquid culture with a sterile 50 % (v/v) glycerol solution to a final glycerol concentration of 25 % (v/v) and stored at -80 °C.

3.1.2. Strain cultivation

Microbial suspensions cryo-tubes were thawed in hand. Then, an inoculation loop was used to spread them on corresponding agar plates following the T-streak method and incubated over night at 37 °C for bacteria and over two nights at 30 °C for yeast, followed by 48 h at 4 °C. Liquid cultures were inoculated with single colonies from the incubated agar plates.

3.1.3. Organism growth tests

E. coli, *C. necator*, *S. cerevisiae*, *P. pastoris*, and *Y. lipolytica* were screened for growth in different hydrolysate concentrations diluted with water or in complex medium as similarly done by Ong et al.[28]. Briefly, 5 mL pre-cultures of NR medium for bacteria or YPD medium for yeast were cultivated for 48 h, transferring 10 % into a fresh tube twice. 2 µL of exponentially growing culture was inoculated in 96-well microtiter plates containing 198 µL of supplemented medium or hydrolysate. The 200 µL cultures were grown in each of the following supplemented hydrolysates: 2 % Glc and 0.9 % NaCl in 5 % - 90 % hydrolysate corrected for growth in only water or in YPD/NR with 2 % Glc and 0.9 % NaCl in up to 75 % hydrolysate. The MTP plates were shaken for one min with 900 rpm then incubated at 30 °C for 24 h and read every 15 min using a Tecan Infinite M200 multimode plate reader.

3.1.4. Shake flask experiments

P. pastoris cultivation was done in 50 mL unbaffled shake flasks, starting with 10 mL pre-culture of BMGY 0.4 % for 48 h at 30 °C and 150 rpm inoculated from an agar plate. Then 10 mL BMGY/BMGlc or hydrolysate with 2 % glycerol or glucose were inoculated with 1 mL of the pre-culture and again incubated for 48 h at 30 °C and 150 rpm.

3.1.5. Batch and fed-batch fermentations

All fermentations were conducted in 1 L DASGIP bioreactors (Eppendorf, Germany) with initial volume of 500 mL BMGY 4 % or MSM (4 % GY) and at 30 °C. For pulsed batch, 25 mL of 50 % (w/v) glycerol was injected once after 12 h with a syringe into the sample port and flushed once with sterile air. Fed batch fermentations were continuously fed with a total amount of 200 g of 50 % (w/v) glycerol depending on the strategy. The stirrer was equipped with a 6-plate-rushton impeller placed 2.5 cm from the bottom of the shaft stirring with an initial rate of 400 rpm and maximum stirring rates were 1200 rpm. For optimized fermentations, the maximum stirring was reduced to 900 rpm. Batch and pulsed batch fermentations were performed with an aeration of 0.2 – 0.5 vvm. Optimized fed batch fermentations were performed with 0.5 – 1.2 vvm. Agitation and aeration were automatically adjusted to maintain the level of dissolved oxygen over 30 %. The pH was maintained at 5.0 and automatically adjusted with 20 % (v/v) NH_4OH (directly into the broth) or with 7 % (v/v) H_2SO_4 as required. Foam control was done using 1 % (v/v) antifoam B (Merk, Germany). For monitoring process parameters, the reactors were equipped with probes for pH and dissolved oxygen. 3 mL samples were drawn every 3 – 5 h. Cell growth was determined as OD_{600}; cell dry weight was determined by centrifuging 1 mL cell culture broth at 500 x g for 10 min and drying the cell pellet over night at 105 °C. The supernatant was analyzed for glycerol by HPLC-RID after 1:10 dilution in 2.5 mM H_2SO_4 and filtration (0.2 µm, PVDF) and later for phytase activity as well. The OD, DCW, and phytase activity values in the fed batch fermentations were normalized to the starting volumes.

Scripts

Antifoam script:

```
p.FCSP = 0
if p.LvlPV >50
   p.FCSP = 30
   end if
```

Exponential feed script using $\mu_{max} = 0.3$

```
p.FDSP = 0
if p.VDPV < 200 and p.DOPV > 30
  p.FDSP = 0.0456*EXP(0.3*p.InoculationTime_H)
  else p.FDSP = 0
   end if
```

Feeding strategies & process evaluation

In order to evaluate the fermentations, a feeding strategy was developed along with an exponential feed and several key parameters for growth and product kinetics were calculated. The substrate utilization rate q_S was calculated using Eq. (1).

$$q_S = \frac{(s_n - s_{n\_1})}{(x_n - x_{n\_1}) * (t_n - t_{n\_1})} \tag{1}$$

where *s* is substrate concentration, *x* is biomass concentration and *t* fermentation time. The specific growth rate *μ (t)* was calculated using Eq. (2) and the activity formation rate $q_{A/x}$ was calculated using Eq. (3).

$$\mu\ (t) = \frac{\ln(x) - \ln(x_o)}{(t - t_o)} \tag{2}$$

$$q_{A/x} = \frac{(A_n - A_{n\_1})}{(x_n - x_{n\_1}) * (t_n - t_{n\_1})} \tag{3}$$

where *A* is the activity in Units per mL. Further, the specific productivity as relationship between product formation and specific growth rate $q_A(\mu)$ was calculated using Eq. (4).

$$q_A\ (\mu) = \mu\ *\ q_{A/x} \tag{4}$$

Two substrate feeding strategies, standard exponential feed and DO-*stat* feed were carried out in fed-batch fermentation. 200 g of glycerol as carbon source was additionally added for all fermentations. For the exponential feed, the medium feed profiles were calculated according to Eq. (5).

$$F\ (t) = F_o * e^{\mu * t} \tag{5}$$

where F_o is the initial feed rate, which can be calculated using Eq. (6).

$$F_o = \left(\frac{\mu}{Y_{x/s,,max}} + m_s\right) * \frac{V_o * x_o}{W_{in}} \tag{6}$$

where $Y_{x/s,max}$ is the maximum yield (biomass/substrate), m_s is the specific maintenance rate, V_o is the initial working volume, and w_{in} is the mass fraction of substrate in the feed solution. Finally, the space-time yield (*STY)* was calculated using Eq. (7).

$$STY = \frac{A_n}{t_n} \tag{7}$$

3.2. Biomass processing methods

3.2.1. Sequential extraction & mass balance

10 g of biomass were weighed into 500 mL centrifugation buckets. 200 mL of 50 mM sodium phosphate buffer pH 7.0 was added. The samples were mixed and disrupted for 15 min in a sonication water bath with ice and then mixed again. Then, the samples were centrifuged for 20 min at 10,000 x g at 4 °C. The supernatant was collected in a Schott bottle and the residual biomass was dried. Next, 200 mL of methanol were added to the residual biomass. The residual biomass was sonicated again in the water bath for 20 min and again centrifuged for 20 min at 15,000 x g at 4 °C. The supernatant was again collected in a Schott bottle and the residual biomass was dried again. The double extracted residual biomass was used for enzymatic treatment. After enzymatic hydrolysis, the residual biomass was dried again. Residual biomasses were dried over night at 65 °C in the oven and the mass determined gravimetrically. The methanol extract was dried with a vacuum evaporator and the residual mass also determined gravimetrically. The sequential extractions of 10 g biomass were done in triplicates. The hydrolysate was produced from pooled residue and masses extrapolated to the 10 g starting material.

3.2.2. Hydrolysate production

Hydrolysate production for fermentations with *P. pastoris* was done in shake flasks. 5 % (w/v) of dry crude biomass or dry extracted biomass was suspended in 50 mM citrate buffer pH 4.5. The biomass slurry was pre-treated at 80 °C for one hour in the oven. After cooling down, 0.05 % (v/v) DISTILLASE® CS and Viscozyme® L were added for saccharification for 24 h at 50 °C shaking at 150 rpm. After allowing to cool again, 0.05 % (v/v) FERMGEN™ was added for solubilization over another 36 h at 30 °C shaking at 150 rpm. Subsequently, the treatment was ended by heating at 90 °C for 30 min in a pre-heated oven. The biomass slurry was then centrifuged with 15,000 x g for 20 min at RT. The supernatant was sterile filtered (0.2 µm) into a sterile flask and kept at 4 °C until further use.

3.3. Analytical methods

The employed analytical methods for biomass composition were laboratory analytical procedures (LAPs), standard algal biomass analytical methods provided by the National Renewable Energy Laboratory (NREL).

3.3.1. Biomass pre-treatment

Prior to running any procedures, the biomass of the investigated strains was milled in a ball mill (MM 400, Retsch GmbH, Haan) for 1 min at a frequency of 30 Hz using a zirconium oxide coated 35 mL jar and a single bead.

3.3.2. Total solids & ash

For the determination of total solids and ash content in the biomass, the NREL LAP was followed. Crucibles were pre-conditioned at 575 °C to remove contaminates, before they were weighed out and 100 mg of biomass was weighed into the pre-weighed crucibles. The samples were then placed into a vacuum oven (Binder, VDL 53) at 40 °C and dried under vacuum overnight. After cooling to room temperature in a desiccator, samples were weighed again. The crucibles were then placed back in the desiccator.

The same samples that were used for total solids determination were used for ash determination. The biomass samples were ashed in a muffle furnace (Linn High Term GmbH, LM-312.27) with controller (Gefran, 880P) running the following ramping program: RT to 105, hold at 105 for 5 min. 150 to 250 at 10°C min^{-1}. Hold 250 for 30 min. Ramp to 575 at 20°C min^{-1}. Hold for 180 min. Drop to 105 till sample removal. Samples allowed to cool to RT in desiccator prior weighing.

3.3.3. Total starch content

Starch content in the biomass was determined using the Megazyme Total Starch Assay AOAC Official Method 996.11. In brief, 100 mg of biomass (based on starch content to be close to control), as well as 10 mg of starch as control was weighed into 15 mL falcon tubes. 200 µL of an aq. 80 % (v/v) ethanol solution was added to each sample. Immediately, 3.0 mL of thermostable α-amylase (100 U/mL in 100 mM sodium acetate buffer with 5 mM CaCl, pH 5.0) was added and mixed. The samples were then incubated in a boiling water bath (100 °C) on a hot plate for 12 min. Every 4 min, the samples were taken out and vortexed. After cooling to around 50 °C, 100 µL of amyloglycosidase (200 U/mL) was added to each sample. The tubes were vortexed and incubated at 50 °C for 30 min. Then, the volume was adjusted to 10.0 mL with deionized water, followed by centrifugation with 3,000 *x g* for 10 min at RT. 100 µL aliquots of

the supernatant was transferred into 15 mL glass tubes. 3.0 mL of 20:1 in deionized water diluted GOPOD reagent (*p*-hydroxybenzoic acid and sodium azide 0.095% w/v, pH 7.4) containing glucose oxidase and 4-aminoantipyrine was added. The samples were then again incubated for color formation at 50 °C in a water bath for 20 min. Lastly, 200 µL of each sample was transferred into a microtiter plate and the absorbance was read at 510 nm. The starch content in percent of biomass was calculated based on the absorbance of the glucose standard and corrected for hydration.

$$Starch, \% = \Delta A * F * FV * \frac{FV}{0.1} * \frac{1}{1000} * \frac{100}{W} * \frac{162}{180} \quad (8)$$

ΔA = absorbance (reaction) read against the reagent blank 20:1 diluted GOPOD reagent.

F = $\frac{100\ (\mu g\ of\ D-glucose)}{absorbance\ for\ 100\ \mu g\ of\ glucose}$ (conversion from absorbance to µg)

FV = final volume (10 mL)

0.1 = volume of sample analyzed

$\frac{1}{1000}$ = conversion from µg to mg

$\frac{100}{W}$ = factor to express starch as percentage of biomass

W = weight of biomass (mg)

$\frac{162}{180}$ = adjustment from free glucose to anhydro glucose in starch

3.3.4. Protein Content

Protein content of cyanobacterial biomass was determined based on a conversion factor from elemental nitrogen to protein. The freeze-dried biomass was analyzed by elementary analysis (Euro EA 3000, EuroVector) for its nitrogen content. 1-3 mg of biomass was loaded into tin containers for carbon, nitrogen, sulfur, and hydrogen determination. The crude protein content was determined by a nitrogen-to-protein conversion factor of 4.78.

A modified Bradford assay based on Coomassie Brilliant Blue-G250 was used to measure the protein concentration of fermentation broth samples. Standard calibration was performed with 20 – 100 µg/mL bovine serum albumin. 50 µL standard or sample (n = 3) was mixed with 200 µL color reagent (5+2) in each well of a 96-well plate. The absorbance at 595 nm was measured after 15 min incubation at room temperature.

3.3.5. Total lipids as FAMEs

Lipids were determined as fatty acid methyl esters (FAMEs) and GC-MS slightly modified to as described by the NREL LAP. In short, 10 mg of dry biomass was weighed into pre-weighed 1.5 mL crimp cap glass vials. 25 µL of dodecane as internal standard, 200 µL of chloroform:methanol (2:1 v/v), and 300 µL 0.6 M HCl:methanol was added and the vials were quickly closed. All solutions were kept on ice. The vials were then placed on an 85 °C pre-heated metal heating block (StarFish, Heidolph Inst.). After one hour, the vials were removed and allowed to cool to room temperature. Then, the vials were briefly opened, and 1 mL of hexane was added to each vial and quickly closed again. After mixing well, the phases were allowed to separate for two hours. 200 µL of the upper phase were then transferred into pre-labeled GC micro vials and placed in the autosampler. A FAME standard dilution serious was prepared from a 1 mg/mL even carbon FAME standard (49454-U, Sigma) in GC micro vials with internal standard by adding 100 µL standard dilution and 100 µL of the internal standard solution. The GC-MS was carried out using a Rxi®-5Sil-MS column (30 m by 0.53 mm, 20 µm film, Restek) on a TRACE™ GC Ultra gas chromatograph (Thermo Scientific) with a Quadrupole detector. 1 µL of the sample was injected with a split 1:20 and separated on the column (inlet and detector 250°C, 50°C/hold 3 min, 45°C min $^{-1}$ to 220 °C/hold 2 min, 45 °C min^{-1} to 280 °C/hold 2 min, 60 °C min^{-1} to 330 °C/hold 1.5 min). The transfer line and ion source were 250 °C and MS start time was 4.0 min.

Table 14: Oven ramp for analyte separation.

Ramp	°C / min	$Temp._{Final}$ °C)	$Time_{Hold}$ (min)
Start	-	50 °C	3.5 min
1	45 °C	220 °C	2 min
2	45 °C	280 °C	2 min
3	60 °C	330 °C	1.5 min

Table 15: MS operational parameters for the analysis of FAMEs.

Parameter	Setting
Scan mode	TIC (5 scans/s)
Scan start	50 *m/z*
Scan stop	650 m/z
Injector temp.	250 °C (PTV)
Injection vol.	1 µL
Liner	Skyliner
Split	1:20
Transfer line temp.	250 °C
Ion source temp.	250 °C
Ionization energy	70 eV
Start time	4 min

3.3.6. HT-PMP-method

Chemical hydrolysis

Total carbohydrates and monosaccharide profiles were determined by the HT-PMP method for carbohydrate analysis by UHPLC-UV-ESI-MS/MS applied to algal biomass. The analytical chemical hydrolysis was performed by adding 6 mL of 2 M TFA to 12 mg of biomass in 25 mL glass tubes. The tubes were incubated in a heating block (VLM GmbH, EC-Model) for 90 min - 120 min at 121 °C. The hydrolysis was stopped by transferring the samples to ice and adjusting the pH to 8 by adding an aqueous solution of 3.2 % (v/v) NH_4OH. The dilution factor was determined prior in 1.5 mL reaction tubes using the indicator phenol red.

Enzymatic hydrolysis

Enzymatic saccharification screening was performed by weighing in 25 mg of biomass in 1.5 mL Eppendorf tubes. 50 mM ammonium acetate buffer pH 4.5 with 0.02 % (w/v) sodium azide was added to the samples. Enzymes were added from 0.025 % (v/v) - 0.5 % (v/v) for determination of enzyme suitability to a total of 1.0 mL reaction volume. The tubes were incubated in a heating block for 24 h at 50 °C shaking 300 rpm. The hydrolysis was stopped by incubating at 95 °C for 10 min. After allowing the samples to cool down, they were centrifuged for 10 min with 21,000 x g at room temperature (RT). The supernatants were then collected in fresh tubes and the saccharide concentration was brought into calibration range by diluting with a matrix solution of 0.8 M TFA and subsequently adjusting the pH to 8 with 3.2 % (v/v) NH_4OH for derivatization.

Enzymatic solubilization of cyanobacterial biomass was performed by proteolytic hydrolysis with FERMGEN™. For the screening, 50 mM citrate buffer pH 4.5 with 0.02 % (w/v) sodium azide was added to 25 mg of biomass in pre-weighed 1.5 mL reaction tubes. Different enzyme concentrations 0.025 % (v/v) – 0.5 % (v/v) were added to a total of 1.0 mL reaction volume. The tubes were incubated at 30 °C for varying times with mixing at 150 rpm. After the hydrolysis, the samples were centrifuged for 10 min with 21,000 x g at RT. The supernatants were collected in fresh tubes, and the pellets were dried in an oven at 105°C overnight. The dry weights of the residual biomass were determined gravimetrically and the solubilisation by subtracting the residual dry weight from the starting material.

HT-PMP-derivatization

75 µL of derivatization reagent (0.1 M methanolic-PMP-solution: 0.4 % ammonium hydroxide solution 2:1) were added to 25 µL of sample in a 96-well-PCR-plate. The plate was sealed with a TPE cap mat, mixed well, and centrifuged at 2,000 × g for 2 min at 20 °C. After incubation (100 min at 70 °C) in a PCR-cycler and a following automated cool down to 20 °C, an aliquot of 20 µL was transferred to a fresh 96-well MTP and mixed with 130 µL of 19.23 mM acetic acid. The samples were then transferred into a 96-well filter plate and centrifuged at 2,500 × g for 5 min at 20 °C. Finally, the plate was sealed with a 96-well silicon cap mat.

For additional saccharides eluting prior to the regular cut-off of the MS at 3 min run time as described in the next section, PMP was extracted from samples before HPLC-MS analysis. For these samples, the derivatization was done in 1.5 mL Eppendorf tubes in a water bath (100 min at 70 °C). After the derivatization, 650 µL of 19.23 mM acetic acid was added. After mixing the diluted samples, excess PMP was extracted with 500 µL of chloroform (three times). The samples were then filtered through a syringe filter (0.2 µm cellulose) into 1.5 mL glass vials and capped for analysis.

HPLC analysis of monosaccharide-PMP-derivatives

The HPLC system was composed of a degasser, a pump module, an autosampler, a column compartment, a diode array detector, and an ESI-ion-trap unit. The column (Gravity C18, 100 mm length, 2 mm i.d.; 1.8 µm particle size; Macherey-Nagel) was tempered to 50 °C. Mobile phase A consisted of 5 mM ammonium acetate buffer (pH 5.6) with 15 % acetonitrile and a chromatographic flow rate of 0.6 mL/min. The gradient (mobile phase B containing pure acetonitrile) was programmed as following: start of mobile phase B at 1 %, with increase to 5 % over 5 min, hold for 2 min, with following increase to 18 % over 1 min. The gradient was further increased to 40 % over 0.3 min, hold for 2 min and returned within 0.2 min to starting conditions for 1.5 min. The first 3 min of chromatographic flow were refused by a switch valve behind the UV-detector (245 nm). Before entering ESI-MS the flow was splitted 1:20 (Accurate-Post-Column-Splitter, Dionex). Temperature of the autosampler was set to 20 °C and an injection volume of 10 µL was used.

Table 16: HPLC-MS gradient for separation of PMP sugar derivates by using a gradient of mobile phase A (85 % 5 mM ammonium acetate, pH 5.6 with 15 % acetonitrile) and mobile phase B (pure acetonitrile). Changes between points are linear.

Time [min]	Eluent A [%]	Eluent B [%]
0	99	1
5	95	5
7	95	5
8	82	18
8,3	60	40
10,3	60	40
10,5	99	1
12	99	1

ESI-ion-trap parameter

The ion-trap was operated in the ultra-scan mode (26,000 m/z s^{-1}) from 50 to 1,000 *m/z*. The ICC target was set to 200,000 with a maximum accumulation time of 50 ms and four averages. The ion source parameters were set as following: capillary voltage 4 kV, dry temperature 325 °C, nebulizer pressure 40 psi and dry gas flow 6 L/min. Auto-MS-mode with the smart target mass of 600 m/z and a MS/MS fragmentation amplitude of 0.5 V was used. The quantification was performed by using the extracted ion chromatograms (EIC) of the *m/z* value corresponding to the protonated molecules.

Table 17: ESI-MS operational parameters for the HT-PMP method.

Parameter	Setting
Scan mode	ultra (26000 m/z s^{-1})
Scan start	50 *m/z*
Scan stop	1000 m/z
ICC target	200000
ICC max. accumulation time	50 ms
ICC number of averages	4
Ion source capillary voltage	4 kV
Ion source dry temperature	325 °C
Ion source nebulizer pressure	2.76 bar
Ion source dry gas flow	6 L/min
MS mode	Auto
Auto MS smart target	600 *m/z*
MS/MS fragmentation amplitude	0.5 V

3.3.7. Pigments and phycobiliproteins

Pigments and phycobiliproteins were quantified as described by Meixner *et al*[28]. 20 mg of biomass was weighed into 15 mL falcon tubes. For the extraction of chlorophyll a and carotenoids, 5 mL of 90 % (v/v) acetone and for phycobiliproteins 5 mL of 50 mM sodium acetate was added. The samples were vortexed and subsequently incubated for 24 h extraction at 4 °C in the dark. The samples were vortexed several times in between. After extraction, solids were separated by centrifugation for 10 min with 2,000 *x g* at room temperature. 200 µL of the supernatants were then transferred into a quartz microtiter plate in triplicates for absorbance measurements. λ = 647 nm and λ = 664nm (chlorophylls), λ = 480 nm (carotenoids), λ = 615 nm (c-phycocyanin), λ = 652 nm (allophycocyanin), λ = 562 nm (phycoerythrin). Subsequently, pigment concentrations were calculated based on the equations provided in the supporting information (annex 3) and reported as milligrams per gram biomass.

Calculation of the chlorophyll$_a$ concentration using absorption values of λ = 647 nm and λ = 664 nm

$$\text{chlorophyll}_a\ [\mu g/ml] = -1.79 * A_{647} + 11.87 * A_{664} \quad (9)$$

Calculation of the chlorophyll$_b$ concentration using absorption values of λ = 647 nm and λ = 664 nm

$$\text{chlorophyll}_b\ [\mu g/ml] = 18.98 * A_{647} - 4.90 * A_{664} \quad (10)$$

Calculation of the total carotenoid concentration using absorption values of λ = 480 nm

$$\text{total tarotenoids}\ [\mu g/ml] = 4 * A_{480} \quad (11)$$

Calculation of the C-phycocyanin concentration using absorption values of λ = 615 nm, λ = 652 nm & λ = 730 nm

$$\text{c – phycocyanin (PC)}\ [\mu g/ml] = \frac{A_{615} - A_{730} - 0.474 * (A_{652} - A_{730})}{5.34} \quad (12)$$

Calculation of the allophycocyanin concentration using absorption values of λ = 615 nm, λ = 652 nm & λ = 730 nm

$$\text{allophycocyanin (APC)}\ [\mu g/ml] = \frac{A_{652} - A_{730} - 0.2087 * (A_{615} - A_{730})}{5.09} \quad (13)$$

Calculation of the phycoerythrin concentration using absorption values of λ = 562 nm & λ = 730 nm

$$\text{phycoerythrin (PE)}\ [\mu g/ml] = \frac{A_{562} - A_{730} - (2.41 * PC) - (0.849 * APC)}{9{,}62} \quad (14)$$

Calculation of total phycobiliproteins

$$\text{total phycobiliproteins} = PC + PE + APC \quad (15)$$

3.3.8. Glucose assay

50 µL of sample or standard solution were placed in a 96-well plate. Reaction was started by adding 50 µL of assay mixture (40 mM potassium phosphate buffer (pH 6.0), 1.5 mM ABTS, 0.4 U glucose oxidase and 0.02 U horseradish peroxidase). The plate was sealed with a 96-well silicon cap mat. After incubation on a microplate shaker at 400 rpm for 30 min at 30 °C the resulting extinction was measured at 418 nm. The absorption at 480 nm was subtracted to eliminate background signals in the UV. The calibration curve was compiled with eight points in the range of 2.5 to 500 µM (n = 3) of glucose.

Reaction Scheme

D-Glucose oxidase catalyzes the oxidation of D-glucose using molecular oxygen to D-(+)-glucono-1,5-lactone, and hydrogen peroxide (reaction 1). Then, the oxidation of reduced ABTS with hydrogen peroxide to reduced ABTS and water is catalyzed by horseradish peroxidase (reaction 2). Oxidized ABTS can be determined photometrically at 418 nm.

$$2\ \text{D-glucose} + O_2 \rightarrow 2\ \text{D-glucono-1,5-lactone} + 2\ H_2O_2 \quad (16)$$

$$H_2O_2 + 2\ ABTS_{red.} \rightarrow 2\ H_2O + 2\ ABTS_{ox.} \quad (17)$$

3.3.9. Glycerol

Glycerol from culture supernatants was quantified using ion exclusion chromatography (IEC). Samples were diluted 1:10 with 2.5 mM sulfuric acid and filtered through 0.2 µm PVDF filters. The HPLC system (Dionex Corp., USA) was coupled with a refractive index detector (RI 101, Shodex, Tokyo, Japan) and equipped with an Rezex ion exclusion column (Rezex ROA-Organic Acid H+ (8%); 300 x 7.8 mm; Phenomenex Deutschland Ltd.). The column oven temperature was set to 70 °C, and 2.5 mM sulfuric acid was used for isocratic elution at a flow rate of 0.5 mL/min.

3.3.10. Gel electrophoresis

Sodium dodecyl sulfate–polyacrylamide gel electrophoresis (SDS-PAGE) was performed for protein separation as described by Ausubel et al. [21] with modifications. To prepare polyacrylamide gels, the Mini/PROTEAN® Tetra Cell Casting Stand and Clamps (Bio-Rad Laboratories GmbH, München, Germany) were used. For 2 gels, a separating gel was prepared according, the solution was swirled gently, immediately used to load the chambers and covered with water. After polymerization, the water layer was removed, the stacking gel layer added, and the desired comb inserted. After polymerization (RT, 60 min), the gels were stored wrapped in wet paper towels until use at 4 °C. To analyze a protein sample, it was mixed with 5X loading buffer (50 % (v/v) glycerol, 12.5 % (v/v) β-mercaptoethanol, 7.5 % (w/v) SDS, 0.25 g/l bromphenol blue) and heated (95 °C, 10 min). The sample was loaded to the SDS-PAGE, 1X SDS electrophoresis buffer (0.1 % (w/v) SDS, 25 mM Tris, 192 mM glycine) was added to the Mini-PROTEAN® Tetra Vertical Electrophoresis Cell and the gel was run for about 45 min with 40 mA for each gel. Protein size was determined using the PageRuler Prestained Protein Ladder (#26616, Thermo Fisher Scientific, Waltham, MA, USA). After the electrophoretic run, the gel was washed with water, stained using a coomassie-staining solution (0.2 % (w/v) coomassie brilliant blue G250 and R250, 50 % (v/v) ethanol, 10 % (v/v) acetic acid, filtered and stored protected from light) and discolored using water.

Table 18: Preparation of SDS-PAGE gels.

Solution	Separating gel	Stacking gel	Composition
Acrylamide (Conc.)	4 mL	0.83 mL	30 % (v/v) acrylamide / 0.8 % (v/v) bisacrylamide
ddH_2O	3.29 mL	2.77 mL	
Separating gel buffer 4x	2.5 mL	-	0.8 % (w/v) SDS, 1.5 M Tris/HCl, pH 8.8 using HCl
Stacking gel buffer 4x	-	1.25 mL	0.8 % (w/v) SDS, 0.5 M Tris/HCl, pH 6.8 using HCl
APS	100 µL	50 µL	10 % (w/v) ammonium persulfate
TEMED	10 µL	5 µL	N,N,N′,N′-Tetramethylethylendiamine

3.3.11. Phytase activity assay

The phytase activity in the *P. pastoris* culture supernatants was determined by assessing the free phosphate released from phytate using ammonium molybdate as the coloring agent to perform colorimetric quantification as per the protocol of Bae *et al* and adapted for 96-well-plate applications[39]. 100 µL of supernatant was subjected to gel-filtration chromatography to purify the secreted protein from smaller molecules such as free phosphate. 96-Well SpinColumns (Harvard Apparatus, Holliston, MA USA) were used as described by the manufacturer. 13.5 µL of filtrate was diluted using water and transferred into a 96-well assay plate. 53.5 µL freshly prepared 1.5 M phytate substrate in 0.1 M sodium acetate solution was added to each well and the plate was incubated (37 °C, 30 min). To terminate the reaction, 66.6 µL 5 % (w/v) TCA solution as well as

66.6 µL coloring solution were added and absorbance was measured at 700 nm. Coloring solution was freshly prepared before use by mixing four volumes of 1.5 % (w/v) ammonium molybdate in 5.5 % (v/v) sulfuric acid with one volume of 2.7 % (w/v) ferrous sulphate solution. One phytase unit was defined as the amount of enzyme that releases 1 micromole of inorganic phosphate per minute. In order to determine phytase units, samples had to be within a 0.8 - 5 mM calibration curve potassium phosphate.

3.3.12. Optical Density

Optical density (OD) of cell suspensions were measured with a photometer (Ultraspec 10, Amersham Bioscience) in plastic cuvettes at 600 nm (volume 1 mL). The corresponding media were used for blank measurements. Samples with values higher than OD_{600} = 0.7 were diluted to minimize the measurement error.

3.3.13. Dry cell weight

For the determination of dry cell weight (DCW), 1 mL of the culture supernatant was added to pre-weighed Eppendorf tubes and centrifuged for 10 min at 500 x g and RT. The supernatant was collected in fresh tubes and the cell pellets were dried until constant mass at 105 °C over night.

4. Results

4.1. Towards a cyanobacterial biorefinery: Carbohydrate fingerprint, biocomposition and enzymatic hydrolysis of *Nostoc* biomass

Authors: Korbinian Sinzinger, Doris Schieder, Broder Rühmann, and Volker Sieber

This study explores the potential of *Nostoc* strains as biorefinery feedstock through a detailed analysis of their carbohydrate profiles, biochemical composition, and enzymatic hydrolysis efficiency. The saccharide profiles of seven *Nostoc* strains using the high-throughput pre-column derivatization method with 1-phenyl-3-methyl-5-pyrazolone (HT-PMP) were characterized. The analysis revealed the presence of various monosaccharides, including rare sugars, and indicated complex heteroglycan structures. Specifically, *Nostoc* sp. De1, *Nostoc* sp. Cc3, and *Nostoc* muscorum I were analyzed for their complete biochemical composition. *Nostoc* sp. De1, for instance, contained 4.8 % moisture, 6.7 % ash, 1.4 % starch, 2.7 % lipids, and 48.6 % protein. Enzymatic hydrolysis was conducted using several industrial enzymes (OPTIMASH™ BG, DISTILLASE® CS, and FERMGEN™). Saccharification yields were assessed after 24 hours at 50°C, showing that *Nostoc* muscorum I had the highest yield at 0.38 g/g biomass. The saccharide yields per biomass after 24 and 48 h of hydrolysis at 60 °C, following an 8 h protease pre-treatment at 30 °C, were also measured. For instance, after 48 h, the saccharification yield of *Nostoc* sp. De1 increased to 35 mg/g biomass. The study highlighted significant variability in enzyme efficiency due to the structural complexity of the heteroglycans. Nonetheless, *Nostoc* sp. De1 exhibited a remarkable solubilization rate, reaching up to 57 % biomass solubilization. This variability suggests the necessity for tailored enzymatic treatments to optimize saccharification yields across different strains. This research demonstrates the potential of *Nostoc* strains for biorefinery applications, despite the challenges posed by their complex carbohydrate structures.

Korbinian Sinzinger designed and conducted all experiments, analyzed the data and wrote the original draft. Doris Schieder contributed to the conceptualization, reviewed, and edited the manuscript. Broder Rühmann contributed to the data analysis and reviewing and editing the manuscript. Volker Sieber contributed to reviewing and editing the manuscript.

The supplemental information for this publication can be found in the appendix, section 6.1.

Towards a cyanobacterial biorefinery: Carbohydrate fingerprint, biocomposition and enzymatic hydrolysis of Nostoc biomass

Korbinian Sinzinger, Doris Schieder, Broder Rühmann Volker Sieber

Algal Research

2022

https://doi.org/10.1016/j.algal.2022.102744

Algal Research 65 (2022) 102744

Contents lists available at ScienceDirect

Algal Research

journal homepage: www.elsevier.com/locate/algal

Towards a cyanobacterial biorefinery: Carbohydrate fingerprint, biocomposition and enzymatic hydrolysis of *Nostoc* biomass

Korbinian Sinzinger [a], Doris Schieder [a,*], Broder Rühmann [a], Volker Sieber [a,b,c]

[a] Chair of Chemistry of Biogenic Resources, Technical University of Munich, Campus for Biotechnology and Sustainability, 94315 Straubing, Germany
[b] Catalysis Research Center, Technical University of Munich, 85748 Garching, Germany
[c] The University of Queensland, School of Chemistry and Molecular Biosciences, 68 Cooper Road, St. Lucia 4072, Australia

ARTICLE INFO

Keywords:
Cyanobacteria
Nostoc
Polysaccharide analysis
UHPLC-UV-ESI-MS/MS
Enzymatic hydrolysis
Biorefinery

ABSTRACT

High investment costs have switched the perspective of cyanobacterial biorefinery concepts from biofuels towards approaches with multiple high-value products including residual biomass utilization. For the purpose of residual biomass utilization, this study investigated the biomass of several *Nostoc* strains. The saccharide profiles of the highly complex heteroglycans in seven *Nostoc* strains was elucidated. Besides neutral sugars, uronic acids, amino sugars, other substituted sugars as well as different methylated sugars and their methylation patterns were identified. Also, the biocomposition of the exemplary strains *Nostoc* sp. De1, *Nostoc* sp. Cc3, and *Nostoc muscorum* I was investigated totaling 77.4%, 91.8%, and 71.4% biomass, respectively. Ash and moisture made up 11–15%, lipids 2–2.7%, starch 1.4–8.4%, structural saccharides 12.6–16.8%, and protein 37.7–49.3%. While overall the detected masses were 28.6%–8.2% short to full recovery, many identified sugars could not be quantified. Further, different industry enzymes were tested on these three *Nostoc* strains for saccharification and solubilization. The highest saccharification results for all three strains were 36 mg g^{-1}, 73 mg g^{-1}, and 75 mg g^{-1} for *Nostoc* sp. De1, *Nostoc* sp. Cc3 and *N. muscorum* I, respectively. The obtained results demonstrate the extremely complex heteroglycans in *Nostoc* biomass as well as the difficulty for industrial utilization of these saccharides. Yet, the achieved biomass solubilization of 57%, 49%, and 56% for *Nostoc* sp. De1, *Nostoc* sp. Cc3, *N. muscorum* I, respectively could still allow for efficient biomass utilization.

1. Introduction

The research of using microalgae and cyanobacteria biomass as a renewable source of energy and fuel is currently trending [1–6]. The interdisciplinary field of multiproduct biorefineries of microalgal biomass is still at the beginning focusing mainly on primary metabolites [7–9]. Many studies have reported the cultivation of algal biomass with a high lipid or starch content to produce biodiesel or fermentable sugars, respectively [10–14]. The transition from fossil fuels to this more renewable option is hindered due to the high initial investment and cultivation costs associated with the use of microalgal biomass [15]. But the range of applications for microalgae is broad, ranging from nutrition, feed, cosmetics, colorants, fine chemicals and even biotechnological and pharmaceutical applications [5]. Concepts for algal biorefineries have thus started to emerge at a higher frequency [7]. Economically feasible biorefinery models from microalgae need to focus on establishing multiple product streams of significant values [8,16–18]. Identifying high-value primary products from microalgae is the first step in developing such biorefinery concepts. Many high-value compounds have already been identified from microalgae and cyanobacteria [9,16,19–21]. Exopolysaccharides, pigments, polyhydroxyalkanoates, phycobiliproteins or secondary metabolites have been suggested as such products [22–24]. So far, applying additional extraction steps or fractionation of the biomass has only resulted in higher costs for downstream processing, totaling up to 50–60% of the whole process [8]. This has made such biorefinery concepts hardly economically feasible [25]. Hence, schemes for complete utilization of this biomass are of utmost importance to increase the number of revenue streams. In order to do so, the complete biocomposition of the biomass needs to be analyzed and the residual biomass further utilized. The increasing political support and environmental awareness among the public aim to dismiss raw oil as an industry feed and protect our ecosphere. With these measures in action, the emphasis for the need of a biomass-based biorefinery are in high demand [25].

* Corresponding author at: TUM Campus Straubing, Schulgasse 16, 94315 Straubing, Germany.
E-mail address: doris.schieder@tum.de (D. Schieder).

https://doi.org/10.1016/j.algal.2022.102744
Received 15 October 2021; Received in revised form 25 March 2022; Accepted 7 May 2022

The utilization of microalgae and cyanobacteria residual biomass after extraction of high value compounds poses a significant challenge. The biocomposition with content of primary metabolites depends on the cultivation strategy and will differ strongly for each chosen biorefinery approach [8,15]. Cultivation strategies targeting the production of secondary metabolites do not necessarily result in large amounts of storage compounds, such as starch or lipids. This means mainly structural saccharides are available from the biomass as fermentable sugars. Yet, microalgae and cyanobacteria have developed robust structural saccharides to withstand any harsh environmental conditions. Besides cellulose, carrageenan or alginate, different polysaccharides, which are more difficult to break down have been identified [26]. Thus, the extraordinarily diverse saccharide compositions present in the biomass, make it extremely difficult to adopt a utilization concept when identifying strains. Therefore, a thorough analysis of the saccharides in each strain is inevitable. The previously presented procedure for quick saccharide fingerprinting of microalgae has made it possible to investigate crude microalgal biomass as well as processed biomass, such as enzymatic hydrolysates [27]. The high-throughput pre-column derivatization 1-phenyl-3-methyl-5-pyrazolone (HT-PMP) method allows the elucidation of rare saccharides and even allows the identification of residue substitution positions such as methyl groups, sulfates or pyruvate residues.

Several cyanobacterial genera with potentially valuable bioactive compounds have been identified [28]. For the genus *Nostoc*, several species show a number of interesting bioactive compounds and a few have also been investigated on structure and composition of their polysaccharide fractions [29]. The majority of the found polysaccharides were complex heteroglycans comprised of mannose, arabinose, galactose, xylose, rhamnose, ribose, galacturonic acid and glucuronic acid connected mainly by beta linkages [29–31]. Yet, the detailed compositions and structures were always different depending on species, environmental stress, or cultivation conditions. Indicating the difficulty of developing a one-fits-all strategy for enzymatic hydrolysis and utilization of microalgae and cyanobacterial biomass.

In this study, seven *Nostoc* strains were investigated for their biocomposition. The HT-PMP method for fingerprinting algal carbohydrates was utilized to investigate the broad range of saccharides present in the seven *Nostoc* strains. Besides the quantification of common monosaccharides, rare sugars have been identified and methylation patterns have been elucidated based on retention times and MS^2 spectra of methyl-glucose standards. Further, the representative biomass of three *Nostoc* strains was evaluated as biorefinery substrate feeds by summative biocomposition analysis. Finally, different industrial enzymes have been investigated on their hydrolysis efficiency on the three *Nostoc* strains.

2. Materials & methods

2.1. Chemicals, enzymes, biomass, and pre-treatment

All chemicals, unless otherwise stated, were purchased in analytical grade from Sigma Aldrich (Germany), Merck KGaA (Germany) and Carl Roth GmbH (Germany). OPTIMASH™ BG, DISTILLASE® CS, and FERMGEN™ were kindly provided by Genencor (DuPont) and Viscozyme® L (Novozymes) was acquired from Sigma Aldrich.

Freeze dried whole cells from *Nostoc* sp. De1, *Nostoc* sp. Cc3, *N. muscorum* I, *N. piscinale*, *N. viola*, *Nostoc* sp. F 15c, *N. linckia* VT-15 were kindly provided by Centre Algatech, Institute of Microbiology, The Czech Academy of Sciences (Třeboň): *N. linckia* VT-15 had been cultivated in Allen Arnon medium, all other strains in BG-11 medium. The strains had been grown in 300 mL glass columns (light path 2.5 cm) bubbled with enriched air (1.5% CO_2) at 28 °C and constant illumination of 100 μmol photon m^{-2} s^{-1}. For *Nostoc* sp. De1, *Nostoc* sp. Cc3, and *N. muscorum* I, additional cultivation had been performed in a 100 L glass flat-panel bioreactor (light path 10 cm) under the same conditions. Strains had been harvested at early stationary phase by centrifugation at 4500 rpm for 10 min, stored at −70 °C and freeze dried.[1]

Freeze dried biomass from the 100 L scale was used for the experiments with *Nostoc* sp. De1, *Nostoc* sp. Cc3, and *N. muscorum* I, and from the 300 mL scale for analysis of all other strains. All analytical procedures were done following slightly modified laboratory analytical procedures (LAPs), standard algal biomass analytical methods provided by the National Renewable Energy Laboratory (NREL) or the PMP method for saccharides [32]. Prior to running any procedures, the biomass of the investigated strains was milled in a ball mill (MM 400, Retsch GmbH, Haan) for 1 min at a frequency of 30 Hz using a zirconium oxide coated 35 mL jar and a single bead.

2.2. Carbohydrate fingerprinting of Nostoc biomass

2.2.1. Chemical hydrolysis of biomass

Total carbohydrates and monosaccharide profiles were determined by a previously developed HT-PMP derivatization method for carbohydrate analysis by UHPLC and MS applied to algal biomass [27]. Briefly: the analytical chemical hydrolysis was performed by adding 6 mL of 2 M trifluoroacetic acid (TFA) to 12 mg of biomass in 25 mL glass tubes. The tubes were incubated in a heating block (VLM GmbH, EC-Model) for 105 min at 121 °C. The hydrolysis was stopped by transferring the samples onto ice and adjusting the pH to 8 by adding an aqueous solution of 3.2% NH_4OH [33].

2.2.2. HT-PMP derivatization of algal hydrolysates

The derivatization of the saccharolytic hydrolysates was performed in a 96-well format as described originally [34]. In short, a 25 μL aliquot of the hydrolysate adjusted to pH 8 was transferred to a 96-well-PCR plate (781,350, Brand) and 75 μL of derivatization reagent (0.1 M methanolic-PMP-solution: 0.4% NH_4OH solution, 2:1) were added. After incubation (100 min, 70 °C) in a PCR-cycler (Biorad, My-cycler), a 20 μL aliquot was mixed with 130 μL of 19.23 mM acetic acid. The samples were then filtered through a 96-well plate (0.2 μm Supor, Pall Corporation) by centrifugation at 2500 ×*g* for 5 min into a microtiter plate. The plate was subsequently sealed with a silicon cap mat (7704-0105, Whatman).

For additional saccharides eluting prior to the regular cut-off of the MS at 3 min retention time as described in the next section, PMP was extracted from samples before HPLC-MS analysis. For these samples, the derivatization was done in 1.5 mL Eppendorf tubes in a water bath (100 min at 70 °C). After the derivatization, 650 μL of 19.23 mM acetic acid was added. After mixing the diluted samples, excess PMP was extracted with 500 μL of chloroform (three times). The samples were then filtered through a syringe filter (0.2 μm cellulose) into 1.5 mL glass vials and capped for analysis.

2.2.3. UHPLC-UV-ESI-MS/MS analysis of derivatized monosaccharides

The chromatographic analysis of the derivatized sugars was conducted as shown and validated before [27,34]. In brief: a mobile phase A consisting of 5 mM ammonium acetate buffer (pH 5.6) with 15% (w/w) acetonitrile and a mobile phase B containing pure acetonitrile were used. The column (Gravity C18, 100 mm length, 2 mm i.d.; 1.8 μm particle size, Macherey-Nagel) was tempered to 50 °C. The flow rate was set to 0.6 mL min^{-1}. The gradient was run as described. The temperature of the autosampler was set to 20 °C and an injection volume of 10 μL was used. All calibration standards were prepared with the TFA-hydrolysis matrix pH 8 to compensate its influence on the derivatization process. Data were collected and analyzed with Bruker Hystar, QuantAnalysis, Data Analysis and Dionex Chromeleon software. Detailed parameters can be found in the original publication of the method [34].

[1] Data communicated by Algaltech.

2.3. Total solids & ash

For the determination of total solids and ash content in the biomass, the NREL LAP was followed [35]. 100 mg of biomass was used for the determination of total solids in a vacuum oven (Binder, VDL 53) and ash in a muffle furnace (Linn High Term GmbH, LM-312.27) with controller (Gefran, 880P).

2.4. Starch analysis

Starch content in the biomass was determined using the Megazyme Total Starch Assay AOAC Official Method 996.11 [36]. 100 mg of biomass (based on starch content), as well as 10 mg of starch as control was investigated for starch content. The starch content in percent of biomass was calculated based on the absorbance of the glucose standard and corrected for hydration. The equation as provided by Megazyme can be found in the supporting information (supplementary, Annex 3).

2.5. Determination of protein

Protein content was determined based on a conversion factor from elemental nitrogen to protein. Freeze dried *Nostoc* biomass was analyzed by elementary analysis (Euro EA 3000, EuroVector) for its nitrogen content. 1–3 mg of biomass was loaded into tin containers for carbon, nitrogen, sulfur, and hydrogen determination. The crude protein content was determined by a nitrogen-to-protein conversion factor of 4.78, as revised by Lourenço et al. [37].

2.6. Determination of lipids as FAMEs

Lipids were determined as fatty acid methyl esters (FAME) and GC–MS as described by the NREL LAP [38]. In short, 10 mg of dry biomass was trans-esterified with 200 μL of chloroform:methanol (2:1 v/v), and 300 μL 0.6 M HCl in methanol on an 85 °C pre-heated metal heating block (StarFish, Heidolph Inst.) for 1 h. 1 mL of hexane was added to each vial and quickly closed again. After mixing well, the phases were allowed to separate for 2 h. 200 μL of the upper phase were then transferred into pre-labeled GC micro vials and placed in the autosampler. A FAME standard dilution series was prepared from a 1 mg/mL even carbon FAME standard (49454-U, Sigma) in GC micro vials with internal standard by adding 100 μL standard dilution and 100 μL of internal standard. The GC–MS was carried out using a Rxi®-5Sil-MS column (30 m by 0.53 mm, 20 μm film, Restek) on a TRACE™ GC Ultra gas chromatograph (Thermo Scientific) with a Quadrupole detector. 1 μL of the sample was transferred in the injector (250 °C) with a split 1:20 and separated on the column (50 °C/hold 3 min, 45 °C min^{-1} to 220 °C/hold 2 min, 45 °C min^{-1} to 280 °C/hold 2 min, 60 °C min^{-1} to 330 °C/hold 1.5 min). The transfer line and ion source were 250 °C and MS start time was 4.0 min.

2.7. Enzymatic hydrolysis

Enzymatic saccharification was performed by adding 50 mM ammonium acetate buffer pH 4.5 with 0.02% (w/v) sodium azide to 25 mg of biomass in 1.5 mL Eppendorf tubes. Enzymes were added with 0.5% (v/v) for determination of enzyme suitability to a total of 1.0 mL reaction volume. The tubes were incubated in a heating block for up to 24 h or 48 h at different temperatures shaking 300 rpm. The hydrolysis was stopped by incubating at 95 °C for 10 min. After allowing the samples to cool down, they were centrifuged for 10 min with 21,000 ×*g* at room temperature. The supernatants were then collected in fresh tubes and the saccharide concentration was brought into calibration range by diluting with a matrix solution of 0.8 M TFA adjusted to pH 8 with aqueous 3.2% NH_4OH for PMP derivatization. The subsequent derivatization and analysis was done as described in Section 2.2.

3. Results & discussion

3.1. Saccharide profile of seven Nostoc strains

3.1.1. Identification of monosaccharides

The standardized, fast, and reliable HT-PMP method for algal carbohydrate fingerprinting was used on crude biomass of seven *Nostoc* strains. The biomass was treated with 2 M TFA for complete hydrolysis, the hydrolysate then derivatized with PMP, as described in Section 2.2.1. Different incubation times (75 min–120 min) for hydrolysis were tested with 105 min showing the highest yields of monosaccharides for three biomass strains (results not shown). Saccharides derivatized with PMP absorb strongly at 245 nm, which allows for sensitive UV detection. Additionally, co-eluting sugars can be distinguished based on the MS analysis. Extracted ion chromatograms (EIC) permit the cross-verification of the identities of the detected sugars, with the exception of xylose and arabinose. The monosaccharides that were detected and quantified in the hydrolysates of the investigated seven *Nostoc* strains are reported in Table 1.

Saccharides from different *Nostoc* strains have been broadly investigated before with focus on possible applications [39]. Nevertheless, this is the first study to report an in-depth analysis of the saccharide composition of multiple *Nostoc* strains. The monosaccharide profiles of all the *Nostoc* strains investigated in here are diverse, consisting mostly of mannose, glucosamine, glucuronic acid, rhamnose, galactose, glucose, and xylose. Only minor amounts of fucose, galacturonic acid and ribose were detected in all the investigated strains. Although the detected monosaccharides in the investigated *Nostoc* biomasses are quite similar, the overall saccharide contents differ strongly. Other authors have reported similar saccharide compositions of mannose, rhamnose, glucuronic acid, galactohydric acid, glucose, galactose, arabinose and galactosidonic acid methyl ester [29,31,39]. The total saccharide content established in the present work ranges from 15 to 40% depending on the strain with glucose being the most abundant monosaccharide in all samples. These findings are in line with other reports [3]. The glucose yield is usually higher for algal biomass with high starch content, but the *Nostoc* strains used in this work were not exposed to any abiotic stress factors during cultivation. This can be drawn from low storage compounds concentrations (Table 4). The mentioned monosaccharides compose a large part of structural polysaccharides in algal biomass [27,40]. The actual glucose concentration from starch or structural saccharides can be precisely elucidated with specific enzymes. This is discussed further in Section 3.2.1.

3.1.2. Analysis of unknown saccharides

The advantage that sets the applied HT-PMP method apart from others in identifying sugars is the additional MS^2 determination of unknown signals in the chromatograms. For most rare sugars, there are no standards available and therefore these cannot be quantified. Nevertheless, based on the elution profile, the *m/z* ratio and the MS^2 fragmentation pattern postulates can be formulated about their constitution. The derivatization of saccharides with PMP gives the chemical species for $[M + H]^+$ distinct *m/z*. The produced *bis*-PMP derivatives result in masses of plus *m/z* 331 ($+2 \times$ PMP and $-1 \times H_2O + H^+$). Additionally, mass differences and distinct fragments can be allocated to specific substituents such as methyl, amino, carboxyl, deoxy or even phosphoryl and sulfuryl groups. Therefore, considering a non-functionalized hexose has a $[M + H]^+$ of *m/z* 511, a methyl hexose results in *m/z* 525. Additionally, dimers can also be detected, and identities postulated for the unknown saccharides. Dimers often give additional insight into polysaccharide structure and retention times can even give clues about stereo chemical characteristics of the glycosidic bonds [34].

The method allows to separate many different saccharides, though for some an additional step has to be included to elucidate their identity. In order to identify saccharides eluting from the column prior to 3 min, excess PMP has to be extracted to not flood the ion source with PMP. On

Table 1
Saccharide amounts in TFA hydrolysates of crude cyanobacterial biomass from investigated *Nostoc* strains. Monosaccharide quantification was primarily performed based on EIC. Glucose and galactose were quantified by UV. In this case, values are reported as the mean of $mg_{sugar}\ g^{-1}$ dry biomass ± one standard deviation, n = 3. *<LOQ*: below limit of quantification.

	Nostoc sp. De1	*Nostoc* sp. Cc3	*Nostoc muscorum* I	*Nostoc piscinale*	*Nostoc viola*	*Nostoc* F 15c	*Nostoc linckia*
Mannose	8.7 ± 0.5	21.8 ± 1.2	7.8 ± 0.4	22.0 ± 1.7	43.7 ± 3.8	75.8 ± 2.1	41.2 ± 2.7
Glucosamine	6.4 ± 0.3	5.3 ± 0.1	5.7 ± 0.2	18.4 ± 1.3	5.3 ± 0.3	4.4 ± 0.4	19.1 ± 0.5
Glucuronic acid	18.8 ± 1.7	5.2 ± 0.4	10.2 ± 0.7	6.2 ± 0.6	22.9 ± 2.1	4.0 ± 0.2	9.0 ± 0.5
Galacturonic acid	*<LOQ*	*<LOQ*	*<LOQ*	3.8 ± 0.3	10.5 ± 1.0	3.4 ± 0.03	4.4 ± 0.2
Ribose	5.4 ± 0.3	5.0 ± 0.4	2.9 ± 0.1	8.8 ± 0.4	2.4 ± 0.05	10.5 ± 0.2	4.9 ± 0.3
Rhamnose	3.1 ± 0.2	5.9 ± 0.4	3.5 ± 0.02	3.6 ± 0.1	11.1 ± 0.8	3.4 ± 0.1	8.8 ± 0.2
Glucose	70.2 ± 2.8	128.8 ± 2.7	137.9 ± 2.4	86.5 ± 7.7	148.1 ± 7.5	205.5 ± 11.4	126.0 ± 3.7
Galactose	16.4 ± 1.4	36.4 ± 2.0	10.8 ± 0.6	21.0 ± 1.8	26.7 ± 2.8	76.3 ± 4.1	50.6 ± 2.9
Xylose/Arabinose	17.1 ± 1.1	25.1 ± 1.2	17.1 ± 0.5	10.8 ± 0.8	49.2 ± 5.9	13.0 ± 0.7	64.3 ± 2.3
Fucose	*<LOQ*	17.9 ± 0.9	4.8 ± 0.1	11.5 ± 1.3	14.1 ± 0.7	4.1 ± 0.1	15.5 ± 0.4
Total	146.0 ± 8.2	251.5 ± 9.2	200.6 ± 5.1	192.7 ± 16.0	334.0 ± 25.0	400.3 ± 19.4	343.8 ± 13.9

doing so, MS acquisition can be done from the start for the full 12 min run time. Especially more hydrophilic saccharides can be identified, which might otherwise co-elute with PMP and therefore disappear under the large UV peak of PMP. For the strains *Nostoc* sp. Cc3 and *Nostoc muscorum* I especially interesting saccharides were found to elute this early. An overlay of the UV- (black) and EIC (color) -chromatograms (1.5–4.5 min) of PMP derivatized and with chloroform extracted TFA hydrolysates of these two strains are shown in Fig. 1. Additional to the reported monosaccharides in Table 1, peaks corresponding to the here reported ones, further saccharides could be identified. Additional chromatograms (3–9 min) for all seven *Nostoc* strains with identified saccharides can be found in the supporting information (supplementary, Annex 1).

The first peak in Fig. 1A, the hydrolysate of *Nostoc* sp. Cc3 elutes at 2.1 min. The peak (purple) shows an *m/z* of 687, which corresponds to the mass of a dimer composed of hexose and a hexuronic acid. The MS^2 fragmentation for dimers in this case as does in general shows a distinct main fragment with the *m/z* of *bis*-PMP derivatized monomer of 511.

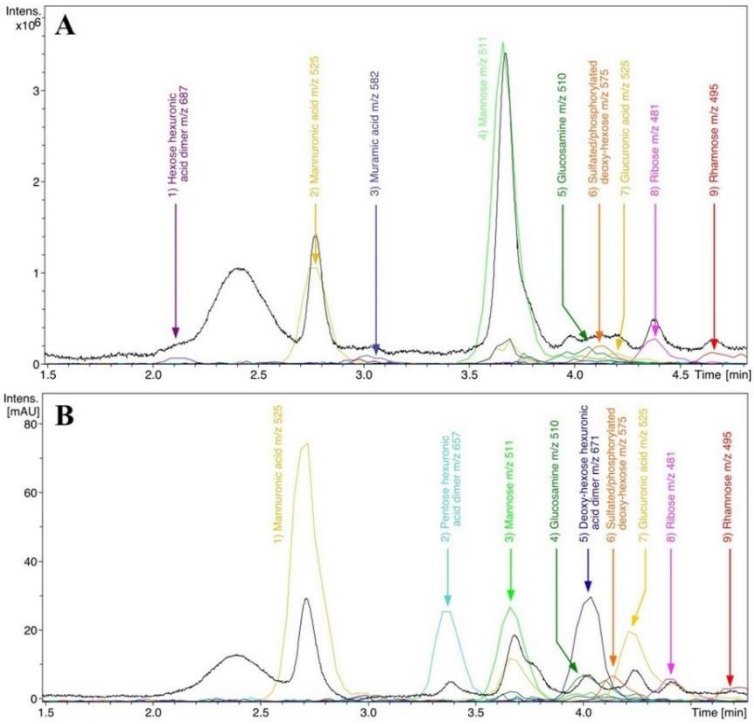

Fig. 1. Overlay of UV 245 nm (black) and MS extracted ion chromatograms (color, 1.5–4.5 min) of PMP extracted A: *Nostoc* sp. *Cc3* and B: *Nostoc muscorum I* monosaccharide analysis. EIC colors have been chosen to help differentiate peaks. Corresponding *m/z* values are shown in the figs. A retention time shift between PMP extracted and non-extracted samples can occur.

Meaning the glycosidic bond at the anomeric center of the uronic acid has not been cleaved. This is due to the protective properties of the uronic acid with its C-6 carboxyl group against hydrolysis of the glycosidic bond at the anomeric carbon [41]. Dimers with uronic acids appear therefore more often. On the other hand, uronic acids degrade quicker when released from its polymer, which can be seen by the presence of their degradational products. Due to these reasons, a reliable quantification is not possible. For uronic acids eluting prior to 3 min, the degradation products are the only clue to their presence in the normal mode of the HT-PMP method.

The second peak in the hydrolysate of *Nostoc* sp. Cc3 as well as in *Nostoc muscorum* I elutes at 2.7 min. The peak (yellow) shows an *m/z* of 525, which corresponds to uronic acids or methyl hexoses. A methylated hexose elutes later than a neutral hexose in this reversed chromatography. No hexose elutes this early and hence this peak can be identified to be a uronic acid. Also, the MS^2 fragmentation pattern did not show a loss of a methyl group (*m/z* 14) but the loss of a carboxy group (*m/z* 44) can be observed. Uronic acids, which are differentiated based on retention time are rare besides glucuronic acid and galacturonic acid, but this *m/z* 525 peak could be identified here as mannuronic acid. The identity was confirmed based on the retention time against a standard. The presence of mannuronic acid could indicate the presence of alginate as one structural component in the biomass of these two *Nostoc* strains [42]. The fact that no guluronic acid as second residue of alginate was detected might indicate that only the precursor form was produced until the time of harvest [43]. The precursor form is a linear homopolymer of mannuronic acid residues. For all seven investigated *Nostoc* strains, several unknown peaks were identified by mass spectrometry, albeit some of them in trace amounts. Postulations for each sugar, based on *m/z*, elution pattern and mass fragmentation was done in the same manner as described above and detailed MS^2 fragmentation below in Section 3.1.3. A summary is given in Table 2. In addition to the chromatograms, MS^2 spectra of all investigated *Nostoc* strains for the identified sugars can be found in the supplementary information (supplementary, Annex 2).

Diverse and complex structures of polysaccharides pose a big challenge to utilizing saccharides from any sources. Biomass treatment to enhance sugars solubility and to improve substrate availability requires elucidation of saccharide structures. A complete analysis of the saccharide profile, as well as the linkage patterns are key to making saccharide sources such as *Nostoc* biomass industrially available. Rare saccharides could be found in all strains as the unknown sugar found in *Nostoc piscinale* at 4.7 min with *m/z* 583 showing the mass of a hydroxypropyl/carboxyethyl hexuronic acid or a lactate-hexose. The fragmentation pattern allowed to conclude this sugar to be a lactate-hexose. Yet, the loss of specific fragments could not always be unequivocally assigned. In literature reported structural findings of polysaccharides in *Nostoc* strains were similar to our findings. The presence of a xylogalactoglucan backbone was identified with residues from ribose, mannose, galactose, glucose, and xylose to carboxyethyl-glucuronic acid (nosturonic acid) and other uronic acids. The complex structural saccharides further utilize heavy substitution for increased stress tolerance of the strains. This is achieved by different substitutions such as multiple methylations, acetylations or other groups such as propyl, or carboxyethyl as in the case of nosturonic acid. Propositions about stereo chemical conformations were mostly β-(1-4)-linked (glucose) backbones, branching 1–3, 4, 6 with different residues in α or β position [31,39]. As shown in Table 2, many different methylated or amino monosaccharides were identified in this study. Especially diversely methylated hexoses were found.

3.1.3. Elucidation of methylation patterns on saccharides

The HT-PMP method allows a detailed elucidation of sugar structures including stereo isomeric constitution of monosaccharides. Epimers such as glucose, mannose and galactose elute well in a separated manner. It is highly interesting and notable that the C-2-hydroxy group conformation shows a larger effect in the *bis*-PMP derivatives, being axial for mannose but equatorial for glucose and galactose. The separation capability of this method even allows to separate substituted saccharides differing in position of the substitution group. Here, this is shown for the first time for the four methyl-glucoses and 6-*O*-methyl-galactose. An overlay of the UV- (black) and EIC (yellow) -chromatograms (6–9 min) of PMP derivatized standard methyl-glucoses and 6-*O*-methyl-galactose are shown in Fig. 2. Glucose and galactose (EIC in green) are also included as reference peaks. It can be seen the methyl-glucoses are almost completely baseline separated using the applied conditions in the UV (245 nm) trace and only the MS traces of 2-*O*-methyl-glucose and 6-*O*-methyl-glucose due to the much higher sensitivity are not completely baseline separated.

The HT-PMP method utilizes an ion trap MS and therefore does not only give discrete *m/z* values from corresponding EIC but allows further structural elucidation. The fragmentation pattern in the MS^2 spectra reveal the position at which substitutions are located on sugar molecules. In order to validate the postulations on methylation positions, the MS^2 spectra of the methyl glucose standards were used for comparison. These MS^2 spectra of the methyl-glucoses are presented in Fig. 3. In addition to the methylated fragments, the PMP *mono*- and *bis*-derivatives are marked with symbols in the MS^2 spectra.

Distinct fragments for each of the sugars reveal the position of each methyl group. These distinct fragments can usually be found in the range of the PMP *mono*-derivative, which is below *m/z* 351 and can be transferred to other hexoses. The fragment *m/z* 231 is specific for 2-*O*-methyl-hexoses, while *m/z* of 285 corresponds to a hexose with 3-*O*-methyl

Table 2
Rare and unknown sugars found in all seven investigated *Nostoc* species. Chromatograms and MS^2 spectra can be found in the supporting information (supplementary, Annex 1 and 2). The identity of the sugars was postulated analogously to those discussed in the text.

Mass [*m/z*]	*Nostoc* sp. De1	*Nostoc* sp. Cc3	*Nostoc muscorum* I	*Nostoc piscinale*	*Nostoc viola*	*Nostoc* F15c	*Nostoc linckia*	Postulated SUGAR
	R_t [min]	R_t [min]	R_t [min]	R_t [min]	R_t [min]	R_t [min]	R_t [min]	
495	–	–	8.6, 8.9	–	–	8.6	–	3/2-Methyl-xylose/arabinose
495	–	–	–	–	–	5.6	–	6-Deoxy talose
509	8.2	9.1	–	–	9.1	8.0	8.0	Methyl-deoxy-hexose
525	–	2.7	2.7	–	–	–	–	Mannuronic acid
525	8.7	8.5, 8.7	6.7, 8.7	7.6, 8.7	8.7	5.7, 7.6, 8.7	8.7	Methyl-hexoses
539	–	5.1	5.1	–	–	–	–	Methyl-hexuronic acid
539	8.9	–	–	–	–	–	–	Dimethyl-hexose
575	4.1	4.1	4.4	3.8	3.8	–	–	Sulphated/phosphorylated deoxy-hexose
582	–	3.0	–	–	–	–	–	Muramic acid
583	–	–	–	4.7	–	–	–	Lactate-hexose
657	3.1	–	3.3	–	4.3	–	4.2	Pentose hexuronic acid dimer
671	–	–	–	–	4.1	–	–	Deoxy hexose hexuronic acid dimer
687	3.9	2.1	–	–	–	–	–	Hexose hexuronic acid dimer

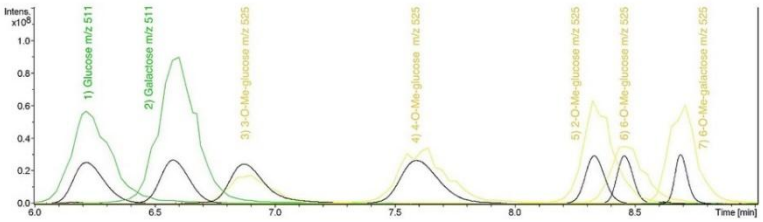

Fig. 2. Overlay of UV 245 nm (black) and MS extracted ion (color) chromatograms (6–9 min) of PMP derivatized methyl hexose standards with *m/z* 525 in yellow. As references, glucose, and galactose (EIC in green) are shown with *m/z* 511. (For interpretation of the references to color in this figure legend, the reader is referred to the web version of this article.)

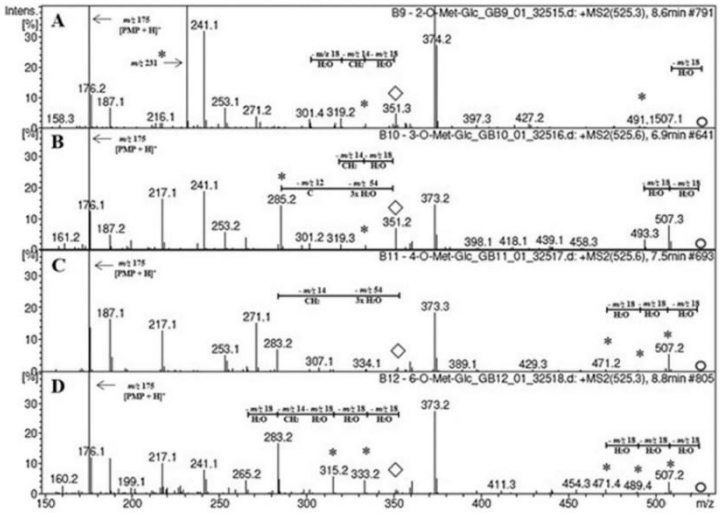

Fig. 3. Mass spectra (*m/z* 150–550) of PMP derivatized methyl glucose standards with *m/z* 525. A: 2-*O*-methyl-glucose (R_t = 8.6 min), B: 3-*O*-methyl-glucose (R_t = 6.9 min), C: 4-*O*-methyl-glucose (R_t = 7.5 min), D: 6-*O*-methyl-glucose (R_t = 8.8 min); ○: parent ion; ◊: mono-derivative ion. Masses marked with * correspond to methylated fragments.

group. 4-*O*-methyl hexoses lack distinct fragments, but the distinct lack of the fragment *m/z* 241 points out the position of substitution. Lastly, 6-*O*-methyl-hexoses show more clearly losses of water resulting in distinct methylated fragments with the masses of *m/z* 315 and *m/z* 333. These masses are theoretically not distinctive, but it appears, for the other methyl-hexoses these fragments are not produced with such high intensity. The analysis of the fragmentation in the MS^2 of the methyl-hexoses found in the investigated *Nostoc* strains was done, similar as

Table 3
Overview of identified methyl hexoses in investigated *Nostoc* strains based on retention time and MS^2 fragmentation pattern.

Methyl hexose	Standard	*Nostoc* sp. De1	*Nostoc* sp. Cc3	*Nostoc muscorum* I	*Nostoc piscinale*	*Nostoc viola*	*Nostoc* F 15c	*Nostoc linckia*
	R_t [min]	R_t [min]	R_t [min]	R_t [min]	R_t [min]	R_t [min]	R_t [min]	R_t [min]
2-*O*-methyl-glucose	8.5[2]	8.5	8.5[1]	–	–	–	–	–
3-*O*-methyl-glucose	6.9	–	–	6.7[2]	–	–	–	–
4-*O*-methyl-glucose	7.6	–	–	–	7.5	–	–	–
6-*O*-methyl-glucose	8.7[2]	–	–	–	–	–	–	–
2-*O*-methyl-galactose	–	–	8.7	8.7	8.7	8.7	8.7	8.7
3-*O*-methyl-mannose	–	–	–	–	–	–	5.7	–
3-*O*-methyl-galactose	–	–	–	–	–	–	7.5	–
6-*O*-methyl-galactose	8.9[2]	–	–	–	–	–	–	–

[1] Mixed spectra of 2-*O*-methyl-glucose and 6-*O*-methyl hexose (based on retention time).
[2] A retention time shift over one sequence or between different runs can occur.

discussed above for the methyl-glucose standards. The findings of the methyl-hexoses of the *Nostoc* strains are listed in Table 3.

Considering all rare saccharides in the investigated strains as well as the diverse methylation patterns especially on the hexoses, it can be concluded that a big fraction of these polymers will be difficult to hydrolyze by enzymatic treatments for fermentative utilization. This has the repercussion that in a biorefinery approach, the saccharides may rather be exploited as nutraceutical or pharmaceutical [44]. Alongside the extractable saccharides, as many as possible other valuable compounds need to be co-extracted and utilized. The remaining primary metabolite fractions need to be evaluated for alternative utilization. Only then a full biorefinery approach can be evaluated.

3.2. Evaluation of three Nostoc strains for biorefinery

3.2.1. Biocomposition analysis

The multidisciplinary research to design cyanobacterial biorefineries requires the complete biocomposition profile of each specific strain in order to utilize the complete biomass. *Nostoc* strains with reportedly many different bioactive compounds are of particular interest for biorefineries. The three *Nostoc* strains *Nostoc* sp. De1, *Nostoc* sp. Cc3 and *N. muscorum* I were hence further characterized to investigate the utilization potential of the biomass, e.g. as residue after extraction of bioactive compounds. Here, we report the percentage content of inorganics, lipids, proteins and saccharides, represented by sum parameter. The biocomposition of the three *Nostoc* strains is shown in Table 4.

Overall, the mass balance is not complete. The total detected mass was between 91.8% and 71.4% and therefore 28.6%–8.2% short to full recovery of the biomass. The difference can partly be explained by components, which have not been quantified. *N. muscorum* I with only 71.4% total mass quantified, shows for example to have a 2-*O*-methyl-xylose/arabinose in large quantity present (supplementary, Annex 2.3). In total, eight rare saccharides were detected in the mentioned strain. Due to the lack of standards, quantification was not possible and therefore not included into the mass balance of *N. muscorum* I. For all three strains, saccharides which were not quantified most likely account to a large amount of the discrepancy in the mass balance. The utilizable saccharides, e. g. starch, were determined to be rather low. Saccharides in total were found to be 14.6% to 25.2% in the three strains, of which maximum 60% was starch in one of the strains (*N. muscorum* I). In addition, the quantification of protein in the biomass is only a relative measure. The elemental nitrogen conversion to protein is based on a conversion factor and even though elemental analysis is a very accurate method, the result has to be considered as only a good estimation as it is based on a conversion factor. Components such as carotenoids, sterols or nucleic acids were not quantified but should only contribute in small quantities to the total biomass. Yet, the general composition of the investigated biomasses from the three investigated *Nostoc* strains reveal that they were not cultivated under any abiotic stress but harvested latest at the end of the log phase. The storage compounds such as starch, lipids or PHB (data not shown) were low or not detected in the case of PHB. Rarer unfermentable and unquantified saccharides such as the mentioned methyl-pentose in *N. muscorum* I (supplementary, Annex 2.3) made up a large fraction of the detected sugars. Such a low fermentable sugar content in the biomass is due to the cultivation strategy. For viable cyanobacteria biorefinery concepts secondary metabolites are of highest interest. Such cultivation approaches without stress conditions result in protein being the major component of the biomass, here ranging from 37.7% to 49.3% [45]. Such large protein fractions also need to be utilized and can potentially serve after the extraction of high-value compounds as N-source e. g. for fermentation, as well as the lower saccharide content as C-source.

Table 4
Summative biocomposition of three *Nostoc* strains for the evaluation of the biomass as feedstock for biorefineries. Reported values for all components are the mean of triplicates ± standard deviation. FAME: fatty acid methyl esters.

Component	*Nostoc* sp. De1	*Nostoc* sp. Cc3	*Nostoc muscorum* I
% Moisture	4.8 ± 0.3	6.1 ± 0.2	5.4 ± 0.1
% Ash	6.7 ± 0.2	9.1 ± 0.7	6.3 ± 0.1
% Protein	48.6 ± 0.2	49.3 ± 0.1	37.7 ± 1.0
% FAME	2.7 ± 0.1	2.1 ± 0.1	2.0 ± 0.2
% Starch	1.4 ± 0.1	8.4 ± 0.2	7.5 ± 0.2
% Structural saccharides*	13.2 ± 0.8	16.8 ± 0.9	12.6 ± 0.5
% Total	77.4 ± 1.7	91.8 ± 2.2	71.4 ± 2.1

* The values for structural saccharides are total saccharides (TFA) corrected for glucose determined as starch.

Another fraction in algal biomass are lipids. Here, lipids were analyzed as fatty acid methyl esters (FAMEs) using GC–MS. The total FAME content in the three strains was also low ranging from 2.0% to 2.7% of the total biomass. The fatty acids found in all three strains were palmitic acid, palmitoleic acid, stearic acid, linoleic acid, and α-linolenic acid (supplementary, Annex 4). Such extremely low concentrations allow to neglect FAME as a major product stream in a biorefinery approach. Nevertheless, utilization of biomass with abundant protein fraction still requires a multi-product stream approach to make a biorefinery concept feasible. High-value compounds are certainly the concept driving products. For the utilization as residual component in a biorefinery concept, the hydrolysis of the protein and saccharide fraction needs to be investigated further. It is to be noted that the high protein content demands mild reaction conditions to prevent yield losses due to the Maillard reaction. An enzymatic hydrolysis approach described here poses a chance for higher yields compared to harsh chemical hydrolysis.

3.2.2. Enzymatic hydrolysis

Different industrial saccharolytic enzymes were tested for the hydrolysis of *Nostoc* sp. De1, *Nostoc* sp. Cc3 and *N. muscorum* I. The enzymes were chosen based on the physiology of the cells. OPTIMASH™ BG a combination of beta glucanases and xylanase enzymes which modifies, and digests non-starch carbohydrates, DISTILLASE® CS that produces glucose from liquefied starch, and Viscozyme® L blend of glucanases, pectinases, hemicellulases and xylanases were tested for 24 h hydrolysis on the biomass of the three cyanobacterial strains (Fig. 4).

DISTILLASE® CS released besides small amounts of mannose exclusively glucose from all three strains, indicating that, as described, DISTILLASE® CS is meant to hydrolyze preliminary starch but may also contain side activities acting on other polysaccharides. The yields (saccharides/biomass) achieved were 30 mg g^{-1}, 67 mg g^{-1} and 67 mg g^{-1} for *Nostoc* sp. De1, *Nostoc* sp. Cc3 and *N. muscorum* I, respectively. In *Nostoc* sp. De1 the released amount of glucose was higher than the starch fraction determined by the Megazyme kit (16 mg g^{-1}). The Megazyme photometric assay was compared to analysis by the HT-PMP method (supplementary, Annex 5) showing that the detected glucose by PMP-HPLC-UV with 32 mg g^{-1} was much higher than by the assay. Whereas for the other two strains as well as for the starch control the results were quite the same with both methods. OPTIMASH™ BG and Viscozyme® L released besides glucose and mannose also galactose in all three strains (Fig. 4). These enzymatically released fractions of mannose and galactose account for around 13% and 30% in *Nostoc* sp. De1, 5% and 21% in *Nostoc* sp. Cc3, and 15% and 42% in *N. muscorum* I. Showing the two enzymes hydrolyze also structural saccharides. Surprisingly, although the enzyme blends contain xylanase or hemicellulase activities no pentoses such as xylose were detected.

Overall, the maximum released saccharides from the cyanobacterial biomasses were 20%, 27%, and 33% from *Nostoc* sp. De1, *Nostoc* sp. Cc3, *N. muscorum* I, compared to the total saccharide findings in Table 1. The detected dissolved saccharides in the biomass control samples (i.e. without enzymes) accounted for not more than 2.7% in all three strains. Ribose was only detected in the biomass control samples, which was due to the higher dilution factors applied for analysis of the enzymatic treated samples, making low concentrations of saccharides such as

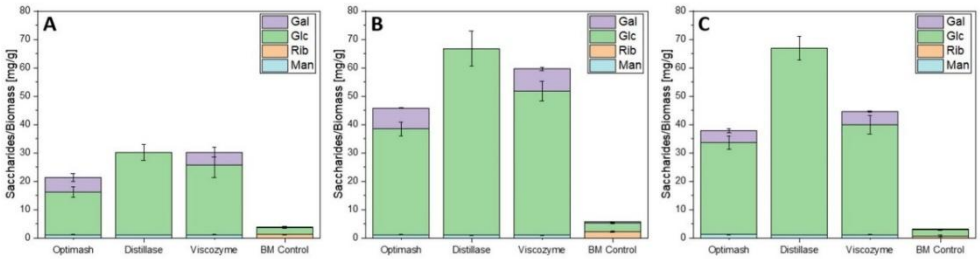

Fig. 4. Saccharification yields per biomass after 24 h using industrial enzymes at 50 °C on (A) *Nostoc* sp. De1 (B) *Nostoc* sp. Cc3 and (C) *Nostoc muscorum* I analyzed by the HT-PMP method. Enzyme concentrations per total sample volume were 0.5% (v/v). Data presented are the average of triplicates and standard deviation.

ribose disappear under the *LOQ*. Ribose has been reported in *Nostoc spec* as constitute of released extracellular and cellular saccharides but can also be found as part of nucleotides [29,46].

For further improvement of the biomass saccharification, several methods can be considered. Here, as one intention could be to utilize the biomass as fermentation feed, a protease was used to increase saccharification yields as well as solubilize the protein as main component of the biomass. The hydrolysate could serve as N-rich medium. A combination of OPTIMASH™ BG and DISTILLASE® CS was used over a total of 24 h and 48 h for a one pot approach. Additionally, a pre-treatment of 8 h at 30 °C with a protease (FERMGEN™, DuPont) was tested for better saccharification (Fig. 5). The saccharification yield with OPTIMASH™ BG on *Nostoc* sp. De1 was 30% higher at 60 °C than at 50 °C before. Yet, the yield on the other two strains was unchanged over also 48 h hydrolysis. The addition of DISTILLASE® CS did not show the expected increase in yield. On the *Nostoc* sp. De1 biomass, the combination of the two enzymes resulted in a lower yield overall with 23 mg g^{-1} and 26 mg g^{-1} after 24 h and 48 h, respectively. The additional FERMGEN™ treatment increased the overall yield slightly to 35 mg g^{-1} but showed no difference for 24 h and 48 h treatment time. For the strains *Nostoc* sp. Cc3 and *N. muscorum* I higher yields were reached with the addition of DISTILLASE® CS. Yet, the yields after 48 h were still just below what was reached by DISTILLASE® CS alone before (67 mg g^{-1}). The addition of FERMGEN™ resulted on all three biomasses in increased yields, resulting in 36 mg g^{-1} (24 h), 73 mg g^{-1}, and 75 mg g^{-1} (both 48 h) for *Nostoc* sp. De1, *Nostoc* Cc3 and *N. muscorum* I, respectively.

The saccharification with the chosen industry enzymes has resulted in relatively low yields. In combination, only the pre-treatment with FERMGEN™ helped to increase the final saccharification yields on the three *Nostoc* strains. Overall, the maximum released saccharides were 25%, 29%, and 37% of the total saccharides detected by chemical hydrolysis in *Nostoc* sp. De1, *Nostoc* sp. Cc3, *N. muscorum* I, respectively (Table 1). Also, the released mannose and galactose did not increase. The enzymatic saccharification depends strongly on the saccharides present in the biomass (starch vs. structural saccharides) as well as the specific enzymes [47]. For more efficient saccharification in low starch cyanobacterial biomass, the enzymes specificities are therefore elemental for efficient hydrolysis of the structural saccharides. On the other hand, the fermentative utilization of the *Nostoc* biomass requires besides saccharification also efficient solubilization. The solubilization of the investigated three *Nostoc* strains by the tested enzymes was also recorded (supplementary, Annex 6). The treatment with the saccharolytic enzymes showed higher solubilization in *Nostoc* sp. Cc3 and *N. muscorum* I compared to the biomass control but not on *Nostoc* sp. De1. This could be an indication for which saccharides were hydrolyzed, as the hydrolysis of structural saccharides should lead to better solubilization of the biomass. The additional proteolytic treatment increased the biomass solubilization for all three strains differently but overall, up to 57%, 49%, and 56% for *Nostoc* sp. De1, *Nostoc* sp. Cc3, *N. muscorum* I, respectively. The enzymatic treatment scheme could also serve for processing of prior high-value compound extracted biomass. Saccharification and solubilization ought to be investigated on extracted residual biomasses. A mass balance should assist in providing valuable data for such biorefinery concepts and their techno-economic evaluation.

4. Conclusions

In this study, the saccharide profiles of seven *Nostoc* strains were elucidated using the fast and reliable HT-PMP method. The quantified monosaccharides and rare sugars from diversely substituted monosaccharides to uronic acid dimers indicate the presence of very complex heteroglycans. The complete biocomposition, including starch, lipids, and protein of three *Nostoc* strains have been characterized. The *Nostoc* biomass as biorefinery feedstock was further characterized by different

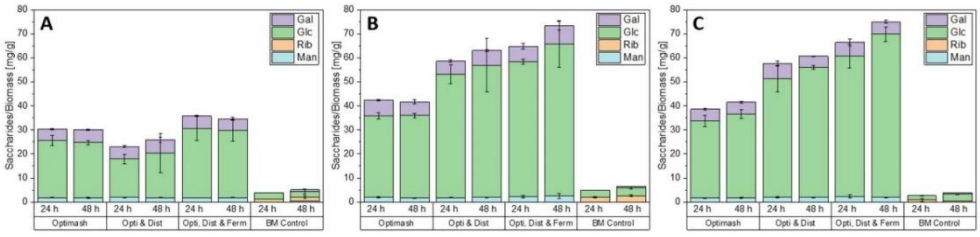

Fig. 5. Saccharide yields per biomass over 24 h and 48 h hydrolysis using industrial enzymes at 60 °C after 8 h protease pre-treatment at 30 °C on (A) *Nostoc* sp. De1 (B) *Nostoc* sp. Cc3 and (C) *Nostoc muscorum* I analyzed by the PMP method. Enzyme concentrations were 0.5% (v/v) of each enzyme. Data presented are the average of triplicates and one standard deviation. The enzymes used were Opti: OPTIMASH™ BG, Dist: DISTILLASE® CS, and Ferm: FERMGEN™.

saccharolytic and proteolytic industry enzymes. The results demonstrated the challenge of the utilization of such structurally complex heteroglycans. Yet, a multi-product biorefinery concept including a utilization of the residual biomass as enzymatic hydrolysate seems feasible.

CRediT authorship contribution statement

Korbinian Sinzinger: Conceptualization, Methodology, Investigation, Writing – original draft. **Doris Schieder:** Conceptualization, Project administration, Supervision, Writing – review & editing. **Broder Rühmann:** Methodology, Supervision, Writing – review & editing. **Volker Sieber:** Supervision, Funding acquisition, Writing – review & editing.

Declaration of competing interest

There are no additional relationships, no patents, and no additional activities to disclose.

Acknowledgements

The project Joint Research on "Natural Compounds from Cyanobacteria" as a Model of Cross-Border Scientific Partnership (Interreg ZIEL ETZ Cross- Border cooperation Czech-Bavaria, 2017 - 2020, project no. 41) was funded by the European Union. Many thanks to Algatech, The Czech Academy of Sciences, Třeboň, for providing the biomass.

Appendix A. Supplementary data

Supplementary data to this article can be found online at https://doi.org/10.1016/j.algal.2022.102744.

References

[1] S. Aikawa, K. Inokuma, S. Wakai, K. Sasaki, C. Ogino, J.-S. Chang, T. Hasunuma, A. Kondo, Direct and highly productive conversion of cyanobacteria Arthrospira platensis to ethanol with CaCl2 addition, Biotechnol. Biofuels 11 (1) (2018), https://doi.org/10.1186/s13068 018 1050 y.

[2] T. J. Chow, H. Y. Su, T.-Y. Tsai, H. H. Chou, T. M. Lee, J. S. Chang, Using recombinant cyanobacterium (Synechococcus elongatus) with increased carbohydrate productivity as feedstock for bioethanol production via separate hydrolysis and fermentation process, Bioresour. Technol. 184 (2015) 33–41, eng.

[3] G.A. Cuevas-Castillo, F.S. Navarro-Pineda, S.A. Baz Rodríguez, J.C. Sacramento Rivero, Advances on the processing of microalgal biomass for energy-driven biorefineries, Available from, Renew. Sustain. Energy Rev. [Internet] 125 (2020), https://doi.org/10.1016/j.rser.2019.109606, https://www.scopus.com/inward/record.uri?eid=2 s2.0 85082121243&doi=10.1016%2fj.rser.2019.109606&partnerID=40&md5=a8f874882129ffc2462154e33deb4ca1.

[4] K.B. Möllers, D. Cannella, H. Jørgensen, N.-U. Frigaard, Cyanobacterial biomass as carbohydrate and nutrient feedstock for bioethanol production by yeast fermentation, Biotechnol. Biofuels [Internet] 7 (2014) 64, https://doi.org/10.1186/1754-6834-7-64, eng.

[5] Y. Tang, J.N. Rosenberg, P. Bohutskyi, G. Yu, M.J. Betenbaugh, F. Wang, Microalgae as a feedstock for biofuel precursors and value-added products: green fuels and golden opportunities, BioResources [Internet]. 11 (1) (2015), https://doi.org/10.15376/biores.11.1.Tang.

[6] S.S. Rahpeyma, J. Raheb, Microalgae biodiesel as a valuable alternative to fossil fuels, Available from, Bioenergy Res. [Internet] 12 (4) (2019) 958–965, https://doi.org/10.1007/s12155-019-10033-6, https://www.scopus.com/inward/record.uri?eid=2 s2.0 85071294684&doi=10.1007%2fs12155 019 10033 6&partnerID=40&md5=45efbd79ed6b31184b1e3b4864edf66d.

[7] A.K. Koyande, P.-L. Show, R. Guo, B. Tang, C. Ogino, J.-S. Chang, Bio-processing of algal bio-refinery: A review on current advances and future perspectives, Bioengineered [Internet] 10 (1) (2019) 574–592, https://doi.org/10.1080/21655979.2019.1679697. Available from.

[8] G.P. Lam, M.H. Vermuë, Eppink MHM, R.H. Wijffels, C. van den Berg, Multi-product microalgae biorefineries: from concept towards reality, Available from, Trends Biotechnol. [Internet] 36 (2) (2018) 216–227, https://doi.org/10.1016/j.tibtech.2017.10.011, http://www.sciencedirect.com/science/article/pii/S0167779917302755.

[9] K. Saurav, M. Macho, A. Kust, K. Delawská, J. Hájek, P. Hrouzek, Antimicrobial activity and bioactive profiling of heterocytous cyanobacterial strains using MS/MS-based molecular networking, Folia Microbiol. 64 (5) (2019) 645–654, eng.

[10] Z.U. Rehman, A.K. Anal, Enhanced lipid and starch productivity of microalga (Chlorococcum sp. TISTR 8583) with nitrogen limitation following effective pretreatments for biofuel production, eng. Available from, Biotechnol. Rep. [Internet] 21 (2019), e00298, https://doi.org/10.1016/j.btre.2018.e00298, https://www.sciencedirect.com/science/article/pii/s2215017x18302388.

[11] Laurens LML, N. Nagle, R. Davis, N. Sweeney, S. van Wychen, A. Lowell, P. T. Pienkos, Acid-catalyzed algal biomass pretreatment for integrated lipid and carbohydrate-based biofuels production, en. Available from, Green Chem. [Internet] 17 (2) (2015) 1145–1158, https://doi.org/10.1039/C4GC01612B, https://pubs.rsc.org/en/content/articlehtml/2015/gc/c4gc01612b.

[12] K. Ullah, M. Ahmad, Sharma V.K. Sofia, P. Lu, A. Harvey, M. Zafar, S. Sultana, C. N. Anyanwu, Algal biomass as a global source of transport fuels: overview and development perspectives, Available from, Progr. Nat. Sci. Mater. Intl. [Internet] 24 (4) (2014) 329–339, https://doi.org/10.1016/j.pnsc.2014.06.008, https://www.sciencedirect.com/science/article/pii/s1002007114000860.

[13] W. L. Chu, Strategies to enhance production of microalgal biomass and lipids for biofuel feedstock, Eur. J. Phycol. [Internet] 52 (4) (2017) 419–437, https://doi.org/10.1080/09670262.2017.1379100.

[14] K.M. Rahman, Food and high value products from microalgae: market opportunities and challenges [Internet], in: Microalgae Biotechnology for Food, Health and High Value Products, Springer, Singapore, 2020, pp. 3–27, https://doi.org/10.1007/978-981 15-0169-2_1, en. Available from.

[15] M.R. Tredici, L. Rodolfi, N. Biondi, N. Bassi, G. Sampietro, Techno-economic analysis of microalgal biomass production in a 1 ha Green Wall Panel (GWP®) plant, Available from, Algal Res. [Internet] 19 (2016) 253–263, https://doi.org/10.1016/j.algal.2016.09.005, http://www.sciencedirect.com/science/article/pii/S2211926416303320.

[16] N.H. Thuan, T.T. An, A. Shrestha, N.X. Canh, J.K. Sohng, D. Dhakal, Recent advances in exploration and biotechnological production of bioactive compounds in three Cyanobacterial genera: Nostoc lyngbya, and microcystis, Front. Chem. [Internet]. 7 (2019) 604, https://doi.org/10.3389/fchem.2019.00604, eng.

[17] A. Fidor, R. Konkel, H. Mazur Marzec, Bioactive peptides produced by Cyanobacteria of the genus nostoc: a review, Mar. Drugs [Internet] 17 (10) (2019) 561, https://doi.org/10.3390/md17100561, eng.

[18] J. Ruiz, G. Olivieri, J. de Vree, R. Bosma, P. Willems, J.H. Reith, M.H.M. Eppink, D. M.M. Kleinegris, R.H. Wijffels, M.J. Barbosa, Towards industrial products from microalgae, Energy Environ. Sci. 9 (10) (2016) 3036–3043, https://doi.org/10.1039/C6EE01493C.

[19] B. Nowruzi, S. Haghighat, H. Fahimi, E. Mohammadi, Nostoc cyanobacteria species: A new and rich source of novel bioactive compounds with pharmaceutical potential, J. Pharm. Health Serv. Res. 9 (1) (2018) 5–12, https://doi.org/10.1111/jphs.12202.

[20] M.H. Bule, I. Ahmed, F. Maqbool, M. Bilal, Iqbal HMN, Microalgae as a source of high-value bioactive compounds, Front. Biosci. 10 (1) (2018) 197–216, https://doi.org/10.2741/s509 (Scholar edition) [Internet].

[21] S. Mobin, F. Alam, Some promising microalgal species for commercial applications: a review, Available from, Energy Procedia [Internet] 110 (2017) 510–517, https://doi.org/10.1016/j.egypro.2017.03.177, https://www.sciencedirect.com/science/article/pii/s1876610217302072.

[22] S.S. Costa, A.L. Miranda, B.B. Andrade, C.O. Souza, Morais MGD, Costa JAV, J. I. Druzian, D.J. de Assis, Influence of nitrogen on growth, biomass composition, production, and properties of polyhydroxyalkanoates (PHAs) by microalgae, Available from, Int. J. Biol. Macromol. [Internet] 116 (2018) 552–562, https://doi.org/10.1016/j.ijbiomac.2018.05.064, https://www.sciencedirect.com/science/article/pii/S0141813018314132.

[23] G. Pierre, C. Laroche, P. Michaud, C. Delattre, Production, extraction and characterization of microalgal and cyanobacterial exopolysaccharides, Available from, Biotechnology Advances 34 (7) (2016) 1159–1179, https://doi.org/10.1016/j.biotechadv.2016.08.001, https://www.sciencedirect.com/science/article/pii/S0734975016300921.

[24] K.W. Chew, J.Y. Yap, P.L. Show, N.H. Suan, J.C. Juan, T.C. Ling, D.-J. Lee, J.-S. Chang, Microalgae biorefinery: high value products perspectives, Available from, Bioresour. Technol. [Internet] 229 (2017) 53–62, https://doi.org/10.1016/j.biortech.2017.01.006, https://www.sciencedirect.com/science/article/pii/S0960852417300263.

[25] S.M. Zahraee, N. Shiwakoti, P. Stasinopoulos, Biomass supply chain environmental and socio-economic analysis: 40-Years comprehensive review of methods, decision issues, sustainability challenges, and the way forward, Available from, Biomass and Bioenergy 142 (2020), 105777, https://doi.org/10.1016/j.biombioe.2020.105777, http://www.sciencedirect.com/science/article/pii/S0961953420303123.

[26] Veela B. Mehta, B.S. Vaidya, Cellular and extracellular polysaccharides of the blue-green Alga Nostoc, Journal of Experimental Botany 29 (113) (1978) 1423–1430. Available from.

[27] J.G. Ortiz-Tena, B. Rühmann, D. Schieder, V. Sieber, Revealing the diversity of algal monosaccharides: fast carbohydrate fingerprinting of microalgae using crude biomass and showcasing sugar distribution in Chlorella vulgaris by biomass fractionation, Algal Res. 17 (227–235) (2016), https://doi.org/10.1016/j.algal.2016.05.008.

[28] J. Demay, C. Bernard, A. Reinhardt, B. Marie, Natural products from Cyanobacteria: focus on beneficial activities, Mar. Drugs [Internet] 17 (6) (2019) 320, https://doi.org/10.3390/md17060320, eng.

[29] Y. Liu, P. Su, J. Xu, S. Chen, J. Zhang, S. Zhou, Y. Wang, Q. Tang, Y. Wang, Structural characterization of a bioactive water-soluble heteropolysaccharide from Nostoc sphaeroids kütz, Available from, Carbohydr. Polym. [Internet] 200 (2018) 552–559, https://doi.org/10.1016/j.carbpol.2018.08.034, https://www.sciencedirect.com/science/article/pii/S0144861718309329.

[30] K. Kanekiyo, J.-B. Lee, K. Hayashi, H. Takenaka, Y. Hayakawa, S. Endo, T. Hayashi, Isolation of an Antiviral Polysaccharide, Nostoflan, from a Terrestrial Cyanobacterium, Nostoc flagelliforme, J. Nat. Prod. [Internet]. 68 (7) (2005) 1037–1041, https://doi.org/10.1021/np050056c 10.1021/np050056c. Available from.

[31] R.F. Helm, Z. Huang, D. Edwards, H. Leeson, W. Peery, M. Potts, Structural characterization of the released polysaccharide of desiccation-tolerant Nostoc commune DRH-1, Available from, J. Bacteriol. [Internet] 182 (4) (2000) 974–982, https://doi.org/10.1128/JB.182.4.974-982.2000, https://jb.asm.org/content/182/4/974.

[32] Lieve M.L. Laurens, Summative Mass Analysis of Algal Biomass – Integration of Analytical Procedures: Laboratory Analytical Procedure (LAP), Technical report NREL/TP-5100-60943 (revised) [Internet], Available from, National Renewable Energy Laboratory, Golden, CO, USA, 2015, https://www.nrel.gov/docs/fy16osti/60943.pdf.

[33] S. Houda, E. Akao, S. Suzuki, M. Okuda, K. Kakehi, J. Nakamura, High-performance liquid chromatography of reducing carbohydrates as strongly ultraviolet-absorbing and electrochemically sensitive 1-phenyl-3-methyl5-pyrazolone derivatives, Available from, Analytical Biochemistry 180 (2) (1989) 351–357, https://doi.org/10.1016/0003-2697(89)90444-2, http://www.sciencedirect.com/science/article/pii/0003269789904442.

[34] B. Rühmann, J. Schmid, V. Sieber, Fast carbohydrate analysis via liquid chromatography coupled with ultra violet and electrospray ionization ion trap detection in 96 well format, J. Chromatogr. A 1350 (2014) 44–50, eng.

[35] Stefanie Van Wychen, M.L. Lieve, Laurens: NREL., Determination of Total Solids and Ash in Algal Biomass: Laboratory Analytical Procedure (LAP), Technical report NREL/TP-5100-60956 (revised), National Renewable Energy Laboratory, Golden, CO (United States) [Internet]. (2015). Available from: https://www.nrel.gov/docs/fy16osti/60956.pdf.

[36] Megazyme, Total Starch Assay Procedure (Amyloglucosidase/α-Amylase Method) K-TSTA 09/14, Available from, Megazyme International [Internet], Bray, County Wicklow, Ireland, 2014, https://secure.megazyme.com/files/booklet/k-tsta_data.pdf.

[37] S.O. Lourenço, E. Barbarino, P.L. Lavín, U.M. Lanfer Marquez, E. Aidar, Distribution of intracellular nitrogen in marine microalgae: calculation of new nitrogen-to-protein conversion factors, Eur. J. Phycol. 39 (1) (2004) 17–32, https://doi.org/10.1080/0967026032000157156.

[38] S. van Wychen, K. Ramirez, Laurens LML, Determination of Total Lipids as Fatty Acid Methyl Esters (FAME) by In Situ Transesterification: Laboratory Analytical Procedure (LAP), Technical report NREL/TP-5100-60958 (revised), [Internet]., English. Available from, National Renewable Energy Laboratory, Golden, Co, USA, 2015, https://www.nrel.gov/docs/fy16osti/60958.pdf.

[39] Z. Huang, Y. Liu, B.S. Paulsen, D. Klaveness, Studies on polysaccharides from three edible species of Nostoc (cyanobacteria) with different colony morphologies: comparison of monosaccharide composition and viscosities of polysaccharides from field colonies and suspension cultures, J. Phycol. 34 (6) (1998) 962–968, https://doi.org/10.1046/j.1529-8817.1998.340962.x.

[40] T. Fernandes, I. Fernandes, Andrade CAP, A. Ferreira, N. Cordeiro, Marine microalgae monosaccharide fluctuations as a stress response to nutrients inputs, Available from, Algal Res. [Internet] 24 (2017) 340–346, https://doi.org/10.1016/j.algal.2017.04.023, https://www.sciencedirect.com/science/article/pii/S2211926416306774.

[41] K.K. De, T. Timell E, The acid hydrolysis of glycosides: IV: Hydrolysis of aldobiouronic acids, Carbohydr. Res. [Internet] 4 (1967) 177–181, https://doi.org/10.1016/S0008-6215(00)82576-8.

[42] H.S. Kim, C. G. Lee, E.Y. Lee, Alginate lyase: Structure, property, and application, Biotechnology and Bioprocess Engineering 16 (5) (2011) 843, https://doi.org/10.1007/s12257-011-0352-8. Available from.

[43] M. Franklin, D. Nivens, J. Weadge, P. Howell, Biosynthesis of the Pseudomonas aeruginosa Extracellular Polysaccharides, Alginate, Pel, and Psl, Available from: Front. Microbiol. [Internet] 10.3389/fmicb.2011.00167 (2011;2:167.) https://www.frontiersin.org/article/10.3389/fmicb.2011.00167.

[44] M.F. Raposo, Morais AMMB, R. Morais, Bioactivity and applications of polysaccharides from marine microalgae, Available from, Mar Drugs [Internet] 11 (1) (2013) 233–252, https://doi.org/10.3390/md11010233. https://web.archive.org/web/20170814105640id_/http://repositorio.ucp.pt/bitstream/10400.14/17443/1/RMorais_Bioactivity_Springer.pdf.

[45] D. Norena-Caro, M.G. Benton, Cyanobacteria as photoautotrophic biofactories of high-value chemicals, Available from, Journal of CO2 Utilization 28 (2018) 335–366, https://doi.org/10.1016/j.jcou.2018.10.008, https://www.sciencedirect.com/science/article/pii/S2212982018303585.

[46] R. de Philippis, C. Sili, R. Paperi, M. Vincenzini, Exopolysaccharide-producing cyanobacteria and their possible exploitation: A review, J. Appl. Phycol. [Internet] 13 (4) (2001) 293–299, https://doi.org/10.1023/A:1017590425924.

[47] A.N. Bader, L.S. Rizza, V.F. Consolo, L. Curatti, Efficient saccharification of microalgal biomass by Trichoderma harzianum enzymes for the production of ethanol, Available from, Algal Res. [Internet] 48 (2020), 101926, https://doi.org/10.1016/j.algal.2020.101926, https://www.sciencedirect.com/science/article/pii/S2211926420301296.

4.2. The *Pichia pastoris* enzyme production platform: From combinatorial library screening to bench-top fermentation on residual cyanobacterial biomass

Authors: Korbinian Sinzinger, Ulrike Obst, Samed Güner, Manuel Döring, Magdalena Haslbeck, Doris Schieder, Volker Sieber;

This manuscript outlines an innovative approach to enzyme production using the yeast *Pichia pastoris*. This study focuses on creating a sustainable biorefinery platform by utilizing cyanobacterial biomass as feedstock, which is an important step towards greener industrial processes. We developed a combinatorial library to facilitate the engineering of *P. pastoris*, screening for optimal conditions for enzyme production. In this manuscript, we focus on producing phytase, an enzyme of significant industrial relevance. The high-throughput screening of the combinatorial library allowed for the identification of genetic constructs that maximize enzyme expression and secretion. The study demonstrated successful fermentation using a hydrolysate from *Nostoc* sp. De1 cyanobacterial biomass. The engineered *P. pastoris* strains were tested in various cultivation conditions, including shake flask experiments and bench-top batch and fed-batch fermentations. The best-performing strain achieved a phytase activity exceeding 7000 U/mL in fed-batch fermentation over three days. This high level of enzyme activity underscores the potential of utilizing this *Pichia* toolkit. Also, the cyanobacterial biomass proved itself as a viable and sustainable feedstock for industrial enzyme production. The results indicate that the engineered strains and optimized fermentation conditions can significantly enhance the efficiency of enzyme production.

The study emphasizes the potential for cyanobacterial biomass to serve as a cost-effective and renewable feedstock, reducing the environmental impact of enzyme production processes. Overall, the research highlights the importance of integrating synthetic biology, microbiology, and bioprocess engineering to develop sustainable bioproduction platforms. This multidisciplinary approach can address global challenges related to sustainable industrial processes, offering promising solutions for the future.

The two authors Korbinian Sinzinger and Ulrike Obst contributed equally to this publication. Ulrike Obst conducted all the experiments of molecular cloning, library assembly, and strain screening. Korbinian Sinzinger designed and conducted all experiments of hydrolytic enzyme screening, growth screening and fermentations in shake flasks and bench-top reactors. Both authors wrote the original draft. Samed Güner, Manuel Döring, and Magdalena Haslbeck contributed to different experiments and conceptualization. Doris Schieder contributed to the conceptualization, reviewed, and edited the manuscript. Volker Sieber contributed to reviewing and editing the manuscript.

The supplemental information for this publication can be found in the appendix, section 6.2

The Pichia pastoris enzyme production platform: From combinatorial library screening to bench-top fermentation on residual cyanobacterial biomass

Korbinian Sinzinger, Ulrike Obst, Samed Güner, Manuel Döring, Magdalena Haslbeck, Doris Schieder, Volker Sieber

Journal of Bioresources and Bioproducts

2023

https://doi.org/10.1016/j.jobab.2023.12.005

Journal of Bioresources and Bioproducts 9 (2024) 43–57

Contents lists available at ScienceDirect

Journal of Bioresources and Bioproducts

journal homepage: https://www.keaipublishing.com/en/journals/journal-of-bioresources-and-bioproducts/

Research Article

The *Pichia pastoris* enzyme production platform: From combinatorial library screening to bench-top fermentation on residual cyanobacterial biomass

Korbinian Sinzinger[a,1], Ulrike Obst[a,1], Samed Güner[a], Manuel Döring[a], Magdalena Haslbeck[a], Doris Schieder[a,*], Volker Sieber[a,b,c,d]

[a] *Chair of Chemistry of Biogenic Resources, Campus Straubing for Biotechnology and Sustainability, Technical University of Munich, Straubing 94315, Germany*
[b] *Catalysis Research Center, Technical University of Munich, Garching 85748, Germany*
[c] *SynBiofoundry@TUM, Technical University of Munich, Straubing 94315, Germany*
[d] *School of Chemistry and Molecular Biosciences, The University of Queensland, St. Lucia 4072, Australia*

ARTICLE INFO

Keywords:
Protein secretion
Phytase
Cyanobacterial biomass
Fed-batch fermentation
Pichia pastoris

ABSTRACT

The demand for industrial enzymes is continually rising, fueled by the growing need to shift towards more sustainable industrial processes. However, making efficient enzyme production strains and identifying optimal enzyme expression conditions remains a challenge. Moreover, the production of the enzymes themselves comes with unavoidable impacts, e.g., the need to utilize secondary feedstocks. Here, we take a more holistic view of bioprocess development and report an integrative approach that allows us to rapidly identify improved enzyme expression and secretion conditions and make use of cyanobacterial waste biomass as feed for supporting *Pichia pastoris* fermentation. We demonstrate these capabilities by producing a phytase secreted by *P. pastoris* that is grown on cyanobacterium hydrolysate and buffered glycerol-complex (BMGY) medium, with genetic expression conditions identified by high-throughput screening of a randomized secretion library. When our best-performing strain is grown in a fed-batch fermentation on BMGY, we reach over 7 000 U/mL in three days.

1. Introduction

The transition to a sustainable global society requires greener industrial production processes, including the biochemical valorization of biomass as renewable feedstock. Integrated multi-product biorefinery concepts are needed to overcome the hurdles for profitable commercialization. In a biorefinery concept, biomass is converted efficiently into multiple marketable products, such as fuels, chemicals or enzymes. Among others, this requires a multi-field research approach to handle the complex interplay of developing microbial hosts that can convert residual biomass to valuable products, upcycling a feed to make it accessible for the hosts and engineering the hosts to produce valuable products.

Microalgae and cyanobacteria are a promising renewable feedstock for fermentation processes that deliver high-value compounds (Chandra et al., 2019; Mitra and Mishra, 2019; de Farias Silva et al., 2019). These photosynthetic microorganisms can grow and multiply using light as energy and CO_2 as a carbon source (Chandra et al., 2019). They are characterized by their more rapid growth compared to terrestrial plants and do not require arable land or freshwater; hence don't compete with plant-based food or feed

* Corresponding author.
E-mail address: doris.schieder@tum.de (D. Schieder).
[1] Korbinian Sinzinger and Ulrike Obst contributed equally to this work and should be considered co-first authors.

https://doi.org/10.1016/j.jobab.2023.12.005

Available online 26 December 2023

(de Farias Silva et al., 2019). Cyanobacteria are Gram-negative prokaryotes with a structured cell envelope, but their cell wall contains a peptidoglycan layer, which more closely resembles that of Gram-positive bacteria. Hence, carbohydrates entrapped within the cell wall or stored intracellularly in the form of starch/glycogen are easily degraded by enzymatic hydrolysis and accessible as fermentation substrates (Choi et al., 2010; Möllers et al., 2014). Here, we use the previously investigated biomass of the cyanobacterium species *Nostoc* sp. De1 to produce an enzymatic hydrolysate suitable for fermentation (Sinzinger et al., 2022). However, challenges exist due to the filamentous growth and the presence of bioactive components in *Nostoc* colonies, necessitating the selection of a robust organism for fermentation (Briones-Nagata et al., 2007).

The *Pichia pastoris* (*Komagataella phaffii*) is a methylotrophic yeast known for its robustness and widespread use in protein production processes for various applications. Its advantages include microbial safety, rapid growth to high-cell densities, and ease of genetic manipulation. The *P. pastoris* supports efficient protein secretion, allowing for complex folding processes and facilitating downstream purification (Delic et al., 2013; Zang et al., 2021). Despite extensive engineering efforts of the yeast secretion system, process development remains challenging due to many cross-reacting factors. We focused on the expression and secretion of phytases, crucial enzyme additives in animal feed, which hydrolyze phytate ester bonds, improving phosphate and mineral uptake and reducing environmental pollution (Chen et al., 2015). The phytase market has exceeded 300 million US dollar and continues to grow about 10 % per year with an ongoing interest in enhancing the substrate specificity, catalytic efficiency, and thermostability to improve the pH profile and reduce production costs (Chen et al., 2015; Herrmann et al., 2019). Phytases aimed for the feed and food industry are sold from 1 to 5 US dollar per kg (David, 2018).

Variant libraries using differing genetic designs are usually screened to identify suitable protein expression and secretion conditions. To assist in the design of *P. pastoris* secretion libraries, we previously developed a toolkit of regulatory elements (PTK), which included promoters, secretion signal peptides, and a terminator (Obst et al., 2017). Standardization was key to ensuring parts were interchangeable for creating randomized libraries and multi-component systems (Canton et al., 2008). The PTK follows the widely used Modular Cloning (MoClo) design rules of the *Saccharomyces cerevisiae* Yeast toolkit (YTP) (Lee et al., 2015). Rajkumar et al. (2019) further expanded the number of interchangeable parts available with their toolkit specific for *Kluyveromyces marxianus*, enabling 552 options for a gene to be expressed intracellularly and over 55 000 possibilities if secreted (when these three matching toolkits are combined). Additional expression options arise when parts from other toolkits with different designs are considered, e.g., the promoter toolbox from Vogl et al. (2016), the GoldenPiCS toolkit from Prielhofer et al. (2017), or the secretion toolkits for other methylotrophic yeast from Celińska et al. (2018) for *Yarrowia lipolytica* and from Yarimizu et al. (2015) for *K. marxianus*. The challenge that arises from using these libraries is the lack of methods to screen the resultant designs efficiently for *P. pastoris* because the construction and evaluation of each design individually would be too slow and costly to perform.

Here, we studied four different phytases that previously were successfully expressed in *P. pastoris*: three fungal phytases (PhyA) from *Aspergillus niger* (Han and Lei, 1999), *Thielavia heterothallica* (Ranjan and Satyanarayana, 2016), *Peniophora lycii* (Xiong et al., 2005) and a bacterial phytase (periplasmic phosphoanhydride phosphatase, AppA) from *Escherichia coli* (Akbarzadeh et al., 2015). We took a comprehensive approach, considering all major factors for enzyme production by *P. pastoris* in buffered glycerol-complex (BMGY) medium and showing a proof of principle process that uses cyanobacterial biomass as feedstock. An overview of the study is given in Fig. 1, outlining the process from library design and screening to fed-batch fermentation. We tackled the bottleneck of screening by developing a combinatorial library to facilitate easy *P. pastoris* engineering. The workflow comprised three main steps: plasmid library assembly from toolkit plasmids using Golden Gate shuffling (Engler et al., 2009), yeast transformation and colony isolation, and library screening for identifying best performs. In addition, we demonstrated the successful fermentation of *P. pastoris* in *Nostoc* sp. De1 hydrolysate for AppA *E. coli* phytase expression in flasks and 1 L bench top scales. In the 1 L reactor system, we determine the strain-specific growth kinetics in batch and pulsed batch fermentation in BMGY medium and finally develop a fed-batch fermentation strategy in BMGY medium concluded by a process evaluation.

This is the first time the PTK has been used to generate a diverse library of expression constructs to optimize a broader bioprocess that is able to utilize a sustainable feedstock. It also demonstrates the ability for *P. pastoris*, an industrial workhorse, to productively grow on cyanobacterium hydrolysate, enabling a new source for sustainable bioproduction. More broadly, this work highlights the innovation that is possible when combining technologies from synthetic biology, microbiology, and bioprocess development to create end-to-end solutions for challenging problems.

2. Material and methods

2.1. Chemicals, Nostoc biomass and enzymes

All chemicals were, unless otherwise stated, purchased in analytical grade from Sigma Aldrich (Germany), Merck KGaA (Germany) and Carl Roth GmbH (Germany). Freeze dried whole cells from *Nostoc* sp. De1 was kindly provided by Centre Algatech, Institute o f Microbiology, The Czech Academy of Sciences (Třeboň). The following enzyme mixtures were used: DISTILLASE® CS (amyloglucosidase & α-amylase) and FERMGEN^{TM} (protease) from Genencore, and Viscozyme® L (cellolytic) purchased from Sigma Aldrich.

2.2. The DNA plasmids and molecular cloning

Part plasmids used in this study originated from either the Yeast Toolkit (YTK, Addgene Kit: 1000000061, Cambridge, MA, USA) (Lee et al., 2015), the PTK (Addgene Kit: 1000000108) (Obst et al., 2017), were ordered from Twist Bioscience (Santa Clara, CA, USA)

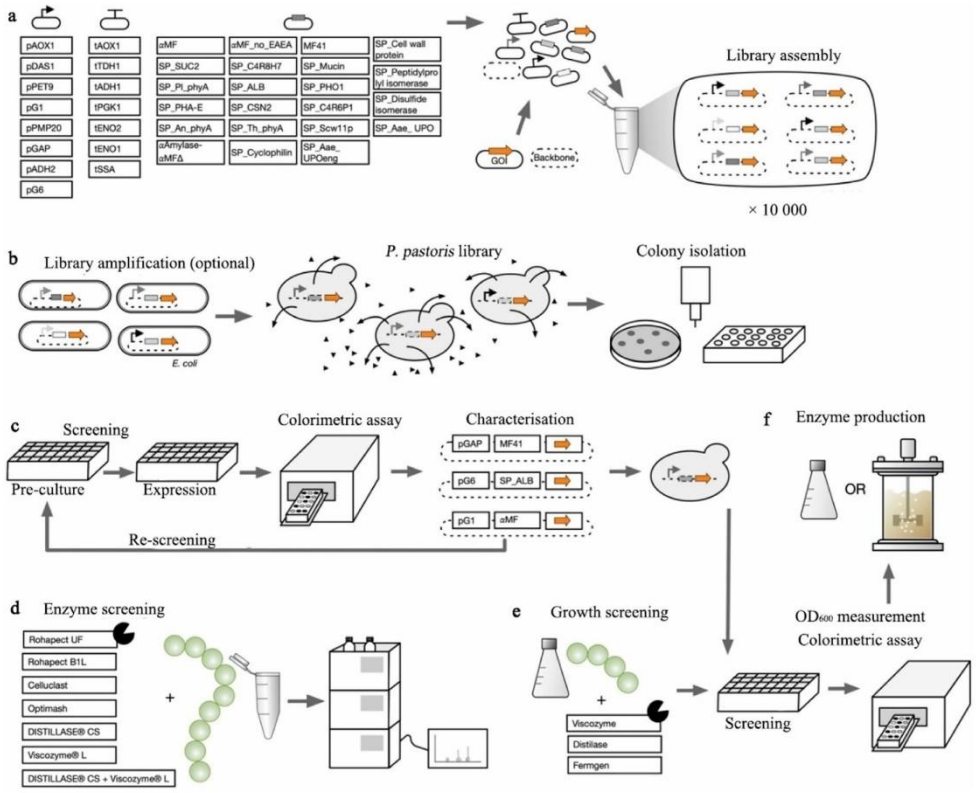

Fig. 1. Overview of work conducted in this study. (a) development of a combinatorial library to facilitate easy *Pichia pastoris* engineering; (b) characterization of the library components. (c) library screenings for industrially relevant phytase enzyme production; (d) investigate preparation of enzymatic hydrolysate from *Nostoc* sp. De1 biomass; (e) demonstration of successful fermentation of *P. pastoris* in this hydrolysate for periplasmic phosphoanhydride phosphatase (AppA) *Escherichia coli* phytase expression; (f) development of a fed-batch fermentation strategy in a 1 L format.

or were constructed by standard molecular cloning techniques. Constructed part plasmids were made with gene fragments (Twist Bioscience) or polymerase chain reaction (PCR) fragments integrated into the pYTP001 backbone vector using Golden Gate assembly with enzymes from New England BioLabs (Beverly, Massachusetts, USA).

Expression libraries were built from part plasmids encoding each functional element and inserted into the backbone vector pPTK051 (made in this study, 4 327 bp in size). Assembly was performed using a Golden Gate reaction (37 °C, 10 min; 50 × (37 °C, 5 min; 16 °C, 5 min); 37 °C, 10 min; 65 °C, 10 min) with T4 ligase and BsaI (Engler et al., 2009). The total concentration of each insert was twice that of the backbone vector pPTK051. For the generation of randomized libraries via shuffling, the DNA concentration of each insert was the total amount of insert divided by the number of plasmids used in the assembly. For example, when using 300 fmol of insert and three different plasmids for shuffling, 100 fmol of each plasmid was used in the assembly.

For the phytase shuffling, an assembly reaction was assembled containing: 20 secretion signals, a terminator part and a linearized backbone from the PTK. This was split into two equally sized reactions to which the respective promoter parts for induced (pAOX1, pDAS1, pPMP20) and constitutive (pGAP, pPET9, pG1, pG6, pADH2) expression were added. These reaction mixes were then each split again into 4 reactions to which the phytases were added. The final reaction mixtures contained: 50 fmol backbone, 100 fmol for each functional part, restriction enzyme, and T4 ligase. Following the Golden Gate reaction, *E. coli* DH5α (Thermo Fisher Scientific, Waltham, MA, USA) or NEB Turbo (New England Biolabs, Ipswich, MA, USA) cells were chemically transformed and grown in lysogeny broth (LB) with relevant antibiotics (25 mg/mL chloramphenicol, 30 mg/mL kanamycin sulfate).

2.3. The P. pastoris strain and transformation

For *P. pastoris attP* (NRRL Y-11430 + *attP* recombinase target site) transformation, competent cells were prepared as described by Madden et al. (2015) and stored at –80 °C until use. Competent cells were combined with 200–500 ng of the BxbI plasmid (Perez-Pinera et al., 2016) and 200–500 ng of the circular expression vector in a 1 mm electroporation cuvette. The reaction mixture was then pulsed at 1 800 V, 25 μF, 200 Ohm (Micro Pulser Electroporator, Bio-Rad Laboratories GmbH, München, Germany) and 1 mL *Pichia* electroporation recovery solution (PERS, 50 % (*V/V*) yeast extract peptone dextrose (YPD), 50 % (*V/V*) 1 mol/L sorbitol) was added. Everything was then transferred into a 2 mL cup for recovery through growth at 30 °C, 100 r/min for 3.5 h. Following this, 100 μL of the cell solution and the cell pellet (8 000 r/min, 30 s; Heraeus Fresco 21 Centrifuge, Thermo Fisher Scientific, Waltham, MA, USA) were plated on YPD media (2 % peptone, 2 % glucose and 1 % yeast extract) containing 75 μg/mL zeocin. The Golden Gate reaction was used directly for *P. pastoris* transformation for strains pUO_pL730–pUO_pL771. Red fluorescent protein (RFP) and yeast-enhanced green fluorescent protein (yEGFP) expression strains previously prepared were used for Reference Obst et al. (2017).

2.4. The P. pastoris cultivation condition

General *P. pastoris* growth was carried out using YPD media. For protein expression, cells were grown in either buffered glycerol/methanol-complex (BMGY/BMMY) or buffered minimal dextrose/methanol (BMD/BMM) media with modifications. Zeocin was added (75 μg/mL final concentration) to the media except when assessing the growth of the wild-type strain.

2.4.1. Strain characterizations and screening

The screening was performed in 96-well deep-well plates with incubation at 30 °C and 900 r/min (Weis et al., 2004). Pre-cultures were inoculated using an automated colony picker (Norgren Systems, Fairlea, WV, USA) from glycerol stocks and grown for 48 h. Constitutive or induced expression cultures were inoculated from this pre-culture using an automated liquid handling platform (Tecan Group Ltd., Männedorf, Switzerland; MCA96 multi-channel arm). While the expression plates were incubated, methanol was added to induce expression in the cultures every 24 h to ensure 1 % (*V/V*) methanol was maintained throughout.

The RFP and yEGFP expression was monitored as described in Qin et al. (2011). Specifically, 900 μL of 0.2 % BMD glucose pre-culture consisting of 100 mmol/L potassium phosphate, 1.34 % (*w/V*) yeast nitrogen base, 0.000 04 % (*w/V*) biotin, 0.2 % (*w/V*) glucose was inoculated manually from a glycerol stock. The expression culture in 1 % BMD glucose (100 mmol/L potassium phosphate, 1.34 % (*w/V*) yeast nitrogen base, 0.000 04 % (*w/V*) biotin, 1 % (*w/V*) glucose) or 1 % BMM methanol (100 mmol/L potassium phosphate, 1.34 % (*w/V*) yeast nitrogen base, 0.000 04 % (*w/V*) biotin, 1 % (*w/V*) methanol] was inoculated with 30 μL of the pre-culture and incubated for 48 h before measurements were taken.

The phytase screening was performed as in Hesampour et al. (2015). Specifically, a 96-well agar plate was used to inoculate 1.2 mL pre-culture, of which 100 μL was used as inoculant for 900 μL of the expression-culture. This was then incubated for 48 h. For inducible expression, the pre-culture was 2 % BMGY-PP (BMGY-phosphate buffer, 1 % (*w/V*) yeast extract, 2 % (*w/V*) peptone, 1.34 % (*w/V*) yeast nitrogen base, 0.000 04 % (*w/V*) biotin, 2 % (*V/V*) glycerol), the expression-culture 1 % BMMY-PP [1 % (*w/V*) yeast extract, 2 % (*w/V*) peptone, 1.34 % (*w/V*) yeast nitrogen base, 0.000 04 % (*w/V*) biotin, 1 % (*V/V*) methanol]. For methanol induction, 10 % BMMY-PP (1 % (*w/V*) yeast extract, 2 % (*w/V*) peptone, 1.34 % (*w/V*) yeast nitrogen base, 0.000 04 % (*w/V*) biotin, 10 % (*V/V*) methanol] was added after 24 h of expression to maintain 1 % (*V/V*) methanol throughout the experiment. For constitutive expression, the pre-culture was 0.4 % BMGY-PP (1 % (*w/V*) yeast extract, 2 % (*w/V*) peptone, 1.34 % (*w/V*) yeast nitrogen base, 0.000 04 % (*w/V*) biotin, 0.4 % (*V/V*) glycerol) and the expression-culture 2 % BMGY-PP. To determine OD_{600} and create cryo-cultures, 180 μL 16.66 % (*V/V*) glycerol was mixed with 20 μL sample in flat bottom assay plates, OD_{600} was measured (Infinite 200 pro microplate reader, Tecan Group Ltd., Männedorf, Switzerland), and plates were stored at –80 °C.

2.4.2. Shake flask experiments

The *P. pastoris* cultivation was done in 50 mL shake flasks, starting with 10 mL pre-culture of 0.4 % BMGY (from here on forth -PP) for 48 h at 30 °C and 150 r/min inoculated from an agar plate. The 10 mL expression cultures in BMGY/BMD or pure hydrolysate with 2 % (*w/V*) glycerol or glucose were inoculated with 1 mL of pre-culture and again incubated for 48 h at 30 °C and 150 r/min. The OD_{600} was measured using an Ultraspec 10 spectrophotometer (Amersham Bioscience, UK). The cultures were transferred to 15 mL Falcon® tubes and subsequently the samples were centrifuged at 500 × g for 10 min. The supernatants were then analyzed with the Bradford assay using bovine serum albumin (BSA) as standard for protein content and the phytase activity was determined as described below.

2.4.3. Batch and fed-batch fermentation

All fermentations were conducted in 1 L DASGIP® bioreactors (Eppendorf, Germany) with an initial volume of 500 mL 4 % BMGY and at 30 °C. For the pulsed batch, 25 mL of 50 % (*w/V*) glycerol was injected once after 12 h with a syringe into the sample port and flushed once with sterile air. Fed-batch fermentations were continuously fed with a total amount of 200 g of 50 % (*w/V*) glycerol depending on the strategy. The stirrer was equipped with a 6-plate-rushton impeller placed 2.5 cm from the bottom of the shaft stirring with an initial rate of 400 r/min. Maximum stirring rate was initially 1 200 r/min, which was reduced to 900 r/min for optimized fermentations. Batch and pulsed batch fermentations were performed with an aeration of 0.2–0.5 ($m^3/(m^3 \cdot min)$). Fed-batch fermentations were performed additionally with 0.5–1.2 ($m^3/(m^3 \cdot min)$). Agitation and aeration were automatically adjusted to maintain the level of dissolved oxygen over 30 %. The pH was maintained at 5.0 and automatically adjusted with 20 % NH_4OH

(directly into the broth) or with 7 % H_2SO_4 as required. Foam control was done using 1 % antifoam B (Merk, Germany). For monitoring process parameters, the reactors were equipped with probes for pH and dissolved oxygen. The 3 mL samples were taken every 3–5 h. Cell growth was determined as above; cell dry weight was determined by centrifuging 1 mL cell culture broth at 500 × g for 10 min and drying the cell pellet overnight at 105 °C. The supernatant was analyzed for glycerol after 1:10 dilution in 2.5 mmol/L H_2SO_4 and filtration (0.2 μm, PVDF) by high-performance liquid chromatography-RID (Dionex Corp., USA, RI 101, Shodex, Tokyo, Japan) equipped with an Rezex ion exclusion column (Rezex ROA-Organic Acid H+ (8 %); 300 mm × 7.8 mm; Phenomenex Deutschland Ltd.). The column oven temperature was set to 70 °C, and 2.5 mmol/L sulfuric acid was used for isocratic elution at a flow rate of 0.5 mL/min. Later the phytase activity was determined as described in Section 2.6. The OD_{600}, DCW, and phytase activity values in the fed batch fermentations were normalized to the starting volumes.

2.5. Fluorescence assay for RFP and yEGFP determination

To measure fluorescence, 100 μL culture or supernatant after centrifugation at 4 °C and 500 × g for 10 min were used, and intensity was normalized to OD_{600}, if not otherwise stated. To determine OD_{600}, samples were diluted in phosphate-buffered saline (PBS) buffer, pH 7.4. The parental *P. pastoris* strain not expressing the fluorescent protein was assayed in parallel and used to determine background fluorescence, which was averaged over all parent strains and removed from the fluorescence of the expression strains.

2.6. Colorimetric assay determining phytase activity

Phytase activity was measured using a colorimetric assay by monitoring the free phosphate released from phytate with ammonium molybdate. First, the culture was centrifuged (4 °C, 500 × g, 10 min) and the secreted protein in the supernatant was purified via gel-filtration using 96-Well SpinColumns (25–100 μL) (Harvard Apparatus, Holliston, MA, USA). Columns were centrifuged at room temperature at 2 000 × g for 2 min, before being hydrated with 200 μL water per well for 20 min and subsequently centrifuged as before. Each of these columns was then washed three times with 150 μL water. During this step, the first two centrifugations were at 2 000 × g and the final one at 1 000 × g (room temperature (RT), for 2 min). To purify the secreted proteins, 35 μL of the supernatant was loaded into wells and the plate was centrifuged (RT, 1 000 × g, 2 min) to collect the filtrate.

Finally, phytase activity was quantified using the method of Bae et al. (1999), but adapted to higher-throughput (i.e., 96-well-plates). Specifically, 13.5 μL gel filtrate, or water dilutions thereof, were combined with 53.5 μL of phytate substrate solution (1.5 mmol/L sodium phytate in 0.1 mol/L sodium acetate buffer, pH 5.0 using acetic acid) in a 96-well plate and incubated at 37 °C for 30 min. The 66.6 μL of a stop solution (5 % (*w/V*) trichloroacetic acid (TCA)) was added to terminate the reaction, followed by 66.6 μL of coloring solution (4 volumes reagent A (1.5 % (w/v) ammonium molybdate, 5.5 % (v/v) sulfuric acid solution) and 1 volume of reagent B (2.7 % (*w/V*) ferrous sulfate)). To calculate phytase units (U), potassium phosphate from 0.8 to 20 mmol/L was measured alongside each plate for the screening and up to 5 mmol/L for all other experiments. Absorbance at 700 nm was then measured.

2.7. Hydrolysate production

The *Nostoc* sp. De1 hydrolysate production was done in a 500 mL shaking flask. 5 % (*w/V*) of *Nostoc* sp. De1 biomass was suspended in 100 mL of 50 mmol/L citrate buffer pH 4.5. The biomass was pre-treated at 80°C for one hour. After cooling down, 0.05 % (v/v) DISTILLASE® CS and Viscozyme® L were added for saccharification for 24 h at 50 °C, while shaking at 150 r/min. After allowing it to cool again, 0.05 % (*V/V*) FERMGEN™ was added for solubilization over another 36 h at 30 °C and shaking at 150 r/min. Subsequently, the treatment ended by a heating step: 90 °C for 30 min in a preheated oven. The biomass slurry was then transferred into 500 mL centrifugation buckets and spun with 8 000 × g for 30 min at RT. The supernatant was sterile filtered (0.2 μm) into a sterile flask and kept at 4 °C until further use.

3. Results and discussion

3.1. Characterization of extended PTK

To develop an optimal phytase production host, we first extended our previous PTK (Obst et al., 2017) with 25 additional regulatory elements from *P. pastoris* (6 promoters, 19 secretion tags) and tested another 13 parts from the YTK (Lee et al., 2015) (7 promoters, 6 terminators). For characterization, we used a red fluorescent protein (RFP) and a yeast-enhanced green fluorescent protein (yEGFP) as reporters, which allowed for the simple measurement of bulk fluorescence (Fig. 2).

For higher product yields and precise tuning of gene expression, we tested the promoters for intracellular expression levels of RFP and yEGFP. We studied two strong methanol inducible promoters (pDAS1 (Vogl et al., 2016), pPMP20 (Vogl et al., 2016)), four constitutive promoters (pPET9 (Stadlmayr et al., 2010), pG1 (Prielhofer et al., 2013), pG6 (Prielhofer et al., 2013), pADH2 (Vogl et al., 2016)) and seven *S. cerevisiae* YTK promoters for their applicability in *P. pastoris* (pTDH3, pCCW12, pHHF2, pTEF2, pHHF1, pHTB2, pRPL18B) (Lee et al., 2015). We compared the intracellular expression levels of RFP and yEGFP from genomically integrated expression constructs (Fig. 2a). The newly added *P. pastoris* promoters resulted in high expression levels, both for GFP and RFP. The newly tested *S. cerevisiae* promoters, except for pTDH3 all promoted protein expression in *P. pastoris*. However, we did see better expression for RFP over yEGFP. Therefore, we selected the endogenous promoters for screening phytase production strains as they result in stronger expression levels and cover the desired spectrum of expression strengths.

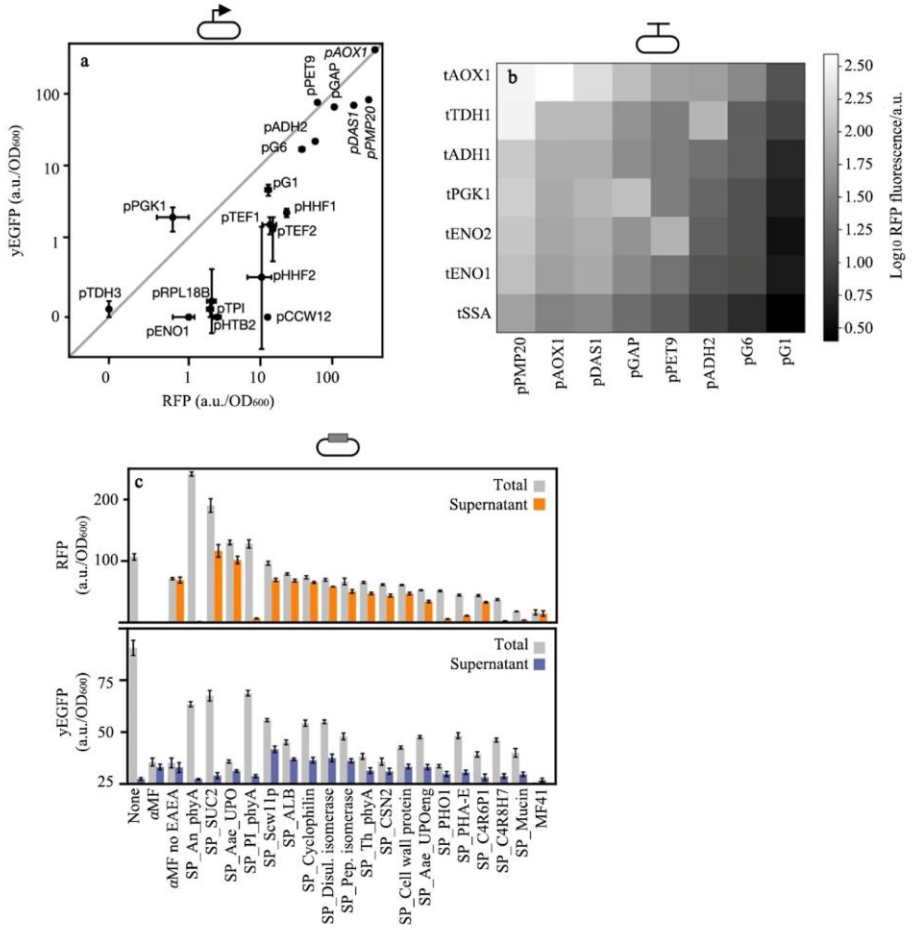

Fig. 2. Characterization of extended *Pichia* Toolkit (PTK) and additional Yeast Toolkit (YTP) regulatory elements. (a) relative promoter strength was evaluated for intracellular red fluorescent protein (RFP) and yeast-enhanced green fluorescent protein (yEGFP) expression. (b) characterization of promoter-terminator combinations. Heat map of RFP fluorescence values given in a.u. (fluorescence normalized to OD_{600}) in a logarithmic scale. (c) for secretion analysis, tags under the control of the constitutive promoter pGAP were analysed for RFP and yEGFP expression and secretion. For all samples, the total fluorescence, as well as the fluorescence of the supernatant after centrifugation, was determined. Three biological replicates were analysed, and the mean fluorescence normalized to the OD_{600} (a.u./OD_{600}) is presented with error bars that denote ± 1 standard deviation. Characterization was performed in 1 % buffered Minimal Methanol (BMM) for the inducible promoter pAOX1 and 1 % buffered minimal dextrose (BMD) for all other constitutive promoters. (For interpretation of the references to color in this figure, the reader is referred to the web version of this article).

In *S. cerevisiae* the terminator is important in tuning protein expression by up to 35-fold through impacts on mRNA stability (Curran et al., 2013; Morse et al., 2017). In *P. pastoris* terminators studied by Vogl et al. (2016) showed only minor differences in expression levels when different terminators were used. Here, eight *P. pastoris* promoters were coupled to six different YTK terminators (tTDH1, tADH1, tPGK1, tENO2, tENO1, tSSA1) or the *P. pastoris* terminator tAOX1 (Fig. 2b) to drive intracellular expression of RFP and test this idea further. We found that terminator choice significantly impacted expression levels by up to 5-fold across the promoter-terminator combinations, except for when the pAOX1 promoter was used where differences up to 10-fold were observed. Terminators were sorted according to their ability to tune expression for each promoter with tAOX1 typically causing higher expression levels,

and tSSA1 negatively impacting expression strength. This ranking was found to be similar for almost all promoters (other than the combinations: pGAP-tPGK1, pPET9-tENO2, pADH2-tTDH1), suggesting a systematic effect underlies the changes.

In eukaryotes, protein secretion primarily occurs via the endoplasmic reticulum (ER)—Golgi pathway, requiring a signal peptide on the N-terminal of the nascent polypeptide for translocation through the ER membrane (Delic et al., 2013; Liang et al., 2013). To fine-tune secretion, we included an additional 9 endogenous *P. pastoris*, 8 exogenous and 2 synthetic signal peptides to our toolkit. We selected tags based on previous knowledge regarding signal peptides and their prediction and initial signal peptide characterization was performed using RFP and yEGFP controlled by the strong constitutive promoter pGAP. Fluorescence of the total culture and supernatant were measured and OD_{600} was normalized (Fig. 2c). The secretion efficiency of the signal sequences varied for the reporter proteins RFP and yEGFP, as previously seen for synthetic tags (Obst et al., 2017), highlighting the importance of the signal peptide and gene of interest (GOI) combination when designing a secretion system. Here, we found that more RFP is expressed for the signal peptides SP_An_phyA, SP_SUC2, SP_Aae_UPO, or SP_Pl_phyA., while only SP_SUC2 and SP_Aae_UPO enabled higher secretion efficiencies than the commonly used mating factor α αMF_no_EAEA signal peptide. For yEGFP, the highest expression is seen for the intracellular expression construct without a tag. In comparison to the widely used αMF_no_EAEA or αMF signal peptides, higher secretion levels are achieved when using SP_Scw11p, SP_ALB, SP_Cyclophilin, SP_Disulfideierase, SP_Cell wall protein, SP_Peptidylprolyl isomerase and SP_Aae_UPOeng. Comparing endogenous *P. pastoris* or exogenous signal peptides, there is no noticeable difference. The analysis of the six newly characterized signal peptides shows two (SP_Cyclophilin and SP_Th_phyA) induce efficient secretion, two (SP_An_phyA, SP_Pl_phyA) lead to overall very high protein ex but no secretion, and two (SP_C4R8H7, SP_Mucin) result in only low amounts of secreted RFP and yEGFP. These results demonstrate the functionality of the newly designed regulatory elements and provided insight for part choice during the phytase screening.

3.2. Application of extended PTK on phytase expression

A selection of the extended PTK was used to generate randomized libraries to screen for beneficial combinations of regulatory elements for the phytase genes to achieve high levels of secreted phytases. All sequences were codon optimized for *P. pastoris* and designed to be compatible with the PTK. Secretion libraries with 20 secretion tags for induced and constitutive expression (3 and 5 different promoters, respectively) were made for each phytase. To cover the 60 or 100 possible combinations for the induced and constitutive library, respectively, 182 and 364 *P. pastoris* strains were screened to achieve an expected coverage of at least 95 %. Suitable screening conditions were established and validated (Fig. 1), to differentiate positive hits (active enzyme expression) from negative variants (no expression or inactivity of the enzyme). Expression supernatant after centrifugation was purified to remove small molecules via gel-filtration chromatography and a colorimetric assay was used to determine phytase activity using absorption measurements at 700 nm.

For all phytase screenings, strains producing active enzymes were identified, but the activity level and amount of secreted protein varied significantly. For each phytase, the activity landscape showed similarities between constitutive and induced screening. The decreasing activity for the *A. niger* and *P. lycii* phytases indicates a clear preference for specific promoter and secretion tag combinations. The smaller decrease (with many strains showing high activity) for the *E. coli* phytase suggests that this protein has less of an effect on the performance of the promoter and tag choice. A selection of strains for each library was re-screened, to confirm the initial results. The best performing from the induced and constitutive screening (10 and 22 colonies, respectively) and colonies that were found to not express any phytase (3 and 5 colonies, respectively), and were plated onto fresh agar media. Biological triplicates were screened and for a selection of strains, the genotype of the expression construct was found using sequencing (Fig. 3).

For each phytase, specific tags were found to support secretion better than others, while some were non-functional for all of the phytases tested. To assess this in more detail, 60 of the strains were sequenced. Of these, only six of the tags were not seen in any strain (three phytase signal peptides SP_Pl_phyA, SP_An_phyA, SP_Th_phyA; and signal peptides αAmylase–αMFΔ, SP_SUC2 and SP_PHA-E). For secretion of both fluorescent proteins, we found that both SP_An_phyA and SP_Pl_phyA were also non-functional. This suggests that *P. pastoris* may not be able to recognize these heterologous tags for secretion. The other four tags were shown to enable secretion of the fluorescent proteins previously (Fig. 2c), however, their function could be impacted by the phytase. The tag SP_PHO1 stood out, for its efficient secretion for all constitutive phytase expression strains. In addition, specific secretion tag-phytase combinations seemed to be beneficial. For example, SP_C4R8H7 for *A. niger* and *T. heterothallica*, SP_Mucin for *P. lycii*, and MF41 or the related αMF and αMF_no_EAEA tags for *E. coli*. When the gene was constitutively expressed, we found that the pGAP promoter gave the strongest expression, except for when the *P. lycii* phytase was used, where pG6 and pAHD2 resulted in the highest expression. For these constitutively expressed variants, only the pPET9 promoter did not appear in the sequencing data. For the designs using an inducible promoter, all three were found to lead to strong phytase expression, with pAOX1 and pPMP20 often outperforming pDAS1 as also seen for fluorescent proteins (Fig. 2a).

In summary, our screening identified functional promoter and tag combinations for each phytase. However, the number of suitable combinations varied significantly for each phytase and the secretion efficiency was heavily influenced by the combination of promoter, tag, and gene of interest. This illustrates the need for effective screening tools (Prielhofer et al., 2017). The novel tags SP_C4R8H7 and SP Cyclophillin, or the less commonly used tags SP_CSN2 and SP_PHO1 performed well in many contexts and could provide a suitable alternative to the most widely used tag αMF (Massahi and Çalık, 2015). For example, the application of SP_CSN2 instead of αMF increased the amount of secreted *A. niger* phytase by 20 % providing a simple to apply means for strain improvement.

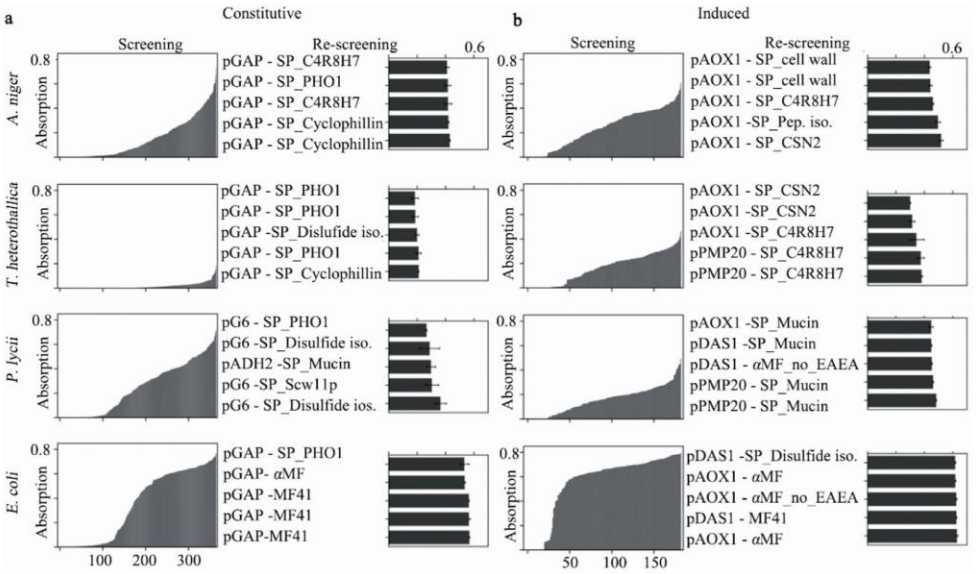

Fig. 3. Screening and Rescreening of phytases. For each phytase a screening for constitutive and induced expression was performed. Constitutive expression was performed in 2 % buffered glycerol-complex-phosphate buffer (BMGY-PP) and induced expression in 1 % buffered methanol-complex-phosphate buffer (BMMY-PP). To remove background noise, absorption values presented are measured absorption for each well subtracted by the average absorption of three medium controls which were assayed on each plate. The screening *x*-axis defines the number of samples screened in a ranked order. For each phytase, a re-screening of the constitutive and induced expression constructs was performed. Bars represent the mean absorption from the phytase assay of three biological replicates, subtracted by the mean absorption of three medium samples. Error bars denote ± 1 standard deviation. From the sequencing analysis, the genetic composition of promoter and secretion tag are indicated. *A.*: *Aspergillus; T.*: *Thielavia; P.*: *Peniophora.*

3.3. Shake flask cultivations for strain selection and media testing

In addition to the selection and combination of regulatory elements (strain design), different cultivation strategies (process design) greatly influence protein expression and secretion. Cultivation conditions often differ significantly between the initial screening and the final production process, which often makes scale-up challenging. Designing the overall process in a new system is essential to maximize yield and quality of phytase secretion (Looser et al., 2015). To demonstrate that the PTK can generate good producer strains, a single strain was selected for process optimization. For this, the 16 best performing strains were tested in shake flask format in two separate screenings. Based on the first screenings, a constitutive expression strain was chosen for methanol-free enzyme production, to prevent oxidative stress and special material handling, enable easier scale-up, and avoid protein degradation (Shen et al., 2016; Navone et al., 2021). The pGAP-MF41 AppA *E. coli* phytase construct was found multiple times in the shuffled screening as the best-performing constitutive strain. Other groups have reported similar observations, that AppA *E. coli* phytase is promising due to its characteristics (e. g., high temperature tolerance and high activity) and the good levels of expressed enzyme in *P. pastoris* (Chen et al., 2004). Hence, this strain was used further for phytase expression studies in shake flasks in complex medium as well as pure *Nostoc* sp. De1 hydrolysate using 2 % (*w/V*) glycerol or glucose as an additional carbon (C) source (Fig. 4). The composition of the *Nostoc* sp. De1 biomass and investigations of the enzymatic hydrolysis on the *Nostoc* sp. De1 biomass were reported by us before (Sinzinger et al., 2022).

The OD_{600} values of the cultures in BMGY and BMD were 23.7 and 18.9, respectively. The cultures did not grow as well in pure hydrolysate as they did in BMGY and BMD with OD_{600} of 18.8 and 14.3 (Fig. 4a). Little growth was observed in pure hydrolysate implying only very little readily available C-source. The phytase activity in BMGY and BMD reached 29.9 U/mL and 33.1 U/mL, respectively (Fig. 4b). In hydrolysate, the activities reached 23.6 U/mL and even 36.5 U/mL with glycerol and glucose as C-sources, respectively. Showing a tendency that glucose might be a good C-source for the expression system used here. The activities determined were still lower than the ones reported by others for the same *E. coli* phytase, e.g., by Akbarzadeh et al. (2015) who reached an activity of more than 200 U/mL with a pAOX1 system in modified BMGY after 96 h induction with methanol. Bai et al. (2009) reached a phytase activity of 243–412 U/mL over 48 h with a pGAP system depending on the medium composition. Shake flasks limit oxygen intake tremendously, which limits the interpretation of how well a producer strain can perform in a controlled system.

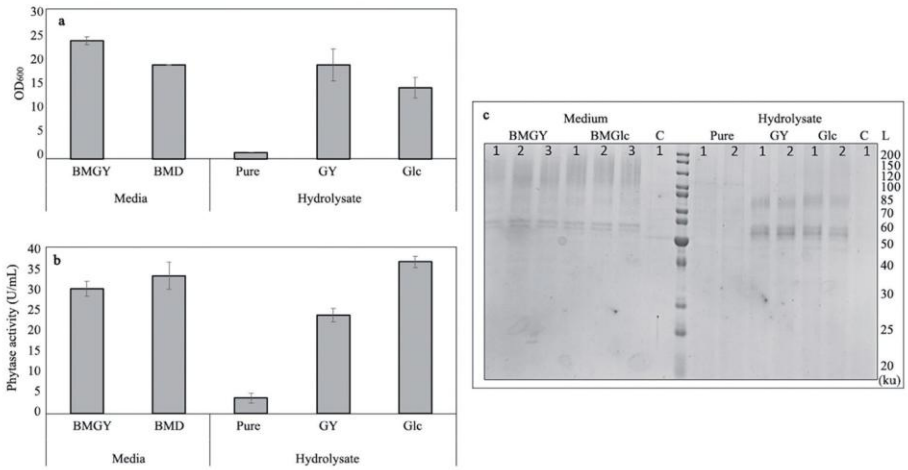

Fig. 4. Expression of pGAP-MF41 AppA *E. coli* phytase in 50 mL shake flasks. Expression in BMGY and BMD was done in triplicates, error bars showing ± 1 standard deviation. Expression in the *Nostoc* sp. De1 hydrolysate was done in duplicates as hydrolysate was limited, error bars showing relative deviation. (a) OD_{600} was measured after 48 h expression; (b) phytase activity was determined by colorimetric assay; (c) sodium dodecyl sulfate-polyacrylamide gel electrophoresis (SDS-PAGE) gel of the culture supernatants. The AppA *E. coli* phytase specific bands appearing at around 56 ku. C are medium controls. GY and Glc are the C-sources being glycerol and glucose, respectively. L is the protein ladder.

The presence of the protein was verified by sodium dodecyl sulfate–polyacrylamide gel electrophoresis (SDS-PAGE) analysis. In all relevant supernatants a clear band at the expected size of 56 ku was observed (Fig. 4c). This is in accordance with other results on this AppA *E. coli* phytase showing the same size of the protein and an unglycosylated native phytase with 45 ku (Chen et al., 2004). The bands in the samples with glycerol as a C-source were more prominent than with glucose in hydrolysate as well as the controlled complex medium. These larger bands might indicate higher enzyme concentrations in the hydrolysate samples, which are unmodified or improperly folded, potentially due to low oxygen availability in the shake flasks. Proceeding in a controlled system, glycerol as a C-source was considered for further testing to achieve higher activity.

3.4. Bench-top batch fermentation

The expression level of heterologous protein with pGAP is reported to be dependent on the protein itself, the medium, and the C-source (Karbalaei et al., 2020). A 1 L batch fermentation of (pGAP-MF41) AppA *E. coli* phytase was performed in BMGY medium as well as in 20 % (*V*/*V*) *Nostoc* sp. De1 hydrolysate (Fig. 5). The fermentations in hydrolysate took almost twice as long as in BMGY. The final activities reached were about the same at over 500 U/mL. The growth and product kinetics in BMGY medium were better than in hydrolysate (Table 1).

The highest phytase activities in BMGY medium were achieved at 24 h (530 and 511 U/mL), while in *Nostoc* sp. De1 hydrolysate, the peak activities were observed at 28 h (522 and 528 U/mL). The BMGY reached the highest OD_{600} value of 112 after 18 h, with corresponding cell dry weights (CDWs) of 25 and 23 g/L. In the hydrolysate, the stationary phase was reached at 32 h, with OD_{600} values of 98 and CDWs of 19 and 20 g/L. Glycerol consumption slowed down after 18 h, indicating nutrient limitations due to dilution with deionized water. Despite this, phytase activity continued to increase until 48 h. Table 1 provides an overview of cultivation conditions and yields for batch and pulsed batch fermentation. The study demonstrates the potential use of 20 % *Nostoc* sp. De1 hydrolysate as a fermentation medium for AppA *E. coli* phytase. The utilization of cyanobacterial hydrolysate thus could be a key in the development of cyanobacterial biorefinery concepts and associated cost economics. Although cyanobacteria are regarded as promising renewable feedstock, the main economic challenges of cyanobacterial biorefineries today are the still low concentration of products and high costs of cultivation and product recovery. Economic analysis such as the study of Fasahati et al. (2019) report a large span of costs for cyanobacterial products depending on the product type, e.g., in the range of 2.74–34.00 US dollar per kg based on product concentrations of 0.5 g/L in open pond cultivation systems. With respect to this, among other demands for improvement, a multiproduct approach including value added utilization even of the residual biomass is of high importance to add the most possible value to such a process. The utilization of cyanobacterial biomass for fermentation medium is to be seen as part of such a strategy.

Further, we aimed to develop a fed-batch bioprocess for AppA *E. coli* phytase in BMGY. Initially, the maximum specific growth rate μ_{max} (1/h) was determined by pulsed-batch fermentation of *P. pastoris* in BMGY (Fig. 5c). Pulses of additional C-source were performed with 25 g/L of glycerol into the fermentation broth after 15 h. The fermentation resulted in a maximum activity of

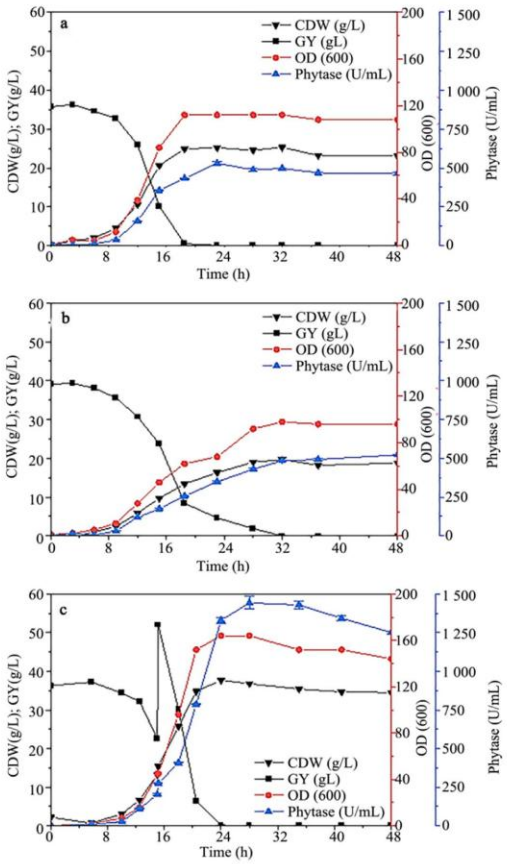

Fig. 5. The *P. pastoris* fermentation constitutively expressing pGAP-MF41 AppA *E. coli* phytase in a 1 L system over 48 h. (a) the batch fermentation in 4 % BMGY; (b) in 20 % (*V/V*) *Nostoc* sp. De1 biomass hydrolysate in *di*H_2O, hydrolysate was produced enzymatically as described in the text; (c) a pulsed-batch fermentation in 4 % BMGY. The glycerol pulse was done as described in the text. Phytase activity is shown as mean of analytical triplicates with one standard deviation. CDW: cell dry weight.

around 1 450 U/mL, which is 2.5-fold higher than the maximum yield obtained with previous batch fermentations run in BMGY. The maximum cell dry weight was around 1.5-fold higher than in the batch fermentations. Most growth and product kinetics, such as the maximum activity formation rate $q_{A,max}(\mu)$, improved when applying the pulsed batch fermentation strategy. The $q_{A,max}$ (μ) increased by more than 30 %, thereby showing that no system limitations were constraining the phytase expression at this point. For a more dynamic process, a second glycerol pulse could be applied to explore the limitations of the bioreactor system early in the process development (Looser et al., 2015). An overview of the determined growth and product kinetics of the conducted batch and pulsed batch fermentation is also shown in Table 1.

Contrary to induced expressions for high-cell density fermentation with three phases (batch phase, fed-batch phase, and induction phase), constitutive expression consists of just two: batch and fed-batch phase (Liu et al., 2019). Hence, the product formation in the fed-batch phase must be specifically tailored to the expression host and the reactor system. The key parameter to be determined for a high yield strategy is the specific productivity $\mu(q_A)$ the product of specific growth rate μ and product formation rate q_A. Hence, it must be investigated to determine the ideal feed rate for an exponential feed strategy. The $\mu(q_{A,max})$ and μ_{max} for the pulsed batch fermentations were determined to be the same with μ_{max} corresponding to a doubling time of 2.5 h. Contrary to induced expressions, which usually show to have their $\mu(q_{A,max})$ close to zero growth on methanol. Reported $\mu(q_{A,max})$ for pGAP regulated constitutive expression were usually just below μ_{max}.

Table 1
Overview of cultivation conditions, growth kinetics and products kinetics of periplasmic phosphoanhydride phosphatase (AppA) *Escherichia coli* phytase production with *Pichia pastoris* in a 1 L system using glycerol for C-source.

Cultivation condition						Growth kinetics				Product kinetics			
Medium	Temperature (°C)	pH	Mode	S_{total} (g/L)	Time (h)	CDW_{max} (g/L)	$Y_{x/s}$ (g/g)	$q_{s,max}$ (g/(g·h))	μ_{max} (1/h)	$A_{p,\ max}$ (U/mL)	$Y_{A/x,\ max}$ (U/g)	$q_{A,max}$ (U/(g·h))	$\mu(q_{A,max})$ (1/h)
BMGY	30	6.0	Batch	40	24	25. 3	0.70	0.72	0.286	530.0	21 378	6 680	0.286
BMGY	30	6.0	Batch	40	24	23. 4	0.59	0.84	0.266	522.0	23 337	6 536	0.266
BMGY	30	6.0	Pulsed Batch	65	28	36.6	0.58	1.10	0.303	1 458.6	42 034	17 515	0.303
BMGY	30	6.0	Pulsed Batch	65	28	37.7	0.57	1.04	0.308	1 342.9	40 395	14 281	0.308
20 % Hydrol.	30	6.0	Batch	40	32	19.7	0.50	1.18	0.300	522.3	27 182	8 408	0.300
20 % Hydrol.	30	6.0	Batch	40	32	19.0	0.48	1.16	0.170	528.3	30 016	1 432	0.170

Notes: The growth and product kinetics were used for the determination of feeding parameters to develop a fed-batch strategy. The hydrolysate was produced from *Nostoc* sp. *De1* biomass. S_{Total}, total substrate; CDW, cell dry weight; $Y_{x/s}$, biomass yield per substrate; q_s, substrate utilization rate; μ, growth rate; A_p, activity yield; $Y_{A/X}$, activity yield per biomass; $q_A(\mu)$, specific product formation rate; $\mu(q_A)$, specific growth rate.

3.5. Fed-batch strategy development

The exponential feed rate for high cell density fermentation of *P. pastoris* requires an ideal C-source feed rate. The μ_{max} of 0.3, determined from a pulsed batch fermentation, served as the exponential feed rate and 75 % of this μmax was also tested. Glycerol feed was limited by bioreactor space, with 4 % (*w/V*) starting glycerol and an additional 0.2 L of 50 % (*w/V*) glycerol solution fed. However, glycerol started accumulating due to the limited capacity of the 1 L system to sustain the organism's high growth rate. Fermentation curves are shown in Fig. 6a (μ_{max}) and 6b (75 % μ_{max}). The maximum activity yield and activity yield per biomass with exponential feeds were around 3 400 U/mL and 59 000 U/g for μ_{max} feed, and over 3 800 U/mL and 76 000 U/g for 75 % μ_{max} feed. Maximum CDW close to 100 g/L was achieved just before glycerol was completely consumed. Phytase activity, especially in μ_{max} feed fermentations, was strongly affected by glycerol accumulation, with a larger drop in activity after approximately 40 h of fermentation. Table 2 compares cultivation conditions, growth, and product kinetics for all fed-batch fermentations.

A notable difference between the two exponential feeds was that glycerol was temporarily consumed between 20 and 26 h in the 75 % μ_{max} feed fermentations, leading to a rise in dissolved oxygen levels. In contrast, dissolved oxygen dropped to zero until complete glycerol consumption in μmax feed fermentations. The low growth rates after 20 h resulted in decreased $q_A(\mu)$ values, indicating limited biomass formation and enzyme expression due to oxygen availability. However, the DO-stat strategy demonstrated lower oxidative stress.

The high cell density fermentation with exponential feed exhibited high phytase activity after 24 h, with minimal increase thereafter. To further increase phytase yield in the 1 L system, a DO-stat fermentation strategy was employed, maintaining DO above 20 %. Two DO-thresholds were tested: 30 % and 20 % DO (Fig. 6c and 6d), reaching over 4 000 U/mL. Glycerol levels were maintained at zero throughout the fed batch phase but DO-stat fermentations took 5–10 h longer than exponential feed strategy fermentations and yielded 20 %–25 % lower biomass (CDW) and max biomass per substrate yields. Growth slowed down after 30 h, particularly in DO-stat fermentations with a 20 % DO-threshold. Significant drops in enzyme activity were observed after approximately 40 h, possibly due to cellular proteases released from *P. pastoris* cells. The change from exponential feed to DO-stat feed strategy reduced growth kinetics but improved product kinetics. Although $q_{A,max}(\mu)$ decreased by more than 100 %, the maximum activity yield increased by more than 20 %. The DO-stat feed with a 30 % threshold showed promising results, with maximum activity yields of around 4 000 U/mL and activity yield per biomass over 4 400 U/g.

The DO-stat controlled feed strategy proved more effective than the exponential feed strategy for *P. pastoris* in a 1 L system, particularly with a 30 % DO threshold. Modifications were made by adjusting the DO-cascade, regulating aeration, agitation, and oxygen supply ratio. The 1 L system provided a maximum air flow of 50 sL/h, allowing for high aeration of 1–1.2 ($m^3/(m^3 \cdot min)$). To minimize protease release, the stir rate was reduced from 1200 rpm to 900 r/min (Fig. 6e). Additionally, a lower fermentation temperature of 25 °C after 12 h was implemented (Fig. 6f).

The modified DO-stat controlled feed strategy with a 30 % threshold, 1–1.2 ($m^3/(m^3 \cdot min)$), and 900 r/min showed improved fermentation results overall. While it did not reach the maximum space-time yield of exponential feed fermentations, it significantly improved activity yields per biomass. The maximum activity yield and activity yield per biomass increased by up to 40 %, reaching 7 200 U/mL and 113 000 U/g after 77 h fermentation, respectively. The lower temperature of 25 °C also resulted in around a 30 % increase in activity yield compared to the non-optimized DO-stat strategy. Studies of other authors on *P. pastoris* fermentation producing *E. coli* phytase ranged from 112.5 U/mL after 72 h in shake flasks to 30 246 U/mL after 180 h in a 50-L fermenter (Tai et al., 2013; Helian et al., 2020). However, the comparison is somewhat limited, as fermentation systems of different laboratories usually have different set-ups and limitations. Limited oxygen supply by the aeration system was an issue in the fermentation system available in our laboratories, which certainly limits activity yields. Yet, our results are very promising. Investigations on expressions in a larger-

Table 2
Overview of cultivation conditions, growth kinetis, and product kinetics of the conducted AppA (periplasmic phosphoanhydride phosphatase) *E. coli* phytase production with *P. pastoris*, namely exponential feed with feed for μ_{max} and 75 % of μ_{max}, DO-*stat* feed with 20 % and 30 % DO-limits, and optimized DO-*stat* feed strategies with reduced stirring rate and increased aeration.

Cultivation condition							Growth kinetics				Product kinetics			
Mode	Temperature (°C)	pH	DO-lvl (%)	Stirring rate (r/min)	Air ($m^3/(m^3 \cdot min)$)	S_{total} (g)	CDW_{max} (g/L)	$Y_{x/s}$ (g/g)	$q_{s,max}$ (g/(g·h))	μ_{max} (1/h)	$A_{p,\ max}$ (U/mL)	$Y_{A/x,\ max}$ (U/g)	$q_{A,max}$ (μ) (U/(g·h))	STY_{max} (U/(L·h))
Exp. Feed μ_{max}	30	6.0	30	400–1 200	0.2–0.5	240	98.8	0.45	142.32	0.246	3,435	59,677	18,090	130,357
Exp. Feed μ_{max}	30	6.0	30	400–1 200	0.2–0.5	240	99.4	0.45	6.74	0.281	3,432	55,940	16,538	128,705
Exp. Feed 75 % μ_{max}	30	6.0	30	400–1 200	0.2–0.5	240	97.5	0.45	1.56	0.357	3,573	76,197	17,522	116,709
Exp. Feed 75 % μ_{max}	30	6.0	30	400–1 200	0.2–0.5	240	96.5	0.44	16.47	0.272	3,880	76,459	16,546	118,518
DO-*stat* (20 %)	30	6.0	30	400–1200	0.2–0.5	240	77.5	0.35	0.59	0.249	4,093	59,293	6,012	81,324
DO-*stat* (20 %)	30	6.0	30	400–1 200	0.2–0.5	240	77.9	0.36	0.61	0.258	3,950	58,337	5,628	79,348
DO-*stat* (30 %)	30	6.0	30	400–1 200	0.2–0.5	240	77.5	0.36	0.57	0.274	4,446	75,449	8,657	96,661
DO-stat (30 %)	30	6.0	30	400–1 200	0.2–0.5	240	75.5	0.35	0.63	0.227	4,177	67,614	8,151	82,458
DO-*stat* (30 %)	30	6.0	30	400–900	1.0-1.2	240	72.4	0.33	0.46	0.186	6,531	104,686	8,622	102,903
DO-*stat* (30 %)	30	6.0	30	400–900	1.0–1.2	240	72.9	0.33	0.42	0.207	7,213	113,337	8,222	93,681
DO-*stat* (30 %)	25	6.0	30	400–900	1.0–1.2	240	97.8	0.45	0.42	0.155	6,317	76,305	4,850	82,042
DO-*stat* (30 %)	25	6.0	30	400–900	1.0–1.2	240	101.6	0.46	0.41	0.230	5,671	60,100	4,050	73,660

Notes: S_{total}, total substrate; CDW, cell dry weight; $Y_{x/s}$: biomass yield per substrate; q_s, substrate utilization rate; μ, growth rate; A_p, activity yield; $Y_{A/X}$, activity yield per biomass; $q_A(\mu)$, specific product formation rate; STY, space time yield.

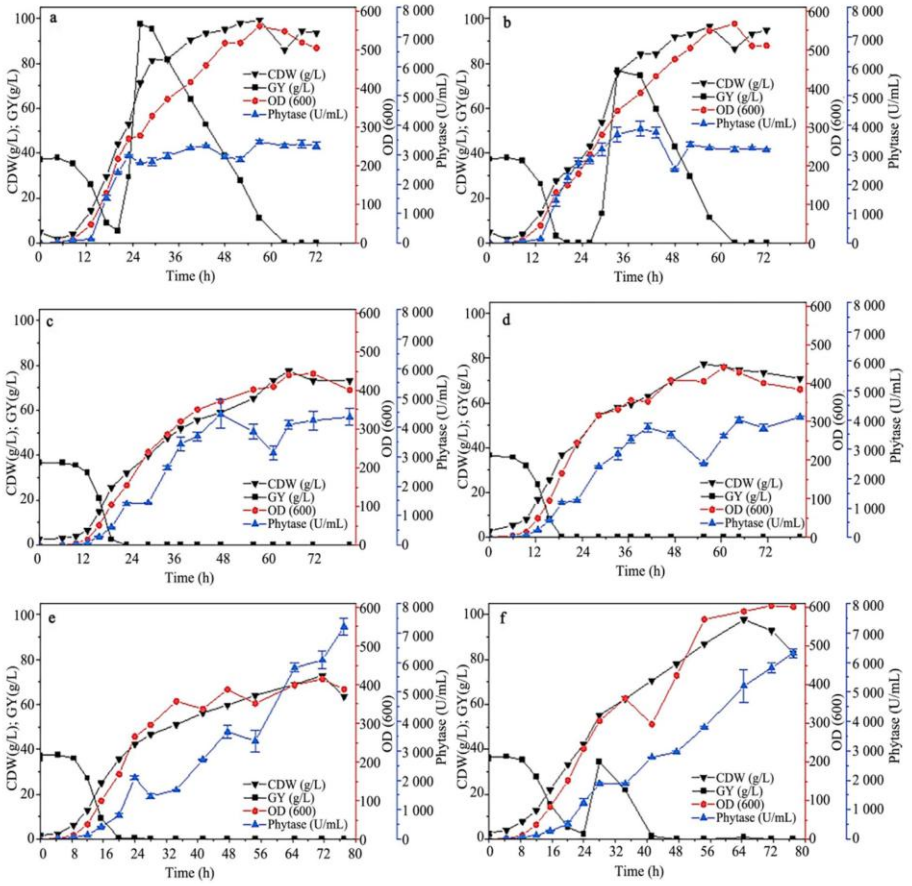

Fig. 6. Fed-batch development of *P. pastoris* fermentation constitutively expressing pGAP-MF41 AppA *E. coli* phytase in a 1 L fermenter system with 4 % BMGY medium feeding 200 g glycerol. We started with an exponential feed based on the calculated μ_{max} from batch and pulsed batch fermentations shown in (a) and a feed based on 75 % of μ_{max} in (b). The following step was a DO-stat feeding strategy with 30 % dissolved oxygen limit shown in (c) and 20 % dissolved oxygen limit in (d). The next step was improving the DO-cascade by lowering the max stir rate from 1 200 to 900 r/min and increasing the aeration to its maximum around 1.2 ($m^3/(m^3 \cdot min)$) shown in (e) and a decrease of temperature from 30 to 25 °C in (f).

scale system with better aeration and lower starting volume, ought to be done to further elucidate the potential of the strain developed in this study.

4. Conclusions

We applied a multi-field research approach to a *P. pastoris* enzyme production platform showing the potential to use cyanobacterial biomass as feedstock. We characterized and extended a combinatorial library to facilitate *P. pastoris* engineering, characterized the library components, and screened libraries for industrially relevant enzyme production. We developed a fed-batch strategy for AppA *E. coli* phytase expression and successfully demonstrated the utilization of *Nostoc* sp. De1 biomass hydrolysate. Thus, we could show that the extended *P. pastoris* toolkit can produce relevant producer strains and the enzyme expression with cyanobacterial biomass as feedstock may be an industrially relevant and more sustainable alternative to currently used sources. Global challenges, such

as economically feasible biobased production, will require creative solutions. This work highlights the value of multidisciplinary approaches to these issues and demonstrates how new biotechnologies can fuel novel solutions.

Declaration of Competing Interest

There are no conflicts to declare.

Acknowledgment

The EFRE—Interreg project 41 "Joint Research on Natural Compounds from Cyanobacteria as a Model of Cross-Border Scientific Partnership" was funded by the European Union ZIEL ETZ. Many thanks to Algatech for providing the biomass and to Prof. Timothy K. Lu (MIT) for providing *P. pastoris attP*.

Supplementary materials

Supplementary material associated with this article can be found, in the online version, at doi:10.1016/j.jobab.2023.12.005.

References

Akbarzadeh, A., Dehnavi, E., Aghaeepoor, M., Amani, J., 2015. Optimization of recombinant expression of synthetic bacterial phytase in *Pichia pastoris* using response surface methodology. Jundishapur J. Microbiol. 8, e27553.
Bae, H.D., Yanke, L.J., Cheng, K.J., Selinger, L.B., 1999. A novel staining method for detecting phytase activity. J. Microbiol. Methods 39, 17–22.
Bai, Y.G., Yang, P.L., Wang, Y.R., Shi, P.J., Luo, H.Y., Meng, K., Wu, B., Yao, B., 2009. Phytase production by fermentation of recombinant *Pichia pastoris* in monosodium glutamate wastewater. World J. Microbiol. Biotechnol. 25, 1643–1649.
Briones-Nagata, M.P., Martinez-Goss, M.R., Hori, K., 2007. A comparison of the morpho-cytology and chemical composition of the two forms of the cyanobacterium, *Nostoc* commune Vauch., from the Philippines and Japan. J. Appl. Phycol. 19, 675–683.
Canton, B., Labno, A., Endy, D., 2008. Refinement and standardization of synthetic biological parts and devices. Nat. Biotechnol. 26, 787–793.
Celińska, E., Borkowska, M., Białas, W., Korpys, P., Nicaud, J.M., 2018. Robust signal peptides for protein secretion in *Yarrowia lipolytica*: identification and characterization of novel secretory tags. Appl. Microbiol. Biotechnol. 102, 5221–5233.
Chandra, R., Iqbal, H.M.N., Vishal, G., Lee, H.S., Nagra, S., 2019. Algal biorefinery: a sustainable approach to valorize algal-based biomass towards multiple product recovery. Bioresour. Technol. 278, 346–359.
Chen, C.C., Cheng, K.J., Ko, T.P., Guo, R.T., 2015. Current progresses in phytase research: three-dimensional structure and protein engineering. ChemBioEng Rev. 2, 76–86.
Chen, C.C., Wu, P.H., Huang, C.T., Cheng, K.J., 2004. A *Pichia pastoris* fermentation strategy for enhancing the heterologous expression of an *Escherichia coli* phytase. Enzyme Microb. Technol. 35, 315–320.
Choi, S.P., Nguyen, M.T., Sim, S.J., 2010. Enzymatic pretreatment of *Chlamydomonas reinhardtii* biomass for ethanol production. Bioresour. Technol. 101, 5330–5336.
Curran, K.A., Karim, A.S., Gupta, A., Alper, H.S., 2013. Use of expression-enhancing terminators in *Saccharomyces cerevisiae* to increase mRNA half-life and improve gene expression control for metabolic engineering applications. Metab. Eng. 19, 88–97.
David, G., 2018. Chapter 26—economics of food and feed enzymes: status and prospectives. In: Enzymes in Human and Animal Nutrition. Academic Press, USA, pp. 487–514.
de Farias Silva, C.E., Barbera, E., Bertucco, A., 2019. Biorefinery as a promising approach to promote ethanol industry from microalgae and Cyanobacteria. Bioethanol Production from Food Crops. Elsevier, Amsterdam, pp. 343–359.
Delic, M., Valli, M., Graf, A.B., Pfeffer, M., Mattanovich, D., Gasser, B., 2013. The secretory pathway: exploring yeast diversity. FEMS Microbiol. Rev. 37, 872–914.
Engler, C., Gruetzner, R., Kandzia, R., Marillonnet, S., 2009. Golden gate shuffling: a one-pot DNA shuffling method based on type IIs restriction enzymes. PLoS One 4, e5553.
Fasahati, P., Wu, W.Z., Maravelias, C.T., 2019. Process synthesis and economic analysis of cyanobacteria biorefineries: a superstructure-based approach. Appl. Energy 253, 113625.
Han, Y.M., Lei, X.G., 1999. Role of glycosylation in the functional expression of an*Aspergillus niger*Phytase (*phyA*) in*Pichia pastoris*. Arch. Biochem. Biophys. 364, 83–90.
Helian, Y.K., Gai, Y.M., Fang, H., Sun, Y.M., Zhang, D.W., 2020. A multistrategy approach for improving the expression of *E. coli* phytase in *Pichia pastoris*. J. Ind. Microbiol. Biotechnol. 47, 1161–1172.
Herrmann, K.R., Ruff, A.J., Infanzón, B., Schwaneberg, U., 2019. Engineered phytases for emerging biotechnological applications beyond animal feeding. Appl. Microbiol. Biotechnol. 103, 6435–6448.
Hesampour, A., Siadat, S.E.R., Malboobi, M.A., Mohandesi, N., Arab, S.S., Ghahremanpour, M.M., 2015. Enhancement of thermostability and kinetic efficiency of *Aspergillus niger* PhyA phytase by site-directed mutagenesis. Appl. Biochem. Biotechnol. 175, 2528–2541.
Karbalaei, M., Rezaee, S.A., Farsiani, H., 2020. *Pichia pastoris*: a highly successful expression system for optimal synthesis of heterologous proteins. J. Cell. Physiol. 235, 5867–5881.
Lee, M.E., DeLoache, W.C., Cervantes, B., Dueber, J.E., 2015. A highly characterized yeast toolkit for modular, multipart assembly. ACS Synth. Biol. 4, 975–986.
Liang, S.L., Li, C., Ye, Y.R., Lin, Y., 2013. Endogenous signal peptides efficiently mediate the secretion of recombinant proteins in *Pichia pastoris*. Biotechnol. Lett. 35, 97–105.
Liu, W.C., Inwood, S., Gong, T., Sharma, A., Yu, L.Y., Zhu, P., 2019. Fed-batch high-cell-density fermentation strategies for *Pichia pastoris* growth and production. Crit. Rev. Biotechnol. 39, 258–271.
Looser, V., Bruhlmann, B., Bumbak, F., Stenger, C., Costa, M., Camattari, A., Fotiadis, D., Kovar, K., 2015. Cultivation strategies to enhance productivity of *Pichia pastoris*: a review. Biotechnol. Adv. 33, 1177–1193.
Madden, K., Tolstorukov, I., Cregg, J., 2015. In: Electroporation of *Pichia pastoris*. Genetic Transformation Systems in Fungi, 1. Springer, Cham, pp. 87–91 2015.
Massahi, A., Çalık, P., 2015. In-silico determination of *Pichia pastoris* signal peptides for extracellular recombinant protein production. J. Theor. Biol. 364, 179–188.
Mitra, M., Mishra, S., 2019. Multiproduct biorefinery from *Arthrospira* spp. towards zero waste: current status and future trends. Bioresour. Technol. 291, 121928.
Möllers, K.B., Cannella, D., Jørgensen, H., Frigaard, N.U., 2014. Cyanobacterial biomass as carbohydrate and nutrient feedstock for bioethanol production by yeast fermentation. Biotechnol. Biofuels 7, 64.
Morse, N.J., Gopal, M.R., Wagner, J.M., Alper, H.S., 2017. Yeast *Terminator* function can be modulated and designed on the basis of predictions of nucleosome occupancy. ACS Synth. Biol. 6, 2086–2095.
Navone, L., Vogl, T., Luangthongkam, P., Blinco, J.A., Luna-Flores, C., Chen, X.J., von Hellens, J., Speight, R., 2021. Synergistic optimisation of expression, folding, and secretion improves *E. coli* AppA phytase production in *Pichia pastoris*. Microb. Cell Fact. 20, 8.
Obst, U., Lu, T.K., Sieber, V., 2017. A modular toolkit for generating *Pichia pastoris* secretion libraries. ACS Synth. Biol. 6, 1016–1025.
Perez-Pinera, P., Han, N.R., Cleto, S., Cao, J.C., Purcell, O., Shah, K.A., Lee, K., Ram, R., Lu, T.K., 2016. Synthetic biology and microbioreactor platforms for programmable production of biologics at the point-of-care. Nat. Commun. 7, 12211.

Prielhofer, R., Barrero, J.J., Steuer, S., Gassler, T., Zahrl, R., Baumann, K., Sauer, M., Mattanovich, D., Gasser, B., Marx, H., 2017. GoldenPiCS: a Golden Gate-derived modular cloning system for applied synthetic biology in the yeast *Pichia pastoris*. BMC Syst. Biol. 11, 123.

Prielhofer, R., Maurer, M., Klein, J., Wenger, J., Kiziak, C., Gasser, B., Mattanovich, D., 2013. Induction without methanol: novel regulated promoters enable high-level expression in *Pichia pastoris*. Microb. Cell Fact. 12, 5.

Qin, X., Qian, J., Xiao, C., Zhuang, Y., Zhang, S., Chu, J., 2011. Reliable high-throughput approach for screening of engineered constitutive promoters in the yeast *Pichia pastoris*. Lett. Appl. Microbiol. 52, 634–641.

Rajkumar, A.S., Varela, J.A., Juergens, H., Daran, J.MG., Morrissey, J.P., 2019. Biological parts for *Kluyveromyces marxianus* synthetic biology. Front. Bioeng. Biotechnol. 7, 97.

Ranjan, B., Satyanarayana, T., 2016. Recombinant HAP phytase of the thermophilic mold *Sporotrichum thermophile:* expression of the *Codon*-optimized phytase gene in *Pichia pastoris* and applications. Mol. Biotechnol. 58, 137–147.

Shen, W., Xue, Y., Liu, Y.Q., Kong, C.X., Wang, X.L., Huang, M.M., Cai, M.H., Zhou, X.S., Zhang, Y.X., Zhou, M., 2016. A novel methanol-free *Pichia pastoris* system for recombinant protein expression. Microb. Cell Fact. 15, 178.

Sinzinger, K., Schieder, D., Rühmann, B., Sieber, V., 2022. Towards a cyanobacterial biorefinery: carbohydrate fingerprint, biocomposition and enzymatic hydrolysis of *Nostoc* biomass. Algal Res. 65, 102744.

Stadlmayr, G., Mecklenbräuker, A., Rothmüller, M., Maurer, M., Sauer, M., Mattanovich, D., Gasser, B., 2010. Identification and characterisation of novel *Pichia pastoris* promoters for heterologous protein production. J. Biotechnol. 150, 519–529.

Tai, H.M., Yin, L.J., Chen, W.C., Jiang, S.T., 2013. Overexpression of *Escherichia coli* phytase in *Pichia pastoris* and its biochemical properties. J. Agric. Food Chem. 61, 6007–6015.

Vogl, T., Sturmberger, L., Kickenweiz, T., Wasmayer, R., Schmid, C., Hatzl, A.M., Gerstmann, M.A., Pitzer, J., Wagner, M., Thallinger, G.G., Geier, M., Glieder, A., 2016. A toolbox of diverse promoters related to methanol utilization: functionally verified parts for heterologous pathway expression in *Pichia pastoris*. ACS Synth. Biol. 5, 172–186.

Weis, R., Luiten, R., Skranc, W., Schwab, H., Wubbolts, M., Glieder, A., 2004. Reliable high-throughput screening with *Pichia pastoris* by limiting yeast cell death phenomena. FEMS Yeast Res. 5, 179–189.

Xiong, A.S., Yao, Q.H., Peng, R.H., Han, P.L., Cheng, Z.M., Li, Y., 2005. High level expression of a recombinant acid phytase gene in *Pichia pastoris*. J. Appl. Microbiol. 98, 418–428.

Yarimizu, T., Nakamura, M., Hoshida, H., Akada, R., 2015. Synthetic signal sequences that enable efficient secretory protein production in the yeast *Kluyveromyces marxianus*. Microb. Cell Fact. 14, 20.

Zang, J.K., Zhu, Y.F., Zhou, Y., Gu, C.J., Yi, Y.F., Wang, S.X., Xu, S.Q., Hu, G.W., Du, S.J., Yin, Y.N., Wang, Y.L., Yang, Y., Zhang, X.Y., Wang, H.K., Yin, F.F., Zhang, C., Deng, Q., Xie, Y.H., Huang, Z., 2021. Yeast-produced RBD-based recombinant protein vaccines elicit broadly neutralizing antibodies and durable protective immunity against SARS-CoV-2 infection. Cell Discov. 7, 71.

4.3. Biorefinery concept for *Cylindrospermum* alatosporum CCALA 988 extracting multiple high-value compounds and residue utilization by *P. pastoris* fermentation producing phytase

Authors: Korbinian Sinzinger, Sebastian Bieringer, Doris Schieder, Herbert Riepl, and Volker Sieber;

The manuscript outlines a novel biorefinery concept for the cyanobacterium *Cylindrospermum* alatosporum CCALA 988, emphasizing the extraction of multiple high-value compounds and the utilization of residual biomass. The study reveals that the cyanobacterial biomass composition includes 52.4% protein, 8.7% structural saccharides, 4.1% lipids, and 2.4% starch. High-value compounds identified are cyclic lipopeptides (PUWs and MINs), phycobiliproteins, and pigments. A sequential extraction process was developed to maximize the recovery of these compounds. Initially, aqueous extraction is performed to avoid denaturation of proteins, followed by organic solvent extraction to recover additional amounts of CLPs and pigments. This process allows for the recovery of 56.2% of the biomass, leaving 43.8% as residue. The residual biomass is enzymatically hydrolyzed and used as a nutrient supplement for *Pichia pastoris* fermentation, which produces appA E. coli phytase. This approach achieved phytase levels comparable to those produced in rich complex media, demonstrating the potential for economic viability. The fermentation process utilized minimal salt medium and showed promising results, indicating that the residual biomass can be effectively valorized. Overall, the study provides a basis for the further development of this biorefinery concept, with the potential for scale-up and economic assessment. The utilization of *C*. alatosporum CCALA 988 biomass for producing multiple high-value products, coupled with the efficient use of residual biomass, supports the feasibility and economic potential of this biorefinery approach.

Korbinian Sinzinger designed and conducted most experiments, analyzed the date and wrote the original draft. Sebastian Bieringer contributed to the analysis of the CLPs and writing this section in the original draft. Doris Schieder contributed to the conceptualization, reviewed, and edited the manuscript. Herbert Riepl contributed to reviewing and editing the manuscript. Volker Sieber contributed to reviewing and editing the manuscript.

The supplemental information for this publication can be found in the appendix, section 6.3.

Biorefinery concept for *Cylindrospermum* alatosporum CCALA 988 extracting multiple high-value compounds and residue utilization by *P. pastoris* fermentation producing phytase

Korbinian Sinzinger, Sebastian Bieringer, Doris Schieder, Herbert Riepl, and Volker Sieber

Algal Research

2023

https://doi.org/10.1016/j.algal.2023.103302

Algal Research 76 (2023) 103302

Contents lists available at ScienceDirect

Algal Research

journal homepage: www.elsevier.com/locate/algal

Biorefinery concept for *Cylindrospermum alatosporum* CCALA 988 extracting multiple high-value compounds and residue utilization by *P. pastoris* fermentation producing phytase

Korbinian Sinzinger [a], Sebastian Bieringer [c], Doris Schieder [a,*], Herbert Riepl [b,c], Volker Sieber [a,d,e,f]

[a] Chemistry of Biogenic Resources, Technical University of Munich, Campus for Biotechnology and Sustainability, 94315 Straubing, Germany
[b] Organic-analytical Chemistry, Weihenstephan-Triesdorf University of Applied Sciences, Straubing, Germany
[c] Campus Straubing for Biotechnology and Sustainability, Technical University of Munich, Straubing, Germany
[d] Catalysis Research Center, Technical University of Munich, 85748 Garching, Germany
[e] SynBiofoundry@TUM, Technical University of Munich, 94315 Straubing, Germany
[f] The University of Queensland, School of Chemistry and Molecular Biosciences, 68 Cooper Road, St. Lucia 4072, Australia

ARTICLE INFO

Keywords:
Cyanobacteria biorefinery
Cylindrospermum alatosporum
Phytase fermentation
Pichia pastoris

ABSTRACT

Economically feasible biorefinery concepts rely on the production of multiple high-value products and valorization even of residual side streams. This generally holds true for biomass from agriculture, forestry, and aquaculture. Cyanobacteria are seen as promising organisms for this purpose. The potential for commercialization, however, strongly depends on the strain being used and the range of products it offers. The cyanobacterial strain *Cylindrospermum alatosporum* CCALA 988 was reported to produce high amounts of the cyclic lipopeptides puwainaphycins (PUWs) and minutisamides (MINs) as high-value products. Hence, this study investigated the biomass of the cyanobacterial strain as a potential feedstock for a biorefinery concept. The study also explored the enzymatic hydrolysis of the residual biomass and its utilization as a medium supplement for appA *E. coli* phytase expression with *Pichia pastoris*. Analysis of the cyanobacterial biomass revealed the following composition: ash 1.9 %, lipids 4.1 %, starch 2.4 %, structural saccharides 8.7 %, and protein 52.4 %. Further, a sequential extraction concept and a bench-scale mass balance were investigated, and products were proposed with 56.2 % of biomass being utilized and 43.8 % being left as residue. PUWs (21.6 mg/g), MINs (101.5 mg/g), phycobiliproteins (34.5 mg/g), and pigments (6.4 mg/g) were selected as products and quantified. The utilization of hydrolysate by fermentation of *P. pastoris* for appA *E. coli* phytase expression was studied in a 1 L system. In batch mode, the hydrolysate allowed to achieve comparable results to a rich complex medium, with over 500 U/mL of appA *E. coli* phytase. The obtained results provide a basis for further development of this biorefinery concept.

1. Introduction

In recent years, there has been a growing interest in the utilization of microalgae and cyanobacteria as third generation biomass in order to effectively establish a circular bioeconomy [1,2]. Biomass can be utilized as renewable raw material and substitute for fossil-based fuels in a biorefinery concept [3–5]. The biorefinery concept, like a traditional refinery, converts raw material into a range of products using various treatments and unit operations. Several integrated biorefinery approaches can be found on the industrial scale that utilizes different biomass and waste streams to produce multiple product streams. In 2019, Hassan et al. reported 67 first and second generation biorefineries utilizing lignocellulosic biomass operating globally, of which, two thirds did not operate on a commercial scale [6]. Hence, extensive research is needed to make biorefineries economically feasible, especially the third and fourth generation biorefineries [7].

Microalgae and cyanobacteria have been recognized as a promising and beneficial biorefinery feed for various reasons. Firstly, they exhibit a high rate of carbon dioxide fixation and biomass growth. Additionally, they have the ability to store carbon in saccharides and lipids, which can

* Corresponding author at: TUM Campus Straubing, Schulgasse 16, 94315 Straubing, Germany.
E-mail address: doris.schieder@tum.de (D. Schieder).

https://doi.org/10.1016/j.algal.2023.103302
Received 25 April 2023; Received in revised form 10 October 2023; Accepted 22 October 2023
Available online 24 October 2023

be utilized for the production of fuels. Moreover, these microorganisms can serve as a valuable source of protein for animal feed. Furthermore, they are known to contain high-value compounds such as vitamins, pigments, and nutraceuticals [3]. As the biomass cultivation and processing is often costly, biorefinery concepts focusing solely on commodity chemicals are not feasible [8,9]. Yet, many different potential high-value products from microalgae and cyanobacteria have been identified. Potential valuable products that might be extracted as side streams are exopolysaccharides, pigments, phycobiliproteins, enzymes, polyunsaturated fatty acids, or polysaccharides [10–12]. The residual biomass after extractions might still carry value for other processes or products such as biogas production, fermentation, fertilizer, or animal feed [13–15]. The co-production of multiple high-value products has been highlighted before and is considered to be promising with a short pay-off time [16–18].

The diversity of bioactive compounds, particularly those derived from cyanobacteria, is extensive. Over 1100 secondary metabolites have been described as anti-inflammatory, antiviral, antifungal, antibiotic, cytotoxic, or anticancer agents [16,19–26]. These metabolites of significant value have the potential to serve as drug leads and enhance the viability of multi-product biorefinery concepts, thereby positively influencing the techno-economic performance. A recent focus of research has been on cyclic lipopeptides (CLPs), a group of potential novel lead compounds derived from cyanobacteria [27–30]. CLPs have been reported to display broad biological effects in various organisms, which raises questions on their possible toxicity to humans but also exhibit interesting bioactivities such as antifungal, antibiotic, cytotoxic, and antiproliferative activities [31]. Due to the number of applications, these large molecules are extremely useful in different industries including pharmacy. The CLPs caspofungin, cyclosporine A, and daptomycin have already found their way into clinical application showing potent antifungal, immunosuppressant, and antimicrobial activity even against methicillin-resistant *Staphylococcus aureus*, respectively [31,32].

The promising strain *Cylindrospermum alatosporum* CCALA 988 produces larger quantities of CLPs, namely puwainaphycin (PUW) and minutisamide (MIN) variants [27,31,33,34]. Several PUW and MIN variants have been isolated by specifically developed methods and their bioactivity characterized on different cell lines [27,28,34]. These high-value secondary metabolites in *C. alatosporum* CCALA 988 make this strain a highly promising candidate for the biorefinery concept. Additional to the extraction of PUWs and MINs from *C. alatosporum* CCALA 988 biomass, further valuable compounds need to be extracted for an economical biorefinery concept. Additionally, we found that cyanobacterial biomass with high protein content can be used as a supplement for a *P. pastoris* fermentation producing the appA *E. coli* phytase [35]. We achieved this by enzymatically treating cyanobacterial biomass, and by supplementing the resulting hydrolysate with an additional C-source as fermentation medium to produce phytase. Based on our findings, we hypothesize this approach to be a cost efficient option for a growth medium for industrially relevant enzymes.

In the present study, we propose a novel multi-product biorefinery concept for the cyanobacterium strain *C. alatosporum* CCALA 988. First, the complete biocomposition of *C. alatosporum* CCALA 988 biomass was analyzed including the saccharide profile. An extraction concept for high-value compounds (CLPs and pigments) was investigated. For the evaluation of the techno-economic performance, a small-scale mass balance with 10 g biomass was conducted. Also, a *P. pastoris* fermentation in a 1 L system with minimal salt medium was investigated for constitutive phytase expression. Lastly, the residual extracted biomass was valorized by utilization as fermentation macronutrient supply. It was enzymatically hydrolyzed, and the hydrolysate was used to supplement the minimal salt medium for improved phytase expression.

2. Materials & methods

2.1. Chemicals, enzymes, and biomass

All chemicals were purchased in analytical grade from Sigma Aldrich (Germany), Merck KGaA (Germany) and Carl Roth GmbH (Germany), unless otherwise stated. The enzymes used were the following industry mixtures kindly provided by Genencore: OPTIMASH™ BG (β-glucanase/xylanase), DISTILLASE® CS (amyloglucosidase & α-amylase), FERMGEN™ (protease). Further, Viscozyme® L (cellulolytic) was purchased from Sigma Aldrich. Freeze dried whole cells from *C. alatosporum* CCALA 988 were kindly provided by Centre Algatech, Institute of Microbiology, the Czech Academy of Sciences (Třeboň). The cyanobacterium was grown in Allen-Arnold medium at 30 °C, with 2 % CO_2 enriched air at 30 °C, with constant irradiation of 150 μmol m^{-2} s^{-1} for 10–14 days [31].

2.2. Biomass composition, high value compounds and mass balance

2.2.1. Biomass composition

Components were analyzed following the standard laboratory procedures (LAPs) published by the National Renewable Energy Laboratory (NREL) [36]. All procedures were conducted as done before and described in detail [37].

In brief, total solids of the biomass were determined gravimetrically after drying under vacuum at 40 °C overnight. Ash content was determined using a muffle furnace ramping to 575 °C [38]. Starch was analyzed using enzymes from the Megazyme Total Starch Assay AOAC Official Method 996.11, followed by PMP-HPLC-UV analysis [39,40]. Protein was estimated by elemental analysis using the nitrogen to protein conversion factor of 4.78 [41]. Lipids were determined as fatty acid methyl esters (FAMEs) by GC–MS [42]. Total saccharides were determined by trifluoroacetic acid hydrolysis followed by PMP-HPLC-UV-MS/MS [37], and identification and quantification based on MS2 fragmentation comparison to standards. Structural saccharides were calculated as total saccharides minus the glucose determined by starch analysis.

2.2.2. Pigments and phycobiliproteins

Pigments and phycobiliproteins were quantified as described by Meixner et al. [43]. 20 mg of biomass was weighed into 15 mL falcon tubes. For the extraction of chlorophyll *a* and carotenoids 5 mL of 90 % (v/v) acetone was added. For phycobiliproteins 5 mL of 50 mM sodium acetate was added in separate tubes. The samples were vortexed and subsequently extracted for 24 h at 4 °C in the dark. The samples were vortexed several times in between. After extraction, solids were separated by centrifugation for 10 min with 2000 ×*g* at room temperature. 200 μL of the supernatants were then transferred into a quartz microtiter plate in triplicates for absorbance measurements. The calculation for quantification was done as described in the supporting information (annex 1).

2.2.3. Puwainaphycin and Minutisamide

For the verification of the lipopeptide extraction, 25 mg of biomass was extracted with 1 mL pure water or pure methanol at 4 °C over night. After centrifugation at 21,000 ×*g* for 5 min, the supernatant was filtered (0.2 μm PVDF syringe filter) and diluted 1:100 with water. 150 μL of the dilutions were transferred into micro-vials for analysis. Lipopeptides were measured with a Shimadzu HPLC/IT-TOF-MS system (LC-20AD, SIL-20AC HT, CTO-20A, SPD-M20) equipped with a C18 column (Phenomenex, Kinetex C18 2.1 × 100 mm ID, 2.6 μm). The samples were eluted with a flow of 0.4 mL/min with a gradient of A (water, 0.1 % formic acid) and B (acetonitrile 0.1 % formic acid) starting from 15 % organic phase with a linear increase to 100 % holding for additional 5 min. The molecular structures were evaluated with the single charged negative ion $(M\text{-}H)^-$ and the double charged positive ion $(M + 2H)^{2+}$

mode. For the estimation of the quantity ratio, the positive mode was expected to give better results, since the ionization primarily occurred at the hydroxyl-groups of the polar head. This polar head is identical in all relevant structures. The negative ionization, in contrast, is assumed to take place at the fatty acid tail, which varies from minutisamides to puwainaphycins.

2.2.4. Biorefinery procedure

10 g of biomass was weighed into 500 mL centrifugation buckets. 200 mL of 50 mM sodium phosphate buffer pH 7.0 was added. The samples were mixed and disrupted for 15 min in a sonication water bath and mixed again by hand. Then, the samples were centrifuged for 20 min at 10,000 ×g at 4 °C. The supernatant was collected in a bottle and the residual biomass was dried. Next, 200 mL of methanol were added to the residual biomass, sonicated in a water bath for 30 min and centrifuged for 20 min at 15,000 ×g at 4 °C. The supernatant was collected in a bottle and the residual biomass was dried again. The double extracted residual biomass was used for enzymatic treatment as specified in Section 2.3.2. After enzymatic hydrolysis, the residual biomass was dried again. Residual biomasses were dried over night at 65 °C in an oven and the mass determined gravimetrically. The methanol extract was dried at 40 °C and 150 mbar with a vacuum rotary evaporator and the residual mass also determined gravimetrically. The sequential extractions of 10 g biomass were done in triplicates. The hydrolysate was produced from pooled residues and the reported masses extrapolated to 10 g.

2.3. Residual biomass utilization by hydrolysis and fermentation

2.3.1. Cultivation conditions and media

P. pastoris attP (pUO_pL963) was always freshly streaked out from a cryo-culture onto YPD agar plates supplemented with 75 μg/mL zeocin and incubated for two days at 30 °C. A single colony was picked and cultivated as pre-culture in buffered complex medium (BMGY), containing 10 g/L yeast extract, 20 g/L peptone, 10 g/L ammonium sulfate, 3.4 g/L yeast nitrogen base without amino acids, 0.4 mg/L biotin, and 10 g/L glycerol. Two salt media were used in this study, D'Anjou and minimal salt medium (MSM) with both containing 2 mL/L *Pichia* trace metals solution (PTM). The D'Anjou medium was composed of 18.84 g/L $(NH_4)_2SO_4$, 5.62 g/L KH_2PO_4, 0.11 g/L $CaCl_2{\cdot}2H_2O$, 1.18 g/L $MgSO_4{\cdot}7H_2O$, and 40 g/L glycerol. The MSM medium was composed of 20 g/L $(NH_4)_2SO_4$, 12 g/L KH_2PO_4, 0.36 g/L $CaCl_2{\cdot}2H_2O$, 4.7 g/L $MgSO_4{\cdot}7H_2O$, and 40 g/L glycerol. The PTM was composed of 8.0 mg/L $CuSO_4{\cdot}5H_2O$, 1.2 mg/L KI, 28.0 mg/L $MnSO_4{\cdot}H_2O$, 5.2 mg/L $Na_2MoO_4{\cdot}2H_2O$, 8.0 mg/L H_3BO_3, 44.0 mg/L $ZnSO_4{\cdot}7H_2O$, 75.0 mg/L $FeCl_3{\cdot}6H_2O$, 8.0 mg/L $CoCl_2{\cdot}6H_2O$ and 1.74 mg/L biotin.

2.3.2. Hydrolysate preparation

C. alatosporum CCALA 988 hydrolysate production for *P. pastoris* fermentations was done in a shaking flask. 5 % (*w/v*) of dry, twice extracted *C. alatosporum* CCALA 988 biomass was suspended in 50 mM citrate buffer pH 4.5. The biomass slurry was pre-treated at 80 °C for one hour in the oven swirling twice. After allowing it to cool, 0.05 % (v/v) DISTILLASE® CS and Viscozyme® L were added for saccharification for 24 h at 50 °C shaking at 150 rpm. After allowing to cool again, 0.05 % (v/v) FERMGEN™ was added for solubilization over another 36 h at 30 °C shaking at 150 rpm. Subsequently, the treatment was ended by heating the suspension to 90 °C for 30 min in a pre-heated oven. The biomass slurry was then centrifuged at 15,000 ×g for 20 min at RT. The supernatant was vacuum sterile filtered (0.2 μm PES, Nalgene™ Rapid-Flow™) into a sterile flask and kept at 4 °C until further use.

2.3.3. Pichia pastoris batch and pulsed batch fermentation

Batch fermentations were conducted in 1 L bioreactors (Dasgip Eppendorf, Germany) with a starting volume of 500 mL. A single colony from a freshly streaked out plate was used to inoculate 250 mL BMGY 1 % medium in a 1 L baffled Erlenmeyer flask following incubation for 18–22 h at 30 °C and 110 rpm. 50 mL of pre-culture was used to inoculate the bioreactors for an initial OD_{600} of 0.2–0.6. Fermentation was performed at 30 °C and a starting aeration of 0.2 vvm. The stirrer was equipped with a 6-plate-rushton impeller placed 2.5 cm from the bottom of the shaft stirring with 400 rpm. Agitation and aeration were automatically adjusted to maintain the level of dissolved oxygen over 30 %. The pH was maintained at 6.0 and automatically adjusted with 20 % NH_4OH (directly into the broth) or with 7 % H_2SO_4 as required. Foam control was done using 1 % antifoam B (Merk, Germany). For pulsed batch, 25 mL of 50 % (w/v) glycerol was injected once after around 12 h. For monitoring the process parameters, the reactors were equipped with probes for pH and dissolved oxygen. 3 mL samples were drawn every 3–5 h and cell growth was determined as OD_{600} using an Ultraspec 10 spectrophotometer (Amersham Bioscience, UK). Cell dry weight was determined by centrifuging 1 mL culture broth at 500 ×g for 10 min and drying the cell pellet over night at 105 °C. The supernatant was analyzed for glycerol by HPLC-RID after 1:10 dilution in 2.5 mM H_2SO_4 and filtration (0.2 μm, PVDF), and for phytase activity.

2.3.4. Glycerol analysis

The HPLC system (Dionex Corp., USA) for glycerol analysis was coupled with a RID (RI 101, Shodex, Tokyo, Japan) and equipped with an Rezex ion exclusion column (Rezex ROA-Organic Acid H+ (8 %); 300 × 7.8 mm; Phenomenex Deutschland Ltd.). The column oven temperature was set to 70 °C, and 2.5 mM sulfuric acid was used for isocratic elution at a flow rate of 0.5 mL/min. The retention time of glycerol was 16.9 min.

2.3.5. Phytase activity assay

The phytase activity was determined in the *P. pastoris* culture supernatants by assessing the free phosphate released from phytate using ammonium molybdate as coloring agent to perform colorimetric quantification according to Bae et al, adapted for 96-well-plate applications [44]. 100 μL of supernatant was subjected to gel-filtration chromatography to purify the secreted protein from smaller molecules such as free phosphate. 96-Well SpinColumns (Harvard Apparatus, Holliston, MA USA) were used as described by the manufacturer. The filtrate was then diluted into the calibration range using water. 13.5 μL of the diluted filtrates were transferred into a 96-well assay plate. 53.5 μL freshly prepared 1.5 M phytate substrate in 0.1 M sodium acetate solution pH 5.0 was added to each well and the plate was incubated (37 °C, 30 min). To stop the reaction, 66.6 μL 5 % (w/v) trichloroacetic acid solution as well as 66.6 μL coloring solution were added and absorbance was measured at 700 nm. The coloring solution was freshly prepared by mixing four volumes of 1.5 % (w/v) ammonium molybdate in 5.5 % (v/v) sulfuric acid with one volume of 2.7 % (w/v) ferrous sulphate solution. In order to determine phytase units (U), samples had to be within a 0.8–5 mM calibration curve of potassium phosphate.

3. Results & discussion

3.1.1. Biomass composition

An integrated biorefinery concept for the cyanobacterium *C. alatosporum* CCALA 988 was investigated extracting high value products and producing the *E. coli* phytase appA using hydrolysate from the residual biomass. Firstly, the saccharide profile of the biomass was studied. Eleven monosaccharides were detected after acid hydrolysis of the biomass obviously making up the storage and structural (poly)saccharides of *C. alatosporum* CCALA 988 (Table 1 and annex 2.1) Eight of the detected sugars could be quantified (Table 1). These sugars were mannose (Man), glucosamine (GlcN), ribose (Rib), rhamnose (Rha), glucose (Glc), galactose (Gal), xylose/arabinose (Xyl/Ara), and fucose (Fuc), altogether making up 11.1 % of the biomass. Glucose as the most

Table 1
Identified saccharides in crude *C. alatosporum CCALA 988* biomass after 105 min TFA hydrolysis. Monosaccharide quantification was primarily performed based on EIC. Glucose and galactose were quantified by UV. $n = 3$ and R_t = retention time. *N. D.*: not determined.

Monosaccharides	R_t (min)	Mass (m/z)	Concentration ($mg_{sugar}/g_{dry\ biomass}$)
Mannose	3.8	511	7.2 ± 0.6
Glucosamine	4.3	510	5.6 ± 0.2
S/P-deoxy-hex	4.4	575	*N. D.*
Ribose	4.7	481	8.1 ± 0.5
Rhamnose	5.2	495	3.7 ± 0.2
3-O-Met-Man	6.2	525	*N. D.*
Glucose	6.8	511	57.7 ± 3.2
Galactose	7.2	511	18.5 ± 0.9
Xylose/Arabinose	7.8	481	6.8 ± 0.2
Fucose	8.6	495	3.7 ± 0.1
6-O-Met-Glc	8.6	525	*N. D.*
Total			111.3 ± 6.0

S/P-deoxy-hex: sulphated/phosphorylated-deoxy-hexose, 3-O-Met-Man: 3-*O*-methyl-mannose, 6-O-Met-Glc: 6-*O*-methyl-glucose.

important C-source for fermentation made up the largest fraction with around 52 % of the quantified saccharides. The identities of the three not quantified saccharides were elucidated by their retention time and fragmentation patterns of their MS2 spectra. Their compounded MS2 spectra are presented in the supporting information (annex 2.2). These three sugars were identified as a sulfated or phosphorylated deoxy-hexose (4.3 min), 3-*O*-methyl-mannose (6.1 min) and 6-*O*-methyl-glucose (8.5 min). The identities of the latter two were verified by methyl-glucose standards. The detected saccharides indicate the diversity of the heteroglycans in cyanobacteria, which are often β-linked backbones with side chains branching 1–3,4,6 [45]. Such glycans are difficult to be enzymatically decomposed by industrial enzymes especially due to the presence of varying substituted side chains [37].

Besides saccharides, the total lipid content of *C. alatosporum* CCALA 988 was analyzed by in-situ transesterification to FAMEs. The identified fatty acid profile was composed of palmitic acid, palmitoleic acid, stearic acid, linoleic acid, and α-linolenic acid, and made up around 4.1 % of the total *C. alatosporum* biomatter (annex 3). These fatty acids are rather common ones. They might be used as nutraceuticals or in cosmetics. Yet, the extraction of fatty acids as additional products in a biorefinery concept at such low amounts might not be feasible from an economical or ecological point of view. An additional extraction step is expected to increase the overall process costs considerably. Therefore, this needs to be investigated in a larger scale to show economic viability. Hence, lipids were not considered as separate biorefinery products in this study.

To sum it up, analysis of the *C. alatosporum* CCALA 988 biomass yielded 4.1 % lipids, 2.4 % starch, at least 8.7 % structural saccharides (as the result of 11.3 % quantified total saccharides minus 2.4 % starch), and 52.4 % protein. The total of the quantified components thus made up 76.4 % of the biomass including 1.9 % moisture and 6.9 % ash (Table 2). The unaccounted 23.6 % in the mass balance can be explained by unquantified DNA, RNA, secondary metabolites and partly by the unquantified saccharides as well. Overall, the *C. alatosporum* CCALA 988 biomass, which was cultivated for high CLP content, was not well suited for the utilization for biofuels or other commodities. The starch and lipid content made up only minor fractions of the biomass. The glucose identified as starch by enzymatic hydrolysis accounted for 42.3 % of the total quantified glucose. The remaining glucose thus is to be attributed to the structural polysaccharides, which are not easily hydrolyzed and seldomly utilized. Here, the low concentration of additional storage compound lipids did not warry for conversion into biofuels. However, possible utilization as nutraceuticals is proposed. The largest fraction of the biomass was composed of protein. The utilization of the biomass after extracting high value compounds will therefore need to be aligned for the highest value utilization of the protein.

Table 2
Overview of *C. alatosporum* CCALA 988 biomass composition and high- value compounds.

Components[a]	
% Moisture	1.9 ± 0.1
% Ash	6.9 ± 0.2
% Protein	52.4 ± 0.1
% FAME	4.1 ± 0.1
% Starch	2.4 ± 0.1
% Structural Saccharides	8.7 ± 0.4
% Total	76.4 ± 1.0
High value compounds[a,b]	
Chlorophyll a (mg/g)[a]	5.3 ± 0.3
Carotenoids (mg/g)[a]	1.1 ± 0. 1
Total (mg/g)[a]	6.4 ± 0.4
Phycocyanin (mg/g)[a]	25.6 ± 1.1
Allophycocyanin (mg/g)[a]	5.1 ± 0.4
Phycoerythrin (mg/g)[a]	3.8 ± 0.1
Total (mg/g)[a]	34.5 ± 1.6
Puwainaphycin (mg/g)[b]	21.6
Minutisamide (mg/g)[b]	101.5
Total (mg/g)[b]	123.1

[a] This study.
[b] Estimated based on the IT-TOF-MS rel. Intensities ratio 4.7:1 and the PUW values report by Mareš et al. [48]

Besides the primary metabolites, the biomass was further investigated for additional potential products such as pigments, phycobiliproteins and other high value compounds. Chlorophyll a and carotenoids were extracted with acetone and photometrically quantified to be 5.3 and 1.1 mg/g biomass, respectively. Additionally, phycobiliproteins (PBPs) were extracted in acetate buffer and determined using their respective absorbance maxima resulting in a total of 34.5 mg/g biomass. The major PBP was identified as phycocyanin yielding 25.6 mg/g. A second and third extraction cycle were also investigated and enhanced the yield of PBPs. The resulting spectra indicated that one extraction cycle might be sufficient for PBPs. This was indicated by the distinct blue color of the aqueous extracts (10:1 dilution) (annex 4). Considering the predominant presence of phycocyanin, one might consider to focus on phycocyanin as main PBP product. The many applications of phycocyanin have been shown including high-value therapeutics [46]. The therapeutic potential of phycocyanin in cancer therapy is promising and its successful application in even nanoparticle cancer therapy has been shown already [47]. Therefore, PBPs ought to be considered among the main high-value products.

The most interesting and highest value product in the *C. alatosporum* CCALA 988 biomass are CLPs, which might be used as lead compounds in pharmaceutical drug discovery. Mareš et al. found 30 putative PUWs, of which they identified 12 variants as congeners of PUW F and PUW G in this specific *Cylindrospermum* strain [48]. Their quantitative analysis of two PUW F variants showed that at least 21.6 mg/g PUWs are produced by *C. alatosporum* CCALA 988. Mareš et al. further provided ranges of concentrations and ratios for the detected and separated congeners of PUW F. By combining their results with the ratio of 4.7:1 (MINs:PUWs) established by the analysis done in this study, we concluded MIN variants could make up 101.5 mg/g totaling at least 123.1 mg/g CLPs per biomass (calculation in annex 5). This estimation was based on all PUWs combined as we could not separate them. Hrouzek et al. had further reported a ratio of 1:0.24 of PUW F to PUW G, which would increase the possible concentration of CLPs in *C. alatosporum* CCALA 988 biomass to around 150 mg/g [27]. We consider this as an estimation as it is only based on the masses of two PUWs. This is still in line with the mass balance of the quantified primary metabolites bringing the total mass to 91 % of total biomass. Considering this potential high CLP concentrations makes this strain a highly interesting candidate for a biorefinery approach.

3.1.2. Sequential extraction and enzymatic hydrolysis

In order to develop a multi-product biorefinery concept, a sequential extraction process has to be determined and validated. The amphiphilic nature of the CLP variants PUW and MIN requires a suitable extraction solvent. An aqueous extraction step ought to be performed initially in order to avoid denaturation of proteins, which would be detrimental to PBPs as additional high-value products. The resulting treatment for a sequential extraction of *C. alatosporum* CCALA 988 biomass including further residual biomass utilization is shown in Fig. 1. In the first extraction step (aq. crude extract), the impure phycobiliproteins were recovered as well as a fraction of the CLPs. In the second extraction step using organic solvents, e.g. methanol (MeOH crude extract), some additional amounts of CLPs were extracted including other valuable pigments, chlorophyl a and carotenoids.

The extraction of the CLPs was verified by IT-TOF-MS as single charged negative ions $(M\text{-}H)^-$ and the double charged positive ions $(M + 2H)^{2+}$ in both aqueous and organic extract. In the corresponding chromatograms two peaks with relevant masses were found eluting at around 6 min (Fig. 2). The HPLC/MS analysis gave an approximate estimation about the ratios between MINs and PUWs; however, quantification was limited due to the lack of appropriate standards. The two peaks were identified as described in Section 2.2.3 by their masses as MINs and PUWs with a ratio of 4.7:1. Based on the compared peak area ratio we also concluded that 97 % of the estimated MINs were present in the aqueous extract. PUWs accounted for 85 % in the aqueous extract. This showed that only a small fraction of CLPs are extracted in a second step with methanol. Yet, further additional compounds were extracted as shown by peaks eluting after 10 min (Fig. 2 B). These need to be identified and their bioactivity characterized. Possibly applying only aqueous extractions might be sufficient. Yet, the organic extraction delivers additional valuable compounds. Hence, only an economic analysis will reveal which extraction concept is most viable.

After the extraction, the residual biomass was hydrolyzed with a combination of industrial saccharolytic and proteolytic enzymes. The enzymes DISTILLASE® CS, OPTIMASH™ BG, and Viscozyme® L, for the hydrolysis of starch and other structural saccharides were investigated in advance on the not extracted dry *C. alatosporum* CCALA 988 biomass (annex 6). Viscozyme® L and DISTILLASE® CS yielded 40 mg/g and 44 mg/g monosaccharides per biomass, respectively. Both released glucose, mannose, and ribose, and Viscozyme® L also galactose. DISTILLASE® CS, a mixture of amylases, released the major part of glucose, even more

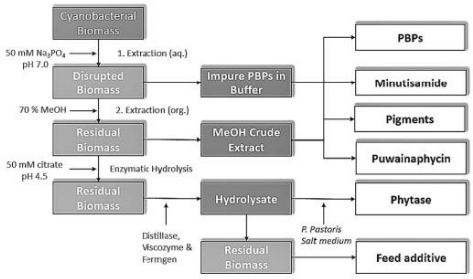

Fig. 1. Scheme of sequential extraction regiment and multi-product biorefinery concept of *C. alatosporum* CCALA 988 biomass. In a first extraction step, an aqueous solvent is used to extract phycobiliproteins (PBPs) and the cyclic lipopeptides minutisamide and puwainaphycin. In a second extraction step, an organic solvent is used to extract remaining cyclic lipopeptides and pigments. The residual biomass from extraction is then enzymatically treated to produce a hydrolysate for a *P. pastoris* fermentation producing phytase. Lastly, the residual biomass from hydrolysis is recovered for further use, e.g. for biogas production or for feed additive.

than related to the starch content of the algal biomass detected by starch analysis, probably due to side activities. OPTIMASH™ BG and Viscozyme® L, both enzyme mixtures for the saccharification of glucans, cellulose and hemicellulose, released somewhat less glucose, but the release of galactose implies that they also attacked other structural parts of the biomass than DISTILLASE® CS. For the final hydrolysate production, the saccharolytic enzymes were chosen also based on their biomass desintegration capacities. Viscozyme® L showed to solubilize the overall biomass better than the other tested enzymes and the control. Thus, the two saccharolytic enzymes DISTILLASE® CS and Viscozyme® L were combined to achieve the highest solubilization of the biomass, accepting a somewhat lower glucose yield. In a second hydrolysis step, the industrial proteolytic enzyme FERMGEN™ was added to solubilize further as much residual biomass as possible, esp. proteins. The hydrolytic efficiency of FERMGEN™ on cyanobacterial biomass had been shown prior on a *Nostoc* strain [37].

The resulting hydrolysate was used as nutrient supplement in a *P. pastoris* fermentation producing appA *E. coli* phytase reported in Section 3.2.2.

3.1.3. Biorefinery mass balance

The following objectives were within the scope of this study: identification of further products from the residual *C. alatosporum* CCALA 988 biomass, utilization of the residual biomass, as well as providing data for a techno-economic analysis. Therefore, a bench scale mass balance with 10 g of *C. alatosporum* CCALA 988 biomass was performed following the presented sequential extraction and biorefinery concept. The distribution analysis of proposed and determined products as well as quantified saccharides in extracts and residual biomasses are shown in Table 3. Additional to the complete mass balance, the results from the elemental analysis of the crude biomass, as well as the dry residual biomass before and after enzymatic hydrolysis are presented in Fig. 3. The mass balance referred to 10 g starting biomass, of which 1.8 g were extracted in the first aq. extraction step. This extracted mass included 985 mg MINs, 184 mg PUWs and 345 mg phycobiliproteins, which resulted in around 300 mg remaining biomass in the extract. The additional extracted extra protein mass (not quantified) ought to be recycled into the process in larger scale for the enzymatic hydrolysis. In the second extraction step using MeOH, 0.4 g were extracted, of which 30 mg and 32 mg are MINs and PUWs, respectively. Further, 53 mg chlorophyl a and 11 mg carotenoids were co-extracted. This means that additional 274 mg biomatter are left in this extract, which might partly be additional products. For instance Devi et al. identified large concentrations of alkaloids, saponins and terpenoids in another *Cylindrospermum* strain with strong anti-oxidative activity [49]. Furthermore, scytonemin, sterols or mycosporin like amino acids might be additional candidates [20].

The remaining 7.8 g (77.8 %) biomass after the two extraction steps were subjected to enzymatic hydrolysis as discussed above. The saccharolytic and proteolytic hydrolysis resulted in a solubilization of 43.8 % of the 7.8 g biomass (being 34.1 % of 10 g). Consequently, 3.4 g solubilized biomass was obtained as hydrolysate of the initial 10 g biomass, leaving 4.4 g of residual biomass. The mass balance gave simple information. Yet, the saccharide analysis is more comprehensive. So, the individual fractions were investigated for their saccharide content to infer future optimized biomass treatment.

The residual biomass after the two extraction steps (Res Biomass 2) exhibited total quantified saccharides contents of 167.8 mg/g, which were 18 % higher compared to the total amount of saccharides in the starting 10 g biomass (111.3 mg/g in Table 1). Interestingly, all monosaccharides were measured at lower concentrations relative to the starting biomass except Glc and Fuc, which were measured at 170.6 % and 175.5 %, respectively. Low detection of these two or more monosaccharides in the starting biomass might be a reason for this, potentially due to incomplete biomass degradation or side reactions during acid hydrolysis of the biomass. Only Glc, Gal and Rib were released as

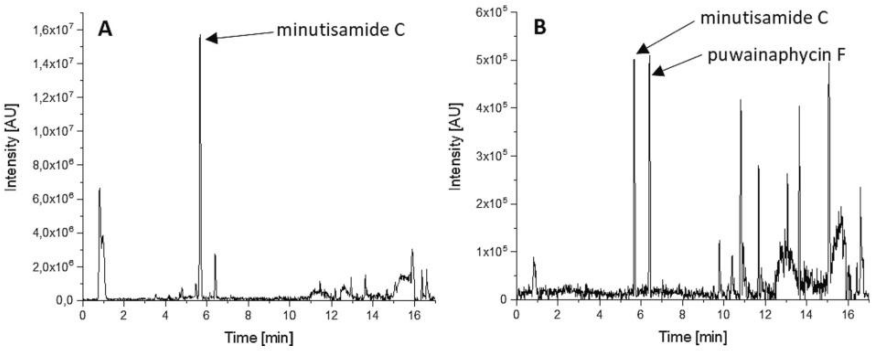

Fig. 2. Chromatograms of IT-TOF-MS (positive ion mode) analysis from A: aqueous crude extract and B: methanol crude extract of *C. alatosporum* CCALA 988 biomass.

Table 3
Distribution analysis of determined products and saccharides in extracts and residual biomasses resulting from the sequential extraction. Given in the brackets is also the detection rate of the saccharides relative to the 10 g starting biomass. The estimation of puwainaphycins (PUWs) and minutisamides (MINs) is described in the text. The quantification of phycocyanin (PC), allophycocyanin (APC) and phycoerythrin (PE) as well as the chlorophyll *a* and carotenoids is described in the methods. Saccharides were quantified after TFA hydrolysis of dry residual biomasses followed by PMP-HPLC analysis as described in the methods, and presented as triplicates with one standard deviation. Monosaccharides in the enzymatic hydrolysate were measured by PMP-HPLC analysis (analytical duplicates).

Extract 1 (aq.)		Extract 2 (org.)		Hydrolysate[b]	
PUWs	18.4 mg/g	PUWs	3.2 mg/g	Rib	21.5 ± 1.4 mg/L (9.3 %)
MINs	98.5 mg/g	MINs	3.0 mg/g	Glc	161.0 ± 0.2 mg/L (2.6 %)
PC	25.6 ± 1.1 mg/g	Chlorophyll a	5.3 ± 0.3 mg/g	Gal	6.34 ± 0.22 mg/L (1.2 %)
APC	5.1 ± 0.4 mg/g	Carotenoids	1.1 ± 0. 1 mg/g	Solubles	21.9 g/L
PE	3.8 ± 0.1 mg/g			Protein[a]	9.4 g/L
		Residual Biomass 2		Residual Biomass 3[c]	
		Man	8.2 ± 0.4 mg/g	Man	7.6 ± 0.9 mg/g (49 %)
		GlcN	< LOQ	GlcN	4.0 ± 0.4 mg/g
		Rib	4.6 ± 0.3 mg/g	Rib	2.6 ± 0.3 mg/g (32 %)
		Rha	3.9 ± 1.3 mg/g	Rha	2.4 ± 0.4 mg/g (35 %)
		Glc	126.2 ± 5.1 mg/g	Glc	10.1 ± 3.3 mg/g (4.5 %)
		Gal	10.9 ± 0.5 mg/g	Gal	6.4 ± 0.9 mg/g (33 %)
		Xyl	5.8 ± 0.6 mg/g	Xyl	4.7 ± 1.0 mg/g (56 %)
		Fuc	8.3 ± 0.7 mg/g	Fuc	5.7 ± 0.5 mg/g (39 %)

[a] Estimated based on the difference in measured N content in Residual Biomass 2 and 3, and on N to protein conversion factor 4.78.
[b] Monosaccharides in the hydrolysate per liter and in % of saccharides in the Residual Biomass 2, resp.
[c] Saccharides in mg/g Residual Biomass 3 and in % of saccharides in Residual Biomass 2, resp.

monosaccharides during enzymatic hydrolysis by the applied enzymes, which showed to be a total of 189 mg/L, making up around 13 % of the initial saccharides in the residual biomass 2, and thus being considerably below the yields of the enzyme hydrolysis tests performed on the native algal biomass (annex 6). It needs to be investigated further, if and to what extend the extraction steps influenced this outcome. Further, the detected saccharides in the hydrolysate and in the remaining residual biomass 3 made up around 15 % of the saccharides in the residual biomass 2, which had been subjected to the enzymatic hydrolysis. Therefore, around 85 % of the saccharides ought to be dissolved in the hydrolysate and most of them still present as oligo- or polysaccharides in the hydrolysate. The utilization of these saccharides obviously requires an improved enzyme regime and ought to be investigated further. The elemental analysis of the crude biomass, and the extracted biomasses before and after the hydrolysis revealed that the extractions did neither change the macro element composition nor the C to N ratio strongly. Yet, the total percentage of the five analyzed macro elements increased slightly from the starting (92.7 %) to the residual biomass after enzymatic hydrolysis (98.5 %), which might be due to preferred solubilization of inorganics. Also, considering 3.4 g biomass were dissolved in the hydrolysate and, with 11 and 12.5 % N-content in the residual biomasses 2 and 3, resp., around 0.308 g N were calculated to be dissolved in the hydrolysate. Using the N to protein factor of 4.78 as mentioned in the methods, this accounted to roughly 1.47 g of protein or 9.4 g/L in the hydrolysate (Table 3). Nevertheless, 43.8 % of the substrate biomass remained recalcitrant to digestion by the applied enzymes and was still left as residue. It may be used for digestion in a biogas plant or possibly for animal feed. This fraction might be reduced further by improved treatment methods.

3.2. Phytase fermentation

3.2.1. Salt media

We could establish that hydrolysate from the cyanobacterium *Nostoc* sp. De1 can also be used as macronutrient in enzyme production with *P. pastoris* [35]. In the present study, different salt media as basic media were investigated prior to supplementation with hydrolysate. The production of appA *E. coli* phytase by *P. pastoris* was studied using a fermenter system of 1 L capacity with 500 mL working volume. The fermentations were performed up to 48 h with 450 mL salt medium of either D'Anjou or MSM medium and 4 % glycerol. Each parameter set was done in duplicates. The time courses of batch and pulsed batch fermentation in MSM medium are shown in Fig. 4 A and C, resp. Time courses of further fermentations in MSM and fermentations in D′Anjou medium are displayed in the supplementals (Annex 7). Fermentation results are summarized in Table 4. Fermentations in basal salt medium (BSM) medium at pH 6 were also tested but significant salt

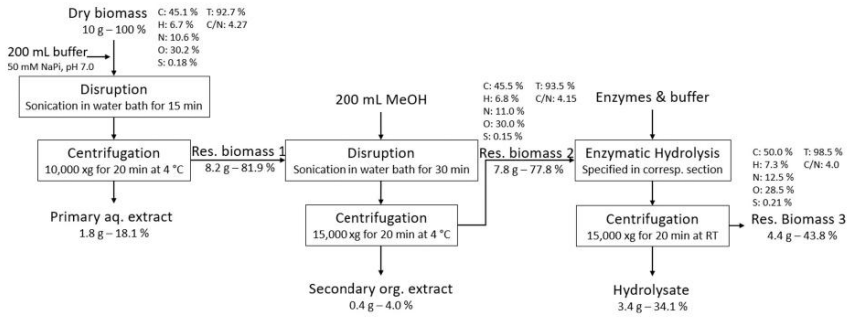

Fig. 3. Mass balance and process steps of the biorefinery concept for 10 g of *C. alatosporum* CCALA 988 biomass conducted in triplicates. Including elemental analysis values CHNOS, total percentage and C to N ratio for crude biomass, dry residual biomass before and after enzymatic hydrolysis.

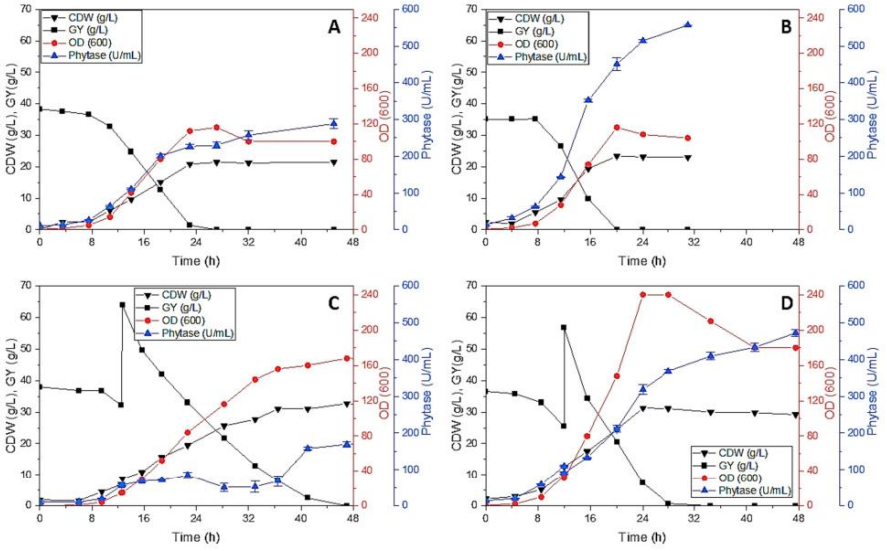

Fig. 4. Phytase production with *P. pastoris* showing A: a batch fermentation in MSM and B: batch fermentation in MSM with 10 % (v/v) hydrolysate from extracted *C. alatosporum* CCALA 988 residual biomass C: a pulsed batch fermentation in MSM. D: a pulsed batch fermentation in MSM with 10 % (v/v) hydrolysate from extracted *C. alatosporum* CCALA 988 residual biomass.

precipitations formed, and the fermentation results were neglected. In both salt media (D'Anjou and MSM), the glycerol was consumed after 28 h of batch fermentation and maximum biomass yields were reached after 30 h. The OD_{max} and CDW_{max} were higher in the D'Anjou medium compared to the MSM medium with 120 and 24 g/L to 112 and 21 g/L, respectively. The highest phytase activity ($A_{p,\ max}$) measured in the salt media were 250 U/mL and almost 290 U/mL for D'Anjou and MSM medium, respectively. Yet, after several hours of fermentation, small amounts of white precipitation were noticed in the D'Anjou medium. Consequently, we proceeded our experiments with the MSM medium of the lower salt concentration and higher final phytase activity. The used *Pichia* trace metals (PTM) concentration was lower than in other reported media. Hence, an investigation of the effect of the PTM concentration was performed in the next step. A doubling of the PTM concentration resulted in slightly higher CDW_{max}, but not OD_{max}. The phytase $A_{p,\ max}$ was lower than with regular PTM concentration with around 160 U/mL after 48 h. This is in line with other reports, which showed that high Fe^{2+}, Zn^{2+} and Co^{2+} inhibit *E. coli* phytase [50]. Further testing was done to check how well the appA *E. coli* phytase would be expressed in MSM medium with larger amounts of C-source by increasing the glycerol. Therefore, after 12 h, 25 g/L glycerol was pulsed into the medium (Fig. 4 C). The glycerol was completely consumed after 48 h. The OD_{max} and CDW_{max} after 58 h reached up to 175 and 35 g/L, respectively. But the phytase $A_{p,\ max}$ reached was only 160 U/mL. A drop in measured phytase activity from 20 h to 35 h could be observed. The decline in activity seems to be correlated to the glycerol pulse. The

Table 4
Overview of phytase fermentations with *P. pastoris* in salt media. Individual results of duplicate runs are displayed S_{Total}: total substrate, CDW: cell dry weight, $Y_{x/s}$: biomass yield per substrate, q_s: substrate utilization rate, μ: growth rate, A_p: activity yield, $Y_{A/X}$: activity yield per biomass, q_A (μ): specific product formation rate.

Cultivation conditions						Growth kinetics				Product kinetics		
Medium	Temp.	pH	Mode	S_{total}	Time	CDW_{max}	$Y_{x/s,\ max}$	$q_{s,max}$	μ_{max}	$A_{p,\ max}$	$Y_{A/x,\ max}$	$q_A\ (\mu)_{max}$
	(°C)			(g)	(h)	(g/ L)	(g g^{-1})	(g g^{-1} h^{-1})	(h^{-1})	(U/ mL)	(U g^{-1})	(U g^{-1} h^{-1})
BMGY[a]	30	6.0	Batch	40	24	25.3	0.70	0.72	0.286	530.0	21,378	6680
BMGY[a]	30	6.0	Batch	40	24	23.4	0.59	0.84	0.266	522.0	23,337	6536
D'Anjou	30	6.0	Batch	40	28	24.4	0.62	0.59	0.092	232.9	10,887	1371
D'Anjou	30	6.0	Batch	40	28	24.8	0.65	0.93	0.092	247.6	11,416	2447
MSM	30	6.0	Batch	40	28	21.4	0.55	0.66	0.137	250.7	11,883	3802
MSM	30	6.0	Batch	40	28	21.5	0.56	0.71	0.140	288.4	13,414	2970
MSM(2xPTM)	30	6.0	Batch	40	28	22.6	0.59	0.74	0.131	157.1	9092	1742
MSM(2xPTM)	30	6.0	Batch	40	28	23.2	0.61	0.84	0.143	194.7	9255	2422
MSM	30	6.0	Pulsed Batch	65	48	35.4	0.57	2.28	0.149	160.4	7806	2216
MSM	30	6.0	Pulsed Batch	65	48	32.7	0.51	2.38	0.138	169.4	7994	2074

[a] Fermentations in BMGY are taken from Ref [35] and are shown as reference.

growth does not seem to be affected as enough N- and C-source were available. Yet, enzyme activity decreased, indicating a simple N-source might not be sufficient for good enzyme biosynthesis. The nitrogen source is usually provided by the addition of ammonium hydroxide. The nitrogen source reportedly affects recombinant protein production in *P. pastoris*. Differing reports show the need for alternatives and a thorough investigation on the N-source. Hence, the batch and pulsed batch fermentation in MSM medium indicated a better N-source might be needed to improve enzyme expression.

For a more detailed analysis the growth kinetics and product kinetics need to be considered. The growth kinetic parameters determined for biomass per substrate yield ($Y_{x/s,\ max}$), maximum substrate utilization rate ($q_{s,max}$), and maximum specific growth rate (μ_{max}) allow to compare the growth of this *P. pastoris* strain in the tested salt media (Table 4). The $Y_{x/s,\ max}$ was the in same range as in complex medium (BMGY). But the μ_{max} was about half of what we found in BMGY medium for this strain [35]. The $q_{s,max}$ in pulsed fermentations was more than twice as high in MSM medium compared to BMGY. Also, the maximum activity yield ($A_{p,\ max}$), maximum activity yield per biomass ($Y_{A/X,\ max}$), and maximum specific product formation rate ($q_A\ (\mu)_{max}$) in MSM were about half of the values achieved in BMGY medium. All these results indicate a lack of macronutrients in MSM medium. The N-source in MSM medium with only ammonium was insufficient to support optimal growth as well as excellent enzyme expression as the growth and product kinetics indicated. Nevertheless, the acceptable growth kinetics results of the fermentations in MSM medium served as a starting point as a cost-efficient minimal growth medium to improve phytase expression with the produced hydrolysate from extracted *C. alatosporum* CCALA 988 biomass.

3.2.2. Salt medium with hydrolysate

Hydrolysate from extracted residual *C. alatosporum* CCALA 988 biomass (Res. Biomass 2) was prepared as described in Section 2.3.2 and tested as fermentation medium to supply complex compounds. Therefore, *P. pastoris* fermentation producing appA *E. coli* phytase in MSM medium was performed with different hydrolysate media concentrations ranging from 0 to 10 Vol% with or without MSM medium. The results are summarized in Table 5, time courses of batch and pulsed batch fermentations with MSM and 10 vol% hydrolysate are exemplarily displayed in Fig. 4 B and 4 D, and additional fermentation time courses in the supplementals (annex 8). Firstly, the fermentation in pure water and in 1 vol% hydrolysate without MSM was investigated to see the effect of the pre-culture medium and small hydrolysate concentrations on the expression in the main culture. The results (annex 8.1) indicate that the enzyme expression and measured activity of appA *E. coli* phytase was negatively affected for fermentations in MSM medium: the effect of 1 % hydrolysate showed no observable accelerated growth, yet it extended the growth to around 40 h reaching an OD_{max} and CDW_{max} of 55 and 11 g/L with 5 g/L glycerol left. This shows that minimal hydrolysate concentrations had an observable effect on cell growth but would not solely suffice as nutrient supplement for phytase expression. So, we tested the phytase expression in MSM medium with 1 vol% hydrolysate. A small improvement in growth could be observed, but $A_{p,max}$ could not be increased compared to the one with MSM medium alone. The next step, supplementation with 5 vol% hydrolysate showed much more promising results. Glycerol was consumed after 20 h with the OD_{max} and CDW_{max} reaching 120 and 21 g/L as observed for the tests with MSM medium. Yet, the $A_{p,max}$ could be improved to 350 U/mL, which is 40 % higher

Table 5
Overview of phytase fermentations with *P. pastoris* in salt media supplemented with hydrolysate from extracted *C. alatosporum* CCALA 988 residual biomass. S_{Total}: total substrate, CDW: cell dry weight, $Y_{x/s}$: biomass yield per substrate, q_s: substrate utilization rate, μ: growth rate, A_p: activity yield, $Y_{A/X}$: activity yield per biomass, q_A (μ): specific product formation rate.

Cultivation conditions							Growth kinetics				Product kinetics		
MSM	Hydrol.	Temp.	pH	Mode	S_{total}	Time	CDW_{max}	$Y_{x/s,\ max}$	$q_{s,\ max}$	μ_{max}	$A_{p,\ max}$	$Y_{A/x,\ max}$	$q_A\ (\mu)_{max}$
(+/−)	(vol%)	(°C)			(g)	(h)	(g/ L)	(g g^{-1})	(g g^{-1} h^{-1})	(h^{-1})	(U/ mL)	(U g^{-1})	(U g^{-1} h^{-1})
+	10	30	6.0	Pulsed Batch	65	28	31.3	0.46	1.28	0.195	472.2	16,172	2420
+	10	30	6.0	Pulsed Batch	65	28	28.7	0.49	0.77	0.228	450.7	16,272	2922
+	10	30	6.0	Batch	40	20	23.1	0.66	0.54	0.169	556.9	24,212	3588
+	10	30	6.0	Batch	40	20	23.6	0.64	0.45	0.169	491.6	20,567	3400
+	5	30	6.0	Batch	40	20	21.5	0.59	0.60	0.195	365.6	17,494	2138
+	5	30	6.0	Batch	40	20	21.2	0.59	0.70	0.192	343.2	16,990	2610
+	1	30	6.0	Batch	40	24	23.8	0.69	0.95	0.117	206.6	8681	3923
+	1	30	6.0	Batch	40	24	24.2	0.71	0.69	0.101	228.2	9431	2179
−	1	30	6.0	Batch	40	40	11.5	0.38	4.02	0.058	391.4	34,035	1839
−	1	30	6.0	Batch	40	40	11.0	0.37	3.04	0.066	387.0	35,182	2219
−	0	30	6.0	Batch	40	31	10.5	0.49	0.97	0.221	273.3	26,026	3739
−	0	30	6.0	Batch	40	31	10.7	0.47	0.94	0.220	333.8	31,196	2382

compared to only MSM medium. Nevertheless, compared to the more costly BMGY medium the $A_{p,max}$ remained 30 % lower.

To further improve putative positive effects of the supplemented hydrolysate, the concentration was doubled to 10 vol% of the starting volume (Fig. 4 B). The glycerol was consumed within 20 h and reached OD_{max} and CDW_{max} of 112 and 23 g/L. The $A_{p,max}$ obtained was above 550 U/mL, which is equivalent to what was reached with BMGY medium. The increasing amount of secreted protein over the fermentation course could be verified on an SDS-PAGE gel (annex 9). Therefore, we could show that 10 vol% hydrolysate and MSM medium could be used as alternative to expensive complex medium for a batch fermentation of *P. pastoris* expressing appA *E. coli* phytase.

The growth and product kinetics can change strongly depending on C-source and nutrient availability. To investigate the appA *E. coli* phytase expression in 10 vol% hydrolysate and MSM medium further, it was tested how well phytase was expressed in a pulsed batch fermentation. After 12 h, additional 25 g/L glycerol were pulsed (Fig. 4 D). The additional C-source increased the OD_{max} and CDW_{max} after 28 h to 200 and 30 g/L. Yet, the $A_{p,max}$ reached only around 470 U/mL. This indicated that more than 10 vol% hydrolysate or additional feeding of hydrolysate will be needed for a fed batch fermentation strategy. Considering the solubilization efficiency reached in the hydrolysate production as described above, 10 vol% hydrolysate is equivalent to only about 2.2 g/L soluble mass with around 0.94 g/L protein. This is less than a tenth of the dissolved mass in BMGY medium. The pulsed batch fermentation elucidated nicely how sensitive *P. pastoris* reacts to additional C-source in a protein limited environment as the protein expression was impaired. Hence, product kinetics such as $q_A\ (\mu)_{max}$ were reduced. Nevertheless, we could show how well suited the hydrolysate from residual *C. alatosporum* CCALA 988 biomass serves as nutrient source for *P. pastoris* fermentation. The use of a different C-source (e.g. glucose) might also bring a different outcome to the enzyme activity yield, but was not in the scope of this study. It is also apparent that the relationship between activity yield and C-source depend on different factors such as gene, medium, strain etc. [51]

The present study outlines a novel biorefinery approach for cyanobacteria *Cylindrospermum alatosporum*. Yet, several aspects need to be investigated in more detail for further process development or economic estimations, mainly fed-batch fermentation, purification of CLPs, and enzymes for saccharide hydrolysis. Industrial saccharolytic enzymes designed for e.g. grain ethanol production are usually available at comparatively low cost, but hydrolyze algal polysaccharides mostly incomplete. Enzyme selection has to be refined and possibly new activities have to be developed to achieve best performance with minimized enzyme consumption.

4. Conclusion

The results of this study revealed that the presented novel multi-product biorefinery concept for the cyanobacterial strain *C. alatosporum* CCALA 988 is feasible. The biocomposition and saccharide fingerprint of this cyanobacterial strain were first characterized. The sequential extraction concept and the identified high-value compounds such as the CLPs PUWs and MINs and the phycobiliproteins and pigments are the basis of this multi-product biorefinery concept. The utilization of the residual biomass as enzymatic hydrolysate in a *P. pastoris* fermentation as first shown here is an important additional valorization step, which can be assumed to make such a biorefinery concept economically more promising. A scale-up of this process, including investigations on improving the enzymatic hydrolysis as well as further fermentations with hydrolysate will be needed to validate the concept and to enable an overall ecological and economic viability of this concept by a life cycle sustainability assessment.

CRediT authorship contribution statement

Korbinian Sinzinger: Investigation, Methodology, Conceptualization, Writing – original draft. **Sebastian Bieringer:** Investigation, Methodology, Writing – original draft. **Doris Schieder:** Conceptualization, Methodology, Supervision, Writing – review & editing. **Herbert Riepl:** Funding acquisition, Supervision, Writing – review & editing. **Volker Sieber:** Funding acquisition, Supervision, Writing – review & editing.

Declaration of competing interest

The authors declare that they have no known competing financial interests or personal relationships that could have appeared to influence the work reported in this paper.

Data availability

Data will be made available on request.

Acknowledgements

The EFRE – Interreg project 41 "Joint Research on Natural Compounds from Cyanobacteria as a Model of Cross-Border Scientific Partnership" was funded by the European Union ZIEL ETZ. Many thanks to Algatech for providing the biomass.

Appendix A. Supplementary data

Supplementary data to this article can be found online at https://doi.org/10.1016/j.algal.2023.103302.

References

[1] J.R. Banu, Kavitha S. Preethi, M. Gunasekaran, G. Kumar, Microalgae based biorefinery promoting circular bioeconomy-techno economic and life-cycle analysis, Bioresour. Technol. 302 (2020) 122822, https://doi.org/10.1016/j.biortech.2020.122822. Available from: https://www.sciencedirect.com/science/article/pii/S0960852420300912.

[2] F. Sarsekeyeva, B.K. Zayadan, A. Usserbaeva, V.S. Bedbenov, M.A. Sinetova, D. A. Los, Cyanofuels: biofuels from cyanobacteria. Reality and perspectives, Photosynth. Res. 125 (1) (2015) 329–340. Available from: https://doi.org/10.1007/s11120-015-0103-3.

[3] K.W. Chew, J.Y. Yap, P.L. Show, N.H. Suan, J.C. Juan, T.C. Ling, D.-J. Lee, J.-S. Chang, Microalgae biorefinery: high value products perspectives, Bioresour. Technol. 229 (2017) 53–62, https://doi.org/10.1016/j.biortech.2017.01.006. Available from: https://www.sciencedirect.com/science/article/pii/S0960852417300263.

[4] M. Bhattacharya, S. Goswami, Microalgae – a green multi-product biorefinery for future industrial prospects, Biocatal. Agric. Biotechnol. 25 (2020) 101580, https://doi.org/10.1016/j.bcab.2020.101580. Available from: https://www.sciencedirect.com/science/article/pii/S1878818119318699.

[5] D.A. Esquivel-Hernández, A. Pennacchio, R.P. Saldívar, V. Faraco, Integrated biorefinery from Arthrospira platensis biomass as feedstock for bioethanol and lactic acid production, bioRxiv (2019), https://doi.org/10.1101/715672. Available from: https://www.biorxiv.org/content/early/2019/07/26/715672.

[6] S.S. Hassan, G.A. Williams, A.K. Jaiswal, Moving towards the second generation of lignocellulosic biorefineries in the EU: drivers, challenges, and opportunities, Renew. Sust. Energ. Rev. 101 (2019) 590–599, https://doi.org/10.1016/j.rser.2018.11.041. Available from: https://www.sciencedirect.com/science/article/pii/S1364032118307937.

[7] P. Fasahati, W. Wu, C.T. Maravelias, Process synthesis and economic analysis of cyanobacteria biorefineries: a superstructure-based approach, Appl. Energy 253 (2019) 113625, https://doi.org/10.1016/j.apenergy.2019.113625. Available from: https://www.sciencedirect.com/science/article/pii/S0306261919312991.

[8] I. Gifuni, A. Pollio, C. Safi, A. Marzocchella, G. Olivieri, Current bottlenecks and challenges of the microalgal biorefinery, Trends Biotechnol. 37 (3) (2019) 242–252, https://doi.org/10.1016/j.tibtech.2018.09.006. Available from: https://www.sciencedirect.com/science/article/pii/S0167779918302592.

[9] G.P'. Lam, M.H. Vermuë, Eppink MHM, R.H. Wijffels, C. van den Berg, Multi-product microalgae biorefineries: from concept towards reality, Trends Biotechnol. 36 (2) (2018) 216–227, https://doi.org/10.1016/j.tibtech.2017.10.011. Available from: https://www.sciencedirect.com/science/article/pii/S0167779917302755.

[10] M. Koller, A. Muhr, G. Braunegg, Microalgae as versatile cellular factories for valued products, Algal Res. 6 (2014) 52–63, https://doi.org/10.1016/j.

algal.2014.09.002. Available from: https://www.sciencedirect.com/science/article/pii/S2211926414000782.
[11] H.-W. Yen, I.-C. Hu, C.-Y. Chen, S.-H. Ho, D.-J. Lee, J.-S. Chang, Microalgae-based biorefinery – from biofuels to natural products, Bioresour. Technol. 135 (2013) 166–174, https://doi.org/10.1016/j.biortech.2012.10.099. Available from: https://www.sciencedirect.com/science/article/pii/S096085241201601X.
[12] R.H. Wijffels, O. Kruse, K.J. Hellingwerf, Potential of industrial biotechnology with cyanobacteria and eukaryotic microalgae, Curr. Opin. Biotechnol. 24 (3) (2013) 405–413, https://doi.org/10.1016/j.copbio.2013.04.004. Available from: https://www.sciencedirect.com/science/article/pii/S0958166913000852.
[13] J. Moncada, J.A. Tamayo, C.A. Cardona, Integrating first, second, and third generation biorefineries: incorporating microalgae into the sugarcane biorefinery, Chem. Eng. Sci. 118 (2014) 126–140, https://doi.org/10.1016/j.ces.2014.07.035. Available from: https://www.sciencedirect.com/science/article/pii/S0009250914003807.
[14] C. Nurra, C. Torras, E. Clavero, S. Ríos, M. Rey, E. Lorente, X. Farriol, J. Salvadó, Biorefinery concept in a microalgae pilot plant. Culturing, dynamic filtration and steam explosion fractionation, Bioresour. Technol. 163 (2014) 136–142, https://doi.org/10.1016/j.biortech.2014.04.009. Available from: https://www.sciencedirect.com/science/article/pii/S0960852414005045.
[15] M. Rizwan, J.H. Lee, R. Gani, Optimal design of microalgae-based biorefinery: economics, opportunities and challenges, Appl. Energy 150 (2015) 69–79, https://doi.org/10.1016/j.apenergy.2015.04.018. Available from: https://www.sciencedirect.com/science/article/pii/S0306261915004730.
[16] Melina Psycha, Antonis Kokossis, Techno-economic evaluation of an integrated microalga biorefinery targeting the co-production of specialty chemicals [internet], in: Antonio Espuña, Moisès Graells, Luis Puigjaner (Eds.), 27th European Symposium on Computer Aided Process Engineering vol. 40, Elsevier, 2017, pp. 1981–1986 (vol. 40). Available from: https://www.sciencedirect.com/science/article/pii/B9780444639653503329.
[17] Melina Psycha, Kostantinos Pyrgakis, Antonis C. Kokossis, Process Design Analysis for the Valorisation and Selection of Integrated Micro-algae Biorefineries [Internet]. In: Jiří Jaromír Klemeš, Petar Sabev Varbanov, Peng Yen Liew, editors. 24th European Symposium on Computer Aided Process Engineering, vol. 33: Elsevier vol. 33, 2014, pp. 1543–1548. Available from: https://www.sciencedirect.com/science/article/pii/B9780444634595500921.
[18] Melina Psycha, Antonis C. Kokossis, Synthesis and Optimization of Microalgae Biorefineries [Internet]. In: Zdravko Kravanja, Miloš Bogataj, editors. 26th European Symposium on Computer Aided Process Engineering, vol. 38: Elsevier vol. 38, 2016, pp. 325–330. Available from: https://www.sciencedirect.com/science/article/pii/B978044463428350059X.
[19] S. Singh, B.N. Kate, U.C. Banerjee, Bioactive compounds from Cyanobacteria and microalgae: an overview, Crit. Rev. Biotechnol. 25 (3) (2005) 73–95. Available from: https://doi.org/10.1080/07388550500248498.
[20] J. Demay, C. Bernard, A. Reinhardt, B. Marie, Natural products from Cyanobacteria: focus on beneficial activities, Mar. Drugs 17 (6) (2019), https://doi.org/10.3390/md17060320. Available from: https://www.mdpi.com/1660-3397/17/6/320.
[21] E. Dittmann, M. Gugger, K. Sivonen, D.P. Fewer, Natural product biosynthetic diversity and comparative genomics of the Cyanobacteria, Trends Microbiol. 23 (10) (2015) 642–652. Available from: https://www.sciencedirect.com/science/article/pii/S0966842X15001572 https://doi.org/10.1016/j.tim.2015.07.008.
[22] T. Encarnação, A.A.C.C. Pais, M.G. Campos, H.D. Burrows, Cyanobacteria and microalgae: a renewable source of bioactive compounds and other chemicals, Sci. Prog. 98 (2) (2015) 145–168. Available from: https://doi.org/10.3184/003685015X14298590596266.
[23] V. Gupta, S.K. Ratha, A. Sood, V. Chaudhary, R. Prasanna, New insights into the biodiversity and applications of cyanobacteria (blue-green algae)—prospects and challenges, Algal Res. 2 (2) (2013) 79–97. Available from: https://www.sciencedirect.com/science/article/pii/S2211926413000234 https://doi.org/10.1016/j.algal.2013.01.006.
[24] D. Noreña-Caro, M.G. Benton, Cyanobacteria as photoautotrophic biofactories of high-value chemicals, J. CO2 Util. 28 (2018) 335–366. Available from: https://www.sciencedirect.com/science/article/pii/S2212982018303585 https://doi.org/10.1016/j.jcou.2018.10.008.
[25] L.T. Tan, Bioactive natural products from marine cyanobacteria for drug discovery, Phytochemistry 68 (7) (2007) 954–979. Available from: https://www.sciencedirect.com/science/article/pii/S0031942207000519 https://doi.org/10.1016/j.phytochem.2007.01.012.
[26] Melina Psycha, Kostantinos Pyrgakis, Patricia J. Harvey, Ami Ben-Amotz, A. Keith Cowan, Antonis C. Kokossis, Design Analysis of Integrated Microalgae Biorefineries [Internet]. In: Mario R. Eden, John D. Siirola, Gavin P. Towler, editors. Proceedings of the 8th International Conference on Foundations of Computer-Aided Process Design, vol. 34: Elsevier vol. 34, 2014, pp. 591–596. Available from: https://www.sciencedirect.com/science/article/pii/B9780444634337500833.
[27] P. Hrouzek, M. Kuzma, J. Černý, P. Novák, R. Fišer, P. Simek, A. Lukešová, J. Kopecký, The cyanobacterial cyclic lipopeptides puwainaphycins F/G are inducing necrosis via cell membrane permeabilization and subsequent unusual actin relocalization, Chem. Res. Toxicol. 25 (6) (2012) 1203–1211, https://doi.org/10.1021/tx300044t.
[28] H.-S. Kang, A. Krunic, Q. Shen, S.M. Swanson, J. Orjala, Minutissamides A-D, antiproliferative cyclic decapeptides from the cultured cyanobacterium Anabaena minutissima, J. Nat. Prod. 74 (7) (2011) 1597–1605, https://doi.org/10.1021/np2002226.
[29] S.N. Hajare, M. Subramanian, S. Gautam, A. Sharma, Induction of apoptosis in human cancer cells by a Bacillus lipopeptide bacillomycin D, Biochimie 95 (9) (2013) 1722–1731. Available from: https://www.sciencedirect.com/science/article/pii/S0300908413001661 https://doi.org/10.1016/j.biochi.2013.05.015.
[30] L.T. Tan, Filamentous tropical marine cyanobacteria: a rich source of natural products for anticancer drug discovery, J. Appl. Phycol. 22 (5) (2010) 659–676. Available from: https://doi.org/10.1007/s10811-010-9506-x.
[31] J. Cheel, P. Urajová, J. Hájek, P. Hrouzek, M. Kuzma, E. Bouju, K. Faure, J. Kopecký, Separation of cyclic lipopeptide puwainaphycins from cyanobacteria by countercurrent chromatography combined with polymeric resins and HPLC, Anal. Bioanal. Chem. 409 (4) (2017) 917–930. Available from: https://doi.org/10.1007/s00216-016-0066-z.
[32] S.M. Mandal, A.E.A.D. Barbosa, O.L. Franco, Lipopeptides in microbial infection control: scope and reality for industry, Biotechnol. Adv. 31 (2) (2013) 338–345. Available from: https://www.sciencedirect.com/science/article/pii/S0734975013000062 https://doi.org/10.1016/j.biotechadv.2013.01.004.
[33] P. Urajová, J. Hájek, M. Wahlsten, J. Jokela, T. Galica, D.P. Fewer, A. Kust, E. Zapomělová-Kozlíková, K. Delawská, K. Sivonen, et al., A liquid chromatography–mass spectrometric method for the detection of cyclic β-amino fatty acid lipopeptides, J. Chromatogr. A 1438 (2016) 76–83. Available from: https://www.sciencedirect.com/science/article/pii/S0021967316300991 https://doi.org/10.1016/j.chroma.2016.02.013.
[34] O. Vašíček, J. Hájek, L. Bláhová, P. Hrouzek, P. Babica, L. Kubala, L. Šindlerová, Cyanobacterial lipopeptides puwainaphycins and minutissamides induce disruptive and pro-inflammatory processes in Caco-2 human intestinal barrier model, Harmful Algae 96 (2020) 101849. Available from: https://www.sciencedirect.com/science/article/pii/S1568988320301281 https://doi.org/10.1016/j.hal.2020.101849.
[35] K. Sinzinger, U. Obst, S. Güner, D. Schieder, V. Sieber, Pichia Pastoris Enzyme Production Platform: From Combinatorial Library Screening to Bench-top Fermentation on Residual Cyanobacterial Biomass. (Manuscript in Preparation), 2022.
[36] Lieve M.L. Laurens: NREL. Summative Mass Analysis of Algal Biomass – Integration of Analytical Procedures; Laboratory Analytical Procedure (LAP) (Revised).
[37] K. Sinzinger, D. Schieder, B. Rühmann, V. Sieber, Towards a cyanobacterial biorefinery: carbohydrate fingerprint, biocomposition and enzymatic hydrolysis of Nostoc biomass, Algal Res. 65 (2022) 102744. Available from: https://www.sciencedirect.com/science/article/pii/S2211926422001151 https://doi.org/10.1016/j.algal.2022.102744.
[38] Stefanie Van Wychen, Lieve M.L. Laurens, NREL. Determination of Total Solids and Ash in Algal Biomass: Laboratory Analytical Procedure (LAP) (Revised) [Internet]. Golden, CO (United States), Available from, https://www.nrel.gov/docs/fy16osti/60956.pdf, 2015.
[39] Megazyme., Total Starch Assay Procedure (Amyloglucosidase/α-Amylase Method) K-TSTA 09/14, Megazyme International [Internet], Bray, County Wicklow, Ireland, 2014. Available from: https://secure.megazyme.com/files/booklet/k-tsta_data.pdf.
[40] B. Rühmann, J. Schmid, V. Sieber, Fast carbohydrate analysis via liquid chromatography coupled with ultra violet and electrospray ionization ion trap detection in 96-well format, J. Chromatogr. A 1350 (2014) 44–50, https://doi.org/10.1016/j.chroma.2014.05.014.
[41] S.O. Lourenço, E. Barbarino, P.L. Lavín, U.M. Lanfer Marquez, E. Aidar, Distribution of intracellular nitrogen in marine microalgae: calculation of new nitrogen-to-protein conversion factors, Eur. J. Phycol. 39 (1) (2004) 17–32, https://doi.org/10.1080/0967026032000157156.
[42] S. van Wychen, K. Ramirez, L.M.L. Laurens, Determination of Total Lipids as Fatty Acid Methyl Esters (FAME) by in situ Transesterification: Laboratory Analytical Procedure (LAP) [Internet]. Golden, CO (United States), Available from: https://www.nrel.gov/docs/fy16osti/60958.pdf, 2016.
[43] K. Meixner, A. Kovalcik, E. Sykacek, M. Gruber-Brunhumer, W. Zeilinger, K. Markl, C. Haas, I. Fritz, N. Mundigler, F. Stelzer, et al., Cyanobacteria Biorefinery - production of poly(3-hydroxybutyrate) with *Synechocystis salina* and utilisation of residual biomass, J. Biotechnol. 265 (2018) 46–53, https://doi.org/10.1016/j.jbiotec.2017.10.020.
[44] H.D. Bae, L.J. Yanke, K.J. Cheng, L.B. Selinger, A novel staining method for detecting phytase activity, J. Microbiol. Methods 39 (1) (1999) 17–22, https://doi.org/10.1016/s0167-7012(99)00096-2.
[45] Z. Huang, Y. Liu, B.S. Paulsen, D. Klaveness, Studies on polysaccharides from three edible species of nostoc (Cyanobacteria) with different colony morphologies: comparison of Monosaccharide compositions and viscosities of polysaccharides from field colonies and suspension cultures, J. Phycol. 34 (6) (1998) 962–968, https://doi.org/10.1046/j.1529-8817.1998.340962.x.
[46] Tolulope Joshua Ashaolu, Katarzyna Samborska, Chi Ching Lee, Merve Tomas, Ezra Capanoglu, Özgür Tarhan, Bengi Taze, Seid Mahdi Jafari, Phycocyanin, a super functional ingredient from algae; properties, purification characterization, and applications, Int. J. Biol. Macromol. 193 (2021) 2320–2331. Available from: https://www.sciencedirect.com/science/article/pii/S0141813021024624 https://doi.org/10.1016/j.ijbiomac.2021.11.064.
[47] L. Jiang, Y. Wang, Q. Yin, G. Liu, H. Liu, Y. Huang, B. Li, Phycocyanin: a potential drug for cancer treatment, J. Cancer 8 (17) (2017) 3416–3429, https://doi.org/10.7150/jca.21058.
[48] J. Mareš, J. Hájek, P. Urajová, J. Kopecký, P. Hrouzek, A hybrid non-ribosomal peptide/polyketide synthetase containing Fatty-Acyl Ligase (FAAL) synthesizes the β-amino fatty acid Lipopeptides Puwainaphycins in the cyanobacterium Cylindrospermum alatosporum, PLoS One 9 (11) (2014) 1–11. Available from: https://doi.org/10.1371/journal.pone.0111904.

[49] S. Devi, N. Rani, A. Sagar, GC-MS Analysis and Antioxidant Activity of Two Species of Cyanobacteria Isolated From Drang Salt Mine of District Mandi, Himachal Pradesh, India [Internet]. In, 2020.
[50] T. Santos, C. Connolly, R. Murphy, Trace element inhibition of phytase activity, Biol. Trace Elem. Res. 163 (1–2) (2015) 255–265, https://doi.org/10.1007/s12011-014-0161-y.
[51] A.B. Zepeda, A. Pessoa, J.G. Farías, Carbon metabolism influenced for promoters and temperature used in the heterologous protein production using Pichia pastoris yeast, Braz. J. Microbiol. 49 (2018) 119–127. Available from: https://www.sciencedirect.com/science/article/pii/S1517838217306901 https://doi.org/10.1016/j.bjm.2018.03.010.

4.4. LCSA of the biorefinery concept for *Cylindrospermum* alatosporum CCALA 988 extracting multiple high-value compounds and residue utilization by *P. pastoris* fermentation producing phytase

Authors: Korbinian Sinzinger, Doris Schieder, and Volker Sieber;

The manuscript presents a lifecycle sustainability assessment (LCSA) of a biorefinery concept for *Cylindrospermum alatosporum* CCALA 988, focusing on the extraction of high-value compounds and utilizing residual biomass for phytase production through *Pichia pastoris* fermentation. The biorefinery concept involves six subsystems: supply, production, product recovery, fermentation, extract purification, and enzyme purification. The assessment is based on data extrapolated to industrial scale, evaluating environmental, economic, and social impacts. The environmental analysis, modeled using the ReCiPe method, covers 16 impact categories, including climate change, acidification, and freshwater eutrophication. Citric acid, glycerol, and electricity are identified as the primary contributors to environmental impact, accounting for over 50% of the total eco-points. The study suggests that switching to renewable energy and sourcing glycerol from biodiesel production could significantly improve sustainability. The economic analysis estimates total investment costs of approximately €4.74 million and annual operational costs of €1.62 million. A financial evaluation using the Net Present Value (NPV) method indicates that cumulative earnings of €18.66 million over five years would be required for a 10% return on investment. Sensitivity analysis reveals that investment costs have the greatest influence on economic feasibility. The manuscript concludes that the biorefinery concept is potentially economically viable but faces uncertainties related to market demand and product purity, particularly for cyclic lipopeptides and phycobiliproteins. Further research is recommended to validate the process and scale up production.

Korbinian Sinzinger designed the work process, collected the assumption, synthesized the porcess, alyzed the date and wrote the original draft. Doris Schieder contributed to the conceptualization, reviewed, and edited the manuscript. Volker Sieber contributed to reviewing and editing the manuscript.

LCSA of the biorefinery concept for *Cylindrospermum* alatosporum CCALA 988 extracting multiple high-value compounds and residue utilization by *P. pastoris* fermentation producing phytase

Korbinian Sinzinger, Doris Schieder, Volker Sieber

Algal Research

2025

Manuscript in preparation

LCSA of the biorefinery concept for *Cylindrospermum* alatosporum CCALA 988 extracting multiple high-value compounds and residue utilization by *P. pastoris* fermentation producing phytase

Korbinian Sinzinger[a], Doris Schieder[a] and Volker Sieber[a,b,c,d]

[a] *Chair of Chemistry of Biogenic Resources, Technical University of Munich, Campus for Biotechnology and Sustainability, 94315 Straubing, Germany*

[b] *Catalysis Research Center, Technical University of Munich, 85748 Garching, Germany*

[c] *Fraunhofer IGB, Branch BioCat, 94315 Straubing, Germany*

[d] *The University of Queensland, School of Chemistry and Molecular Biosciences, 68 Cooper Road, St. Lucia 4072, Australia*

Corresponding author:

Dr. Doris Schieder
Tel.: +49 (0) 9421 187-303
doris.schieder@tum.de
TUM Campus Straubing
Schulgasse 16
94315 Straubing
Germany

Abstract

This study assesses the life cycle sustainability of a biorefinery concept based on *Cylindrospermum alatosporum* CCALA 988, focusing on the extraction of high-value compounds and the fermentation of residual biomass for phytase production. Using Life Cycle Sustainability Assessment (LCSA), the environmental, social, and economic impacts of the biorefinery are analyzed. The process, which produces and processes 1.8 tons of dry cyanobacterial biomass annually, is divided into six subsystems: supply, biomass production, high-value product extraction, fermentation, extract purification, and enzyme purification. The environmental assessment yields an aggregated footprint of approximately 7,500 eco-points, with climate change, non-carcinogenic effects, and fossil depletion contributing most to the impact. Economically, the estimation yields a required initial investment of €4.74 million for the project, with annual operational costs of €1.61 million, largely driven by labor. Sensitivity analysis indicates that investment cost fluctuations significantly affect financial viability. Overall, the biorefinery is deemed economically feasible, with results highlighting the need to optimize resource inputs for enhanced sustainability. This evaluation establishes a foundational framework for advancing cyanobacterial biorefinery technologies and promoting sustainable biomass utilization.

Key words: Cyanobacteria, biomass, biorefinery, *Cylindrospermum alatosporum,* LCSA,

1. Introduction

The global transition toward a sustainable, bio-based economy has intensified the need for innovative biomass utilization strategies[1,2]. Among the most promising candidates for biomass-based processes are cyanobacteria and microalgae, which have attracted attention for their rapid growth, low nutrient requirements, and ability to produce a diverse array of valuable compounds[3–6]. Cyanobacteria, in particular, offer significant potential as feedstock for biorefineries due to their capacity to synthesize bioactive compounds such as pigments, proteins, and secondary metabolites[7]. Furthermore, their ability to fix atmospheric carbon dioxide provides a critical advantage in reducing greenhouse gas emissions, positioning cyanobacteria-based biorefineries as a key contributor to global efforts to reduce fossil fuel dependency and promote sustainable resource utilization.

A biorefinery, similar to a petroleum refinery, aims to convert biomass into multiple high-value products, ensuring the efficient use of raw materials while reducing waste[8]. The economic feasibility of such systems hinges on their ability to produce diverse products from biomass streams[9]. This multi-product approach not only increases the overall profitability of biorefineries but also enhances their sustainability by utilizing residual biomass. For third-generation feedstocks like microalgae and cyanobacteria, the potential to extract bioactive compounds such as phycobiliproteins, pigments, and cyclic lipopeptides (CLPs) has been demonstrated[10,11]. These compounds hold significant value in industries such as pharmaceuticals, nutraceuticals, and cosmetics. However, despite

their promise, large-scale implementation of cyanobacteria-based biorefineries remains a challenge due to technical, environmental, and economic considerations[3].

In previous work, we developed a biorefinery concept utilizing the cyanobacterium *Cylindrospermum alatosporum* CCALA 988[12]. This concept explored the extraction of multiple high-value compounds, including cyclic lipopeptides (puwainaphycins and minutisamides), pigments, and phycobiliproteins. Additionally, the residual biomass was employed in a fermentation process with *Pichia pastoris* to produce phytase, an enzyme used in animal feed to enhance phosphorus uptake and reduce phosphate pollution. Our bench-scale research demonstrated that 56.2% of the biomass could be utilized for product extraction and served as substrate for enzyme production, while 43.8%. remained as residue. Our findings indicated the economic viability and technical feasibility of *C. alatosporum* 988 as a feedstock for a multi-product biorefinery at the lab scale.

While our initial biorefinery concept demonstrated the feasibility of extracting and utilizing multiple compounds from *C. alatosporum 988*, a comprehensive evaluation of its sustainability at a larger scale is necessary to determine its long-term viability. This is particularly important given the growing emphasis on sustainability in industrial processes. To address this gap, we are now focusing on the Life Cycle Sustainability Assessment (LCSA) of the biorefinery concept. LCSA is a holistic methodology that integrates environmental, economic, and social assessments into a single framework[13–15]. By applying LCSA, we aim to evaluate the sustainability performance of the biorefinery process across its entire lifecycle, from biomass cultivation to product recovery and waste management. This approach allows us to identify key areas where the process can be optimized to reduce its environmental footprint, improve economic efficiency, and address social considerations such as labor and community impact.

In this study, we build upon our previously published biorefinery concept by scaling the process to an industrial superstructure and conducting a detailed LCSA to assess its sustainability. The analysis focuses on six main subsystems: supply, production, product recovery, fermentation, extract purification, and enzyme purification. By evaluating the environmental, economic, and social impacts of each subsystem, we aim to provide a comprehensive understanding of the sustainability of the biorefinery model. These findings will not only optimize the current process but also serve as a foundation for future research and development in cyanobacterial biorefineries, advancing sustainable practices in biomass utilization.

2. Material and methods

2.1 Life Cycle Sustainability Assessment Framework

The sustainability of the biorefinery concept for *Cylindrospermum alatosporum* CCALA 988 was evaluated using the Life Cycle Sustainability Assessment (LCSA) framework. In this LCSA two methodologies were integrated—Life Cycle Environmental Assessment (LCA) and Life Cycle Costing (LCC) to provide a comprehensive evaluation of the environmental and economic impact of the proposed biorefinery. The system boundary was defined as "cradle-to-gate," including biomass cultivation, extraction of high-value compounds, and fermentation processes.

2.2 Goal and Scope Definition

The primary goal of the LCSA was to evaluate the sustainability performance of the *C. alatosporum* biorefinery model. In order to be able to develop such a complex assessment, a working plan needed to be set up outlined by the following four steps: collecting assumptions, process synthesis, environmental analysis, and economic

assessment. The complexity of the process made it necessary to break it down into subsystems. Different approaches are possible. The superstructure-based approach by Fasahati *et. al.* with their detailed process synthesis and economic analysis of cyanobacteria biorefineries served as a blueprint for this study[3]. Based on the superstructure investigated in this study, the process was divided into the following six subsystems:

1. Supply
2. Production of cyanobacterial biomass
3. Recovery of high-value compounds (phycobiliproteins, cyclic lipopeptides)
4. Fermentation process for phytase production using *P. pastoris*
5. Purification of extracted compounds
6. Enzyme purification

2.3 Assumptions & process synthesis

Necessary assumptions for the process synthesis used in the current study was based on the multi-product biorefinery concept for *C. alatosporum* CCALA 988 previously published by us[12]. The first two subsystems, supply, and biomass production were not part of the biorefinery concept but data for cyanobacteria cultivation at a commercial scale were provided by Centre Algatech, Institute of Microbiology, The Czech Academy of Sciences (Třeboň), taken from current literature or assumed as suitable. The assumptions for supply and cyanobacterial biomass production in flat panel reactors are listed in **Table 1**. A process plan was developed on these assumptions. Further, a parameterized reverse LCA methodology was used in the python-based LCA-software brightway2. The database which was used here has been used for other studies prior and was publsihed by Bussa[16].

For the first two subsystems including individual process steps, material streams, and material amounts were planned out first.. For the subsystem supply, three steps were

considered, 1) Onsite supply of fresh water, 2) urea as N-source, and 3) fertilizer as P-source. Supply of CO_2 and heat from a nearby powerplant was an economically favorable solution. Additionally, needed amounts of wastewater containing nutrients from a wastewater facility (WWF) were taken. These material streams were utilized in the cultivation in the biomass production subsystem of the concept. The requirements were scaled to achieve an overall annual production of 1.8 tons of dry biomass as confirmed by Centre Algatech. Cultivation is assumed to be done in large flat panel reactors of 180 L from the company Subitec GmbH[17]. Each year 300 days of operation are considered necessary accounting for downtime and cleaning. This allows to assume 21 batches cyanobacterial biomass production needing 720 m^3 of water each year. Additional substances such as citric acid or hydrogen peroxide are needed for cleaning but are not shown in the process plan. These are also included in operational costs for economic benefits. Spent water is returned to the WWF and the 1.8 tons of dry biomass per year enter the next subsystem: product recovery.

Table 1: Assumptions for the supply and cyanobacterial biomass production subsystems.

Specification	Quantity	Unit	Description	Reference
Final biomass concentration	0.25	%	Equals 2.5 g/L cell dry mass	Fasaei *et al*[18]
Annual dry biomass production	1.8	tons	Assumed as necessary	Algatech
Biomass concentration after pressure filtration	25	%	biomass/water	Fasaei *et al.*[18]
Biomass concentration after centrifugation	20	%	biomass/water	Fasaei *et al.*[18]
Water content in product after drying	5	%	water/ biomass	Fasaei *et al.*[18]
Cultivation time for one batch	14	days	Including cleaning	Cheel *et al.*[10]
Operation time	300	days	In each year	Kumar *et al.*[4]
Flat panel reactor	180	Liter	Large reactor	Subitec GmbH[17]
Number of batches	21		Resulting from 300 days/year	
Resulting water usage	720	m^3	From biomass conc. and production/year	
Annual productivity dry biomass	45	t/ha/year	0.04 ha area needed	Fasaei *et al.*[18]

The other four subsystems product recovery, fermentation, extract purification, and fermentation purification are closely intertwined having multiple common material

year. The other high-value compounds such as cyclic lipopeptides in the aqueous extract are first separated from the phycobiliproteins by salt precipitation (ammonium sulfate). The cyclic lipopeptides from the aq. extract are then combined with the organic extract, which are subsequently separated and purified by counter current chromatography (CCC) followed by multiple runs of reversed phase chromatography as published for these compounds by Cheel *et al*[10]. The assumptions made for the extracts and enzyme purification subsystems are listed in **Table 3**. The supernatant from the fermentation is treated with a low-cost aqueous two-phase system (ATPS) which includes a 10.5 % polyethylene glycol (PEG 6000 & 8000) phase and 20.5 % sodium citrate phase[23]. Four cycles allow to reduce the annual amount of PEG needed to 3.14 tons. The final phytase yield with a 98.5 % recovery and a purification factor of 2.5 results therefore in 3,563 GU per year.

Table 3: Assumptions for the two subsystems extracts purification and enzyme purification. Abbreviations: PC: phycocyanin, PE: phycoerythrin, SEC: size exclusion chromatographie, HIC: hydrophobic interaction chromatographie, CCC: countercurrent chromatographie, HPLC: high performance liquid chromatographie, PEG: polyethylene glycol.

Specification	Quantity	Unit	Description	Reference
Phycobiliprotein purification method			PC and PE precipitation, SEC and HIC	Kannaujiya *et al.*[22]
Ammonium sulfate precipitation	60	%	Two step precipitation	Kannaujiya *et al.*[22]
DF after protein precipitation	25		Necessary for	Kannaujiya *et al.*[22]
Factor for water usage for ultrafiltration	10		Assumed as necessary	
Sample to bed factor	25		Assumed as ideal	
Phycobiliprotein Recovery	75	%	With highest purity	Kannaujiya *et al.*[22]
Purification of small compounds			Targeting cyclic lipopeptides	Cheel *et al.*[10]
Enrichment of crude extract			100 L column with 310 kg bed	
CCC separation			Four solvent system	Cheel *et al.*[10]
Preparative HPLC			Reversed Phase	Cheel *et al.*[10]
Aqueous two-phase system (ATPS)			Downstream of extracellular phytase	Bhavsar *et. al.*[23]
Two phases of the ATPS			PEG (6000, 8000) 10.5 % & Na citrate 20.5 %	Bhavsar *et. al.*[23]
ATPS conditions			pH 5.6 and 25 °C ± 2 °C	Bhavsar *et. al.*[23]
Process time, PEG cycles & enzyme recovery			3 h, 4 & 98.5 %	Bhavsar *et. al.*[23]

streams. In general, the product recovery subsystem includes cell pre-treatment, the two extraction steps, and the preparation of biomass hydrolysate for the fermentation planned out in the next subsystem. The two crude extracts containing high-value compounds cyclic lipopeptides, pigments and phycobiliproteins are further treated in the extract purification subsystem. The aqueous extract is 28.8 m^3 per year and the organic extract 18.9 m^3 per year, which are both moved to the purification subsystem. Ideally, all of the organic solvent is recovered in the process but in the product recovery subsystem 4.7 m^3 are recovered and reintroduced into the extraction. The biomass hydrolysate process step is based on the data from our previously reported biorefinery concept including biomass and enzyme concentration. The annual produced hydrolysate is therefore 21.0 m^3 cyanobacterial biomass hydrolysate with 33 L in surplus of the needed amount in the fermentation.

The main consideration for the hydrolysate is that 15 % (v/v) cyanobacterial biomass hydrolysate is used in the fermentations[12]. Additionally, it is assumed that 10 % (v/v) yeast biomass hydrolysate is needed in the fermentation for sufficient nutrients in a fed-batch enzyme production approach. This is met with 18.7 m^3 yeast hydrolysate production per year. Wet residual cyanobacterial as well as wet yeast biomass from the hydrolysis process is moved into the purification subsystem for drying and is listed as animal feed a co-product. The assumptions for the subsystems product recovery and fermentation are listed in **Table 2**. For the fermentation, two seed reactors and a 10 m^3 main vessel with 35 batches per year were chosen to determine production costs and extrapolate a fed-batch strategy. A final phytase activity yield of 30,246 U/mL is assumed for each batch[19].

Table 2: Assumptions for the two subsystems product recovery and fermentation.

Specification	Quantity	Unit	Description	Reference
Mass balance & process conditions			10 g lab scale scenario	Sinzinger *et al.*[12]
Biomass concentration for extraction	5	%	Dry biomass/ solvent	Sinzinger *et al.*[12]
CY biomass concentration for hydrolysis	5	%	Dry biomass/ solvent	Sinzinger *et al.*[12]
Yeast biomass concentration for hydrolysis	15	%	Dry biomass/ solvent	Sinzinger *et al.*[12]
Yeast biomass solubilisation	50	%	Solubilized biomass/starting biomass	Bayarjargal *et al.*[20]
Loss due to centrifugation	25	%	Solvent remaining in pellet	Fasaei *et al.*[18]
Biomass concentration after centrifugation	20	%	biomass/water	Fasaei *et al*[18].
Number of fermentation batches	35		Resulting from 300 days/year	Kumar *et al.*[4]
Starting volume main fermentation	4000	Liter	Assumed as ideal for 10 m^3 reactor	
Feed volume (50% (w/w) glycerol)	3000	Liter	Assumed as ideal for 10 m^3 reactor	
CY hydrolysate concentration in fermentation	15	%	Transposed from Sinzinger *et al.*	Sinzinger *et al.*[12]
YE concentration in fermentation	10	%	Transposed from Sinzinger *et al.*	Sinzinger *et al.*[12]
Final yeast cell wet weight	622	g/L	Highest reported	Helian *et al.*[19]
Final phytase activity	30,246	U/mL	Highest reported	Helian *et al.*[19]
Ratio wet cell weight to dry cell weight	5.646		Wet biomass/dry biomass	Guo *et al.*[21]

Thus, accounting for the 25 % loss of fermentation broth due to centrifugation, leaves us with 119.6 m^3 phytase containing supernatant each year[18]. The overall annual production of crude phytase in the supernatant is therefore 3,617 GU. The supernatant is moved further into the enzyme purification subsystem. Simultaneously, the resulting wet yeast biomass of 142.5 tons per year (deducted the yeast needed for the hydrolysate) containing the 25 % supernatant is moved to the product purification subsystem for drying[18].

The products cyclic lipopeptides, pigments, phycobiliproteins, and phytase are purified towards the end in the extracts purification subsystem. The phycobiliproteins in the aqueous extract (**Fig. 2** extract E1) are precipitated, dialyzed, separated, and purified by size exclusion and hydrophobic interaction chromatography as reported by Kannaujiya *et al.* for highest purity[22]. For the phycobiliproteins a conservative 75 % recovery was assumed, which would lead to a productivity of 46.6 kg highly pure phycobiliproteins per

year. The other high-value compounds such as cyclic lipopeptides in the aqueous extract are first separated from the phycobiliproteins by salt precipitation (ammonium sulfate). The cyclic lipopeptides from the aq. extract are then combined with the organic extract, which are subsequently separated and purified by counter current chromatography (CCC) followed by multiple runs of reversed phase chromatography as published for these compounds by Cheel *et al*[10]. The assumptions made for the extracts and enzyme purification subsystems are listed in **Table 3**. The supernatant from the fermentation is treated with a low-cost aqueous two-phase system (ATPS) which includes a 10.5 % polyethylene glycol (PEG 6000 & 8000) phase and 20.5 % sodium citrate phase[23]. Four cycles allow to reduce the annual amount of PEG needed to 3.14 tons. The final phytase yield with a 98.5 % recovery and a purification factor of 2.5 results therefore in 3,563 GU per year.

Table 3: Assumptions for the two subsystems extracts purification and enzyme purification. Abbreviations: PC: phycocyanin, PE: phycoerythrin, SEC: size exclusion chromatographie, HIC: hydrophobic interaction chromatographie, CCC: countercurrent chromatographie, HPLC: high performance liquid chromatographie, PEG: polyethylene glycol.

Specification	Quantity	Unit	Description	Reference
Phycobiliprotein purification method			PC and PE precipitation, SEC and HIC	Kannaujiya *et al.*[22]
Ammonium sulfate precipitation	60	%	Two step precipitation	Kannaujiya *et al.*[22]
DF after protein precipitation	25		Necessary for	Kannaujiya *et al.*[22]
Factor for water usage for ultrafiltration	10		Assumed as necessary	
Sample to bed factor	25		Assumed as ideal	
Phycobiliprotein Recovery	75	%	With highest purity	Kannaujiya *et al.*[22]
Purification of small compounds			Targeting cyclic lipopeptides	Cheel *et al.*[10]
Enrichment of crude extract			100 L column with 310 kg bed	
CCC separation			Four solvent system	Cheel *et al.*[10]
Preparative HPLC			Reversed Phase	Cheel *et al.*[10]
Aqueous two-phase system (ATPS)			Downstream of extracellular phytase	Bhavsar *et. al.*[23]
Two phases of the ATPS			PEG (6000, 8000) 10.5 % & Na citrate 20.5 %	Bhavsar *et. al.*[23]
ATPS conditions			pH 5.6 and 25 °C ± 2 °C	Bhavsar *et. al.*[23]
Process time, PEG cycles & enzyme recovery			3 h, 4 & 98.5 %	Bhavsar *et. al.*[23]

2.4 Environmental Life Cycle Assessment (LCA)

The environmental analysis for the presented biorefinery concept is based on the work and modeling done with the ReCiPe 2016 method with SimaPro 9.0.029[24,25]. We analysed all of the available areas of protection within ReCiPe 2016: human health, ecosystem quality and resources, as well as the contribution of the available midpoint categories: global-warming potential, ozone layer depletion potential, ionising radiation, photochemical oxidant formation potential, particulate matter formation, terrestrial acidification, freshwater eutrophication, marine eutrophication, terrestrial ecotoxicity potential, freshwater ecotoxicity potential, marine ecotoxicity poten tial, human carcinogenic toxicity potential, human non-carcinogenic toxicity potential, land use, mineral resource depletion, fossil resource depletion and water consumption. The preparation, database, and paramters for the calculations were done as published by Maresa Bussa[16].

2.5 Economic Life Cycle Costing (LCC)

The economic evaluation of the biorefinery was conducted using the Life Cycle Costing (LCC) methodology. Costs were categorized into the following: Capital expenditures (CAPEX): Including equipment for biomass cultivation, compounds extraction, fermentation, and product purification. Operational expenditures (OPEX): Including energy, labor, chemicals, and water usage during the biorefinery process.

Data for economic analysis were derived from a combination of experimental data, literature, and publicly available industrial reports. The process plan synthesized and modeled in here presented study was combined with a detailed economic analysis to

elucidate the financial impact of multiple high-value compounds from cyanobacterial biomass. The first step for the economic analysis was to elucidate the investment costs for the equipment needed which includes land, building, tax & insurance for the biorefinery concept. Tax & insurance was assumed to be 1 % of the total purchase price[26]. The total investment costs include purchase price, installation costs, engineering & supervision, and annual maintenance. Installation costs and annual maintenance accounted to 10 % of the purchase price and engineering & supervision accounted to 5 % of the purchase price[26].

In the next step, the operating expenditure for the biorefinery concept was assessed. The operating costs include the cost of materials and services used in the process plan as consumables, labor and other overhead expenditure. Costs for consumables were estimated. Labor costs were calculated based on 15 workers[27].

Further, for the sensitivity and uncertainty analysis, the net present value (NPV) method and the payback period method were chosen to evaluate the project over a five-year period[28]. The NPV method analyses the intrinsic value of a project and considers the time value of money. For operational costs an annual increase of 2 % is assumed. The sales or earnings cannot be forecasted but must be assumed. For this reason, the analysis was set up the following way: The NPV was set to zero, which means the return on investment (ROI) or internal rate of return is equal to the cost of capital. Here, the weighted average cost of capital (WACC) was chosen to be 10 %. This is a metric that has been reported often in literatur[4]. The WACC is used to discount the annual cashflow to a present value. Hence, the NPV is zero when the sum of all discounted cash flows equals the initial investment. Earnings were assumed to never be zero and increase dynamically without weighting.

3. Results & Discussion

3.1 Process superstructure

The material amounts and process specifications were all specified and calculated for this superstructure approach and are presented in the **Supporting Information (annex 1**). The visual representation of the biorefinery process plan, as shown in **Figures 1** and **2**, not only provides a clear overview but also underscores the complexity and interconnectedness of its six subsystems. These detailed illustrations serve as a roadmap, guiding the understanding of the intricate material flows and interactions within the biorefinery: The supply subsystem focuses on the acquisition and preparation of essential resources for the biorefinery, including water, nutrients, and carbon dioxide. The process flow diagram in **Figure 1** details the annual quantities of these inputs, highlighting the significant water demand of 720 m^3 per year, which underscores the importance of water management and potential recycling strategies. The primary nutrients utilized in this system are urea as the nitrogen source and a phosphorus-based fertilizer. Notably, the integration of wastewater treatment facility effluent as a nutrient source showcases a circular economy approach, reducing environmental impact and resource consumption.

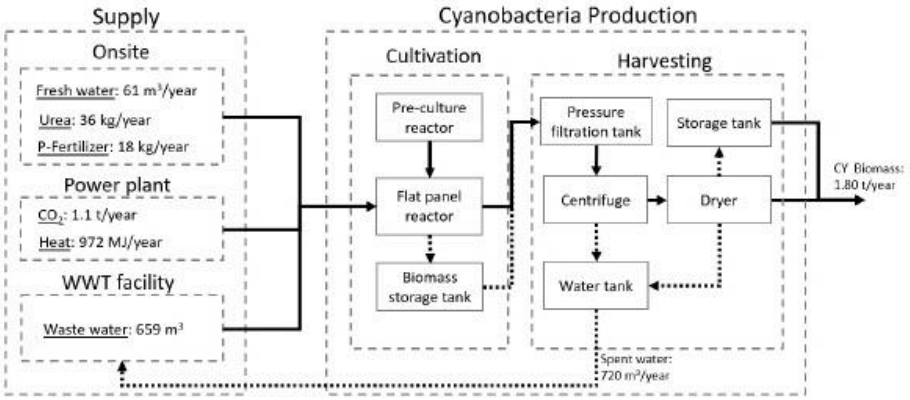

Figure 1: Biorefinery process plan for the subsystems supply and cyanobacterial biomass production. Including process steps, material streams and annual amounts

The production subsystem encompasses the cultivation of *C. alatosporum* 988 in large flat panel reactors aims to produce 1.8 tons of dry biomass annually. **Figure 1** also shows that the process operates in 14-day batches, yielding 45 tons/ha/year dry biomass. This illustrates the efficiency and scalability of biomass production. The cultivation process parameters taken from literature, such as the final biomass concentration of 0.25% and the annual productivity of 45 tons/ha/year, provide insights into the efficiency and scalability of biomass production.

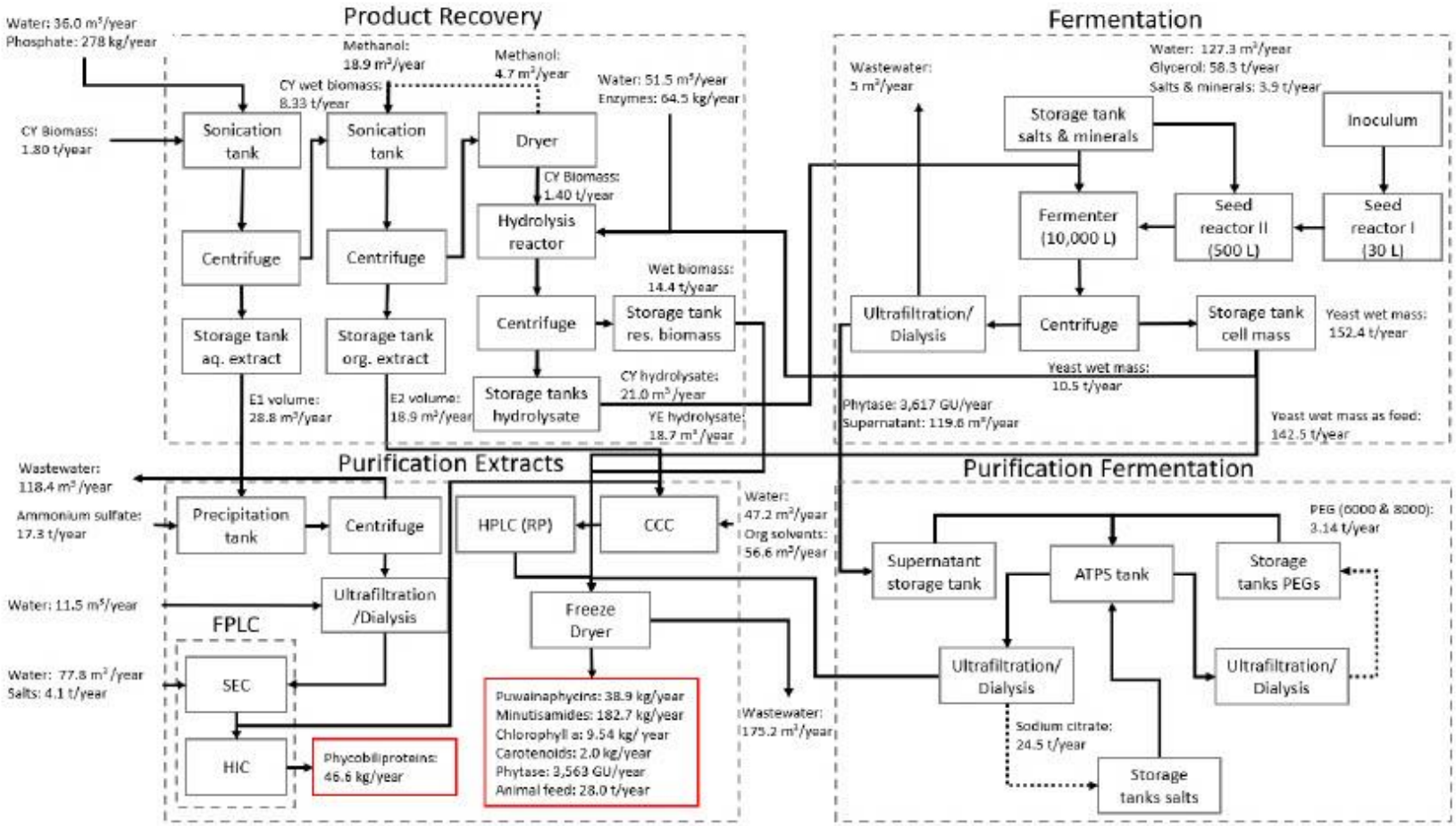

Figure 2: Biorefinery process plan for the four subsystems: product recovery, fermentation, extracts purification, and enzyme purification. Including process steps, material streams and annual amounts. Abbreviations: CY: cyanobacteria, CCC: countercurrent chromatographie, HPLC: high perfomrance chromatographie, FPLC: fast protein liquid chromatographie, SEC: Size exclusion chromatographie, HIC: hydrophobic interaction chromatographie, ATPS: aqueous two-phase system.

The product recovery subsystem focuses on the extraction of high-value compounds, such as the cyclic lipopeptides puwainaphycins and minutisamides, as well as phycobiliproteins, from the cultivated biomass. The process flow diagram in **Figure 2** details the extraction steps, including cell pre-treatment using ultrasonication, solvent extraction with methanol, and centrifugation to separate the biomass from the solvent. It also highlights the recovery and reuse of organic solvents, contributing to the overall sustainability of the biorefinery. The biomass concentration for extraction is set at 5%, and a 25% loss due to centrifugation is accounted for, reflecting practical considerations in the extraction process.

The fermentation subsystem utilizes the residual biomass from the product recovery subsystem as a substrate for phytase production through fermentation with *P. pastoris*. The process involves seed reactors and a main fermentation vessel with a 10 m^3 capacity, operating in a fed-batch mode with glycerol as the primary carbon source. Visualization in **Figure 2** illustrates the material flow from the product recovery subsystem to the fermentation subsystem, emphasizing the efficient utilization of residual biomass. The fermentation process parameters, such as the use of 15% (v/v) cyanobacterial biomass hydrolysate and 10% (v/v) yeast hydrolysate, and the final phytase activity yield of 30,246 U/mL, provide insights into the productivity and efficiency of enzyme production.

The extract purification subsystem focuses on the purification of the extracted high-value compounds to achieve the desired purity levels. The process involves various techniques tailored to each compound. Phycobiliproteins undergo precipitation, dialysis, and chromatography, while cyclic lipopeptides are purified using counter-current chromatography and reversed-phase HPLC. The material flow diagram in **Figure 2** showcases the purification steps and the final product streams, with a conservative 75% recovery assumed for phycobiliproteins.

The enzyme purification subsystem focuses on the purification of the phytase enzyme produced in the fermentation subsystem. The process involves an aqueous two-phase system (ATPS) using PEG and sodium citrate for initial separation and concentration. The ATPS conditions, including pH and temperature, are optimized for phytase partitioning. The material flow diagram in **Figure 2** illustrates the purification process, with a final phytase yield of 3,563 GU per year, reflecting a 98.5% recovery and a purification factor of 2.5.

The superstructure facilitates the overall evaluation of the biorefinery's efficiency and sustainability, and the identification of potential bottlenecks and optimization opportunities. For instance, the substantial water usage of 720 m^3 per year in the biomass production subsystem, as indicated in **Figure 1**, prompts consideration of water recycling or alternative cultivation strategies to minimize environmental impact. Similarly, the recovery of 4.7 m^3 of organic solvent in the product recovery subsystem, as shown in **Figure 2**, highlights the potential for further optimization to reduce solvent consumption and associated costs. The superstructure thus serves as a valuable tool for guiding both technical and economic decision-making in the development and operation of the biorefinery.

3.2 Environemental life cycle assessment

The environmental analysis for the presented biorefinery concept was done with the ReCiPe method[24]. The results of the contribution of the 16 categories at midpoint levels can be found in **Supporting Information (annex 2)**. As the different categories have different units, it is more convenient to convert the values to eco-points to compare and evaluate their impact on the environment. Eco-points are a very useful unit of measurement for such comparisons. Used in an LCA, eco-points take into account the many aspects of environmental burden and impact – from resources and emissions through to wastes[29]. The aggregated environmental

impact of the 16 used impact categories expressed in eco-points comes out at just below 7,500 as shown in **Figure 3**.

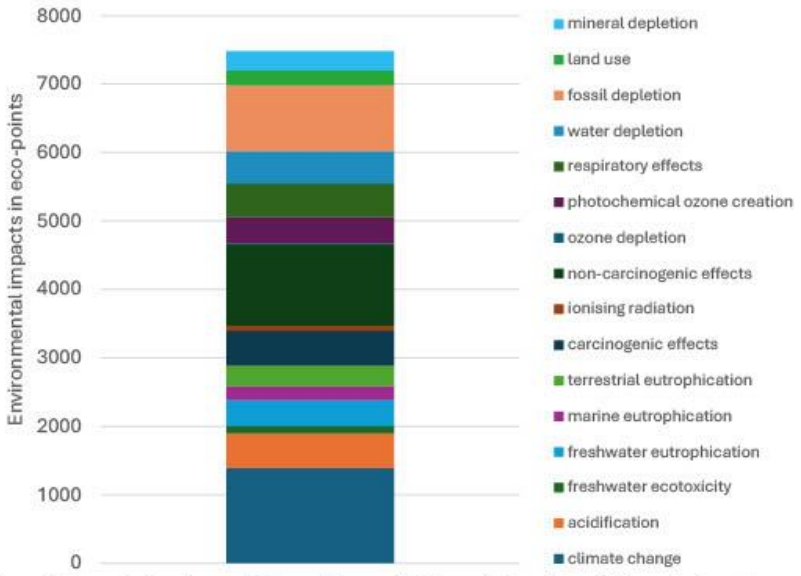

Figure 3: Aggregated environmental impact in eco-points for unified ranking of 16 impact categories.

The three categories with the highest impact are climate change with 18.6 %, non-carcinogenic effects with 15.8 %, and fossil depletion with 12.9 %. These three categories combined make up almost 50 % of the total impact. None of the other categories reache up to 7 % of the aggregated environmental impact. This implies improving the environmental impact from this biorefinery is most efficiently achieved by reducing the impact from the three categories mentioned above. Hence, a contribution analysis for each category might allow to investigate, which material stream or process step would have the highest impact on the environment.

A contribution analysis of all impact categories was therefore performed. The results are presented in **Figure 4**. Five of the process components showed to contribute the most, while other factors contributed to max. 11 % (mineral depletion) to each category. Overall, it was shown that the following three components had the highest contribution for all 16 categories: citric acid, glycerol, and electricity. Except for photochemical ozone creation for which the drying steps contributed about 60 %. These three factors contributed 77 – 98 % of all eco-points for the other 15 categories. The three categories climate change, non-carcinogenic effects, and fossil depletion accounted for 50 % of all eco-points for which over 90 % were contributed by citric acid, glycerol, and electricity. Hence, the overall process can significantly be made more sustainable by finding green alternatives for these three factors. The glycerol is assumed to be utilized glycerol as waste product from bio-diesel production, which makes it already more sustainable as from a commercial source. The electricity can be made much more sustainable by switching from the regular electricity mix (German national) to electricity from only renewable energy sources. As nations are transitiong more and more to renweable energy anyway, this might become a self-elimitaing problem.

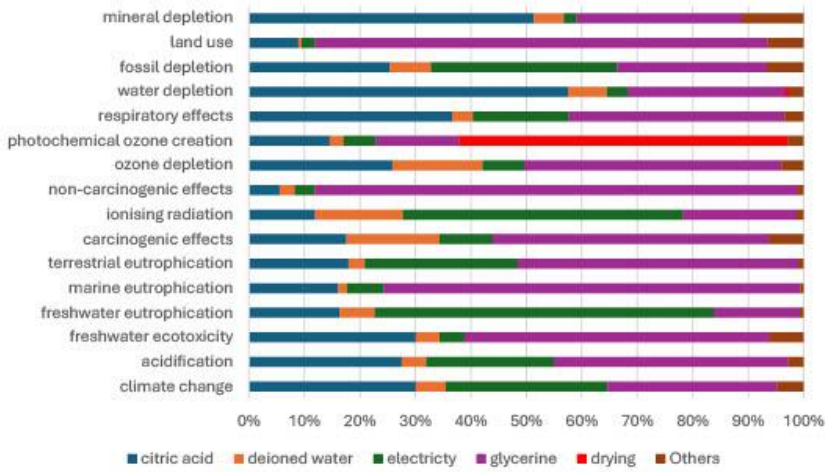

Figure 4: Contribution analysis of process plan components to the 16 environmental impact categories.

3.3 Life cycle costing

The economic evaluation of the biorefinery was conducted using the life cycle costing (LCC) methodology. Costs were categorized into: Capital expenditures (CAPEX): Including equipment for biomass cultivation, compound extraction, fermentation, and product purification. Operational expenditures (OPEX): Including energy, labor, chemicals, and water usage during the biorefinery process.

Data for economic analysis were derived from a combination of experimental data, literature, and publicly available industrial reports. The process plan synthesized and modeled in this study was combined with a detailed economic analysis to elucidate the financial impact of multiple high-value compounds from cyanobacterial biomass. The first step for the economic analysis was to elucidate the investment costs for the equipment needed, which includes land, building, tax & insurance for the biorefinery concept. Tax & insurance were assumed to be 1 % of the total purchase price[30]. The total investment costs shown in **Table 5**

include purchase price, installation costs, engineering & supervision, and annual maintenance. The installation costs and annual maintenance were assumed to be 10 % of the purchase price, and engineering & supervision as 5 % of the purchase price[30].

Table 4: Estimated investment costs for the equipment needed. Purchase costs were either adapted from literature or a contribution factor (CF) was applied[30,31]. The auxiliary euqipment for the fermentation and the purification subysystems were estimated on the costs for the biomass equipment. Installation costs and annual maintenance are assumed 10 % of purchase price each and engineering & supervision 5 % of purchase price. Tax & insurances was 1 % of the total costs.

Equipment	CF	Purchase Price	Installation costs	Engineering & Supervision	Annual maintenance
Flat Panel PBR		529,884.04 €	52,988.40 €	26,494.20 €	52,988.40 €
Piping, fitting, and pumps		919,054.78 €	91,905.48 €	45,952.74 €	91,905.48 €
Auxiliary equipment (Fermentation)	0.4	579,575.53 €	57,957.55 €	28,978.78 €	57,957.55 €
Auxiliary equipment (Purification)	0.4	579,575.53 €	57,957.55 €	28,978.78 €	57,957.55 €
Instrumentation	0.2	521,617.98 €	52,161.80 €	26,080.90 €	52,161.80 €
Electrical	0.1	260,808.99 €	26,080.90 €	13,040.45 €	26,080.90 €
Land (0.12 ha, 6€/m2)[32]		- €	- €	- €	7,200.00 €
Building	0.3	782,426.96 €	78,242.70 €	39,121.35 €	78,242.70 €
Tax & insurances		41,729.44 €	4,172.94 €	2,086.47 €	4,172.94 €
Total		**4,214,673.24 €**	**421,467.32 €**	**210,733.66 €**	**428,667.32 €**

The total CAPEX is estimated to be €4.74 million. This investment includes a vast array of gear and structures required in the biorefinery process, including input, conversion, separation, energy production, product purification, and waste disposal. The main components that contribute to the bulk of CAPEX include plant and construction, piping and associated equipment, photobioreactors, and unique analytical instruments such as HPLC-MS. The extensive requirement of piping and related equipment is evidence that the process is involved and requires proper connection and transfer of materials between the sub-systems. Importantly, CAPEX counts not only the price of the equipment but also all expenses associated with installation costs, engineering, and supervision, together with the yearly maintenance costs, which gives a more realistic picture of the total expenditure needed.

These costs are in line with recent cost estimates for scaled biorefineries of a similar size range. For instance, a techno-economic evaluation by Chew *et al.* of a microalgae biorefinery for high-

include purchase price, installation costs, engineering & supervision, and annual maintenance. The installation costs and annual maintenance were assumed to be 10 % of the purchase price, and engineering & supervision as 5 % of the purchase price[30].

Table 4: Estimated investment costs for the equipment needed. Purchase costs were either adapted from literature or a contribution factor (CF) was applied[30,31]. The auxiliary euqipment for the fermentation and the purification subysystems were estimated on the costs for the biomass equipment. Installation costs and annual maintenance are assumed 10 % of purchase price each and engineering & supervision 5 % of purchase price. Tax & insurances was 1 % of the total costs.

Equipment	CF	Purchase Price	Installation costs	Engineering & Supervision	Annual maintenance
Flat Panel PBR		529,884.04 €	52,988.40 €	26,494.20 €	52,988.40 €
Piping, fitting, and pumps		919,054.78 €	91,905.48 €	45,952.74 €	91,905.48 €
Auxiliary equipment (Fermentation)	0.4	579,575.53 €	57,957.55 €	28,978.78 €	57,957.55 €
Auxiliary equipment (Purification)	0.4	579,575.53 €	57,957.55 €	28,978.78 €	57,957.55 €
Instrumentation	0.2	521,617.98 €	52,161.80 €	26,080.90 €	52,161.80 €
Electrical	0.1	260,808.99 €	26,080.90 €	13,040.45 €	26,080.90 €
Land (0.12 ha, 6€/m2)[32]		- €	- €	- €	7,200.00 €
Building	0.3	782,426.96 €	78,242.70 €	39,121.35 €	78,242.70 €
Tax & insurances		41,729.44 €	4,172.94 €	2,086.47 €	4,172.94 €
Total		**4,214,673.24 €**	**421,467.32 €**	**210,733.66 €**	**428,667.32 €**

The total CAPEX is estimated to be €4.74 million. This investment includes a vast array of gear and structures required in the biorefinery process, including input, conversion, separation, energy production, product purification, and waste disposal. The main components that contribute to the bulk of CAPEX include plant and construction, piping and associated equipment, photobioreactors, and unique analytical instruments such as HPLC-MS. The extensive requirement of piping and related equipment is evidence that the process is involved and requires proper connection and transfer of materials between the sub-systems. Importantly, CAPEX counts not only the price of the equipment but also all expenses associated with installation costs, engineering, and supervision, together with the yearly maintenance costs, which gives a more realistic picture of the total expenditure needed.

These costs are in line with recent cost estimates for scaled biorefineries of a similar size range. For instance, a techno-economic evaluation by Chew *et al.* of a microalgae biorefinery for high-

value-added compounds found that investment costs for such a facility would be in the range of €3.5–€6.2 million for a similar production level[33]. However, it is important to note that these costs can vary significantly depending on the specific location, technology, and scale of the biorefinery.

In the next step, the OPEX for the biorefinery concept was assessed. OPEX includes the cost of materials and services used in the process plan as chemicals, consumables, labor, and other overhead expenditures as shown in **Table 6.** Costs for consumables were estimated with 1%[26]. Labor costs were calculated according to eurostat labor costs (lc_ncost_r2) based on 15 workers[34]. The need for 15 workers was calculated based on the number of unit operations in the five work needed susbsystems (excluding supply). In those five subsystems on average five unit operations are assumed, which makes 75 unit operations. From literature one operatore is needed for five unit operations[18]. Therefore, 15 workers are estimated to be needed to run the whole operation.

Table 5: Operational costs for the equipment needed in all six subsystems of the biorefinery process plan. The full list can be found in the **supporting information annex 3**. Solvents, salts, enzymes and all other operating supplies are summarized in one position with an averaged unit cost and summed up annoul amount. Consumables were estimated with 1%[26]. Labour cost were taken from eurostat[35]. Overhead & administration was estimated to 20% of everything else[26].

Substance	Unit cost	Unit	Annual Amount	Unit	Annual cost
Heat, natural gas	0.014	€/MJ	972	MJ	14.08 €
Electricity, medium voltage	0.239	€/kWh	268,878	kWh	64,288.63 €
Water	2.230	€/m^3	414	m	923.22 €
Operating supplies	23.614	€/kg	147,683	kg	203,675.54 €
Consumables		€/kg		kg	40,897.80 €
Labour	90,000	€/labour	15	labour	1,350,000.00 €
overhead & administration					324,317.89 €
Total					**1,945,907.36 €**

The annual OPEX of the biorefinery is estimated to be €1.9 million for the current year. The largest component of OPEX is labor costs, which account for around 70% of the total OPEX, corresponding to the labor-intensive operations of the biorefinery. This estimation might be a little high. The second largest category is for raw materials and consumables, where glycerol,

ethanol, and sodium citrate costs are quite high. Other expenses are large in part due to the amount of power used by some processes, predominantly in the form of electricity. The employment of specialized resin used in the extraction and purification process contributes to the annual operating costs due to the complexity of the process. In current microalgal biorefinery designs costs of downstream processes are 50–60%[36]. Typically, biotechnological bulk processes this accounts only for up to 30% to the total costs. To reduce such costs, the downstream processes will need to be developed that require fewer unit operations[36,37].

The costs can rather easily be estimated based on the designed process. Yet, a potenitial economic viability cannot be easily forecasted as many uncertanties lay within the assumptions. So, to financially evaluate the project the net present value (NPV) method was used. The NPV was set to zero, which means the weighted average cost of capital (WACC) is equal to the internal rate of return (IRR). A payback period of 5 years was chosen to evaluate the project over a five-year period. The NPV method analyzes the intrinsic value of a project and considers the time value of money. Here, the weighted average cost of capital (WACC) was chosen to be 10 %[26]. This is a metric that seemed suitable for such a project at hand. The WACC is used to discount the annual cash flow to the present value. Hence, the NPV is zero when the sum of all discounted cash flows equals the initial investment. For operational costs, an annual increase of 2 % is assumed. The revenue was assumed to never be zero and increase coherent to the total expenditure (including WACC). Also, it was assumed the initial investment was recoped only in the last two years with around 65% of it in the fifth year. The results are shown in the **supporting information annex 4**. Overall, €17.6 million of total expenditure accumulate over the five years. Against this, there is a total revenue needed of €20.2 million of the five years. This estimation relies on a relatively large number of

assumptions, making it essential to further investigate how changes in the most critical factors influence the outcome.

The outcome of the financial evaluation was therefore investigated further by a sensitivity analysis. The results of the sensitivity analysis reveals information on the most influential factors that determine the profitability of the biorefinery concept. The sensitivty analysis considered a change of ±20 % for investment costs, operational and labor costs and as well as 4 % change for the WACC. The greatest cost pressure is on operational costs, and for each 20 % rise, it is necessary to obtain an increase in revenue up to €22.1 million to reach NPV equal to zero with the here devloped model as shown in **Figure 5**. Regarding the tangible investment, most parameters exhibit a substantial impact on the investment costs, while the WACC demonstrates a moderate impact on the investments. From this analysis, it becomes quite clear that operational expenses, particularly labor expenses, need to be kept in check for economic stability. But it also calls for further evaluation of how initial investment costs might be ameliorated, which promises vast enhancement for the project. The sensitivity to these factors points out the need to be extra cautious or even begin evaluating the possibility of ways of cutting costs among the most sensitive areas of the biorefinery operation. Changing assumptions such as the 5 year payback period or the assumed ditribution of annual revenues would also have a great influence on the outcome of this analysis. Therefore, such a model can provide valuable insight into economic possibilies yet the limitations due to the assumptions need to be considered. Here, the completely assumed revenue forecast implicates a considerable limitation to this model.

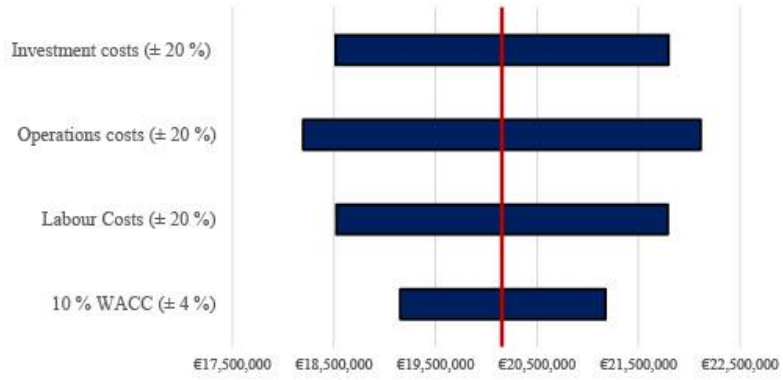

Figure 5: Sensitivity analysis of the financial evaluation for the biorefinery concept investigating four factors and their effect on the needed revenue to reach a NPV of zero. A change of ±20 % was considered for investment, operational and labor costs and as well as ±4 % change for the weighted average cost of capital (WACC).

3.4 Product Portfolio Analysis

The strength of this biorefinery concept lies in its diverse product portfolio, particularly the production of high-value bioactive compounds such as puwainaphycins and minutisamides. The potential annual sales of the product portfolio are well above the needed earning to reach a the NPV of zero. The overview can be found in the **supporting information annex 5**. The numbers have to be evaluated with caution as they are only estimated partially on similar products. So, the potential amount for the products is indicated not to be the bottleneck, but rather the potential market penetration. So, it is important to note that the market for some of these products, such as phycobiliproteins, may become saturated if production volumes are too high or entry hurdles are high.

The biorefinery's focus on high-value bioactive compounds aligns with current market trends, which show increasing demand for such compounds in pharmaceutical and nutraceutical applications. A recent market analysis projected a CAGR of 8.5 % for marine

bioactive compounds from 2022 to 2030, highlighting the significant market potential for these products. While the potential annual sales of €2.48 billion are encouraging, it is important to consider the potential for market saturation, particularly for products like phycobiliproteins. As noted by Morales-Sánchez et al. (2015), the market size for phycobiliproteins is estimated to reach $1.2 billion by 2030[38]. Excessive production volumes could lead to oversaturation and price drops, impacting on the economic viability of the biorefinery. Therefore, a gradual market entry strategy, customer segmentation as well as diversification of the product portfolio are crucial for long-term success.

Diversification can be achieved by exploring new product applications, targeting niche markets, or expanding the range of compounds produced. For instance, phycobiliproteins have potential applications in cosmetics, diagnostics, and as fluorescent markers in biomedical research[33]. Additionally, the biorefinery could explore the production of further high-value compounds, such as polyunsaturated fatty acids (PUFAs), which have a growing market in the food and supplement industries[39].

3.5 Comparison with Other Biorefinery Concepts

This *C. alatosporum* CCALA 988 biorefinery concept distinguishes itself through its multifaceted product strategy, resource-efficient residual biomass utilization, and eco-conscious water-saving technologies. In line with recent advancements in biorefinery design, as highlighted in a 2022 review by Sivaramakrishnan et al., this concept maximizes value extraction from biomass[40]. Its diversified product range caters to various markets, minimizing reliance on single products and mitigating market risks for enhanced economic stability. This approach is further strengthened by the efficient use of residual biomass for phytase production and animal feed, generating additional revenue streams and reducing waste, echoing Centella et al.'s (2017) findings on the profitability boost from residual biomass

utilization[41]. Further, Sano et al. (2021) had presented a techno-economic assessment of microalgae biodiesel plant based on the conversion of sugarcane molasses into microalgae lipids demonstrating the need for multiple higher value products to be competitive[42].

The integration of water-saving technologies, such as flat-panel photobioreactors and the use of wastewater treatment effluent, aligns with the trend towards reduced water consumption in large-scale cultivation systems. This is reflected in the findings of Novoveská et al. (2016) on water usage in open pond systems[43]. This research demonstrats the lower environmental footprint of high-value compound-oriented biorefineries[44]. When compared to traditional chemical synthesis routes for similar compounds, the environmental benefits are even more pronounced, as highlighted by Pérez-López et al. (2014) in their study on eicosapentaenoic acid production[39].

Economically, the biorefinery concept shows promise with a low payback period of 4.24 years, falling within the typical range for novel biorefineries as reviewed by Ubando et al. (2020)[45]. This is particularly encouraging considering the uncertainties associated with emerging markets for high-value compounds like puwainaphycins and minutisamides. While the projected annual sales are substantial, a gradual market entry strategy and product diversification are crucial to avoid oversaturation, especially for phycobiliproteins with their projected market size of $1.2 billion by 2030[38]. This biorefinery concept for *C. alatosporum* CCALA 988 presents a compelling case for a balanced approach to economic viability and environmental sustainability within a sustainable bioeconomy framework. However, it is important to acknowledge that the process plan and LCA calculations rely heavily on assumptions and literature data, and there is currently no proof-of-concept for the overall process. This is because experimentally (even on a laboratory scale) the full process has not

yet been fully conducted. That said, it can be argued that such a preliminary estimate can still very well provide a useful indication of whether the process has the potential to be efficient.

4. Conclusion

This study demonstrates that the biorefinery concept based on *Cylindrospermum alatosporum* CCALA 988 shows promising economic feasibility. However, further research is required to validate the process. First, the entire process needs to be set up in a coherent process flow. Particularly the sequential extraction and residual biomass utilization need to be validated. Subsequently, larger quantities at technical scale can be produced to fully validate the process plan. The greatest uncertainty aside from the technical performance lies in the commercial potential of cyclic lipopeptides (CLPs) and the associated costs of product purification. Despite this, there are established markets for the other high-value products, which suggests that scaling up this biorefinery could be economically viable even without immediate CLP commercialization. Future work should focus on refining product purity, particularly for phycobiliproteins, to meet market demands. Additionally, expanding the biorefinery's enzyme portfolio beyond phytase, using *Pichia pastoris* to produce other enzymes, could further enhance the commercial viability of the concept. Continued research will be critical to address these uncertainties and optimize the biorefinery for broader industrial application.

5. Acknowledgements

The EFRE – Interreg project 41 "Joint Research on Natural Compounds from Cyanobacteria as a Model of Cross-Border Scientific Partnership" was funded by the European Union ZIEL ETZ. Many thanks to Algatech for providing biomass and their process data.

6. Author contributions

Korbinian Sinzinger: Investigation, methodology, conceptualization, writing – original draft

Doris Schieder: Conceptualization, methodology, supervision, writing - review & editing

Volker Sieber: Funding acquisition, supervision, writing – review & editing

7. Declaration of competing interest and conflict of interests

The authors report no commercial or proprietary interest in any product or concept discussed in this article.

References

(1) Hinderer, S.; Brändle, L.; Kuckertz, A. Transition to a Sustainable Bioeconomy. *Sustainability* **2021**, *13* (15), 8232. DOI: 10.3390/su13158232.

(2) Lange, L.; Connor, K. O.; Arason, S.; Bundgård-Jørgensen, U.; Canalis, A.; Carrez, D.; Gallagher, J.; Gøtke, N.; Huyghe, C.; Jarry, B.; Llorente, P.; Marinova, M.; Martins, L. O.; Mengal, P.; Paiano, P.; Panoutsou, C.; Rodrigues, L.; Stengel, D. B.; van der Meer, Y.; Vieira, H. Developing a Sustainable and Circular Bio-Based Economy in EU: By Partnering Across Sectors, Upscaling and Using New Knowledge Faster, and For the Benefit of Climate, Environment & Biodiversity, and People & Business. *Frontiers in bioengineering and biotechnology* **2020**, *8*, 619066. DOI: 10.3389/fbioe.2020.619066. Published Online: Jan. 21, 2021.

(3) Fasahati, P.; Wu, W.; Maravelias, C. T. Process synthesis and economic analysis of cyanobacteria biorefineries: A superstructure-based approach. *Applied Energy* **2019**, *253*, 113625. DOI: 10.1016/j.apenergy.2019.113625.

(4) Kumar, A. K.; Sharma, S.; Dixit, G.; Shah, E.; Patel, A. Techno-economic analysis of microalgae production with simultaneous dairy effluent treatment using a pilot-scale High Volume V-shape pond system. *Renewable Energy* **2020**, *145*, 1620–1632. DOI: 10.1016/j.renene.2019.07.087.

(5) Rizwan, M.; Lee, J. H.; Gani, R. Optimal design of microalgae-based biorefinery: Economics, opportunities and challenges. *Applied Energy* **2015**, *150*, 69–79. DOI: 10.1016/j.apenergy.2015.04.018.

(6) Chia, S. R.; Chew, K. W.; Show, P. L.; Yap, Y. J.; Ong, H. C.; Ling, T. C.; Chang, J.-S. Analysis of Economic and Environmental Aspects of Microalgae Biorefinery for Biofuels Production: A Review. *Biotechnology journal* **2018**, *13* (6), e1700618. DOI: 10.1002/biot.201700618. Published Online: Feb. 9, 2018.

(7) Prabha, S.; Vijay, A. K.; Paul, R. R.; George, B. Cyanobacterial biorefinery: Towards economic feasibility through the maximum valorization of biomass. *The Science of the total environment* **2022**, *814*, 152795. DOI: 10.1016/j.scitotenv.2021.152795. Published Online: Jan. 1, 2022.

(8) Thomassen, G.; Egiguren Vila, U.; van Dael, M.; Lemmens, B.; van Passel, S. A techno-economic assessment of an algal-based biorefinery. *Clean Techn Environ Policy* **2016**, *18* (6), 1849–1862. DOI: 10.1007/s10098-016-1159-2.

(9) Tejada Carbajal, E. M.; Martínez Hernández, E.; Fernández Linares, L.; Novelo Maldonado, E.; Limas Ballesteros, R. Techno-economic analysis of Scenedesmus dimorphus microalgae biorefinery scenarios for biodiesel production and glycerol valorization. *Bioresource Technology Reports* **2020**, *12*, 100605. DOI: 10.1016/j.biteb.2020.100605.

(10) Cheel, J.; Urajová, P.; Hájek, J.; Hrouzek, P.; Kuzma, M.; Bouju, E.; Faure, K.; Kopecký, J. Separation of cyclic lipopeptide puwainaphycins from cyanobacteria by countercurrent chromatography combined with polymeric resins and HPLC. *Analytical and bioanalytical chemistry* **2017**, *409* (4), 917–930. DOI: 10.1007/s00216-016-0066-z. Published Online: Nov. 30, 2016.

(11) Fewer, D. P.; Jokela, J.; Heinilä, L.; Aesoy, R.; Sivonen, K.; Galica, T.; Hrouzek, P.; Herfindal, L. Chemical diversity and cellular effects of antifungal cyclic lipopeptides from cyanobacteria. *Physiologia plantarum* **2021**, *173* (2), 639–650. DOI: 10.1111/ppl.13484. Published Online: Jul. 1, 2021.

(12) Korbinian Sinzinger; Sebastian Bieringer; Doris Schieder; Herbert Riepl; Volker Sieber. Biorefinery concept for Cylindrospermum alatosporum CCALA 988 extracting multiple high-value compounds and residue utilization by P. pastoris fermentation producing phytase. *Algal Research* **2023**, *76*, 103302. DOI: 10.1016/j.algal.2023.103302.

(13) Bhambhani, A.; van der Hoek, J. P.; Kapelan, Z. Life cycle sustainability assessment framework for water sector resource recovery solutions: Strengths and weaknesses. *Resources, Conservation and Recycling* **2022**, *180*, 106151. DOI: 10.1016/j.resconrec.2021.106151.

(14) Kua, H. W. On Life Cycle Sustainability Unified Analysis. *Journal of Industrial Ecology* **2017**, *21* (6), 1488–1506. DOI: 10.1111/jiec.12665.

(15) Finkbeiner, M.; Schau, E. M.; Lehmann, A.; Traverso, M. Towards Life Cycle Sustainability Assessment. *Sustainability* **2010**, *2* (10), 3309–3322. DOI: 10.3390/su2103309.

(16) Bussa, M. Ex-ante life cycle assessment of biorefineries: The potential of microalgae for the production of PLA and commodity chemicals in the Bavarian-Czech border region, Technische Universität München. https://mediatum.ub.tum.de/?id=1615138.

(17) SUBITEC. *Produkt - SUBITEC*. https://www.subitec.com/industrie/kultivierungsmodul/ (accessed 2022-03-15).

(18) Fasaei, F.; Bitter, J. H.; Slegers, P. M.; van Boxtel, A. Techno-economic evaluation of microalgae harvesting and dewatering systems. *Algal Research* **2018**, *31*, 347–362. DOI: 10.1016/j.algal.2017.11.038.

(19) Helian, Y.; Gai, Y.; Fang, H.; Sun, Y.; Zhang, D. A multistrategy approach for improving the expression of E. coli phytase in Pichia pastoris. *Journal of industrial microbiology & biotechnology* **2020**, *47* (12), 1161–1172. DOI: 10.1007/s10295-020-02311-6. Published Online: Sep. 15, 2020.

(20) Bayarjargal, M.; Munkhbat, E.; Ariunsaikhan, T.; Odonchimeg, M.; Uurzaikh, T.; Gan-Erdene, T.; Regdel, D. Utilization of spent brewer's yeast Saccharomyces cerevisiae for the production of yeast enzymatic hydrolysate. *Mong. J. Chem.* **2014**, *12*, 88–91. DOI: 10.5564/mjc.v12i0.179.

(21) Guo, M.; Wu, K.; Zhuang, Y.; Chu, J.; Zhang, S. Studies on characteristics of kinetics and metabolic shift of genetically engineered yeast Pichia pastoris in high-density chemostat cultivation. *Wei sheng wu xue bao = Acta microbiologica Sinica* **2001**, *41* (5), 617–623.

(22) Kannaujiya, V. K.; Sinha, R. P. An Efficient Method for the Separation and Purification of Phycobiliproteins from a Rice-Field Cyanobacterium Nostoc sp. Strain HKAR-11. *Chromatographia* **2016**, *79* (5-6), 335–343. DOI: 10.1007/s10337-016-3025-0.

(23) Bhavsar, K.; Ravi Kumar, V.; Khire, J. M. Downstream processing of extracellular phytase from Aspergillus niger: Chromatography process vs. aqueous two phase

extraction for its simultaneous partitioning and purification. *Process Biochemistry* **2012**, *47* (7), 1066–1072. DOI: 10.1016/j.procbio.2012.03.012.

(24) *LCIA: the ReCiPe model | RIVM*. https://www.rivm.nl/en/life-cycle-assessment-lca/recipe (accessed 2022-03-15).

(25) Huijbregts, M. A. J.; Steinmann, Z. J. N.; Elshout, P. M. F.; Stam, G.; Verones, F.; Vieira, M.; Zijp, M.; Hollander, A.; van Zelm, R. ReCiPe2016: a harmonised life cycle impact assessment method at midpoint and endpoint level. *Int J Life Cycle Assess* **2017**, *22* (2), 138–147. DOI: 10.1007/s11367-016-1246-y.

(26) Tredici, M. R.; Rodolfi, L.; Biondi, N.; Bassi, N.; Sampietro, G. Techno-economic analysis of microalgal biomass production in a 1-ha Green Wall Panel (GWP®) plant. *Algal Research* **2016**, *19*, 253–263. DOI: 10.1016/j.algal.2016.09.005.

(27) *Labour cost, wages and salaries, direct remuneration (excluding apprentices) by NACE Rev. 2 activity) - LCS surveys 2008, 2012 and 2016 - Products Datasets - Eurostat*. https://ec.europa.eu/eurostat/web/products-datasets/-/lc_ncost_r2 (accessed 2022-03-15).

(28) Institute, Corporate Finance. Net Present Value (NPV). *Corporate Finance Institute*, Jan 22, 2018. https://corporatefinanceinstitute.com/resources/knowledge/valuation/net-present-value-npv/ (accessed 2022-03-15).

(29) Federal Office for the Environment, Ed. *Swiss Eco-Factors 2021 according to the Ecological Scarcity Method:Methodological fundamentals and their application in Switzerland*; Environmetal studies no. 2121: 252 pp., 2021.

(30) Banerjee, S.; Ramaswamy, S. Comparison of productivity and economic analysis of microalgae cultivation in open raceways and flat panel photobioreactor. *Bioresource Technology Reports* **2019**, *8*, 100328. DOI: 10.1016/j.biteb.2019.100328.

(31) Sano Coelho, R.; Cuellar, M. C.; Franco, T. T.; van der Wielen, L. A. M. Techno-economic assessment of heterotrophic microalgae biodiesel production integrated with a sugarcane bio-refinery. *Biofuels Bioprod Bioref* **2021**, *15* (2), 416–429. DOI: 10.1002/bbb.2174.

(32) Statista. *Pachtpreise für landwirtschaftlich genutzter Flächen in Deutschland bis 2023 | Statista*. https://de.statista.com/statistik/daten/studie/953408/umfrage/pachtpreise-fuer-landwirtschaftlich-genutzter-flaechen-in-deutschland/ (accessed 2025-02-03).

(33) Chew, K. W.; Yap, J. Y.; Show, P. L.; Suan, N. H.; Juan, J. C.; Ling, T. C.; Lee, D.-J.; Chang, J.-S. Microalgae biorefinery: High value products perspectives. *Bioresource Technology* **2017**, *229*, 53–62. DOI: 10.1016/j.biortech.2017.01.006.

(34) *Database - Labour market - Eurostat*. https://ec.europa.eu/eurostat/web/labour-market/database (accessed 2025-02-02).

(35) *Labour cost levels by NACE Rev. 2 activity (lc_lci_lev)*. https://ec.europa.eu/eurostat/cache/metadata/en/lc_lci_lev_esms.htm (accessed 2025-02-02).

(36) Lam, G. P. 't; Vermuë, M. H.; Eppink, M.; Wijffels, R. H.; van den Berg, C. Multi-Product Microalgae Biorefineries: From Concept Towards Reality. *Trends in Biotechnology* **2018**, *36* (2), 216–227. DOI: 10.1016/j.tibtech.2017.10.011.

(37) Yadav, K.; Vasistha, S.; Nawkarkar, P.; Kumar, S.; Rai, M. P. Algal biorefinery culminating multiple value-added products: recent advances, emerging trends, opportunities, and challenges. *3 Biotech* **2022**, *12* (10), 244. DOI: 10.1007/s13205-022-03288-y.

(38) Morales-Sánchez, D.; Martinez-Rodriguez, O. A.; Kyndt, J.; Martinez, A. Heterotrophic growth of microalgae: metabolic aspects. *World journal of microbiology & biotechnology* **2015**, *31* (1), 1–9. DOI: 10.1007/s11274-014-1773-2. Published Online: Nov. 12, 2014.

(39) Pérez-López, P.; González-García, S.; Allewaert, C.; Verween, A.; Murray, P.; Feijoo, G.; Moreira, M. T. Environmental evaluation of eicosapentaenoic acid production by Phaeodactylum tricornutum. *The Science of the total environment* **2014**, *466-467*, 991–1002. DOI: 10.1016/j.scitotenv.2013.07.105. Published Online: Aug. 28, 2013.

(40) Sivaramakrishnan, R.; Suresh, S.; Kanwal, S.; Ramadoss, G.; Ramprakash, B.; Incharoensakdi, A. Microalgal Biorefinery Concepts' Developments for Biofuel and Bioproducts: Current Perspective and Bottlenecks. *International Journal of Molecular Sciences* **2022**, *23* (5), 2623. DOI: 10.3390/ijms23052623. Published Online: Feb. 27, 2022.

(41) Centella, M. H.; Arévalo-Gallegos, A.; Parra-Saldivar, R.; Iqbal, H. M. Marine-derived bioactive compounds for value-added applications in bio- and non-bio sectors. *Journal of Cleaner Production* **2017**, *168*, 1559–1565. DOI: 10.1016/j.jclepro.2017.05.086.

(42) Sano Coelho, R.; Cuellar, M. C.; Franco, T. T.; Wielen, L. A. M. Techno-economic assessment of heterotrophic microalgae biodiesel production integrated with a sugarcane bio-refinery. *Biofuels, Bioprod. Bioref.* **2021**, *15* (2), 416–429. DOI: 10.1002/bbb.2174.

(43) Novoveská, L.; Zapata, A. K.; Zabolotney, J. B.; Atwood, M. C.; Sundstrom, E. R. Optimizing microalgae cultivation and wastewater treatment in large-scale offshore photobioreactors. *Algal Research* **2016**, *18*, 86–94. DOI: 10.1016/j.algal.2016.05.033.

(44) Arias, A.; Feijoo, G.; Moreira, M. T. Biorefineries as a driver for sustainability: Key aspects, actual development and future prospects. *Journal of Cleaner Production* **2023**, *418*, 137925. DOI: 10.1016/j.jclepro.2023.137925.

(45) Ubando, A. T.; Felix, C. B.; Chen, W.-H. Biorefineries in circular bioeconomy: A comprehensive review. *Bioresource Technology* **2020**, *299*, 122585. DOI: 10.1016/j.biortech.2019.122585. Published Online: Dec. 10, 2019.

5. Discussion

5.1. Evaluation of biomass

Evaluating cyanobacterial biomass composition is a critical first step in developing a biorefinery concept [117,118]. This thesis presents a detailed analysis of biomass composition for various *Nostoc* and *Cylindrospermum* strains, including quantifying proteins, lipids, saccharides, and high-value compounds like cyclic lipopeptides and phycobiliproteins. A key finding is the complexity and diversity of saccharides in the biomass, with many rare, substituted sugars identified that would be challenging to break down enzymatically. This underscores the need for careful carbohydrate profiling to determine the potential for utilization of structural polysaccharides. Enzymatic hydrolysis tests demonstrate the difficulty in achieving high yields of fermentable sugars from *Nostoc* and *Cylindrospermum* biomass using typical industrial enzyme cocktails. While yields up to 75 mg sugars/g biomass of mainly glucose and little galactose and mannose were obtained after additional protease pre-treatment, this was still only 29-37 % of total sugars measured by chemical hydrolysis. Significant optimization of enzymatic treatment will be required to improve the utilization of cyanobacterial sugars.

This thesis also highlights the known importance of a multi-product approach, with cyclic lipopeptides, phycobiliproteins, and pigments quantified as potential high-value coproducts. However, the concentrations reported, while significant, may not be sufficient to offset the high costs of microalgal cultivation and processing. The proposed sequential extraction and demonstration of phytase production from residual biomass provides a good starting point, but further techno-economic analysis is needed to assess the commercial potential. Extending the product portfolio beyond phytases to higher-value enzymes or optimizing cultivation and extraction to increase product yields could enhance economic feasibility.

The detailed profiling provides critical insights into cyanobacterial composition and demonstrates the challenges in finding uses for all biomass components. A systematic biorefinery design approach accounting for mass flows, bioactive extraction, and optimized conversion of residuals is and will be essential to make such concepts economically viable [119]. The research provides a strong foundation, but there are opportunities to expand the scope, improve material balances, and assess sustainability more holistically.

5.2. Fermentative hydrolysate utilization

The phytase production by *Pichia pastoris* fermentation of *Nostoc* hydrolysate demonstrates the potential utilization of cyanobacterial biomass residuals[120]. Using 20 % *Nostoc* hydrolysate as a supplement enabled phytase titers over 500 U/mL in bench-scale batch cultures, comparable to

rich YPD medium. This represents a promising proof-of-concept, indicating residual protein and sugars in the hydrolysate can support yeast growth and recombinant enzyme secretion.

Several areas could benefit from further investigation to advance this approach. First, optimization of the hydrolysate production, as enzymatic sugar release was low and nitrogen solubilization was not quantified. Higher enzyme loadings or more active enzyme cocktails tailored to cyanobacteria cell walls may improve hydrolysate quality. Tracking overall mass balances and losses during hydrolysis will also help identify areas for improvement. Second, assessing hydrolysate suitability across various yeast and bacteria strains and products would provide more insight into its value as a generic supplement. Testing shake flask cultures cannot predict performance in controlled, high-density fermentations, so 10 -30 L reactor studies should be conducted. Third, developing a process model for cyanobacteria cultivation through hydrolysate preparation would enable techno-economic analysis. This could guide the selection of target products and process configurations to enhance economic feasibility.

The fed-batch fermentation engineering provides a valuable framework for translation to industrial systems [121]. The stepwise procedure from batch/pulsed batch characterization to optimized DO-stat feeding is a robust strategy for maximizing productivity. While specific conditions would need re-optimization (e. g. μ_{max}, for different yeast strains and products, the general approach of correlating growth kinetics to feeding rate and modeling effects of oxygen limitation provides a blueprint. Integrating the hydrolysate utilization with high-density fermentation and purifying representative amounts of the product would be logical next steps toward commercial implementation[122].

Overall, the research makes excellent progress in demonstrating an integrated biorefinery concept from cyanobacteria cultivation to utilizing residuals. Additional work on hydrolysate optimization, broader testing across microorganism systems, quantitative process modeling, scale-up, and product purification/validation is recommended. However, the initial results are optimistic and indicate good potential.

5.3. Development of a fermentation strategy

Developing a high-density *P. pastoris* fermentation process for constitutive phytase production provides a valuable case study in bioprocess optimization. The stepwise approach - beginning with fundamental growth kinetics in batch/pulsed cultures and progressing towards optimized DO-stat feeding, offers a robust, generalizable framework [123,124]. Optimizing multiple parameters, including the expression host strain, temperature, inducer concentration, pH,

induction time, and culture medium composition, is crucial for achieving high expression yields [125]. Several vital aspects of this research could improve further process engineering efforts:

- Growth Kinetics and Yield: The specific growth rate (μ_{max}) of 0.30 h^{-1} and biomass yield of 0.6 g/g on glycerol obtained in controlled batch cultures align with previous reports for *P. pastoris* on glycerol, such as 0.28 h^{-1} and 0.53 g/g[126]. Maintaining growth near μ_{max} was ideal for constitutive phytase expression, whereas many inducible systems benefit from lower specific growth rates[127]. This highlights the importance of tailoring fermentation strategies to the specific expression mechanism.
- Nutrient Limitations and Oxygen Supply: Pulsed batch cultures revealed nutrient limitations and uncoupling constraints like oxygen supply, identifying maximum potential productivity. Literature generally reports air saturations around 20-30%[80]. Comparing batch and pulse-fed kinetics was insightful for identifying bottlenecks for process optimization. For example, the initial exponential feed based solely on μmax rapidly increased biomass density but led to dissolved oxygen depletion, prompting the shift to DO-stat feeding. Identifying such limitations through multiple pulses prior to fed-batch mode is critical.
- Multi-Parameter Optimization: Reducing temperature from 30°C to 25°C slowed growth but minimized protease degradation and increased phytase yield, demonstrating the necessity for multi-parameter optimization (Stirring rate and air supply have also been shown to be important parameters. Further, minimal starting and maximum feed volumes are parameters to be optimized but are also intrinsic to the used system[128]. Achieving a titer of 7,200 U/mL in 1 L reactors after 72 hours is promising, though still below technical targets of around 30,000 U/mL.
- Economic and Scale-Up Considerations: The stepwise fermentation development strategy, starting from fundamental growth characterization, effectively improved phytase productivity[124]. However, detailed process modeling incorporating engineering constraints like oxygen transfer and economic analysis is needed to minimize costs at a larger scale. High-yielding operating conditions may be economically suboptimal if they incur excessive utility or equipment costs when scaled up. An integrated techno-economic evaluation should guide the selection of a balanced operating window, maximizing titer while controlling capital and operating expenses.

In summary, the structured approach provides a template for developing *P. pastoris* processes from scratch, which is crucial for new products. Critical knowledge, such as matching feed strategy to expression and navigating equipment constraints, has broad applicability. However, translating even high-yielding laboratory processes to manufacturing scale remains challenging. Techno-economic analysis should guide the selection of balanced operating strategies for productivity, quality, robustness, and costs.

5.4. Biorefinery Concept and LCSA

Our life cycle sustainability assessment (LCSA) indicates the proposed biorefinery concept to be promising. Similarly, Ruiz et al. discussed a cyanobacteria biorefinery concept with sequential extraction of high-value compounds, which has the potential to offer environmental and economic advantages over standard manufacturing approaches [129]. The LCSA provides valuable insights into the conceptual process's ecological impacts and economic feasibility. Several key findings emerged:

- Climate change, fossil fuel depletion, and non-carcinogenic effects accounted for over 50% of eco-points, with glycerol, electricity, and citric acid as significant contributors. Targeting greener alternatives for these inputs could significantly improve sustainability.
- The proposed biorefinery was estimated to equate to the environmental impact of 75 EU citizens annually across 16 impact categories. While not negligible, this is relatively low and could be further reduced by addressing the significant hotspots identified.
- Preliminary economics indicated the potential for the biorefinery to break even within five years with $18.6M cumulative earnings at 10 % ROI. However, sales projections are highly speculative without market validation.
- Assuming idealized selling prices, the proposed product portfolio could generate $2.5B annually. This suggests financial viability may hinge on market development rather than technical or product limitations.

While promising, the LCSA has several limitations requiring further work:

- Process data is based on lab/pilot studies and has not been demonstrated at a large scale, introducing uncertainties into the modeling.
- Many parameters for cultivation, extraction, and hydrolysis steps are assumed rather than experimentally measured.
- Financials rely heavily on literature benchmarks not matched here; rigorous on-site data is needed.
- Market demand and achievable pricing for all products, especially novel cyclic lipopeptides, remain unclear.
- Sustainability assessment focuses only on the environment and economics; social impacts should also be considered.

- Sensitivity analysis evaluates parameter uncertainty but cannot account for model uncertainty and inherent biases.

This initial LCSA provides a functional screening-level analysis to identify priorities for more detailed techno-economic and life cycle studies. Large-scale demonstrations, systematic sustainability assessment, and market analysis will be critical next steps toward commercial maturity. While promising, the full impacts of the biorefinery cannot be projected without reliable data at the manufacturing scale[130].

Prabha et al. presented extensive foundational research on cyanobacterial biomass profiling, extraction schemes, and phytase production from residuals[99]. However, several limitations to the current scope could be addressed through future work. Firstly, the studies have all been conducted at laboratory or bench scales of up to 1L; demonstrating the proposed processes at pilot or commercial scales will be essential to validate the concepts. Secondly, the techno-economic and life cycle analyses rely heavily on assumed parameters and benchmarks from literature rather than experimentally measured data. Detailed on-site mass balance and cost modeling will be required to project sustainability and profitability accurately. Thirdly, the focus has been narrowly on analytics, extraction, and fermentation processes; market assessment and supply chain logistics are needed to create an integrated business plan. Finally, the social impacts and ethics of cyanobacteria biorefining have not been considered; these "people" aspects are vital to sustainability alongside the environment and economics.

Logical next steps after reproducing the lab-scale results to build on this research while addressing current limitations would include:

1) experiments on a technical scale; 2) establish- and assessment of down-stream processes; 3) collection of large-scale operational data for process modeling and LCSA; 4) expanded product portfolio evaluation and market research; 5) assessment of local job creation, labor practices, and social acceptance; and 6) development of an integrated business plan evaluating all aspects of commercial viability and life cycle performance.

This phased approach from fundamental studies to mature business plan will require multidisciplinary collaboration and investment but holds exciting potential to realize sustainable and ethical cyanobacterial biorefineries. This thesis provides an excellent knowledge base to progress towards this goal with additional applied research and development.

6. Conclusion

It is evident from this dissertation that the primary objective was to contribute to the industrial availability of cyanobacterial biomass through the development of a multi-product cyanobacterial-based biorefinery concept, complemented by a comprehensive lifecycle sustainability assessment. Emphasis was placed on utilizing residual biomass after extracting high-value compounds, which would then undergo enzymatic conversion into a hydrolysate, serving as a complex nutrient supplement in subsequent fermentation processes.

The global shift towards sustainable alternatives necessitates the exploration of new energy sources and chemical feedstocks. This study underscores the evolving role of biomass, not merely as a source for biofuels but as a reservoir for chemicals and novel compounds. While microalgal and cyanobacterial biofuels have been demonstrated at smaller scales, the feasibility and impacts at an industrial scale require careful evaluation and a multi-product approach utilizing the complete biomass. The exploration of diverse strains, particularly from the genera *Nostoc* and *Cylindrospermum,* which are promising candidates with high-value secondary metabolites, revealed complex heteroglycans in their saccharide profiles. The enzymatic hydrolysis of *Nostoc* biomass demonstrated its potential as a cost-effective fermentation medium from waste, particularly evident in phytase expression with *Pichia pastoris*. Further fermentation studies with a promising strain revealed significant phytase yields, showcasing its potential as an industrially relevant producer strain.

The identification of *Cylindrospermum alatosporum* CCALA 988 as a highly promising candidate for a multi-product biorefinery concept marked a crucial milestone. The characterization of bioactive compounds, such as cyclic lipopeptides, highlighted the potential for diversified product streams. While this lab scale concept indicated viability, only investigation of this concept in an upscaled format will allow us to find out about its commercial deployability. The integration of a lifecycle sustainability assessment (LCSA) further indicates the feasibility of the biorefinery concept, considering both ecological and economic aspects. The LCSA encompassed a thorough examination of material and equipment bills, material streams, and resulting product quantities. The environmental assessment revealed a moderate ecological impact. The techno-economic analysis, employing net present value (NPV) and payback period methods, demonstrated the potential economic viability of the biorefinery concept. The sensitivity analysis underscored the importance of managing investment costs for sustained financial feasibility. Yet, up-scale experiments are needed to confirm the results.

Future work on the *Cylindrospermum alatosporum* CCALA 988 biorefinery concept should focus on different aspects to improve the overall process. Firstly, investigating the sequential extraction process in a more up-scaled format and optimizing the enzymatic hydrolysis of the

residual biomass. Advancing downstream processing techniques for the identified products within the lab context and investigating the optimization of the utilization of the residual biomass will be paramount. Moreover, fine-tuning the *P. pastoris* fermentation conditions with hydrolysate in salt medium and upscaling the developed fed-batch strategy. This involves a comprehensive exploration of fermentation conditions, including nutrient optimization, culture medium composition, and cultivation parameters.

In summary, this dissertation not only advances our understanding of cyanobacterial biomass utilization but also presents a tangible and potentially economically viable biorefinery concept. The integration of sustainable practices and comprehensive assessments positions this research at the forefront of contributing to a greener and economically feasible industrial landscape.

7. Appendix A

7.1. Supporting Information: Towards a cyanobacterial biorefinery: Carbohydrate fingerprint, biocomposition and enzymatic hydrolysis of *Nostoc* biomass

Algal Research

Towards a cyanobacterial biorefinery: Carbohydrate fingerprint, biocomposition and enzymatic hydrolysis of Nostoc biomass

Supporting Information

Korbinian Sinzinger[a], Doris Schieder[a], Broder Rühmann[a] and Volker Sieber[a,b,c]

[a] *Chair of Chemistry of Biogenic Resources, Technical University of Munich, Campus for Biotechnology and Sustainability, 94315 Straubing, Germany*

[b] *Catalysis Research Center, Technical University of Munich, 85748 Garching, Germany*

[c] *The University of Queensland, School of Chemistry and Molecular Biosciences, 68 Cooper Road, St. Lucia 4072, Australia*

Annex 1. Overlay of UV 245 nm (black) and MS extracted ion (color) chromatograms (3 – 9 min) of *Nostoc* sp. De1*, Nostoc* sp. Cc3*, Nostoc muscorum I, Nostoc piscinale, Nostoc viola, Nostoc F 15c, Nostoc linckia*, monosaccharide analysis. EIC colors have been chosen to help differentiate peaks. Corresponding m/z values are shown in the figures.

Annex 1.1. Overlay of UV 245 nm (black) and MS extracted ion (color) chromatograms (3 – 9 min) *Nostoc* sp. De1.

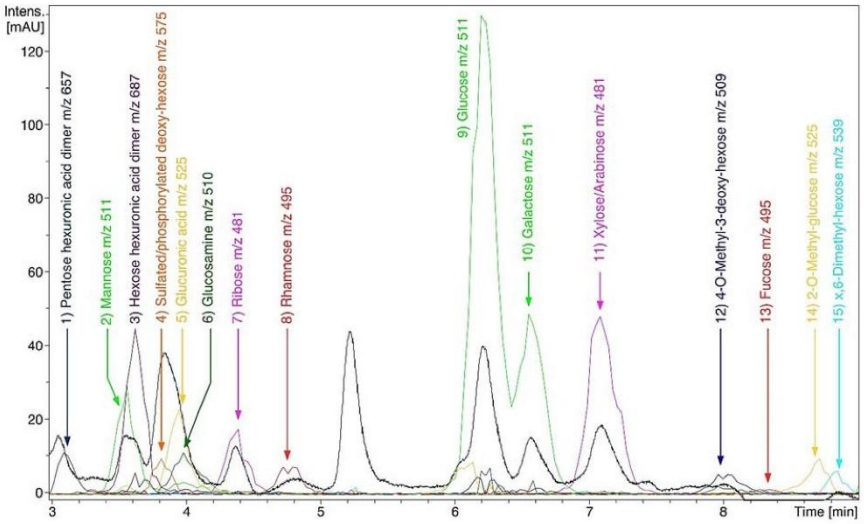

Annex 1.2. Overlay of UV 245 nm (black) and MS extracted ion (color) chromatograms (3 – 9 min) *Nostoc* sp. Cc3.

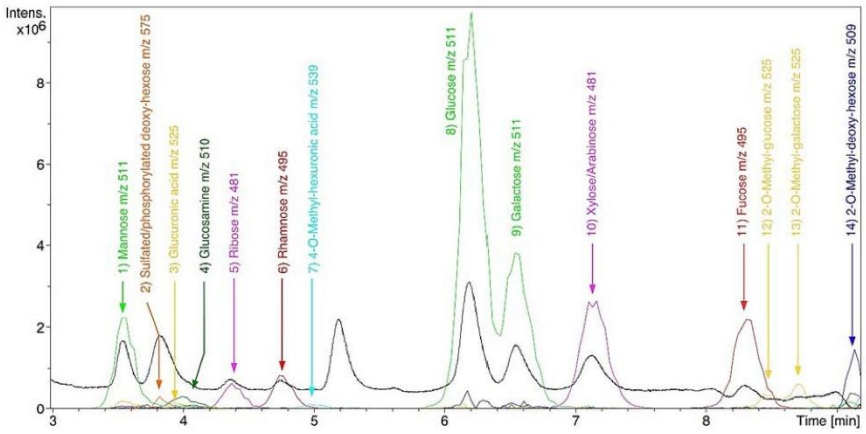

Annex 1.3. Overlay of UV 245 nm (black) and MS extracted ion (color) chromatograms (3 – 9 min) *Nostoc muscorum I.*

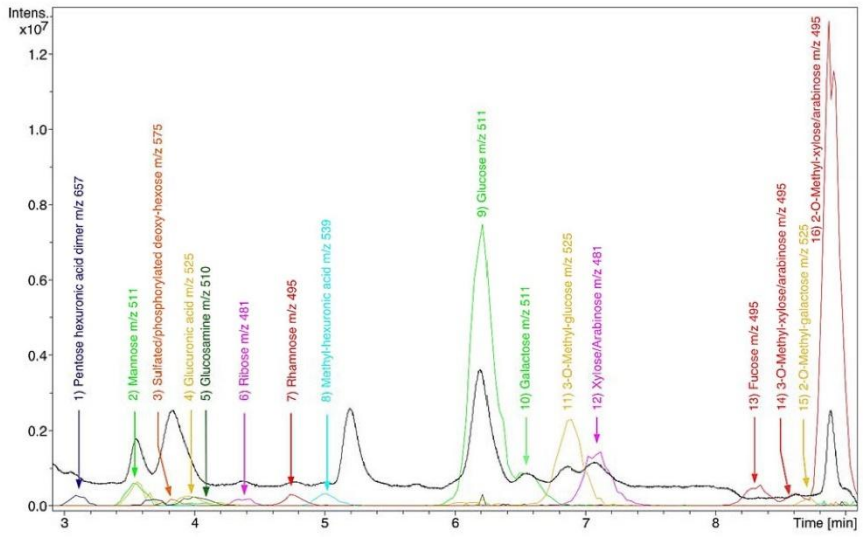

3

Annex 1.6. Overlay of UV 245 nm (black) and MS extracted ion (color) chromatograms (3 – 9 min) *Nostoc* F15c.

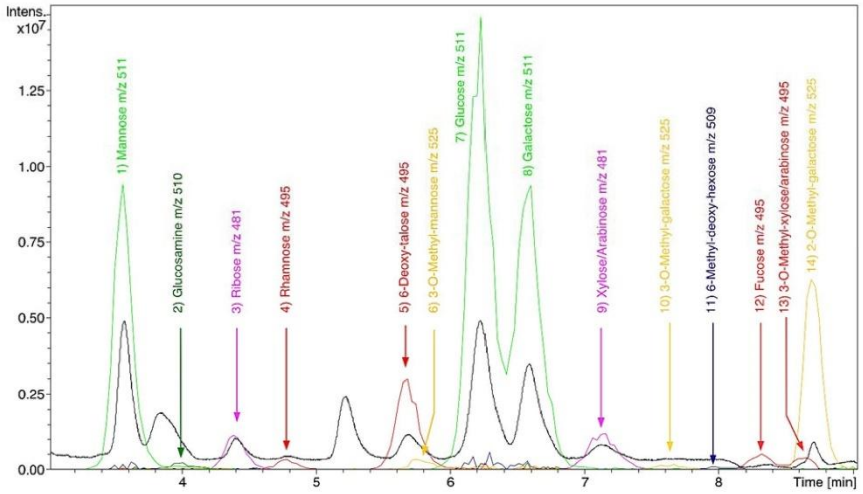

Annex 1.7. Overlay of UV 245 nm (black) and MS extracted ion (color) chromatograms (3 – 9 min) *Nostoc linckia.*

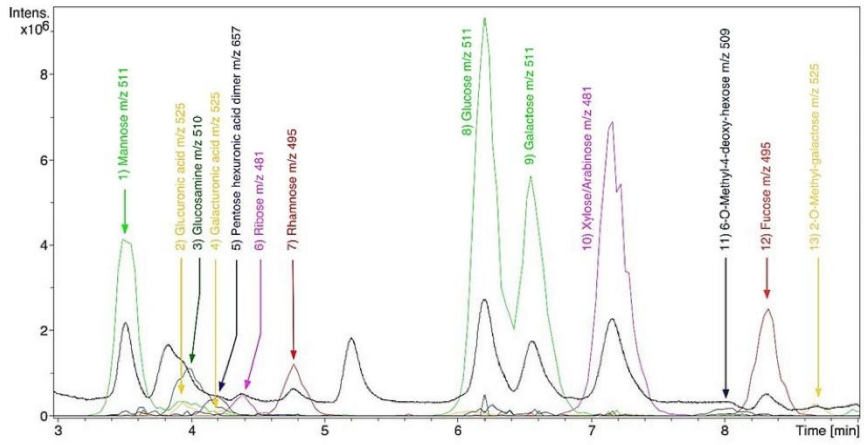

5

Annex 1.4. Overlay of UV 245 nm (black) and MS extracted ion (color) chromatograms (3 – 9 min) *Nostoc piscinale.*

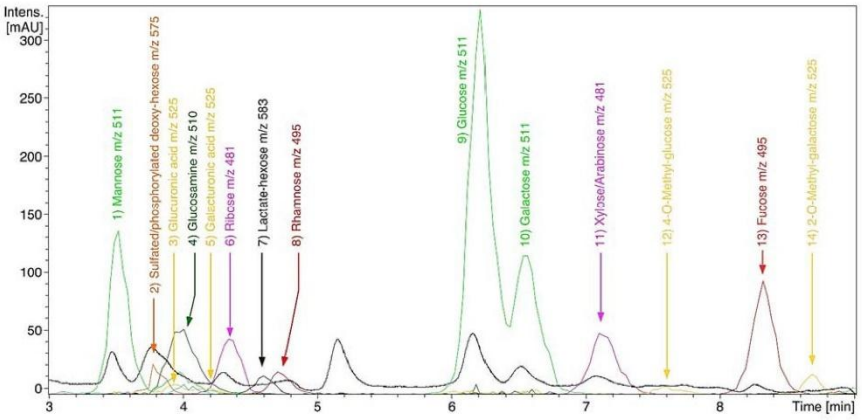

Annex 1.5. Overlay of UV 245 nm (black) and MS extracted ion (color) chromatograms (3 – 9 min) *Nostoc viola.*

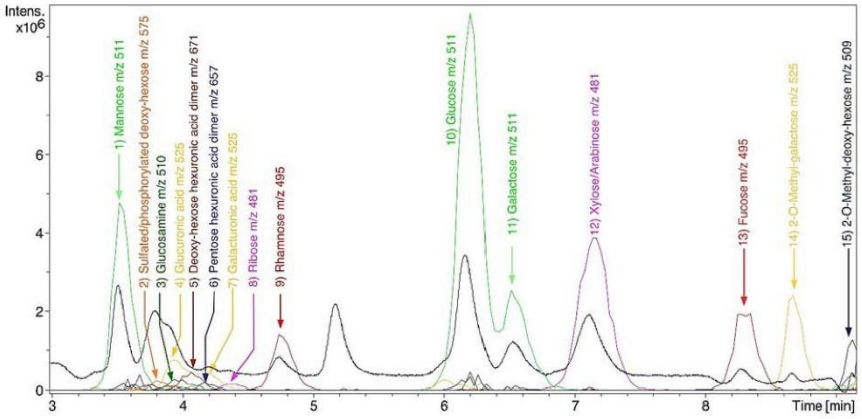

4

Annex 2. Fragmentation pattern of the saccharides detected in *Nostoc* sp. De1, *Nostoc* sp. Cc3, and *Nostoc muscorum* I, *Nostoc piscinale, Nostoc Viola, Nostoc* F 15c*, Nostoc linckia*. Masses marked with ○are parent ions, ◊ are mono-derivative ions and * correspond to methylated or substituted fragments.

Annex 2.1. Fragmentation pattern of identified peaks of *Nostoc* sp. De1 biomass.

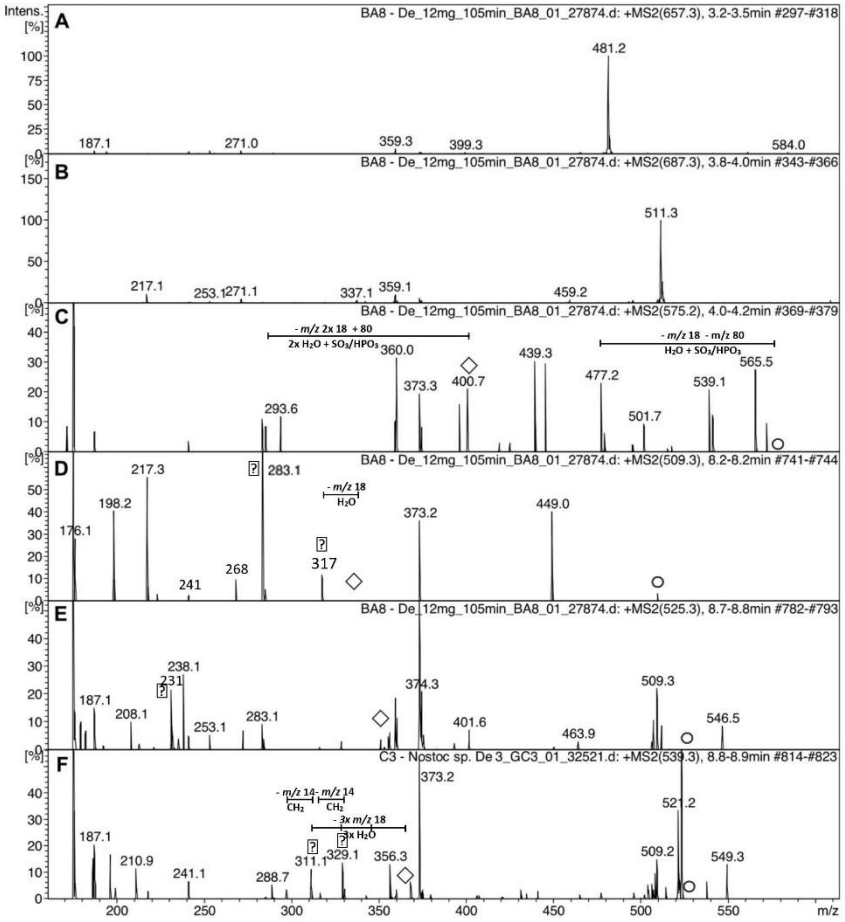

Fragmentation patterns, MS^2, (*m/z 100-610*) of unknown peaks from *Nostoc* sp. De1 biomass. (**A**) Pentose hexuronic acid dimer: fragment m/z 481 indicates the *bis*-PMP pentose fragment. The difference to m/z 657 is 176 for a hexuronic acid and a water 18. (**B**) Hexose hexuronic acid dimer: m/z 511 the *bis*-PMP hexose fragment is shown. The m/z difference to 687 is 176

for a hexuronic acid and a water 18. (**C**) Sulphated/phosphorylated deoxy-hexose: The fragment m/z 477 indicates the loss of a water and the sulphate/phosphate group. (**D**) Methyl-deoxy-hexose: the m/z 449 fragment is present, representing the loss of two terminal carbons without functional groups from m/z 509, which allows to exclude any functional group on C-6. The fragments m/z 317 and m/z 283 are methylated fragments. The absence of fragments m/z 231 or m/z 215 indicate no functional group on C-2. The high intensity of the m/z 283 fragment might be due to the deoxy function to be on C-3. This would mean this sugar is a 4-methyl-3-deoxy-hexose. (**E**) 2-O-methyl-galactose: the fragment m/z 231 is present. (**F**) Dimethyl-hexose: The fragments m/z 329 and 311 are dimethyl *mono*-PMP hexose fragments, which lost two and three water, respectively. The fragments (very low intensity) which show the losses of the methyl groups are m/z 315 and m/z 297. The fragment m/z 289 has lost two methyl groups and a carbon from the fragment m/z 329. The absence of a m/z 231 fragment and the presence of a m/z 241 fragment allow to exclude a methyl group to be on C-2 and C-4 position. Also, the absence of m/z 285 or m/z 299 indicate, there is no methyl group on C-3 position. Therefore, the position of the second methyl group could not be finally elucidated.

7

Annex 2.2. Fragmentation pattern of identified peaks of *Nostoc sp.* Cc3 biomass.

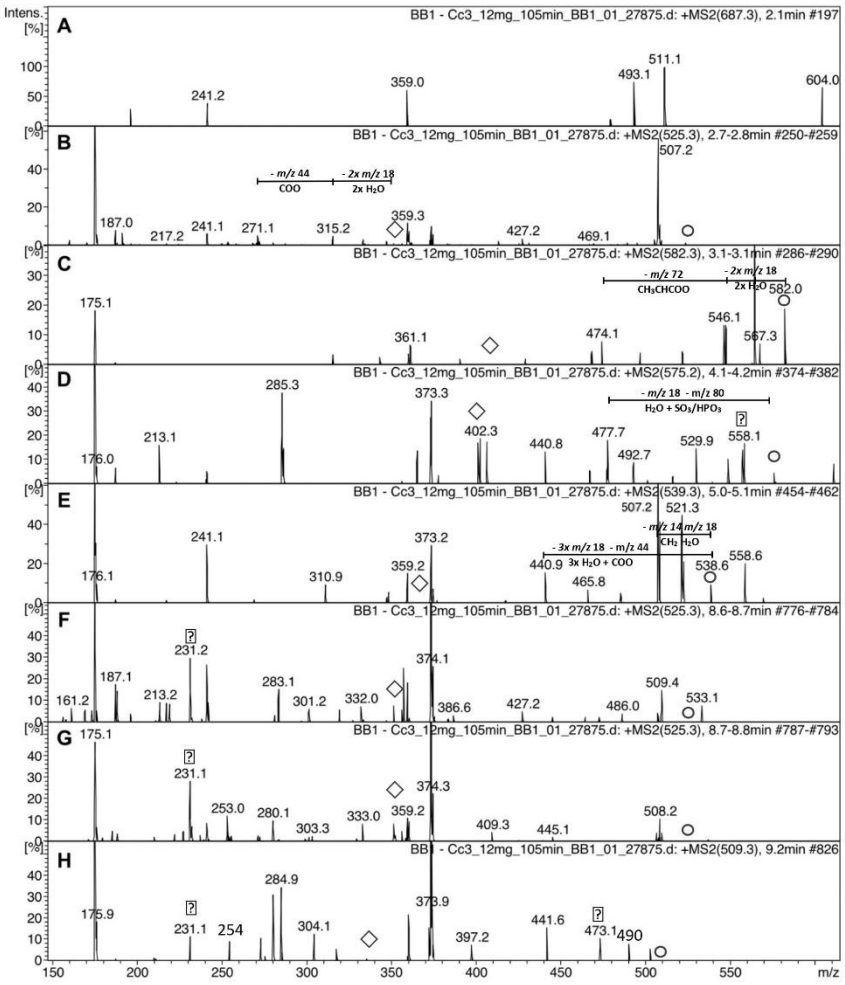

Fragmentation patterns, MS^2, (*m/z 100-610*) of unknown peaks from *Nostoc* sp. Cc3 biomass. (**A**) Hexose hexuronic acid dimer: m/z 511 the *bis*-PMP hexose fragment is shown. The m/z difference to 687 is 176 for a hexuronic acid and a water 18. (**B**) Mannuronic acid: the fragment m/z 271 indicates the loss of a carboxy group m/z 44 from the fragment m/z 315, which has lost two water molecules from the *mono*-PMP mannuronic acid fragment. (**C**) Muramic acid: The even mass indicates it is an amino sugar. The remaining main ion and large fragments m/z

564 and 546 further show water loss and the indicative stability of an amino sugar. The fragment m/z 474 is a typical amino sugar fragment and is the fragment that indicates the loss of the lactate m/z 72. (**D**) Sulphated/phosphorylated deoxy-hexose: The fragment m/z 477 indicates the loss of a water and the sulphate/phosphate group. (**E**) Methyl-hexuronic acid: the fragments m/z 521 and 507 indicate the loss of a water and a methyl group. Further, the fragment m/z 441 results from the loss of three water and a carboxy group (but no methyl group). The absence of the fragment m/z 231 and the presence of the fragment m/z 241 allows to postulate the methyl position to be on the C-3. (**F**) 2-O-methyl-glucose: The fragment m/z 231 indicates it is a 2-O-methyl hexose. The presence of the m/z 283 fragment on the other hand is typical for 4/6-O-methyl hexoses and is not present in 2-O-methyl-hexoses. Therefore, it is apparent that a mixed spectrum is here at hand. (**G**) 2-O-methyl-galactose: The fragment m/z 231 indicates, it is a 2-O-methyl hexose. (**H**) Methyl-deoxy-hexose: The presence of the fragments m/z 231 and m/z 473, which are methylated fragments and the absence of the fragments m/z 217 and m/z 241 allow to make this postulation. The presence of the fragments m/z 231 could be indicative for the methyl group to be on the C-2 position making this a 2-O-methyl-deoxy-hexose. The position of the deoxy function was not unequivocally elucidated.

Annex 2.3. Fragmentation pattern of identified peaks of *Nostoc muscorum* I biomass.

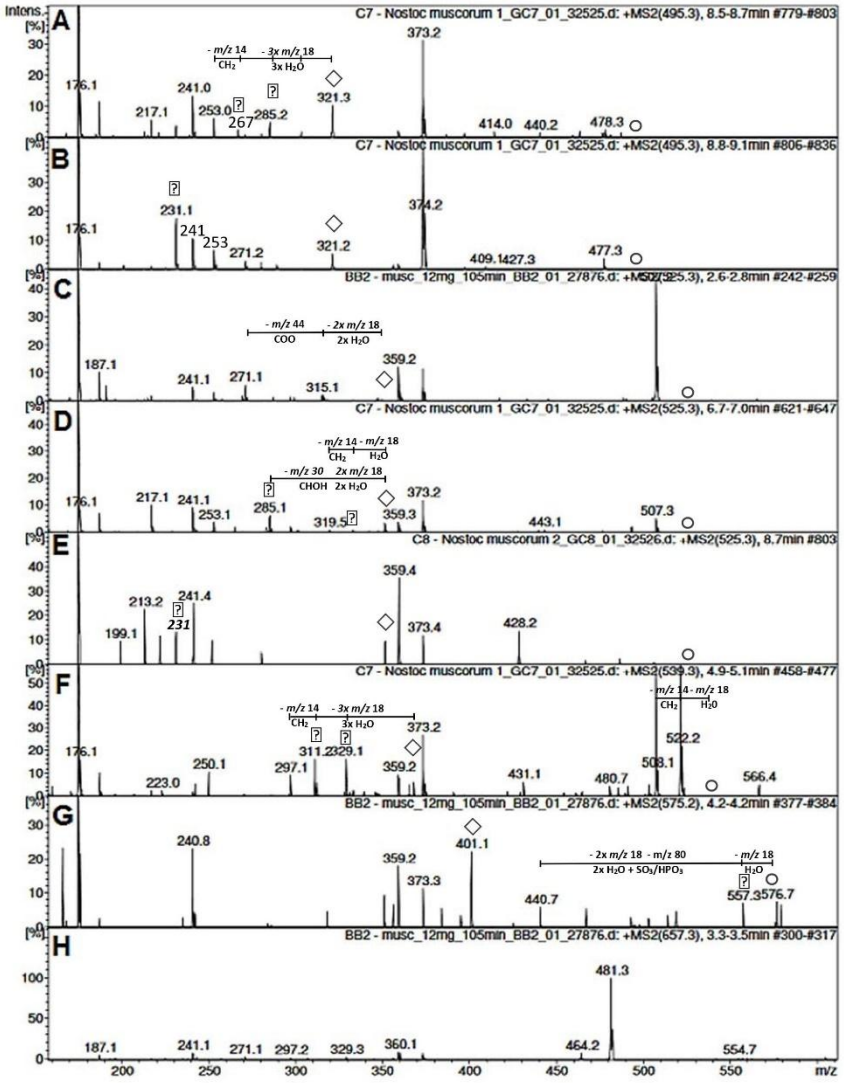

Fragmentation patterns, MS^2, (*m/z 100-600*) of unknown peaks from *Nostoc muscorum I* biomass. (**A**) 3-O-methyl-xylose/arabinose: the fragment m/z 285 is indicative for the substitution at the C-3 position. The presence of fragment m/z 253 indicates, this is not a deoxy hexose. The fragment m/z 321 is indicative for a deoxy-hexose but might also be the

mono-PMP methyl-pentose fragment. The loss of the methyl group is accounted for by the fragments m/z 267 and m/z 253 with a mass difference of m/z 14. (**B**) 2-O-methyl-xylose/arabinose: the fragment m/z 231 is indicative for the substitution at the C-2 position. (**C**) Mannuronic acid: the fragment m/z 271 indicates the loss of a carboxy group m/z 44 from the fragment m/z 315, which has lost two water from the *mono*-PMP mannuronic acid fragment. (**D**) 3-O-methyl-glucose: the fragment m/z 285 is indicative for the substitution at the C-3 position. (**E**) 2-O-methyl-galactose: the fragment m/z 231 is indicative for the substitution at the C-2 position. (**F**) Methyl-hexuronic acid: Many fragments with losses of water are present. Fragment m/z 481 indicates the loss of a methyl and a carboxy group, which might indicate this to be a 6-O-methyl-hexuronic acid. (**G**) Sulphated/phosphorylated deoxy-hexose: The fragment m/z 477 indicates the loss of a water and the sulphate/phosphate group and the fragment m/z 401 is the *mono*-PMP sugar. (**H**) Pentose hexuronic acid dimer: fragment m/z 481 indicates the *bis*-PMP pentose fragment. The m/z difference to 657 is 176 for a hexuronic acid and a water 18.

Annex 2.4. Fragmentation pattern of identified peaks of *Nostoc piscinale* biomass.

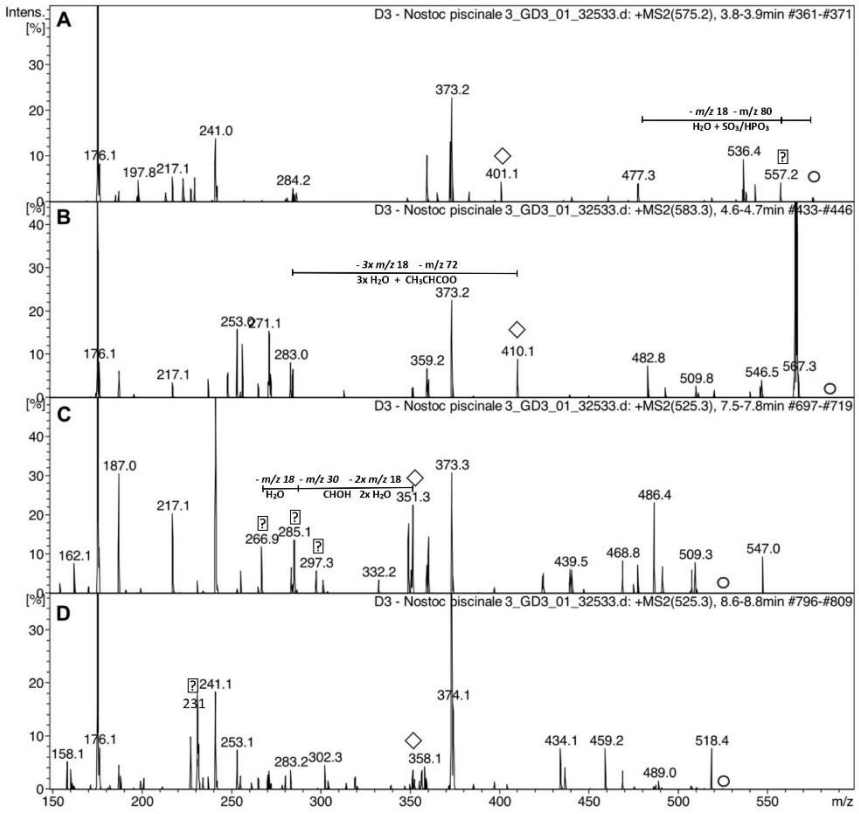

Fragmentation patterns, MS^2, (*m/z 100-600*) of unknown peaks from *Nostoc piscinale* biomass. (**A**) Sulphated/phosphorylated deoxy-hexose: The fragment m/z 477 indicates the loss of a water and the sulphate/phosphate group and the fragment m/z 401 is the *mono*-PMP sugar. (**B**) Lactate-hexose: the mass difference of only regular water losses could be identified. The loss of the lactate m/z 72 and three waters 3 x m/z 18 could be accounted for between the *mono*-PMP fragment m/z 409 and m/z 283. The fragment m/z 271 indicates a further loss of a terminal single carbon. The lack of m/z 241 might indicate a substitution at the C-4 position. (**C**) 3-O-methyl-galactose: the fragment m/z 285 is indicative for the substitution at the C-3 position. The loss of the methyl group is accounted for by the fragments m/z 267 and

m/z 253. (**D**) 2-O-methyl-galactose: the fragment m/z 231 is indicative for the substitution at the C-2 position.

Annex 2.5. Fragmentation pattern of identified peaks of *Nostoc viola* biomass.

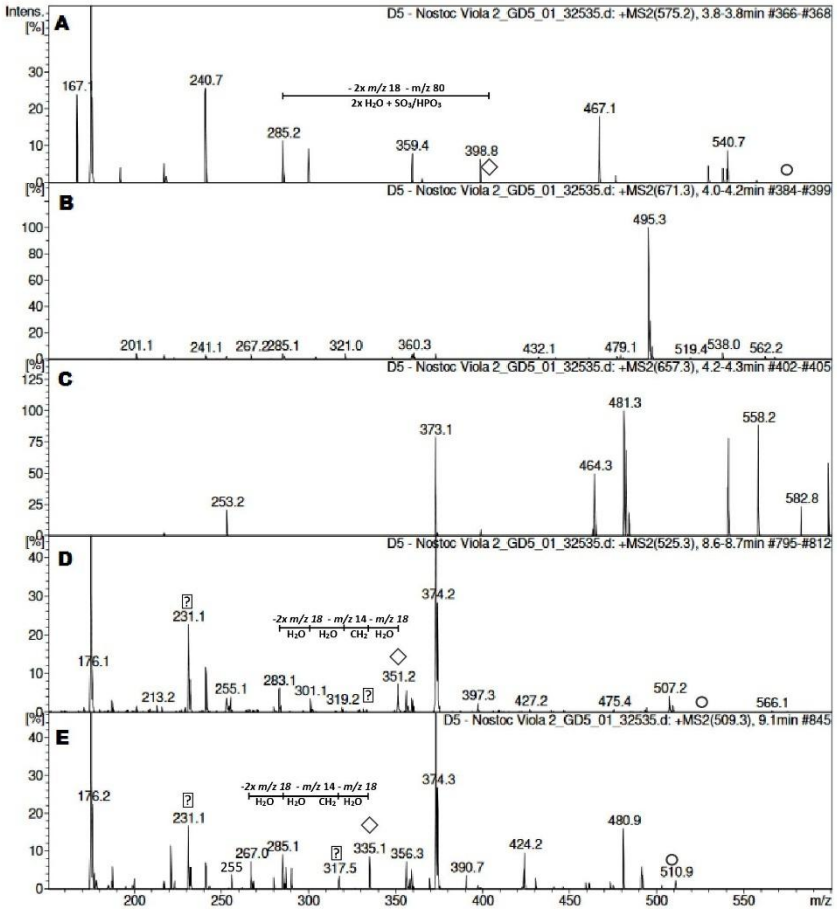

Fragmentation patterns, MS^2, (*m/z 100-600*) of unknown peaks from *Nostoc viola* biomass. (**A**) Sulphated/phosphorylated deoxy-hexose: The fragment m/z 285 indicates the loss of a water and the sulphate/phosphate group from the *mono*-PMP sugar. (**B**) Deoxy-hexose hexuronic acid dimer: m/z 495 the *bis*-PMP deoxy-hexose fragment is shown. (**C**) Pentose hexuronic acid dimer: the fragment m/z 481 indicates the *bis*-PMP pentose fragment. The

m/z difference to m/z 657 is 176 for a hexuronic acid and a water 18. (**D**) 2-O-methyl-galactose: the fragment m/z 231 is indicative for the substitution at the C-2 position. (**E**) Methyl-deoxy-hexose: the fragment m/z 231 is methylated fragment and indicative for the substitution at the C-2 position. The fragment m/z 317 lost a water from the *mono*-PMP derivate. The fragment m/z 285 lost another water and a methyl group. The fragment m/z 267 lost another water and seems to be the equivalent in methyl-deoxy-hexoses to a m/z 283 in methyl-hexoses, making this a 2-O-methyl-deoxy-hexose. The position of the deoxy function could not be elucidated. The fragment m/z 481 is rare and drew the postulation towards a dimethyl-pentose. No double methylated pentose or hexose standards were available, which would allow to verify or exclude the here made postulations.

Annex 2.6. Fragmentation pattern of identified peaks of *Nostoc* F15c biomass.

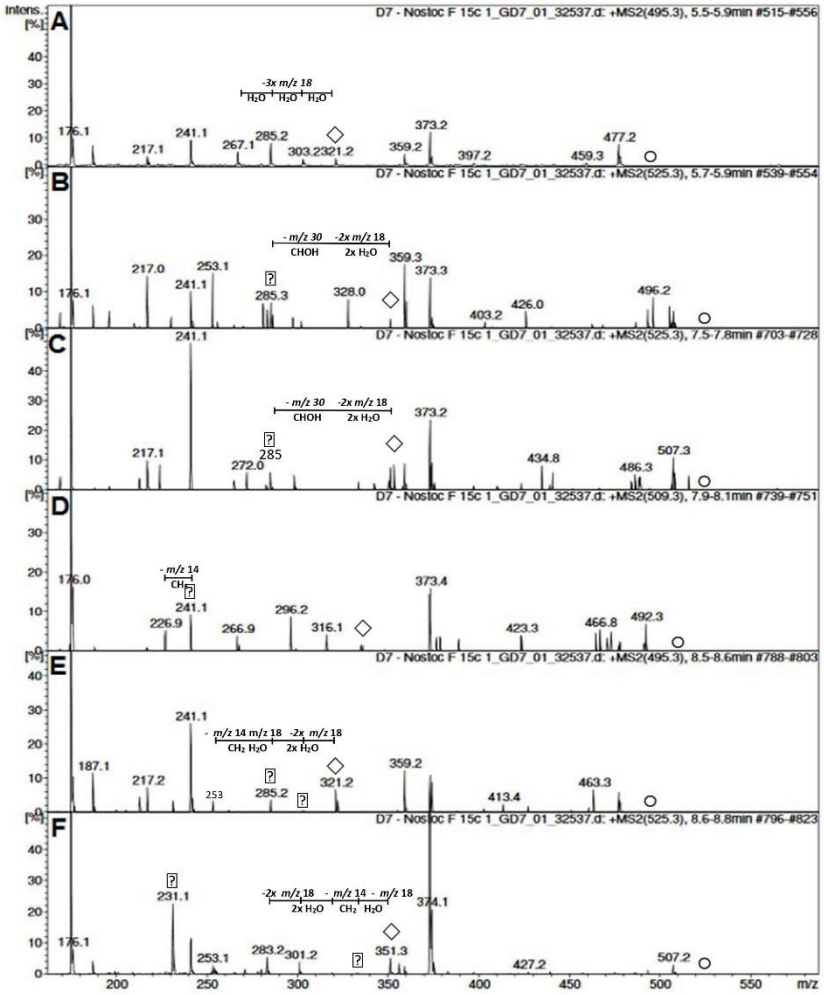

Fragmentation patterns, MS^2, (*m/z 100-600*) of unknown peaks from *Nostoc F15c* biomass. (**A**) 6-deoxy-talose: verified by standard, the fragments m/z 321, 303, 285 and 267 show the losses of water molecules. (**B**) 3-O-methyl-mannose: The fragment m/z 285 is indicative for the substitution at the C-3 position. (**C**) 3-O-methyl-galactose: the fragment m/z 285 is indicative for the substitution at the C-3 position. (**D**) Methyl-deoxy-hexose: the fragment m/z 267 is the *mono*-PMP fragment, which lost three water and a methyl. That is the equivalent

fragment to a m/z 283 of a methyl-hexose due to the deoxy function (- m/z 16). The absence of the fragment m/z 217 and m/z 231 means the deoxy function is on the C-2. The loss of the methyl group is accounted for by the fragments m/z 241 and m/z 227. Therefore, the fragment m/z 241 is a methylated fragment. The fragment m/z 267 instead of a fragment m/z 269 indicates the methyl group to be on C-4/6 instead of C-3. For the methyl group to be on C-6/3, one would expect to find a fragment m/z 225, therefore this sugar might be a 4-O-methyl-2-deoxy-hexose. (**E**) 3-O-methyl-xylose/arabinose: The presence of the fragment m/z 285 and the absence of the fragment m/z 283 are indicative for the substitution to be on C-3 position. The presence of the fragment m/z 217 excludes a substitution to be on C-2. (**F**) 2-O-methyl-galactose: the fragment m/z 231 is indicative for the substitution at the C-2 position.

Annex 2.7. Fragmentation pattern of identified peaks of *Nostoc linckia* biomass.

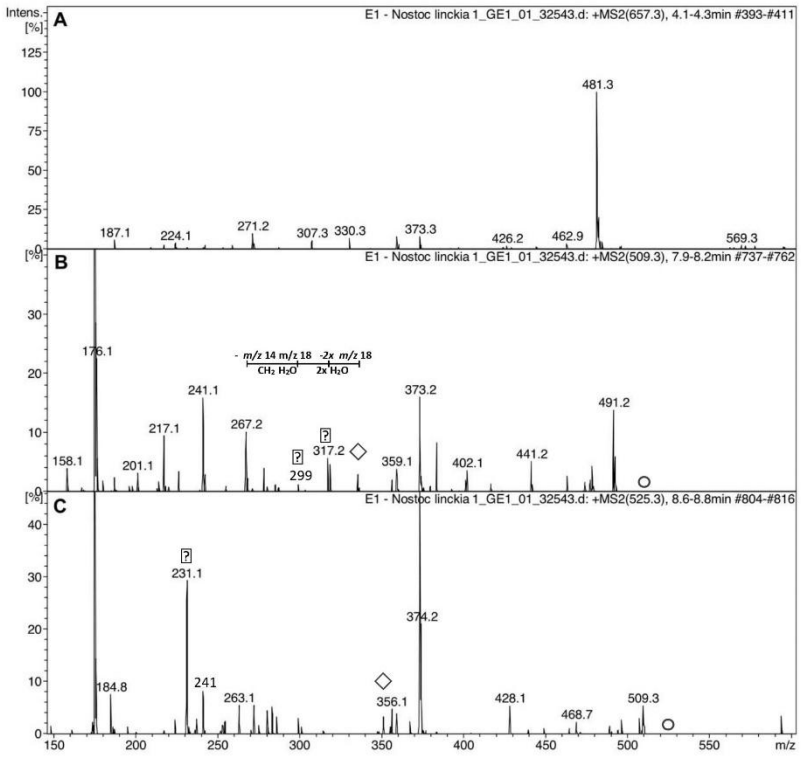

Fragmentation patterns, MS^2, (*m/z 100-600*) of unknown peaks from *Nostoc linckia* biomass. (**A**) Pentose hexuronic acid dimer: the fragment m/z 481 indicates the *bis*-PMP pentose fragment. The m/z difference to m/z 657 is 176 for a hexuronic acid and a water 18. (**B**) Methyl-deoxy-hexose: the fragments m/z 335 is the *mono*-PMP sugar and the m/z 317 indicates the loss of a water and m/z 267 the loss of three water and the methyl group. The fragment m/z 267 is also the equivalent to the m/z 283 in a neutral methyl-hexose. The fragment m/z 317 is an equivalent to the fragment m/z 333 in a neutral methyl-hexose, which allows to postulate the methyl group to be on C-6. The fragment m/z 217 allows to exclude the deoxy function to be on C-2. For the deoxy function to be on the C-3 position, one could expect to see a fragment at m/z 255. Therefore, this sugar might be a 6-O-methy-4-deoxy-hexose. (**C**) 2-O-methyl-galactose: the fragment m/z 231 is indicative for the substitution at the C-2 position.

Annex 3. The starch content in percent of biomass was calculated based on the absorbance of the glucose standard as followed:

$$Starch, \% = \Delta A * F * FV * \frac{FV}{0.1} * \frac{1}{1000} * \frac{100}{W} * \frac{162}{180} \quad (1)$$

ΔA = absorbance (reaction) read against the reagent blank 20:1 diluted GOPOD reagent.

F = $\frac{100\ (\mu g\ of\ D-glucose)}{absorbance\ for\ 100\ \mu g\ of\ glucose}$ (conversion from absorbance to µg)

FV = final volume (10 mL)

0.1 = volume of sample analysed

$\frac{1}{1000}$ = conversion from µg to mg

$\frac{100}{W}$ = factor to express starch as percentage of biomass

W = weight of biomass (mg)

$\frac{162}{180}$ = adjustment from free glucose to anhydro glucose in starch

Annex 4. Fatty acids detected as fatty acid methyl esters (FAMEs) after *in-situ* transesterification and GC-MS analysis. Values are reported in mg per g biomass for triplicates with standard deviation.

Fatty Acid		*Nostoc* sp. De1 [mg/g]	*Nostoc* sp. Cc3 [mg/g]	*Nostoc muscorum* I [mg/g]
palmitic acid	C16:0	16.0 ± 0.6	8.3 ± 0.3	13.3 ± 0.9
palmitoleic acid	C16:1 (9)	4.0 ± 0.2	5.1 ± 0.03	2.2 ± 0.3
stearic acid	C18:0	0.3 ± 0.2	<LOQ	0.3 ± 0.2
linoleic acid	C18:2 (9,12)	1.9 ± 0.1	1.4 ± 0.1	1.2 ± 0.2
α-linolenic acid	C18:3 (9,12,15)	5.1 ± 0.2	6.0 ± 0.1	3.3 ± 0.4
Total		27.3 ± 1.3	20.9 ± 0.5	20.4 ± 2.0

Annex 5. Quantitative analysis of starch content in three *Nostoc* strains by glucose detection with spectrophotometric assay (Megazyme Kit) and HT-PMP method. The enzymatic hydrolysis was done in both cases with the enzymes from the Megazyme kit. The control (corn starch) was corrected for moisture and non-starch solids.

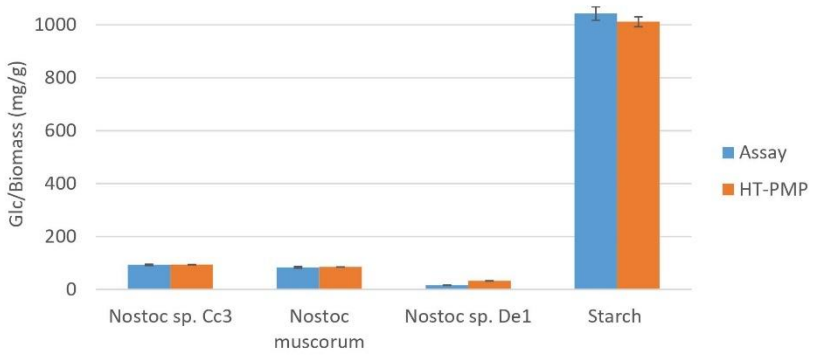

Annex 6. Comparison of percent biomass solubilization yields over 24 h and 48 h hydrolysis using industrial enzymes at 60 °C after 8 h protease pre-treatment at 30 °C on (**A**) *Nostoc* sp. De1 (**B**) *Nostoc* sp. Cc3 and (**C**) *Nostoc muscorum* I based on gravimetric determination of biomass residues. Data presented are the average of triplicates and one standard deviation. The enzymes used were Opti: OPTIMASH™ BG, Dist: DISTILLASE® CS, and Ferm: FERMGEN™.

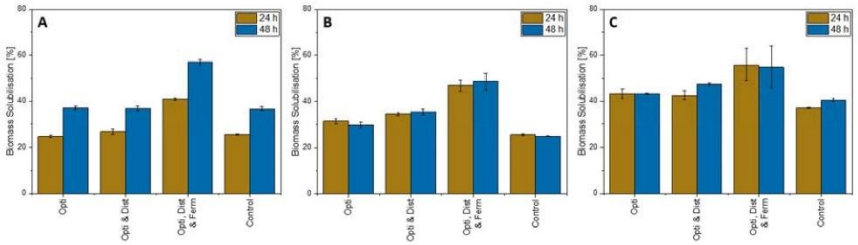

7.2. Supporting Information: The *Pichia pastoris* enzyme production platform: From combinatorial library screening to bench-top fermentation on residual cyanobacterial biomass

Supplementary Materials

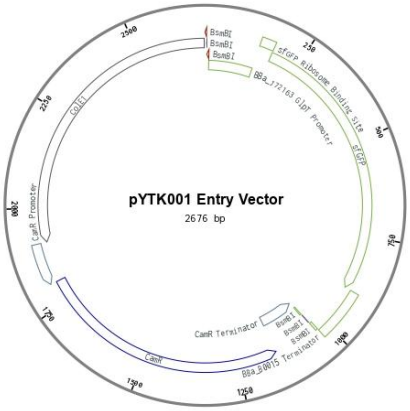

Fig. S1 Plasmid map of pYTK001 entry vector. Map generated with Benching. Plasmid and more information available at Addgene (Plasmid #65108)[1].

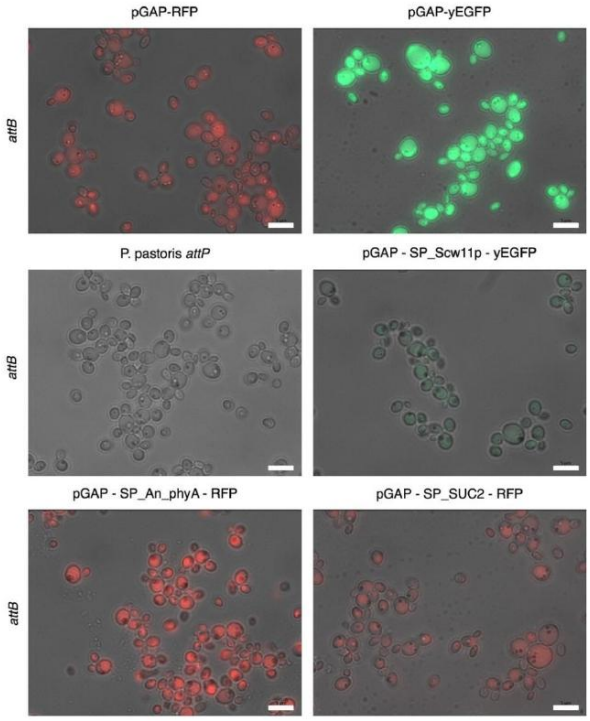

Fig. S2 Microscopical study. The wild-type *P. pastoris attB,* intracellular RFP or yEGP expression under the pGAP promoter and three secretion strains (pGAP–SP_SUC2–RFP, pGAP–SP_Scw11p–yEGFP and pGAP–SP_An_phyA–RFP) where analyzed. The expression constructs are all being genomically integrated and BMD was used for expression. The scale bar denotes 5 µm.

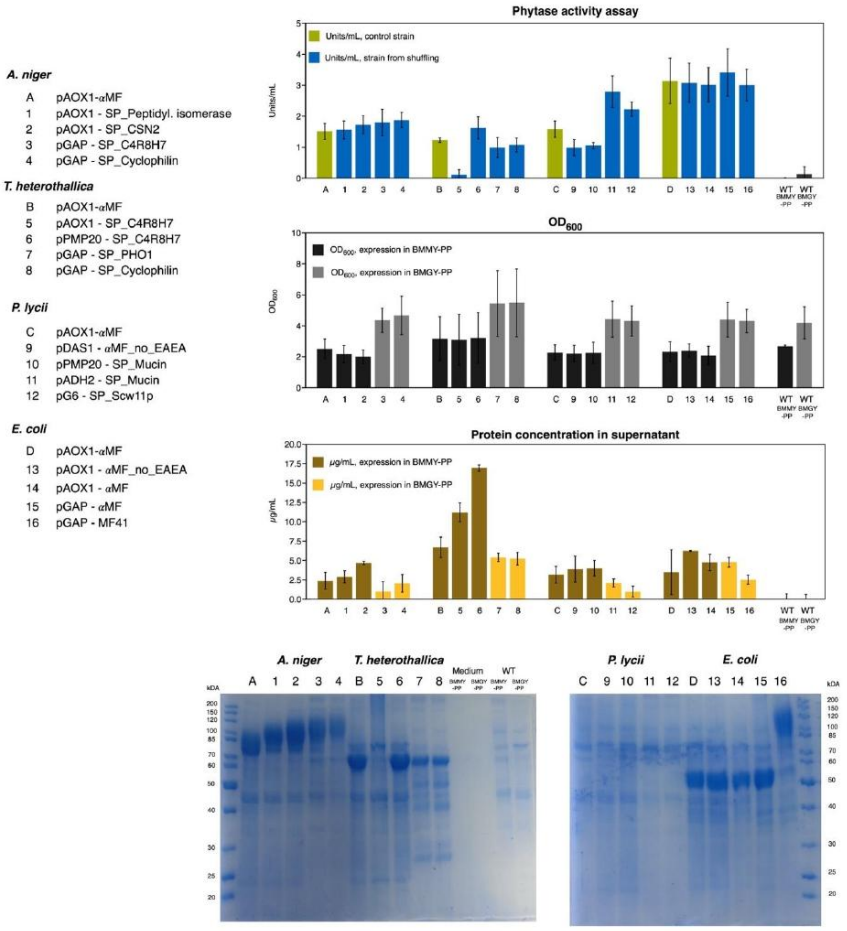

Fig. S3 Expression of phytases in shake flask format. The reference phytase expression strains each having pAOX1-αMF as well as the best two strains of each screening (induced and constitutive) were used for phytase expression in 75 mL medium in shake flasks. The shake flask expression was done twice and values presented are the average absorption of the both expressions measured in triplicate. The error bars denote ± 1 standard deviation. For each expression the phytase activity, OD_{600}, and the protein concentration (Bradford) of the supernatant were measured. The supernatant was concentrated 15 × for the SDS-PAGE analysis.

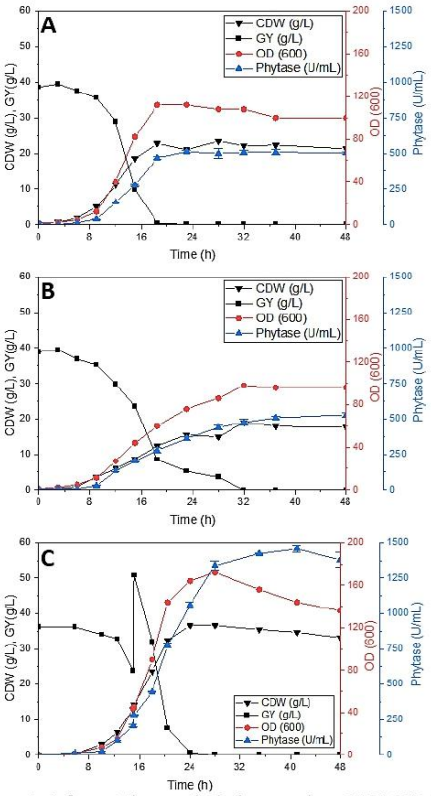

Fig. S4 Duplicates of *P. pastoris* fermentation constitutively expressing pGAP-MF41 AppA *E. coli* phytase in a 1 L system over 48 h. **A** shows the fermentation in 4 % (w/v) BMGY, **B** shows the fermentation in 20 % (v/v) *Nostoc sp. De1* biomass hydrolysate in *di*H_2O, the hydrolysate was produced enzymatically as described in the text and **C** shows a pulsed-batch fermentation in 4 % (w/v) BMGY. The glycerol pulse was done as described in the text. Phytase activity is shown as mean of analytical triplicates with one standard deviation.

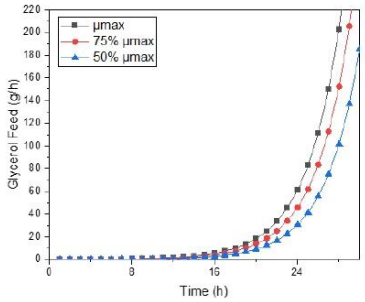

Figures	Value	Unit
μ_{max}	0.300	1/h
$Y_{x/s,max}$	0.59	g/g
m_s	0.005	g/g/L
V_0	0.5	L
x_0	0.08	g
W_{in}	0.45	g/g
F_o	0.0456	g/h

Fig. S5 Determined parameters from *P. pastoris* batch and pulsed batch fermentation for an exponential feed strategy using μ_{max}. The specific maintenance rate for the *P. pastoris* strain was obtained from literature[2]

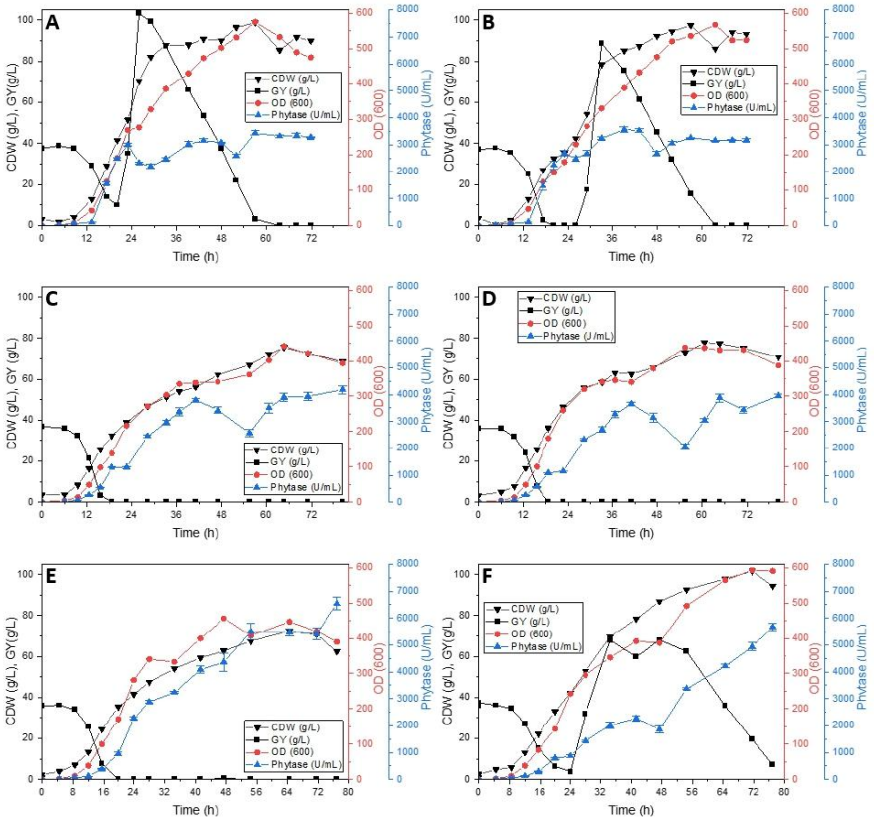

Fig. S6 Duplicates of fed-batch development of *P. pastoris* fermentation constitutively expressing pGAP – MF41 AppA *E. coli* phytase in a 1 L Dasgip system with 4 % (w/v) BMGY medium feeding 200 g glycerol. We started with an exponential feed based on the calculated μ_{max} from the batch and pulsed batch fermentations shown in **A** and a feed based on 75 % of μ_{max} in **B.** The following step was a DO-stat feeding strategy with 30 % dissolved oxygen limit shown in **C** and 20 % dissolved oxygen limit in **D**. The next step was optimizing the DO-cascade by lowering the max. stir rate from 1200 rpm to 900 rpm and increasing the aeration to its maximum around 1.2 ($m^3/(m^3 \cdot min)$) shown in **E** and a decrease of temperature from 30 °C to 25 °C in **F**.

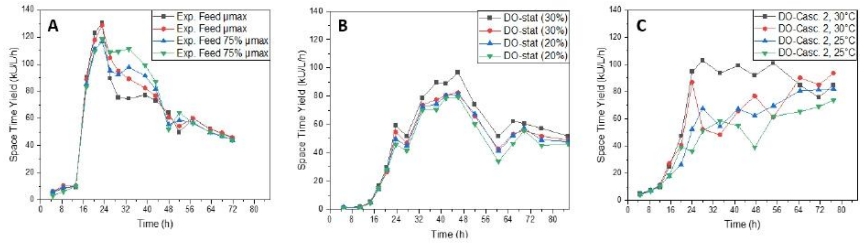

Fig. S7 Comparison of the space time yields of the fermentation optimization processes. **A**: exponential feeds with feeds of μ_{max} and 75 % μ_{max}. **B**: DO-*stat* controlled feeds with 30 % and 20 % dissolved oxygen threshold feed. **C:** Improved DO-*stat* with improved aeration cascade with 30 % dissolved oxygen threshold at 30 °C and 25 °C.

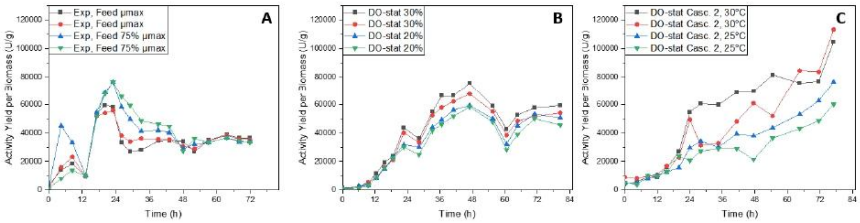

Fig. S8 Comparison of the activity yields per biomass for fed-batch fermentations. **A**: exponential feeds with feeds of μ_{max} and 75 % μ_{max}. **B**: Dissolved oxygen-*stat* controlled feeds with 30 % and 20 % dissolved oxygen threshold feed. **C**: Improved dissolved oxygen cascade with 30 % dissolved oxygen threshold at 30 °C and 25 °C.

Supplementary Notes

Note S1: Development of screening quantifying phytase activity

To allow measurements of phytase activity in higher throughput, an established colorimetric phosphate analysis was used measuring the released phosphate[3]. Positive controls were made (Supplementary Excel Table – Phytase Strains - Pre-screening) for each phytase as previously described in the literature but using the parts of the PTK/YTK[4–7]. Commonly used expression media could not be applied due to their high phosphate content. Therefore, BMMY-PP (buffered complex methanol medium without phosphate buffer) was used for the expressing and expression supernatant was subjected to and gel-filtration chromatography for the removal of small molecules. After further dilution with water, the phytase activity was measured using the colourimetric phosphomolybdate analysis method from Bae *et al.*[8] which was adapted to suit the 96-well format.

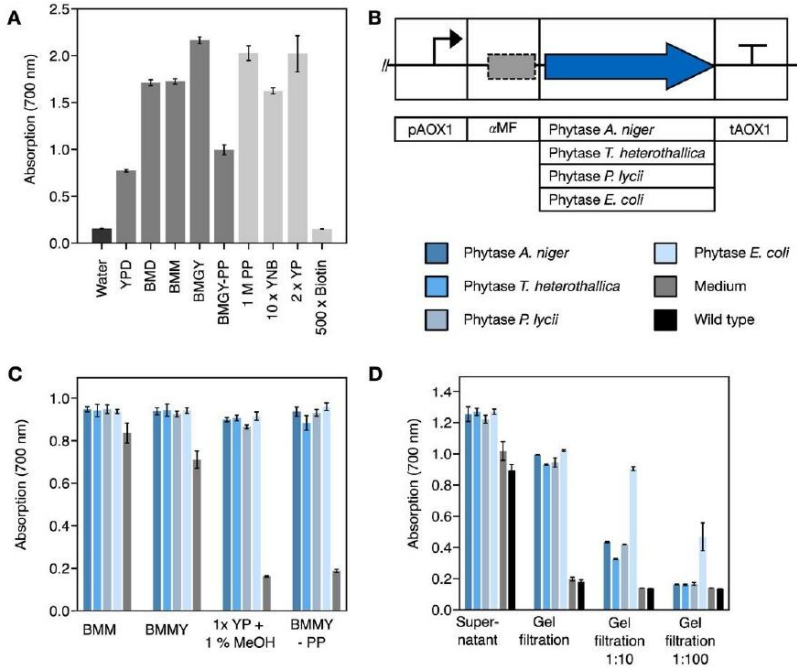

Figure Note S1: Colorimetric phosphate analysis of media and phytase expressions. **A** Widely used media and their components were evaluated for their initial phosphate content. **B** *P. pastoris* controls expressing each phytase were made and **C** the enzyme activity was measured after gel-filtration of the supernatant. **D** Phytase expression in BMMG-PP with gel-filtration of the supernatant and determination of the phytase activity was performed and different dilutions of the gel-filtration filtrate were assayed. Bars represent the mean absorption from the phytase assay of triplicates measured at 700 nm. Error bars denote ± 1 standard deviation.

Note S2: Z-factor determination for phytase screening

The Z-factor was determined, to validate the suitability of the screening and determine the quality of the assay. The Z-factor was introduced by Zhang *et al.* as a simple statistical parameter for the evaluation of assays[9] and is ever since widely used[10]. The screening procedure was performed for one plate of wild type (*i.e.* control) and one plate of the *P. pastoris* strain pUO_pL666 expressing the *E. coli* phytase (*i.e.* sample), **Figure Note S2**. The Z-factor can be calculated according to the formula below (SD standard deviation). The determined Z-factor of 0.8268 stands for an excellent screening with a high degree of confidence and overall, a high-quality screening that can be applied for the targeted secretion libraries.[9]

$$Z = 1 - \frac{3 \cdot \text{SD of sample} + 3 \cdot \text{SD of control}}{|\text{mean of sample} - \text{mean of control}|}$$

$$Z = 1 - \frac{3 \cdot 0.0347 + 3 \cdot 0.0017}{|0.7489 - 0.1186|}$$

$$Z = 0.8268$$

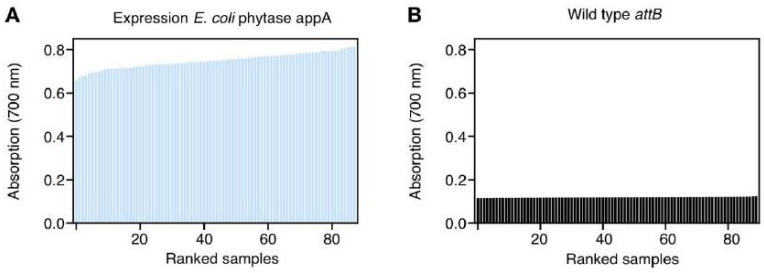

Figure Note S2 Wild type landscape to determine Z-factor. **A** Expression of positive control and **B** the wild type to determine quality of assay. Bars represent absorption at 700 nm after the phytase assay.

Note S3: Phytase library coverage calculation

To confirm sufficient statistical evidence for the phytase shuffling, the expected coverage, *i.e.* the expected percentage of all possible variants that are represented in the library, was calculated according to the formula below. The calculation relies on the assumption that the resulting randomised expression plasmids generated via Golden Gate shuffling are all likely with equal probability. For each constitutive phytase library, the number of equiprobable variants n = 100 and for the inducted phytase library n = 60. After *E. coli* transformation, the number of *E. coli* colonies used to prepare the plasmid library were counted and the expected coverage Yi within *E. coli* was calculated. More than 950 or 400 colonies have been used for the constitutive or induced libraries, respectively, resulting in $Y_i(E.\ coli)$ of at least 99.88 %. After transformation of *P. pastoris* with the respective plasmid library, the library size x was defined as 364 colonies were picked for each constitutive screening and 182 for each induced screening. The expected *P. pastoris* library coverage, as well as the final expected coverage could be calculated[11] . For the constitutive library, the expected coverage of all 100 possible combinations represented in the library is > 97 % and for the induced library with 60 possible combinations the expected coverage is > 95 %.

$$Y_i = 1 - (1 - \left(\frac{1}{n}\right))^x$$

$$Y_i(\text{final}) = Y_i(E.coli) \cdot Y_i(P.pastoris)$$

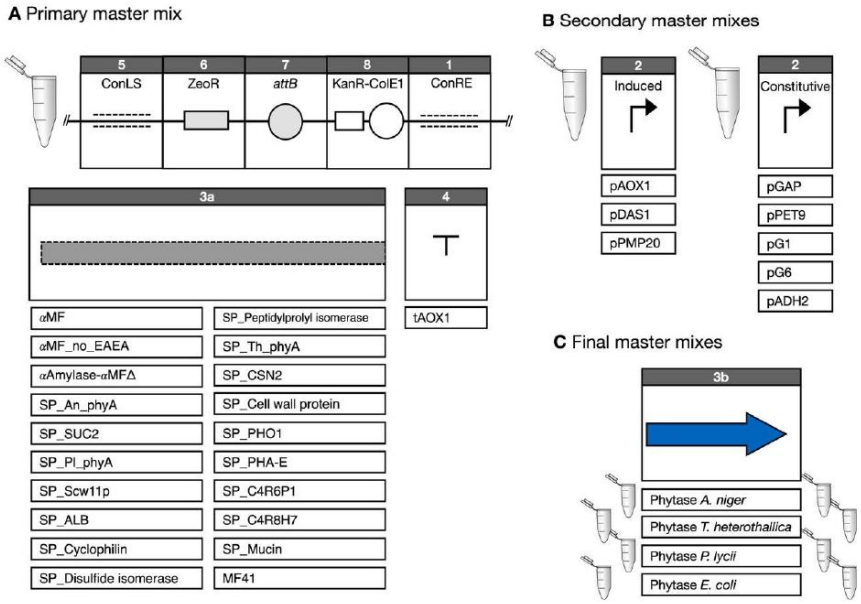

Figure Note S3. Parts for Golden Gate shuffling of phytase library.

Table S1 Predicted endogenous signal peptides for protein secretion

Name	**Description of the coding region**	**Locus in *P. pastoris* genome**	**Amino acid sequence** (N-region **H-region** C-region)
SP_Cyclophilin	Peptidyl-prolyl cis-trans isomerase (cyclophilin) of the endoplasmic reticulum[12]	PAS_chr1-1_0267	MKLLN**FLLSFVTLFGLL**SGSVFA
SP_Disulfide isomerase	Protein disulfide isomerase, multifunctional protein resident in the endoplasmic reticulum lumen[12]	PAS_chr1-1_0160	MK**ILSALLLLF**TLAFA
SP_Peptidylprolyl isomerase	Hypothetical protein (Peptidylprolyl isomerase)[12]	PAS_c131_0001	MKVSTTK**FLAVFLLV**RLVCA
SP_Cell wall protein	Cell wall protein that functions in the transfer of chitin to beta(1-6)glucan[12]	PAS_chr1-1_0293	MRP**VLSLLLLLA**SSVLA
SP_C4R6P1	Hypothetical protein (C4R6P1)[12]	PAS_chr4_0040	MW**SLFISGLLIFY**PLVLG
SP_C4R8H7	Hypothetical protein (C4R8H7)[12]	PAS_chr4_0643	MS**TLTLLAVLLSLQ**NSALA
SP_Mucin	Mucin family member[12]	PAS_chr1-3_0276	MINLNS**FLILTVTLL**SPALA LPKNVLEEQQAKDDLAKR
SP_PHO1	Acid phosphatase PHO1[13]	PPU28658	MFSPI**LSLEIILALATL**QSVFA
SP_Scw11p	Cell wall protein with similarity to glucanases[14 12]	PAS_chr2-1_0052	MLS**TILNIFILLLFI**QASLQ

Table S4 Phytase Information

Taxa	**Fungi**			**Bacteria**
	Ascomycetes	Ascomycetes	Basidiomycetes	Gram-negative
Microorganism	A. niger	*T. heterothallica*	*P. lycii*	*E. coli*
NCBI accession number	CAA78904	KF535924	CAC48195	M58708
Molecular function	3-phytase activity	3-phytase activity	4-phytase activity	4-phytase activity
Gene	phyA	phyA	phyA	appA
bp	2665, 1 intron in tag	1521,1 intron in tag	1568	1296
Amino acids (signal peptide + chain)	467 (23+444)	487 (21+466)	439 (29+410)	432 (22+410)
N-linked glycosylation	10	4	10	3

Table S2 Predicted exogenous signal peptides for protein secretion

Name	Description of the coding region	Locus	Amino acid sequence (N-region H-region C-region)
αMF	Alpha mating factor[15]	*S. cerevisiae* MFAL1_YEAST	M**RFPSIFTAVLFAASS**ALAAPVNTTTEDETAQIPAEAVIGYSDLEG DFDVAVLPFSNSTNNGLLFINTTIASIAAKEEGVSLEKREAEA
αMF_no_EAEA	Alpha mating factor no EAEA[15]	*S. cerevisiae*, Synthetic	M**RFPSIFTAVLFAASS**ALAAPVNTTTEDETAQIPAEAVIGYSDLEG DFDVAVLPFSNSTNNGLLFINTTIASIAAKEEGVSLEKR
SP_An_phyA	3-phytase A	*A. niger* PHYA_ASPNG	MG**VSAVLLPLYLL**SGVTSG(LAVP)
SP_Pl_phyA	Phytase	*P.lycii* Q96VH9_9HOMO	MVSSAFAPS**ILLSLMSSLALSTQFSFVAA**
SP_Th_phyA	Histidine acid phosphatase phytase	*T.heterothallica* V5M269_THIHE	MTG**LGVMVVMVGFLAI**ASLQS
SP_Aae_UPO	Aromatic peroxygenas[16]	*A. aegerita* APO1_AGRAE	MKY**FPLFPTLVFAA**RVVAFPAYASLAGLSQQELDAII PTLEAR
SP_Aae_UPOeng	Aromatic peroxygenase tag engineered[16]	*A. aegerita*, synthetic	MKY**FPLFPTLVYAV**GVVAFPDYASLAGLSQQELDAII PTLEAR
SP_SUC2	Invertase 2[17]	*S. cerevisiae* INV2_YEAST	ML**LQAFLFLLAGFA**AKISA
SP_ALB	Serum albumin[18]	*H. sapiens* ALBU_HUMAN	MK**WVTFISLLFLF**SSAYS
SP_CSN2	Beta-casein[19]	*B. taurus* CASB_BOVIN	MK**VLILACLV**ALALA
SP_PHA-E	Phytohaemag-glutinin [20]	*P. vulgaris* I0J8I4_PHAVU	MASSN**LLSLALFLVLLTHANS**
MF41	Synthetic signal peptide MF41[7]	Synthetic	MAIPR**FPSIFIAVLFAASSALA**APVNTTTEDETAQIPAEAVIGYSDLEG DFDVAVLPFSNSTNNGLLEEAEAEAEPKFINTTIASIAAKEEGVSLE

Table S3 Predicted signal peptides for protein secretion. The likelihood for secretion is given as D-score (discrimination score) determined using SignalP4.1, which looks at the possible cleavage site and the discrimination of different segments to predict signal peptides. Values of D-score >0.7 implies that a peptide is very likely a secretory signal peptide[12]. The secretion efficiency S_e ($S_e = S_S/S_T$) was calculated from the secretion of RFP and yEGFP, genomically integrated, and regulated by the strong constitutive pGAP promoter.

	D-score RFP prediction P4.1	**D-score yEGFP prediction P4.1**	**S*e* RFP and pGAP**	**S*e* RFP and pGAP**
None	-	-	0.00	0.04
SP_Cyclophilin	0.87	0.893	0.89	0.39
SP_Disulfide isomerase	0.862	0.908	0.84	0.42
SP_Peptidylprolyl isomerase	0.858	0.893	0.76	0.49
SP_Cell wall protein	0.867	0.904	0.77	0.48
SP_C4R6P1	0.904	0.912	0.75	0.23
SP_C4R8H7	0.877	0.895	0.07	0.18
SP_Mucin	0.866	0.868	0.22	0.31
SP_PHO1	0.795	0.829	0.11	0.57
SP_Scw11p	0.797	0.854	0.72	0.54
αMF_no_EAEA	0.884	0.884	0.97	0.78
αMF	0.884	0.884	1.84	0.77
SP_An_phyA	0.815	0.807	0.01	0.06
SP_Pl_phyA	0.739	0.743	0.05	0.09
SP_Th_phyA	0.746	0.653	0.72	0.48
SP_Aae_UPO	0.56	0.568	0.78	0.58
SP_Aae_UPOeng	0.56	0.568	0.65	0.36
SP_SUC2	0.79	0.837	0.61	0.10
SP_ALB	0.817	0.868	0.87	0.59
SP_CSN2	0.838	0.899	0.71	0.57
SP_PHA-E	0.837	0.894	0.25	0.24
MF41	0.9	0.9	0.89	16.33

Method S1: Microscopy

Screening for expression of RFP and yEGFP was performed as described by Qin *et al.*, with modifications[21]. A 900 µL 0.2 % BMD (100 mM potassium phosphate (pH 6.0), 1.34 (w/v) % yeast nitrogen base, 4 × 10−5% (w/v) biotin, 0.2% glucose) pre-culture was inoculated from a glycerol stock master plate. The expression-culture in 1 % BMD (100 mM potassium phosphate (pH 6.0), 1.34 (w/v) % yeast nitrogen base, 4 × 10−5% (w/v) biotin, 1 % (w/v) glucose) or 1 % BMM (100 mM potassium phosphate (pH 6.0), 1.34 (w/v) % yeast nitrogen base, 4 × 10−5% (w/v) biotin, 1% methanol) was inoculated with 30 µL of the pre-culture and incubated. Measurements were performed after 48 hours.

Method S2: SDS-PAGE

To separate proteins by their size, gel electrophoresis was performed with separating gel casted with 12% (v/v) and stacking gel casted with 5% (v/v) acrylamide. Protein samples were mixed with 5x loading buffer (50% (v/v) glycerol, 12.5% (v/v) β-mercaptoethanol, 7.5% (w/v) SDS, 0.25 g L^{-1} bromophenol blue) and heated at 95 °C for 10 min. 1x SDS electrophoresis buffer (0.1% (w/v) SDS, 25 mM Tris, 192 mM glycine) was added to the Mini-PROTEAN® Tetra Vertical Electrophoresis Cell, samples were loaded and the gels were run for 45 min at 40 mA. To estimate protein size, the PageRuler Prestained Protein Ladder #26616 (Thermo Fisher Scientific, Waltham, MA, USA) was used. Upon completion of the electrophoretic run, the gel was rinsed with water, stained with Coomassie-staining solution (0.2% (w/v) Coomassie brilliant blue G250) and discolored with water.

Method S3: Feeding strategies & process evaluation

In order to evaluate the fermentations, a feeding strategy was developed along with an exponential feed and several key parameters for growth and product kinetics were calculated as described by Looser *et al.*[22]. The substrate utilization rate q_s was calculated using Eq. (1).

$$q_S = \frac{(s_n - s_{n\_1})}{(x_n - x_{n\_1}) * (t_n - t_{n\_1})} \quad (1)$$

where *s* is substrate concentration, *x* is biomass concentration and *t* fermentation time. The specific growth rate $\mu\ (t)$ was calculated using Eq.(2) and the activity formation rate $q_{A/x}$ was calculated using Eq. (3).

$$\mu\ (t) = \frac{\ln(x) - \ln(x_o)}{(t - t_o)} \quad (2)$$

$$q_{A/x} = \frac{(A_n - A_{n\_1})}{(x_n - x_{n\_1}) * (t_n - t_{n\_1})} \quad (3)$$

where *A* is the activity in Units per mL. Further, the specific productivity as relationship between product formation and specific growth rate $q_A(\mu)$ was calculated using Eq. (4).

$$q_A\ (\mu) = \mu\ *\ q_{A/x} \quad (4)$$

Two substrate feeding strategies, standard exponential feed and DO-*stat* feed were carried out in fed-batch fermentation. 200 g of glycerol as carbon source was additionally added for all fermentations. For the exponential feed, the medium feed profiles were calculated according to Eq. (5).

$$F(t) = F_o * e^{\mu * t} \quad (5)$$

where F_o is the initial feed rate, which can be calculated using Eq. (6).

$$F_o = \left(\frac{\mu}{Y_{x/s,max}} + m_s\right) * \frac{V_o * x_o}{w_{in}} \quad (6)$$

where $Y_{x/s,max}$ is the maximum yield (biomass/substrate), m_s is the specific maintenance rate, V_o is the initial working volume, and w_{in} is the mass fraction of substrate in the feed solution. Finally, the space-time yield (*STY*) was calculated using Eq. (7).

$$STY = \frac{A_n}{t_n} \quad (7)$$

Table Cloning S1A: Part Plasmids - Newly developed in this study

Plasmid	Part Type	Part Description	bp part	Donor	*E. coli* Antibiotic Marker	Backbone	Reference	Description	
pPTK022	2	pPET9	996	ADP, ATP carrier	Chloramphenicol	pYTK001	Stadlmayr et al. 2010	PCR product from genomic DNA (primer FW-2-pPET9, REV-2-pPET9, FW-Fix-pPET9,REV-Fix-pPET9)	pUO-pp-353
pPTK023	2	pG1	965	Hypothetical protein (PAS_chr1-3_0011), Promoter of the high affinity glucose transport	Chloramphenicol	pYTK001	Prielhofer et al. 2013	PCR product from genomic DNA (primer FW-2-pG1, REV-2-pG1)	pUO-pp-354
pPTK024	2	pG6	1000	Hypothetical protein (PAS_chr2-1_0853)	Chloramphenicol	pYTK001	Prielhofer et al. 2013	PCR product from genomic DNA (primer FW-2-pG6, REV-Fix-pG6) and gBlock	pUO-pp-355
pPTK025	2	pADH2	1212	Methylformate synthase, alcohol dehydrogenase	Chloramphenicol	pYTK001	Vogl et al., 2016	PCR product from genomic DNA (primer FW-2-pADH2, REV-2-pADH2, FW-Fix-pADH2, REV-Fix-pADH2)	pUO-pp-356
pPTK026	2	pDAS1	798	Dihydroxyacetone synthase, isoenzymes	Chloramphenicol	pYTK001	Vogl et al., 2016	PCR product from genomic DNA (primer FW-2-pDAS1, REV-2-pDAS1, FW-Fix-pDAS1, REV-Fix-pDAS1)	pUO-pp-357
pPTK027	2	pPMP20	478	Peroxisomal glutathione peroxidase	Chloramphenicol	pYTK001	Vogl et al., 2016	PCR product from genomic DNA (primer FW-2-pPMP20,	pUO-pp-358

								REV-2-pPMP20)	
pPTK028	3a	SP_Disulfide isomerase	48	Protein disulfide isomerase	Chloramphenicol	pYTK001	A. Massahi and P. Çalik, 2015		pUO-pp-360
pPTK029	3a	SP_C4R6P1	54	Hypothetical protein (C4R6P1)	Chloramphenicol	pYTK001	A. Massahi and P. Çalik, 2015		pUO-pp-361
pPTK030	3a	SP_Cell wall protein	51	Cell wall protein	Chloramphenicol	TWIST vector	A. Massahi and P. Çalik, 2015		pUO-pp-362
pPTK031	3a	SP_Cyclophillin	69	Peptidyl-prolyl cis-trans isomerase	Chloramphenicol	TWIST vector	A. Massahi and P. Çalik, 2015		pUO-pp-363
pPTK032	3a	SP_CSN2	45	Beta-casein	Chloramphenicol	TWIST vector	He et al. 2012		pUO-pp-364
pPTK033	3a	SP_PHA-E	63	Phytohaemag-glutinin	Chloramphenicol	pYTK001	R. J. M. Raemaekers et al. 1999		pUO-pp-365
pPTK034	3a	MF41	288	Synthetic signal peptide MF41	Chloramphenicol	TWIST vector	A.-S. Xiong et al. 2006		pUO-pp-366
pPTK035	3a	SP_C4R8H7	57	Hypothetical protein (C4R8H7)	Chloramphenicol	TWIST vector	A. Massahi and P. Çalik, 2015		pUO-pp-367
pPTK036	3a	SP_Peptidylprolyl isomerase	60	Hypothetical protein (Peptidylprolyl isomerase)	Chloramphenicol	pYTK001	A. Massahi and P. Çalik, 2015		pUO-pp-368
pPTK037	3a	SP_ALB	54	Serum albumin	Chloramphenicol	pYTK001	K. Kobayashi et al. 2000		pUO-pp-369
pPTK038	3a	SP_Scw11p	60	Cell wall protein	Chloramphenicol	pYTK001	S. Liang et al. 2013		pUO-pp-370
pPTK039	3a	SP_Mucin	114	Mucin family member	Chloramphenicol	pYTK001	A. Massahi and P. Çalik, 2015		pUO-pp-371
pPTK040	3a	SP_An_phyA	57	*A. niger* 3-phytase A	Chloramphenicol	pYTK001	NYC		pUO-pp-372
pPTK041	3a	SP_Pl_phyA	87	*P. lycii* phytase	Chloramphenicol	TWIST vector	NYC		pUO-pp-373
pPTK042	3a	SP_Th_phyA	63	*T. heterothallica* phytase	Chloramphenicol	TWIST vector	NYC		pUO-pp-374
pPTK043	3a	SP_Aae_UPO	129	Aromatic peroxygenase	Chloramphenicol	TWIST vector	P. Molina-Espeja et al. 2014		pUO-pp-375
pPTK044	3a	SP_Aae_UPOeng	129	Aromatic peroxygenase tag engineered	Chloramphenicol	pYTK001	P. Molina-Espeja et al. 2014		pUO-pp-376
pPTK045	3a	SP_PHO1	67	Acid phosphatase PHO1	Chloramphenicol	pYTK001	H. Heinmo et al. 1997		pUO-pp-377
pPTK046	3a	SP_Suc2	57	Invertase 2	Chloramphenicol	pYTK001	J.-G. Berrin et al. 2000		pUO-pp-378
pPTK047	3b	An_phyA	1332	*A. niger* phytase, *P. pastoris* codon optimised	Chloramphenicol				pUO-pp-380
pPTK048	3b	Th_phyA	1398	*T.heterothallica* phytase, *P. pastoris* codon optimised	Chloramphenicol				pUO-pp-381
pPTK049	3b	Ply_phyA	1230	*P.lycii* phytase, *P. pastoris* codon optimised	Chloramphenicol				pUO-pp-382
pPTK050	3b	Ec_appA	1230	*E. coli* appA, *P. pastoris* codon optimised	Chloramphenicol				pUO-pp-383
pPTK051	Backbone	Backbone_sfGFPdrop	3301	ConLS-sfGFPdrop-ConE-ZeoR-attB-KanaR	Kanamycine				pUO-pp-501

Table Cloning S1B: Part Plasmids - PTK parted used in this study

Addgene plasmid	Part Type	Part Description	bp part	Donor	*E. coli* Antibiotic Marker	Backbone	Available From	Name this study
pPTK001	2	pAOX1	939	Alcohol oxidase 1	Chloramphenicol	pYTK001	Obst et al. 2017	pUO-pp-303-2
pPTK002	2	pGAP	477	Glyceraldehyde-3-phosphate dehydrogenase	Chloramphenicol	pYTK001	Obst et al. 2017	pUO-pp-302-2
pPTK003	2	pENO1	1045	Enolase 1, BsaI and BsmBI site removed	Chloramphenicol	pYTK001	Obst et al. 2017	pUO-pp-321-2
pPTK004	2	pTPI1	603	Triose phosphate isomerase 1	Chloramphenicol	pYTK001	Obst et al. 2017	pUO-pp-322-2
pPTK005	3a	aMF	267	α-mating factor	Chloramphenicol	pYTK001	Obst et al. 2017	pUO-pp-336-3a
pPTK006	3a	aMF no EAEA	255	α-mating factor no EAEA	Chloramphenicol	pYTK001	Obst et al. 2017	pUO-pp-337-3a
pPTK015	3	yEGFP_Intra	763	Green fluorescent protein	Chloramphenicol	pYTK001	Obst et al. 2017	pUO-pp-324-3
pPTK016	3	RFP_Intra	784	Red fluorescent protein, BsaI removed	Chloramphenicol	pYTK001	Obst et al. 2017	pUO-pp-326-3
pPTK017	3b	yEGFP_Sec	763	Green fluorescent protein	Chloramphenicol	pYTK001	Obst et al. 2017	pUO-pp-325-3b
pPTK018	3b	RFP_Sec	784	Red fluorescent protein, BsaI removed	Chloramphenicol	pYTK001	Obst et al. 2017	pUO-pp-327-3b
pPTK019	4	tAOX1	247	Alcohol oxidase 1	Chloramphenicol	pYTK001	Obst et al. 2017	pUO-pp-308-4
pPTK020	7	attB	182	BxbI recognition site, BsaI site removed	Chloramphenicol	pYTK001	Obst et al. 2017	pUO-pp-301-7

Table Cloning S1C: YTK parted used and characterized for *P. pastoris* in this study

Addgene plasmid	Part Type	Part Description	bp part	*E. coli* Antibiotic Marker	Backbone	Available From
pYTK001	entry vector	Part Plasmid Entry Vector		Chloramphenicol		Lee et al. 2015
pYTK002	1	ConLS	143	Chloramphenicol	pYTK001	Lee et al. 2015
pYTK009	2	*pTDH3*	680	Chloramphenicol	pYTK001	Lee et al. 2015
pYTK010	2	*pCCW12*	700	Chloramphenicol	pYTK001	Lee et al. 2015
pYTK011	2	*pPGK1*	*700*	Chloramphenicol	pYTK001	Lee et al. 2015
pYTK012	2	*pHHF2*	700	Chloramphenicol	pYTK001	Lee et al. 2015
pYTK013	2	*pTEF1*	*700*	Chloramphenicol	pYTK001	Lee et al. 2015
pYTK014	2	*pTEF2*	700	Chloramphenicol	pYTK001	Lee et al. 2015
pYTK015	2	*pHHF1*	*700*	Chloramphenicol	pYTK001	Lee et al. 2015
pYTK016	2	*pHTB2*	699	Chloramphenicol	pYTK001	Lee et al. 2015
pYTK017	2	*pRPL18B*	700	Chloramphenicol	pYTK001	Lee et al. 2015
pYTK047	234r	GFP dropout	717	Chloramphenicol	pYTK001	Lee et al. 2015
pYTK051	4	*tENO1*	225	Chloramphenicol	pYTK001	Lee et al. 2015
pYTK052	4	*tSSA1*	225	Chloramphenicol	pYTK001	Lee et al. 2015
pYTK053	4	*tADH1*	225	Chloramphenicol	pYTK001	Lee et al. 2015
pYTK054	4	*tPGK1*	*225*	Chloramphenicol	pYTK001	Lee et al. 2015
pYTK055	4	*tENO2*	225	Chloramphenicol	pYTK001	Lee et al. 2015
pYTK056	4	*tTDH1*	224	Chloramphenicol	pYTK001	Lee et al. 2015
pYTK072	5	ConRE	143	Chloramphenicol	pYTK001	Lee et al. 2015
pYTK080	6	ZeocinR	954	Chloramphenicol	pYTK001	Lee et al. 2015
pYTK084	8	KanR-ColE1	1755	Kanamycin	pYTK001	Lee et al. 2015

Table Cloning S2: RFP and GFP Strains. Light grey shaded indicates strains prepared by directly using the Golden Gate reaction for the *P. pastoris* transformation (pUO_pL730 - pUO_pL771).

Part	Type 1	Type 2	Type 3		Type 4	Type 5	Type 6	Type 7	Type 8
Description	Linker	Promoter	Tag	GOI	Terminator	Linker	Yeast R	Yeast Origin	EC R and Origin
pUO_pL621	ConLS	pTDH3	RFP		tAOX1	ConRE	ZeoR	BxbI	KanR-ColE1
pUO_pL622		pCCW12							
pUO_pL623		pHHF2							
pUO_pL624		pTEF2							
pUO_pL625		pHHF1							
pUO_pL626		pHTB2							
pUO_pL627		pRPL18B							
pUO_pL628	ConLS	pTDH3	GFP		tAOX1	ConRE	ZeoR	BxbI	KanR-ColE1
pUO_pL629		pCCW12							
pUO_pL630		pHHF2							
pUO_pL631		pTEF2							
pUO_pL632		pHHF1							
pUO_pL633		pHTB2							
pUO_pL634		pRPL18B							
pUO_pL680	ConLS	pPET9	RFP		tAOX1	ConRE	ZeoR	BxbI	KanR-ColE1
pUO_pL681		pG1							
pUO_pL682		pG6							
pUO_pL683		pADH2							
pUO_pL684		pDAS1							
pUO_pL685		pPMP20							
pUO_pL686	ConLS	pPET9	GFP		tAOX1	ConRE	ZeoR	BxbI	KanR-ColE1
pUO_pL687		pG1							
pUO_pL688		pG6							
pUO_pL689		pADH2							
pUO_pL690		pDAS1							
pUO_pL691		pPMP20							
pUO_pL621	ConLS	pTDH3	RFP		tAOX1	ConRE	ZeoR	BxbI	KanR-ColE1
pUO_pL622		pCCW12							
pUO_pL623		pHHF2							
pUO_pL624		pTEF2							
pUO_pL625		pHHF1							
pUO_pL626		pHTB2							
pUO_pL627		pRPL18B							
pUO_pL628	ConLS	pTDH3	GFP		tAOX1	ConRE	ZeoR	BxbI	KanR-ColE1
pUO_pL629		pCCW12							
pUO_pL630		pHHF2							
pUO_pL631		pTEF2							
pUO_pL632		pHHF1							
pUO_pL633		pHTB2							
pUO_pL634		pRPL18B							
pUO_pL635	ConLS	pGAP	RFP		tENO1	ConRE	ZeoR	BxbI	KanR-ColE1
pUO_pL636					tSSA1				
pUO_pL637					tADH1				
pUO_pL638					tPGK1				
pUO_pL639					tENO2				
pUO_pL640					tTDH1				
pUO_pL641	ConLS	pGAP	GFP		tENO1	ConRE	ZeoR	BxbI	KanR-ColE1
pUO_pL642					tSSA1				
pUO_pL643					tADH1				
pUO_pL644					tPGK1				
pUO_pL645					tENO2				
pUO_pL646					tTDH1				
pUO_pL730	ConLS	pAOX1	RFP		tENO1	ConRE	ZeoR	BxbI	KanR-ColE1
pUO_pL731					tSSA1				
pUO_pL732					tADH1				
pUO_pL733					tPGK1				
pUO_pL734					tENO2				
pUO_pL735					tTDH1				
pUO_pL736	ConLS	pDAS1	RFP		tENO1	ConRE	ZeoR	BxbI	KanR-ColE1
pUO_pL737					tSSA1				
pUO_pL738					tADH1				
pUO_pL739					tPGK1				
pUO_pL740					tENO2				
pUO_pL741					tTDH1				
pUO_pL742	ConLS	pPMP20	RFP		tENO1	ConRE	ZeoR	BxbI	KanR-ColE1
pUO_pL743					tSSA1				
pUO_pL744					tADH1				
pUO_pL745					tPGK1				
pUO_pL746					tENO2				
pUO_pL747					tTDH1				
pUO_pL748	ConLS	pPET9	RFP		tENO1	ConRE	ZeoR	BxbI	KanR-ColE1
pUO_pL749					tSSA1				
pUO_pL750					tADH1				

pUO_pL751				tPGK1				
pUO_pL752				tENO2				
pUO_pL753				tTDH1				
pUO_pL754	ConLS	pG1	RFP	tENO1	ConRE	ZeoR	BxbI	KanR-ColE1
pUO_pL755				tSSA1				
pUO_pL756				tADH1				
pUO_pL757				tPGK1				
pUO_pL758				tENO2				
pUO_pL759				tTDH1				
pUO_pL760	ConLS	pG6	RFP	tENO1	ConRE	ZeoR	BxbI	KanR-ColE1
pUO_pL761				tSSA1				
pUO_pL762				tADH1				
pUO_pL763				tPGK1				
pUO_pL764				tENO2				
pUO_pL765				tTDH1				
pUO_pL766	ConLS	pADH2	RFP	tENO1	ConRE	ZeoR	BxbI	KanR-ColE1
pUO_pL767				tSSA1				
pUO_pL768				tADH1				
pUO_pL769				tPGK1				
pUO_pL770				tENO2				
pUO_pL771				tTDH1				
pUO_pL692	ConLS	pGAP	SP_Disulfide isomerase	RFP	tAOX1	ConRE	ZeoR	BxbI	KanR-ColE1
pUO_pL693			SP_C4R6P1					
pUO_pL694			SP_Cell wall protein					
pUO_pL695			SP_Cyclophillin					
pUO_pL696			SP_CSN2					
pUO_pL697			SP_PHA-E					
pUO_pL698			MF41					
pUO_pL699			SP_C4R8H7					
pUO_pL700			SP_Peptidylprolyl isomerase					
pUO_pL701			SP_ALB					
pUO_pL702			SP_Scw11p					
pUO_pL703			SP_Mucin					
pUO_pL704			SP_An_phyA					
pUO_pL705			SP_Pl_phyA					
pUO_pL706			SP_Th_phyA					
pUO_pL707			SP_Aae_UPO					
pUO_pL708			SP_Aae_UPOeng					
pUO_pL709			SP_PHO1					
pUO_pL710			SP_Suc2					
pUO_pL711	ConLS	pGAP	SP_Disulfide isomerase	GFP	tAOX1	ConRE	ZeoR	BxbI	KanR-ColE1
pUO_pL712			SP_C4R6P1					
pUO_pL713			SP_Cell wall protein					
pUO_pL714			SP_Cyclophillin					
pUO_pL715			SP_CSN2					
pUO_pL716			SP_PHA-E					
pUO_pL717			MF41					
pUO_pL718			SP_C4R8H7					
pUO_pL719			SP_Peptidylprolyl isomerase					
pUO_pL720			SP_ALB					
pUO_pL721			SP_Scw11p					
pUO_pL722			SP_Mucin					
pUO_pL723			SP_An_phyA					
pUO_pL724			SP_Pl_phyA					
pUO_pL725			SP_Th_phyA					
pUO_pL726			SP_Aae_UPO					
pUO_pL727			SP_Aae_UPOeng					
pUO_pL728			SP_PHO1					
pUO_pL729			SP_Suc2					

Table Cloning S3: Phytase Strains - Pre-screening

	Part	Type 1	Type 2	Type 3		Type 4	Type 5	Type 6	Type 7	Type 8
	Description	Linker	Promoter	Tag	GOI	Terminator	Linker	Yeast R	Yeast Origin	EC R and Origin
1	pUO_pL663	ConLS	pAOX1	aMF	Phytase_A_niger	tAOX1	ConRE	ZeoR	BxbI	KanR-ColE1
2	pUO_pL664				Phytase_S_thermophile					
3	pUO_pL665				Phytase_P_lycii					
4	pUO_pL666				Phytase_E_coli					

Table Cloning S4A: Phytase Shuffling - Constitutive Expression

	Part		Number	Name	Part Plasmid Length [bp]
Shuffling Library_9, Const_AniphyA	3b	1	380	*Ani*phyA	3405
Shuffling Library_10, Const_SthphyA		2	381	*Sth*phyA	3450
Shuffling Library_11, Const_PlyphyA		3	382	*Ply*phyA	3291
Shuffling Library_12, Const_appA		4	383	AppA	3291
	2	1	302	pGAP	2143
		2	353	pPET9	2667
		3	354	pG1	2636
		4	355	pG6	2671
		5	356	pADH2	2883
	4	1	308	tAOX1	1916
	Backbone	1	501	GFPdrop_Linear	3297
	3a	1	336	aMF	1932
		2	337	aMF no EAEA	1920
		3	328	aAmylase-aMFΔ	1896
		4	360	Disulfide isomerase	1713
		5	361	Hypothetical protein	1719
		6	362	Beta(1-6) glucan	2313
		7	363	Cyclophilin	2313
		8	364	CSN2	2313
		9	365	PHA-E	1728
		10	366	MF41	2346
		11	367	Hypothetical protein 1	2313
		12	368	Hypothetical protein 3	1725
		13	369	SA	1719
		14	370	Scw11p	1725
		15	371	Mucin	1779
		16	372	Phytase *A. niger* SP	1722
		17	373	Phytase *P. lycii* SP	2313
		18	374	Phytase *T. heterothallica* SP	2313
		19	377	PHO1	1731
		20	378	Suc2	1722

Table Cloning S4A: Phytase Shuffling - Induced Expression

	Part		Number	Name	Part Plasmid Length [bp]
Shuffling Library_13, Ind_AniphyA	3b	1	380	*Ani*phyA	3405
Shuffling Library_14, Ind_SthphyA		2	381	*Sth*phyA	3450
Shuffling Library_15, Ind_PlyphyA		3	382	*Ply*phyA	3291
Shuffling Library_16, Ind_appA		4	383	AppA	3291
	2	1	303	pAOX1	2605
		2	357	pDAS1	2671
		3	358	pPMP20	2149
	4	1	308	tAOX1	1916
	Backbone	1	501	GFPdrop_Linear	3297
		1	336	aMF	1932
		2	337	aMF no EAEA	1920
		3	328	aAmylase-aMFΔ	1896
		4	360	Disulfide isomerase	1713
		5	361	Hypothetical protein	1719
		6	362	Beta(1-6) glucan	2313
		7	363	Cyclophilin	2313
	3a	8	364	CSN2	2313
		9	365	PHA-E	1728
		10	366	MF41	2346
		11	367	Hypothetical protein 1	2313
		12	368	Hypothetical protein 3	1725
		13	369	SA	1719
		14	370	Scw11p	1725
		15	371	Mucin	1779
		16	372	Phytase *A. niger* SP	1722
		17	373	Phytase *P. lycii* SP	2313
		18	374	Phytase *T. heterothallica* SP	2313
		19	377	PHO1	1731
		20	378	Suc2	1722

Table Cloning S5: Phytase Strains from Shuffling

Part	Type 1	Type 2	Type 3		Type 4	Type 5	Type 6	Type 7	Type 8	
Description	Linker	Promoter	Tag	GOI	Terminator	Linker	Yeast R	Yeast Origin	EC R and Origin	
pUO_pL917	ConLS	pPMP20	SP_Cyclophillin	An_phyA	tAOX1	ConRE	ZeoR	BxbI	KanR-ColE1	Shuffling Library 13
pUO_pL918		pAOX1	SP_Cell wall protein							
pUO_pL919		pAOX1	SP_Cell wall protein							
pUO_pL920		pAOX1	SP_C4R8H7							
pUO_pL921		pAOX1	SP_Peptidylprolyl isomerase							
pUO_pL922		pAOX1	SP_CSN2							
pUO_pL923	ConLS	pDAS1	aMF no EAEA	Th_phyA	tAOX1	ConRE	ZeoR	BxbI	KanR-ColE1	Shuffling Library 14
pUO_pL924		pAOX1	SP_CSN2							
pUO_pL925		pAOX1	SP_CSN2							
pUO_pL926		pAOX1	SP_C4R8H7							
pUO_pL927		pPMP20	SP_C4R8H7							
pUO_pL928		pPMP20	SP_C4R8H7							
pUO_pL929	ConLS	pPMP20	SP_Cyclophillin	Pl_phyA	tAOX1	ConRE	ZeoR	BxbI	KanR-ColE1	Shuffling Library 15
pUO_pL930		pAOX1	SP_Mucin							
pUO_pL931		pDAS1	SP_Mucin							
pUO_pL932		pDAS1	aMF no EAEA							
pUO_pL933		pPMP20	SP_Mucin							
pUO_pL934		pPMP20	SP_Mucin							
pUO_pL935	ConLS	pDAS1	SP_Disulfide isomerase	Ec_phyA	tAOX1	ConRE	ZeoR	BxbI	KanR-ColE1	Shuffling Library 16
pUO_pL936		pAOX1	aMF							
pUO_pL937		pAOX1	aMF no EAEA							
pUO_pL938		pDAS1	MF41							
pUO_pL939		pAOX1	aMF							
pUO_pL940		pAOX1	SP_PHO1							
pUO_pL941	ConLS	pGAP	SP_Disulfide isomerase	An_phyA	tAOX1	ConRE	ZeoR	BxbI	KanR-ColE1	Shuffling Library 9
pUO_pL942		pGAP	SP_C4R8H7							
pUO_pL943		pGAP	SP_PHO1							
pUO_pL944		pGAP	SP_C4R8H7							
pUO_pL945		pGAP	SP_Cyclophillin							
pUO_pL946		pGAP	SP_Cyclophillin							
pUO_pL947	ConLS			Th_phyA	tAOX1	ConRE	ZeoR	BxbI	KanR-ColE1	Shuffling Library 10
pUO_pL948		pG1	SP_ALB							
pUO_pL949		pG1	SP_Cell wall protein							
pUO_pL950		pGAP	SP_PHO1							
pUO_pL951		pGAP	SP_PHO1							
pUO_pL952		pGAP	SP_Cyclophillin							
pUO_pL953	ConLS	pG6	SP_PHO1	Pl_phyA	tAOX1	ConRE	ZeoR	BxbI	KanR-ColE1	Shuffling Library 11
pUO_pL954		pG6	SP_PHO1							
pUO_pL955		pG6	SP_Disulfide isomerase							
pUO_pL956		pADH2	SP_Mucin							
pUO_pL957		pG6	SP_Scw11p							
pUO_pL958		pG6	SP_Disulfide isomerase							
pUO_pL959	ConLS	pGAP	aMF	Ec_phyA	tAOX1	ConRE	ZeoR	BxbI	KanR-ColE1	Shuffling Library 12
pUO_pL960		pGAP	SP_PHO1							
pUO_pL961		pGAP	aMF							
pUO_pL962		pGAP	MF41							
pUO_pL963		pGAP	MF41							
pUO_pL964		pGAP	MF41							

Table Cloning S6A: Primers - Primers for generation of new parts

Name	Sequence 5´-3´
FW-2-pPET9	gcatcgtctcatcggtctcaaacgTAGAAAATTCACCACTGTCGGAAAGTTG
REV-2-pPET9	atgccgtctcaggtctcacatagatctGAAGTCGACGAAGAAGTTAGACTTGTTG
FW-Fix-pPET9	gcatcgtctcacACGGAGCTGCCTCCAC
REV-Fix-pPET9	atgccgtctcaCGTgTCTTGACTCCAATACGACCCCTC
FW-2-pG1	gcatcgtctcatcggtctcaaacgCAAACATTTGCTCCCCCTAGTCTC
REV-2-pG1	atgccgtctcaggtctcacatagatctAAGGGTGGAATTTTAAGGATCTTTTATACTC
FW-2-pPMP20	gcatcgtctcatcggtctcaaacgTTCTGGAGTGTCAAAACAGTAGTGATAAAAGG
REV-2-pPMP20	atgccgtctcaggtctcacatagatctCTTAGATTTTTTTTTTTGCTTGGTGGGATTCC
FW-2-pADH2	gcatcgtctcatcggtctcaaacgCGCAGCGTTTTCTGACGG
REV-2-pADH2	atgccgtctcaggtctcacatagatctTTTCGTAAAGTAAATAAGATAAAAGCTAGTAGCTG
FW-Fix-pADH2	gcatcgtctcacACCCCACATAGTGACAATGATTATGTAAGAAG
REV-Fix-pADH2	atgccgtctcaGGTgTCTACAGTCTCACCCTGCGATC
FW-2-pDAS1	gcatcgtctcatcggtctcaaacgAATAAAAAAACGTTATAGAAAGAAATTGGACTACG
REV-2-pDAS1	atgccgtctcaggtctcacatagatctTTTGTTCGATTATTCTCCAGATAAAATCAACAATAGTTG
FW-Fix-pDAS1	gcatcgtctcagTCGGTTAGCCTCTAGGCAAATTCTG
REV-Fix-pDAS1	atgccgtctcaCGAcACCTGAGGCTAAAAAAGGCAG
FW-2-pG6	gcatcgtctcatcggtctcaaacgTGACCAGCAGTTTAACTACGCAAATC
REV-Fix-pG6	atgccgtctcTTCACCCTAGTCTGCGACTTTTAATTG

Table Cloning S6B: Primers - Sequencing primers

Name	Sequence 5´-3´
FW-BxbILocus	TGGTTTCTCCTGACCCAAAGACTTTAAATTT
REV-BxbILocus	GAACCAATTTAGCTATATATAGTTAACTACCGGCTCG
FW-Sequencing-EntryVector	ccttttgctggccttttgctc
REV-Sequencing-EntryVector	ccagtaatgacctcagaactcc
FW-Seq-ConS	cgacaacgtggcaattcgtcg
FW-Seq-ConE	gaaccagcgccggcgaac
FW-Seq-ZeoTerm	gcgaagttaagtgcgcagaaag
FW-Seq-ColE1	gcggagcctatggaaaaacgc
REV-Seq-ConS	cagatggtcctggagatcgttg
REV-Seq-ConE	catcggtatgatctgtacatgattcg
REV-Seq-Kana	ctcaccggattcagtcgtcactc
REV-Sequ-Mid_RFP	CACCTTCAATTTCGAATTCGTGACCG
REV-Sequ-Mid_GFP	cagcttgccgtaggtggcatc
FW-Seq-pGAP	gcgaacacctttcccaatttggtttc
REV-Seq-tAOX1	GATCAGGAGCAAGCTCGTACGAGAA
FW-Seq-pAOX1	GCGACTGGTTCCAATTGACAAG
FW-Seq-ConS (N-term)	ggtagagccacaaacagccg
Rev-Seq-tAOX1	GCCTGCATCTCTCAGGCAAATG
REV-Seq-Zeocin	caaggagggtattctgggcctc
REV-Seq-Phytase_An	CTGGTCAGGGACTCGTATCTCTGG
REV-Seq-Phytase_Sth	CCAAAGTGTAGTCGTAAGTTCTCAGGAACTC
REV-Seq-Phytase_Ply	CGAATGGCAACAAGTCAGCAACAC
REV-Seq-Phytase_Ec	GCAATAATAGCAACCTGACCGGATTGTG
REV-Seq-Oxidase	GGCCTTCTGCAATTCGAAAGCAG

Supplementary References

1. Lee, M.E., DeLoache, W.C., Cervantes, B., Dueber, J.E., 2015. A highly characterized yeast toolkit for modular, multipart assembly. ACS Synth. Biol. 4, 975–986.[PubMed]
2. Looser V., Bruhlmann B., Bumbak F., Stenger C., Costa M., Camattari A., Fotiadis D., Kovar K., 2015. Cultivation strategies to enhance productivity of *Pichia pastoris:* A review. Biotechnol. Adv. 33, 1177–1193.
3. Qvirist, L., Carlsson, N.G., Andlid, T., 2015. Assessing phytase activity. J. Biol. Meth. 2, e16.
4. Akbarzadeh, A., Dehnavi, E., Aghaeepoor, M., Amani, J., 2015. Optimization of recombinant expression of synthetic bacterial phytase in *Pichia pastoris* using response surface methodology. Jundishapur J. Microbiol. 8, e27553.
5. Han, Y.M., Lei, X.G., 1999. Role of glycosylation in the functional expression of an*Aspergillus niger*Phytase (*phyA*) in*Pichia pastoris*. Arch. Biochem. Biophys. 364, 83–90.
6. Parashar, D., Satyanarayana, T., 2016. Enhancing the production of recombinant acidic α-amylase and phytase in *Pichia pastoris* under dual promoters[constitutive (*GAP*) and inducible (*AOX*)] in mixed fed batch high cell density cultivation. Process. Biochem. 51, 1315–1322.
7. Xiong, A.S., Yao, Q.H., Peng, R.H., Zhang, Z., Xu, F., Liu, J.G., Han, P.L., Chen, J.M., 2006. High level expression of a synthetic gene encoding *Peniophora lycii* phytase in methylotrophic yeast *Pichia pastoris*. Appl. Microbiol. Biotechnol. 72, 1039–1047.
8. Bae, H.D., Yanke, L.J., Cheng, K.J., Selinger, L.B., 1999. A novel staining method for detecting phytase activity. J. Microbiol. Meth. 39, 17–22.
9. Zhang, J.H., Chung, T.D.Y., Oldenburg, K.R., 1999. A simple statistical parameter for use in evaluation and validation of high throughput screening assays. SLAS Discov. 4, 67–73.
10. Zanella, F., Lorens, J.B., Link, W., 2010. High content screening: seeing is believing. Trends Biotechnol. 28, 237–245.
11. Patrick, W.M., Firth, A.E., Blackburn, J.M., 2003. User-friendly algorithms for estimating completeness and diversity in randomized protein-encoding libraries. Protein Eng. Des. Sel. 16, 451–457.
12. Massahi, A., Çalık, P., 2015. In-silico determination of *Pichia pastoris* signal peptides for extracellular recombinant protein production. J. Theor. Biol. 364, 179–188.
13. Heimo, H., Palmu, K., Suominen, I., 1997. Expression in *Pichia pastoris* and purification of *Aspergillus awamori* glucoamylase catalytic domain. Protein Expr. Purif. 10, 70–79.
14. Liang, S.L., Li, C., Ye, Y.R., Lin, Y., 2013. Endogenous signal peptides efficiently mediate the secretion of recombinant proteins in *Pichia pastoris*. Biotechnol. Lett. 35, 97–105.
15. Lin-Cereghino, G.P., Stark, C.M., Kim, D., Chang, J., Shaheen, N., Poerwanto, H., Agari, K., Moua, P.C., Low, L.K., Tran, N., Huang, A.D., Nattestad, M., Oshiro, K.T., Chang, J.W., Chavan, A., Tsai, J.W., Lin-Cereghino, J., 2013. The effect of α-mating factor secretion signal mutations on recombinant protein expression in *Pichia pastoris*. Gene 519, 311–317.
16. Molina-Espeja, P., Garcia-Ruiz, E., Gonzalez-Perez, D., Ullrich, R., Hofrichter, M., Alcalde, M., 2014. Directed evolution of unspecific peroxygenase from *Agrocybe aegerita*. Appl. Environ. Microbiol. 80, 3496–3507.
17. Kuwae, S., Ohyama, M., Ohya, T., Ohi, H., Kobayashi, K., 2005. Production of recombinant human antithrombin by *Pichia pastoris*. J. Biosci. Bioeng. 99, 264–271.
18. Kobayashi, K., Kuwae, S., Ohya, T., Ohda, T., Ohyama, M., Ohi, H., Tomomitsu, K., Ohmura, T., 2000. High-level expression of recombinant human serum albumin from the methylotrophic yeast *Pichia pastoris* with minimal protease production and activation. J. Biosci. Bioeng. 89, 55–61.

19. He, Z.Y., 2012. Comparison of alpha-factor preprosequence and a classical mammalian signal peptide for secretion of recombinant xylanase xynB from yeast *Pichia pastoris*. J. Microbiol. Biotechnol. 22, 479–483.
20. Raemaekers, R.J., de Muro, L., Gatehouse, J.A., Fordham-Skelton, A.P., 1999. Functional phytohemagglutinin (PHA) and *Galanthus nivalis* agglutinin (GNA) expressed in *Pichia pastoris* correct N-terminal processing and secretion of heterologous proteins expressed using the PHA-E signal peptide. Eur. J. Biochem. 265, 394–403.
21. Qin, X., Qian, J., Xiao, C., Zhuang, Y., Zhang, S., Chu, J., 2011. Reliable high-throughput approach for screening of engineered constitutive promoters in the yeast *Pichia pastoris*. Lett. Appl. Microbiol. 52, 634–641.
22. Looser V., Bruhlmann B., Bumbak F., Stenger C., Costa M., Camattari A., Fotiadis D., Kovar K., 2015. Cultivation strategies to enhance productivity of *Pichia pastoris:* A review. Biotechnol. Adv. 33, 1177–1193.

7.3. Supporting Information: Biorefinery concept for *Cylindrospermum* alatosporum CCALA 988 extracting multiple high-value compounds and residue utilization by *P. pastoris* fermentation producing phytase

Algal Research

Biorefinery concept for *Cylindrospermumalatosporum CCALA 988* extracting multiple high-value compounds and residue utilization by by P. pastoris fermentation producing phytase

Supporting Information

Korbinian Sinzinger[a], Sebastian Bieringer[c], Doris Schieder[a], Herbert Riepl[b,c]& Volker Sieber[a,d,e,f]

[a] *Chair of Chemistry of Biogenic Resources, Technical University of Munich, Campus for Biotechnology and Sustainability, 94315 Straubing, Germany*

[b]*Organic-analytical Chemistry, Weihenstephan-Triesdorf University of Applied Sciences, Straubing, Germany*

[c] *Campus Straubing for Biotechnology and Sustainability, Technical University of Munich, Straubing, Germany*

[d] *Catalysis Research Center, Technical University of Munich, 85748 Garching, Germany*

[e]*SynBiofoundry@TUM, Technical University of Munich, 94315 Straubing, Germany*

[f] *The University of Queensland, School of Chemistry and Molecular Biosciences, 68 Cooper Road, St. Lucia 4072, Australia*

Annex 1 Calculation of pigment concentrations afterMeixner*et al*.

Calculation ofchlorophyll_a concentration using absorption values of λ = 647 nm and λ = 664 nm

$$\text{chlorophyll}_a[\mu g/ml] = -1.79 * A_{647} + 11.87 * A_{664} \quad (1)$$

Calculation of the chlorophyll_b concentration using absorption values of λ = 647 nm and λ = 664 nm

$$\text{chlorophyll}_b[\mu g/ml] = 18.98 * A_{647} - 4.90 * A_{664} \quad (2)$$

Calculation of the total carotenoid concentration using absorption values of λ = 480 nm

$$\text{totalcarotenoids}\ [\mu g/ml] = 4 * A_{480} \quad (3)$$

Calculation of the C-phycocyanin concentration using absorption values of λ = 615 nm, λ = 652 nm

$$\text{c – phycocyanin (PC)}\ [\mu g/ml] = \frac{A_{615} - 0.474 * A_{652}}{5.34} \quad (4)$$

Calculation of the allophycocyanin concentration using absorption values of λ = 615 nm, λ = 652 nm

$$\text{allophycocyanin (APC)}\ [\mu g/ml] = \frac{A_{652} - 0.2087 * A_{615}}{5.09} \quad (5)$$

Calculation of the phycoerythrin concentration using absorption values of λ = 562 nm

$$\text{phycoerythrin (PE)}\ [\mu g/ml] = \frac{A_{562} - (2.41 * PC) - (0.849 * APC)}{9{,}62} \quad (6)$$

Calculation of total phycobiliproteins

$$\text{totalphycobiliproteins} = PC + PE + APC \quad (7)$$

2

Annex 2 Overview of saccharides detected in the *C. alatosporum CCALA 988* biomass. Qualitative and quantitative saccharide fingerprint by HT-PMP method and fatty acid profile determined as FAMEs by GC-MS.

Annex 2.1 Overlay of UV 245 nm (black) and MS extracted ion (color) traces in chromatograms (3 – 9 min) of*C. alatosporum CCALA 988.* EIC colors have been chosen to help differentiate peaks. Corresponding m/z values are shown in the figures.

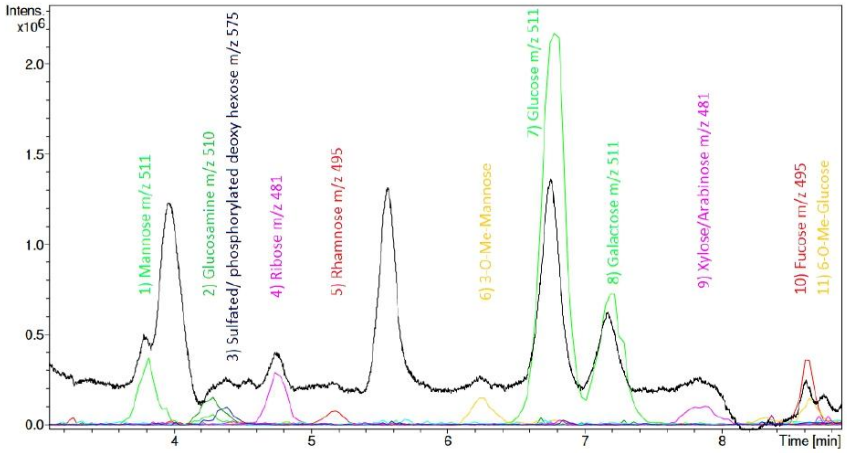

Annex 2.2 Fragmentation pattern of the identified but not quantified saccharidesin *Cylindrospermumalatosporum CCALA988*. Masses marked with * correspond to methylated or substituted fragments and masses markedwith ◊ are the mono-derivative ions.

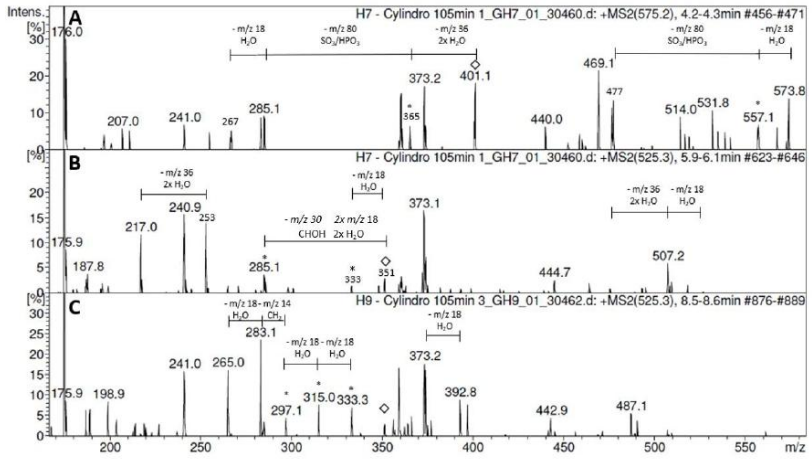

3

Annex 3 Total lipids and fatty acid profile found in *C. alatosporum CCLALA 988* biomass after *in-situ* transesterification and GC-MS analysis. n = 3.

Fatty acids		***C. alatosporum CCALA 988*** (mg fatty acid / g biomass)
palmitic acid	C16:0	13.9 ± 0.2
palmitoleic acid	C16:9	5.7 ± 0.1
stearic acid	C18:0	0.10 ± 0.04
linoleic acid	C18:9,12	11.6 ± 0.4
α-linolenic acid	C18:9,12,15	9.5 ± 0.4
Total		40.7 ± 1.2

Annex 4 Phycobiliprotein content in*Cylindrospermumalatosporum CCALA 988* and phycobiliprotein yields in multiple extraction cycles.

Annex 4.1 Phycocyanin, allophycocyanin and phycoerythrin content in*C. alatosporum CCALA 988* determinedwithin three sequential extraction cycles with 50 mM acetate buffer pH 7 at 4 °C over night.Values are reported as mean of four technical replicates with three analytical replicates each and standard deviation.

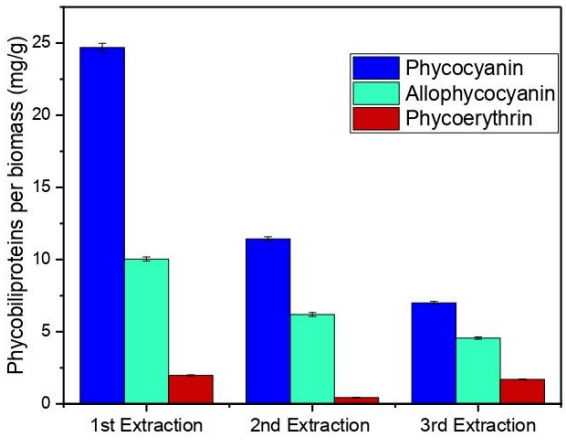

4

Annex 4.2 Absorbance spectra of 1:10 diluted aqueous crude extract of*C. alatosporum CCALA 988*within three sequential extraction cycles showing a picture of the real color of each diluted extract.

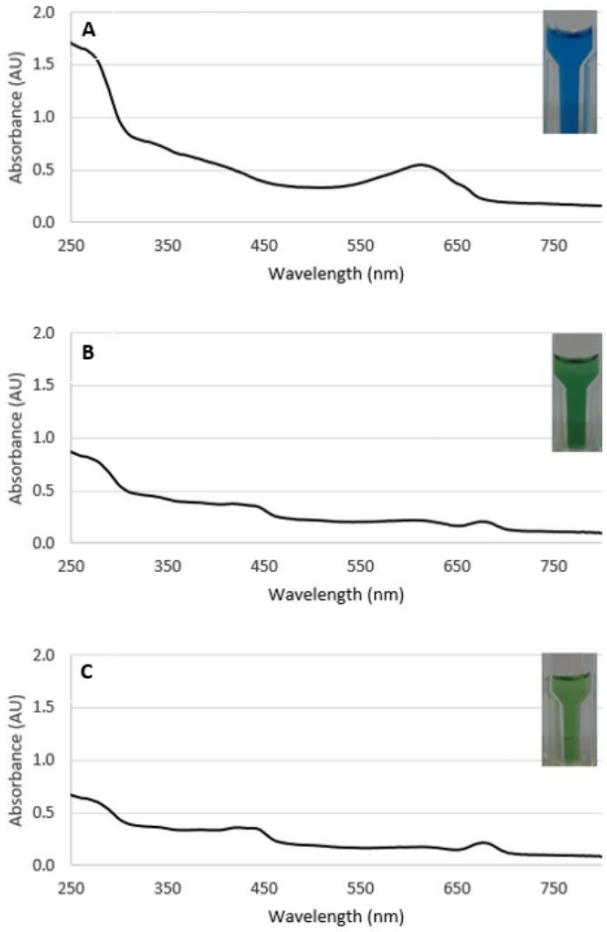

5

Annex 5 Calculations for the estimation of the CLP concentration based onMareš et al. (see ref. 48) and the here found detection ratio of PUW and MIN.

- Mareš et al. quantified two PUW F congeners with 21.6 mg/g
- Combining quantified PUW congeners with the concentration ratio of MIN to PUW of 4.7:1

  21.6 mg/g * 4.7 = 101.5 mg/g

- Results in a combined CLP concentration of 101.5 mg/g + 21.6 mg/g = 123.1 mg/g

Annex 6 Comparison of saccharification yields per biomass. After 1 h heat pre-treatment at 80° C, 25 mg of *C. alatosporum CCLALA 988* biomass washydrolyzed using industrial enzymes at 50 °C in 1 mL total volume with 50 mM ammonium acetate buffer pH 4.5 analyzed by the PMP method. Enzyme concentrations were 0.5 % (v/v) and sodium azide was 0.02 % (w/v). Data presented are the average of triplicates and one standard deviation.

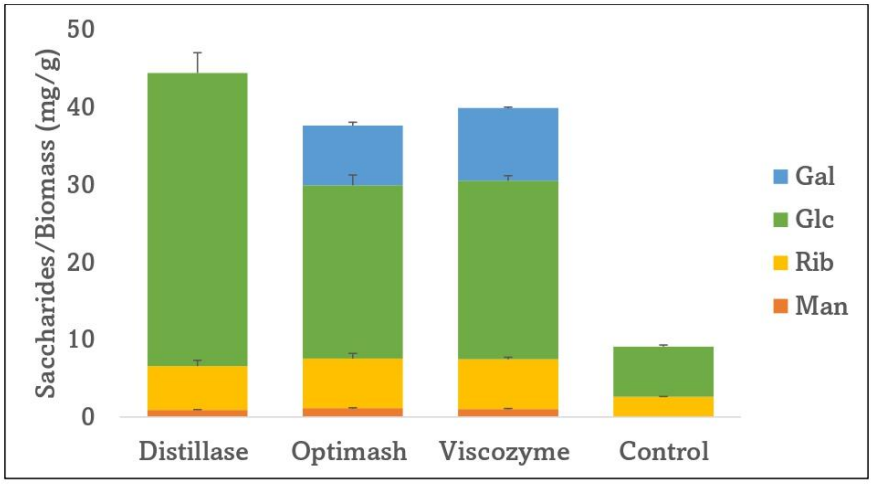

Annex 7 Fermentation graphs of *Pichia pastoris*with MF41 – pGAPproducing the appA*E. coli*phytase in salt media.The medium composition was described in the manuscript.

Annex 7.1 Fermentation graphs of *P. pastoris* producing the appA*E. coli*phytase in D'Anjou medium, **A** and **B** are duplicates.

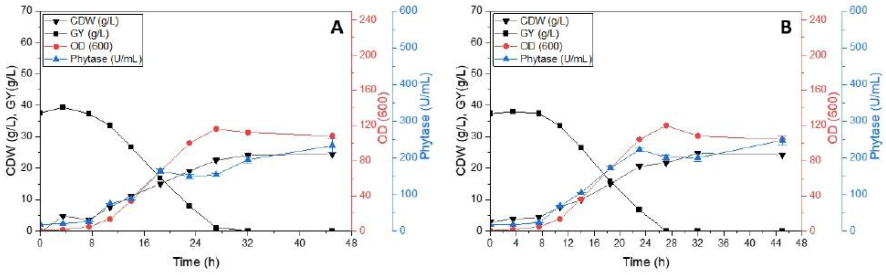

Annex7.2 Fermentation graphs of *P. pastoris* producing the AppA*E. coli*phytase in MSM medium with a double concentration of PTM, **A** and **B** are duplicates.

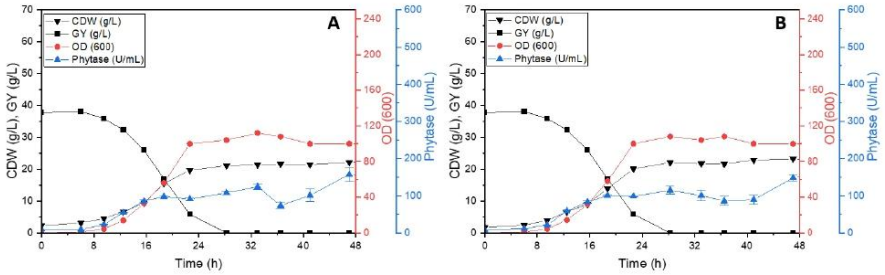

Annex 7.3 Fermentation graphs of *P. pastoris* producing the AppA*E. coli*phytase in MSM medium as batch (**A**) and pulsed batch (**B**) fermentation, (duplicates are shown in the manuscript).

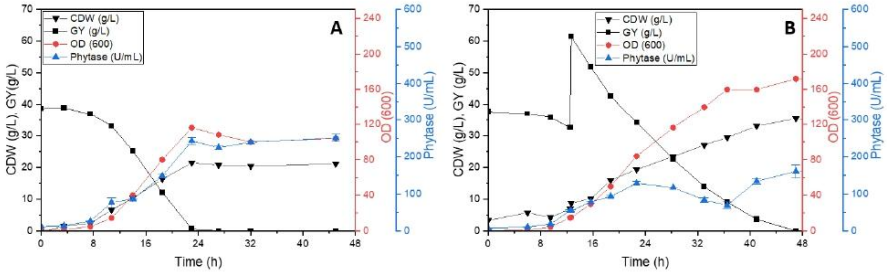

Annex 8 Fermentation graphs of *Pichia pastoris*with MF41 – pGAP producing the appA*E. coli*phytase in water or salt medium with different concentrations of hydrolysate from double extracted residual biomass from *C. alatosporum CCALA 988.*

Annex 8.1 Fermentation graphs of *P. pastoris* producing the appA*E. coli*phytase in onlywater, **A** and **B** are duplicates.

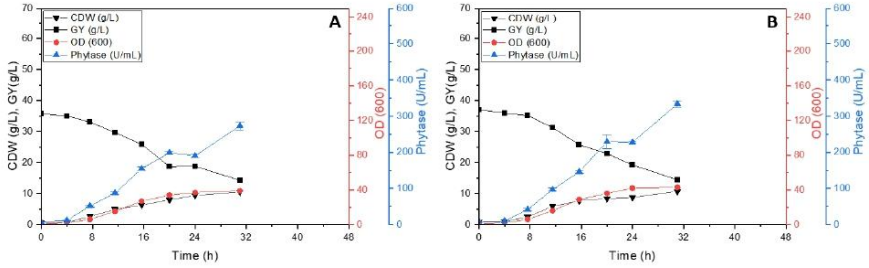

Annex 8.2 Fermentation graphs of *P. pastoris* producing the appA*E. coli*phytase in water with 1 % (v/v) hydrolysate, **A** and **B** are duplicates.

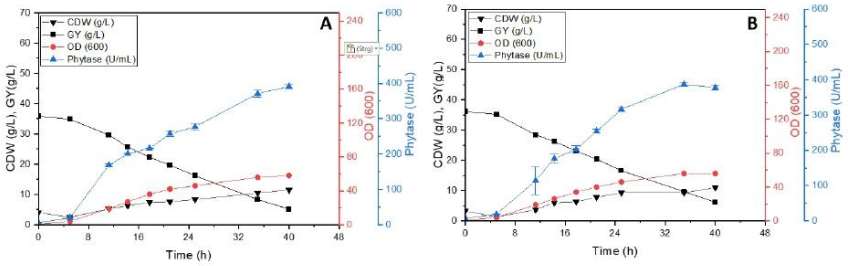

Annex 8.3 Fermentation graphs of *P. pastoris* producing the appA*E. coli*phytase in MSM medium with 1 % (v/v) hydrolysate, **A** and **B** are duplicates.

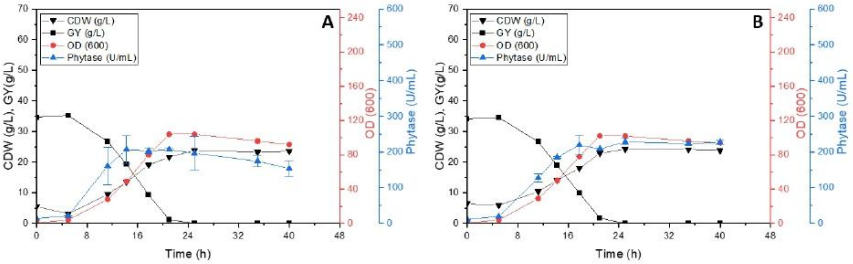

Annex 8.4 Fermentation graphs of *P. pastoris* producing the appA*E. coli*phytase in MSM medium with 5 % (v/v) hydrolysate, **A** and **B** are duplicates.

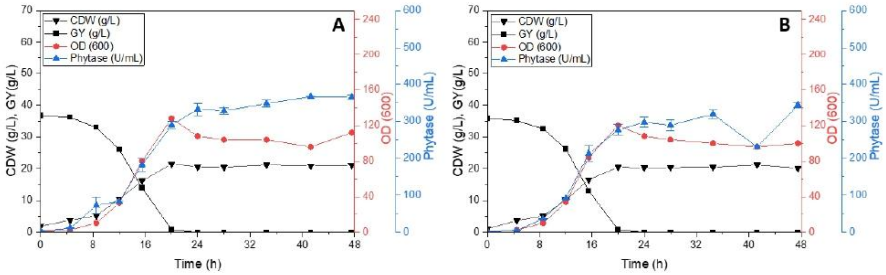

Annex 8.5 Fermentation graphs of *P. pastoris* producing the appA*E. coli*phytase in MSM medium with 10 % (v/v) hydrolysate showing batch (**A**) and pulsed batch (**B**) fermentation (duplicates are shown in the manuscript).

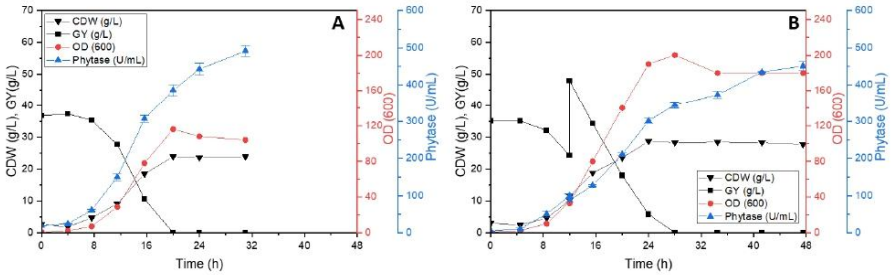

Annex 9SDS-PAGE gel of the fermentation course (timepoints t_0 – t_7 are the sampling points) of *P. pastoris* producing the appA*E. coli*phytase in MSM medium with 10 % (v/v) hydrolysate.The supernatants were concentrated 5-fold and 10 µL were applied to each pocket. The band for the phytase protein is visibly getting thicker over the course of the fermentation.

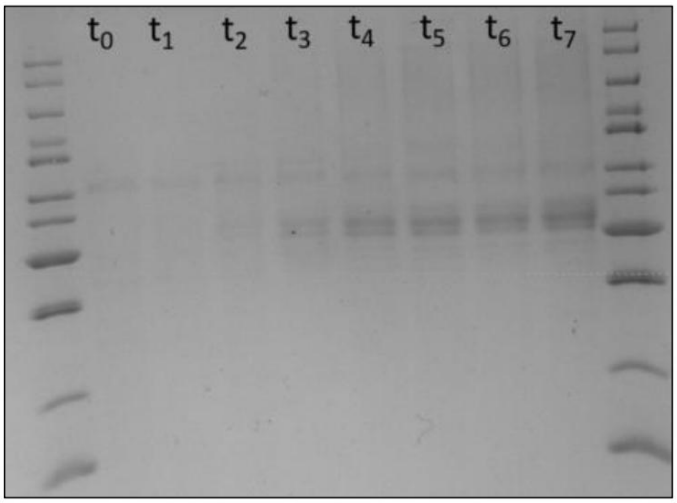

10

7.4. Supporting Information: LCSA of the biorefinery concept for *Cylindrospermum* alatosporum CCALA 988 extracting multiple high-value compounds and residue utilization by *P. pastoris* fermentation producing phytase

Algal Research

LCSA of the biorefinery concept for *Cylindrospermum* alatosporum CCALA 988 extracting multiple high-value compounds and residue utilization by *P. pastoris* fermentation producing phytase

Supporting Information

Korbinian Sinzinger[a], Doris Schieder[a] and Volker Sieber[a,b,c,d]

[a] *Chair of Chemistry of Biogenic Resources, Technical University of Munich, Campus for Biotechnology and Sustainability, 94315 Straubing, Germany*

[b] *Catalysis Research Center, Technical University of Munich, 85748 Garching, Germany*

[c] *Fraunhofer IGB, Branch BioCat, 94315 Straubing, Germany*

[d] *The University of Queensland, School of Chemistry and Molecular Biosciences, 68 Cooper Road, St. Lucia 4072, Australia*

Annex 1: Overview of the material needed as well as the biomass and material streams for the biorefinery concept of *C. alatosporum* CCALA 988 and the six subsystems as described in the main text.

Supply Subsystem and overall

Material	Amount	Unit
Fresh water	61	m3/year
Urea	36	kg/year
P-Fertilizer	18	kg/year
CO_2	1098	kg/year
Heat	972	MJ/year
Waste water	659	m3/year
Carbon dioxide, into air	540	kg/year
Hydrogen peroxide (cleaning)	108	kg/year
Citric acid (cleaning)	90	kg/year
Land occupation	22.5	m^2yr
Land transformation	450	m^2

Cyanobacteria Production Subsystem

Material	Amount	Unit
Productivity	2.5	g/L
Dry CY Biomass	1.80	t/year
Evaporated water	36	m3/year
Total water	720	L/year

Considerations for Product Recovery	
BM load in Extraction	5%
BM load in Hydrolysate	5%
Hydrolysate loss due to centrifugation	25%
Yeast hydrolysate dilution factor for 10 g/L	0

Product Recovery		
Material	**Amount**	**Unit**
Dry CY biomass	1.8	t/year
Water for 1st extraction	36000	L/year
Sodium phosphate	278.0	kg/year
Electricity	0	kWh/year
1st Extract	325.80	kg/year
Volume of 1st Extract (20 % loss)	28800	L/year
Biomass (after 1st extraction)	1474.20	kg/year
2nd Extract	72.00	kg/year
Volume of 2nd Extract (20 %loss)	18869.76	L/year
Methanol	18869.76	L/year
Biomass (after 2nd extraction)	1402.20	kg/year
Water for hydrolysis	51452	L/year
Enzymes	64.52	kg/year
Hydrolysate (25 % loss)	21033	L/year
Residual CY Biomass (after hydrolysis)	788.04	kg/year
Recovered methanol	4717.44	L/year
Solubles in Hydrolysate	614.16	kg/year
yeast CDW (50 % solubilisation)	3511.20	kg/year
Yeast hyrolysate (20% loss)	18726.4	L/year
Residual total wet biomass	14.36210421	t/year

Biomass Streams			From Mass Balance Lab scale	Solubilized in hydrolysate
Material	**Amount**	**Unit**	**Percent**	43.80%
Dry CY biomass	1.80	t/year	100%	
1st Extract	325.80	kg/year	18.10%	
Volume of 1st Extract (20 % loss)	28800	L/year		
Biomass (after 1st extraction)	1474.20	kg/year	81.90%	
2nd Extract	72.00	kg/year	4%	
Volume of 2nd Extract (20 %loss)	18869.76	L/year		
Biomass (after 2nd extraction)	1402.20	kg/year	77.90%	
Solubles in Hydrolysate	614.16	kg/year	34.12%	
Biomass (after hydrolysis)	788.04	kg/year	43.78%	
Total			100.00%	
yeast CDW (50 % solubilisation)	3511.20	kg/year	needs +20%	
Yeast wet residual biomass	9912.6	kg/year		

Other Material Streams		
Material	**Amount**	**Unit**
Water for 1st extraction	36000	L/year
Sodium phosphate (50 mM)	278.0	kg/year
Methanol	23587.2	L/year
recovered Methanol (20%)	4717.44	L/year
Water for hydrolysis (5 % (w/v))	28044	L/year
Enzymes (3x0.05 % (v/v) loading)	50.48	kg/year
hydrolysate (20 % loss)	21033	L/year
Water for yeast hydroylsis (15 % (w/v))	23408	L/year
Enzymes (0.05 % (v/v) loading)	14.04	kg/year
Yeast hyrolysate (20% loss)	18726	L/year
YE in hydrolysate	75.00	g/L
YE hydrolysate needed (below = short)	59.7	L/year

Seed Fermenter I			Starting Volume (L)	# of batches per year
Material	**Amount**	**Unit**	15	35
Water	525	L/year		
Electricity		kWh/year		
Glycerol (20 g/L)	10.5	kg/year		
Salts & minerals (26.1 g/L)	13.70	kg/year		

Seed Fermenter II			Starting Volume (L)	# of batches per year
Material	**Amount**	**Unit**	250	35
Water	8225	L/year		
Electricity		kWh/year		
Glycerol (20 g/L)	175	kg/year		
Salts & minerals (26.1 g/L)	228.38	kg/year		

Considerations for Main Fermenter	
Starting Volume (L)	4000
# of batches per year	35
Denisty of glycerol	1.26
Feed Volume (L)	3000
Glycerol % (w/w)	50%
WCW to DCW	5.65

Main Fermenter

Material	Amount	Unit
Water	92108	L/year
Glycerol (40 g/L)	5600	kg/year
Salts & minerals (26.1 g/L)	3654	kg/year
Hydrolysate (15 %)	21000	L/year
Feed water (3000 L)	66150	L/year
Feed Glycerol (3000 L)	52.5	t/year
Phytase in broth (30,246 U/mL)	7410.27	GU/year
Wet yeast BM (622 g/L)	152.39	t/year
Dry yeast BM	26.99	t/year
Dry YE needed	1.40	t/year
Waste water from wet cell mass	125.40	m3/year
Volume of supernantant	119.6	m3/year
YE hydrolysate needed	18666.7	L/year
Wet YE needed	9.91	t/year
Yeast wet mass as feed	142.48	t/year
Phytase in SN (30,246 U/mL)	3617.40	GU/year

Considerations for Purification Fermentation	
PEG ratio (6000 : 8000)	°1:1
pH	^5.6
PEG conc.	10.50%
Cycles (reuse)	4
Na Citrate	20.50%
Process time	3 h
Recovery	98.50%

Purification Fermentation		
Material	**Amount**	**Unit**
Volume of supernantant	119.6	m3/year
PEG (MW 6000)	1569.7	kg/year
PEG (MW 8000)	1569.7	kg/year
Sodium citrate	24.5	t/year
Recovered Phytase	3563.1	GU/year

Salt Precipitation			Prec. Factor	Dialu. Factor
Material	**Amount**	**Unit**	25	1.125
ammonium sulfate (60% precip.)	17280	kg/year		
Protein faction redissolved in water	1152.00	L/year		
waste water 99%	118403.42	L/year		
water	11520	L/year		
Protein fraction after dialysis	1296	L/year		

Aqeous Extract (FPLC)			Sample/Bed Factor
Material	**Amount**	**Unit**	25
Water for dissolving	144.00	L/year	
Electricity		MJ/year	
1st Extract	325.80	kg/year	
Protein fraction after dialysis	1296.00	L/year	
Water for SEC buffers	64800	L/year	
Phycobiliproteins (34.5 mg/g & 75 % purification recovery)	46.58	kg/year	
extra protein (80 % of remains)	223.4	kg/year	
sodium phosphate (50mM)	500.3	kg/year	
sodium chloride (0.5M)	946.7	kg/year	
Water for HIC buffers	12960	L/year	
ammonium sulfate (1.5M)	2568.8	kg/year	
sodium phosphate (50mM)	100.1	kg/year	
Final volume	2592	L/year	
Total water	77760	L/year	

Organic Extract		
Material	**Amount**	**Unit**
Water	18869.76	L/year
2nd Extract	72.00	kg/year
methanol	18869.76	L/year
ethyl acetate	18869.76	L/year

Purification Extracts		
Material	**Amount**	**Unit**
Phycobiliproteins	46.58	kg/year
extra protein	223.4	kg/year
sodium phosphate	500.3	kg/year
sodium chloride	946.7	kg/year
ammonium sulfate	19848.8	kg/year
methanol	18869.76	L/year
ethyl acetate	18869.76	L/year
Waste water dryer	146862.3	L/year

Amounts of CLPs in each Fraction

Material	Aq.	Org	Unit
Puwainaphycins (21.6 mg/g)	37.7	1.2	kg/year
Minutisamides (101.5 mg/g)	155.3	27.4	kg/year

Final Products (From Biorefinery Manuscript)

Material	Amount	Unit
Puwainaphycins (21.6 mg/g)	38.88	kg/year
Minutisamides (101.5 mg/g)	182.7	kg/year
Phycobiliproteins	46.58	kg/year
Chlorophyll a (5.3 mg/g)	9.54	kg/year
Carotenoids (1.1 mg/g)	1.98	kg/year
Recovered Phytase	3,563	GU/year
Animal Feed	28.0	t/year

Annex 2: Environmental impact analysis: categories and results at midpoint level. ReCiPe 2016 Endpoint v1.02 in the hierarchist version was used as the life-cycle impact assessment method with SimaPro 9.0.0.29. It is based on up-to-date modelling and allows the identification of the influence of midpoint indicators on the results.

Impact category	Value	Unit
climate change	5.12E+05	kg CO_2 eq.
acidification	4.57E+03	kg CFC^{-1} eq.
freshwater ecotoxicity	6.15E+05	CTUh
freshwater eutrophication	3.49E+02	CTUh
marine eutrophication	1.96E+03	death
terrestrial eutrophication	1.43E+04	kBq U-235 eq.
carcinogenic effects	9.20E-03	kg NMVOC eq.
ionising radiation	6.20E+04	mol H^+ eq.
non-carcinogenic effects	3.06E-01	mol N eq.
ozone depletion	7.05E-02	kg P eq.
photochemical ozone creation	3.27E+03	kg N eq.
respiratory effects	3.49E-02	pt
water depletion	6.36E+05	CTUe
fossil depletion	7.58E+06	m^3 water eq. of deprived water
land use	3.64E+07	MJ
mineral depletion	2.10E+00	kg Sb eq.

Annex 3: Operation costs for all six subsystems of the biorefinery including sources and code for the modeling.

Substance	Unit cost	Unit	Annual Amount	Unit	Annual cost	Rel. cost	Source	code
heat, natural gas	0.014	€/MJ	972	MJ	14.08 €	0.001%	https://appsso.eurostat.ec.europa.eu/nui/submitViewTableAction.do	nrg_pc_203
electricity, medium voltage	0.239	€/kWh	268878	kWh	64,288.63 €	3.304%		nrg_pc_205
water	2.230	€/m3	414	m3	923.22 €	0.047%	https://www.statistik-bw.de/Umwelt/Wasser/Trink-Abwasserpreise.jsp	
hydrogen peroxide	0.350	€/kg	108	kg	37.80 €	0.002%	https://trade.ec.europa.eu/access-to-markets/de/statistics	2847
citric acid	1.040	€/kg	360	kg	374.24 €	0.019%		291814
carbon dioxide	0.330	€/kg	1098	kg	362.34 €	0.019%		281121
urea	0.220	€/kg	36	kg	7.92 €	0.000%		31021010
P-fertilizer	0.210	€/kg	18	kg	3.78 €	0.000%		3103
Wastewater	1.950	€/m3	659	m3	1,285.71 €	0.066%	https://www.statistik-bw.de/Umwelt/Wasser/Trink-Abwasserpreise.jsp	
deionized water	0.570	€/kg	3669	kg	2,091.35 €	0.107%	www.alfiltra,de/1000-liter-ve-wasser-im-ibc-behaelter	
sodium phosphate	1.760	€/kg	878	kg	1,545.95 €	0.079%		283522
methanol	0.230	€/kg	23587	kg	5,425.06 €	0.279%		290511
enzymes	8.460	€/kg	65	kg	545.87 €	0.028%		35079090
glycerine, 40g/L, 0.5L used	0.650	€/kg	58286	kg	37,885.58 €	1.947%		290545
iron(III) chloride as proxy for salt medium	1.760	€/kg	3896	kg	6,857.10 €	0.352%	conservative estimation from sodium phosphate	
sodium chloride, powder	0.190	€/kg	947	kg	179.88 €	0.009%		25010091
ammonium sulfate, as N	0.110	€/kg	19849	kg	2,183.37 €	0.112%		310221
Hexane	1.100	€/kg	667	kg	733.41 €	0.038%		290129
Ethyl acetate	0.870	€/kg	5269	kg	4,584.06 €	0.236%		291531
Amberlite XAD-16	278.000	€/kg	200	kg	55,600.00 €	2.857%	https://www.alfa.com/de/catalog/L19565/	
XAD-7 resins	192.800	€/kg	200	kg	38,560.00 €	1.982%	https://www.alfa.com/de/catalog/L19564/	
PEG (MW 6000 & 8000)	3.000	€/kg	3139	kg	9,418.45 €	0.484%	https://www.sigmaaldrich.com/DE/de/product/aldrich/202444?gclid=CjwKCAjw8cCGBhB6EiwAgORey5FkWMDkVbro7X_7nUsa1hwpu_HmEdE-sUo6800EPwMUXmjYX8LIPRoCSOQQAvD_BwE	
sodium citrate	1.460	€/kg	24518	kg	35,796.10 €	1.840%		291815
ethanol	0.840	€/kg	234	kg	196.57 €	0.010%		220710
consumables (1%)					2,689.00 €	0.138%		
labour	90,000	€/labour	15	labour	1,350,000.00 €	69.376%	eurostat	lc_ncost_r2
overhead & administration					324,317.89 €	16.667%		
Total					**1,945,907.36 €**			

Annex 4: Financial evaluation of the biorefinery concept over five years using the net present value (NPV) method. The NPV was set to zero, assuming the return on investment being equal to the weighted average cost of capital (WACC), which was chosen to be 10 % for discounting the cashflow. The payback period was chosen to be five years. Earnings were assumed to develop coherent to the total expenses inlcuding WACC and never be negative. The initial investment was assumed to be recoped in year four and five with 36% in year four and 64% in year five.

	WACC	NPV	Payback (years)
	10.0%	- €	5

T (year)	0	1	2	3	4	5	Sum
CapEx	5,275,542 €	- €	- €	- €	- €	- €	5,275,542 €
OpEx	- €	2,374,575 €	2,422,066 €	2,469,558 €	2,517,999 €	2,567,390 €	12,351,588 €
Yearly OpEx increase (2%)	- €	- €	47,491 €	48,441 €	49,391 €	50,360 €	195,684 €
Total expenditure	- 5,275,542 €	- 2,374,575 €	- 2,422,066 €	- 2,469,558 €	- 2,517,999 €	- 2,567,390 €	- 17,627,129 €
Needed revenue		2,612,032 €	2,930,700 €	3,286,981 €	4,937,457 €	6,388,563 €	20,155,734 €
Cashflow	- 5,275,542 €	237,457 €	508,634 €	817,424 €	2,419,458 €	3,821,173 €	2,528,604 €
Discounted cashflow	- 5,275,542 €	215,870 €	420,359 €	614,142 €	1,652,522 €	2,372,648 €	- €

Annex 5: Overview of annual product yields and assessment of maximum potential sales based on product stream quantities for the financial feasibility of the proposed biorefinery concept including sources for used prices.

Product	Annual amount	Units	Annual Sales	Prize/ Unit	Unit	Source
Puwainaphycins (21.6 mg/g)	38.88	kg	330,480,000.00 €	8.5	€/mg	https://www.abcam.com/daptomycin-lipopeptide-antibiotic-ab141204.html
Minutisamides (101.5 mg/g)	182.70	kg	1,552,950,000.00 €	8.5	€/mg	https://www.abcam.com/daptomycin-lipopeptide-antibiotic-ab141204.html
Phycobiliproteins	46.58	kg	9,734,175,000.00 €	209	€/mg	C-Phycocyanin | Sigma-Aldrich
Chlorophyll a (5.3 mg/g)	9.54	kg	2,032,020,000.00 €	213	€/mg	Chlorophyll A - Chlorophyll a (sigmaaldrich.com)
Carotenoids (1.1 mg/g)	1.98	kg	3,524,400.00 €	1.78	€/mg	Beta Carotene System Suitability United States Pharmacopeia (USP) Reference Standard (sigmaaldrich.com)
Phytase	3563142.8	MU/year	2,672,357.07 €	0.75	€/MU	Phytase Enzyme For Sale
Animal Feed	28000.83	kg	84,002.49 €	3	€/kg	Yeast For Beef & Dairy Cattle | Live Yeast | Biocell Agri
Total			**13,655,905,759.56 €**			

References

(1) Office of Energy Efficiency and Renewable Energy. *Replacing the Whole BarrelTo Reduce U.S. Dependence on Oil*. https://www1.eere.energy.gov/bioenergy/pdfs/replacing_barrel_overview.pdf (accessed 2021-05-04).

(2) Newman, P. Decoupling Economic Growth from Fossil Fuels. *ME* **2017**, *08* (06), 791–805. DOI: 10.4236/me.2017.86055.

(3) Besi, M. de; McCormick, K. Towards a Bioeconomy in Europe:National, Regional and Industrial Strategies. *Sustainability* **2015**, *7* (8), 10461–10478. DOI: 10.3390/su70810461.

(4) Mukhtarov, F.; Gerlak, A.; Pierce, R. Away from fossil-fuels and toward a bioeconomy:Knowledge versatility for public policy? *Environment and Planning C: Politics and Space* **2016**, *35* (6), 1010–1028. DOI: 10.1177/0263774X16676273.

(5) Christian Azar; Kristian Lindgren; Björn A Andersson. Global energy scenarios meeting stringent CO2 constraints—cost-effective fuel choices in the transportation sector. *Energy Policy* **2003**, *31* (10), 961–976. DOI: 10.1016/S0301-4215(02)00139-8.

(6) Kircher, M. The Emerging Bioeconomy:Industrial Drivers, Global Impact, and International Strategies. *Industrial Biotechnology* **2014**, *10* (1), 11–18. DOI: 10.1089/ind.2014.1500.

(7) Morton, S.; Pencheon, D.; Squires, N. Sustainable Development Goals (SDGs), and their implementation: A national global framework for health, development and equity needs a systems approach at every level. *British medical bulletin* **2017**, *124* (1), 81–90. DOI: 10.1093/bmb/ldx031.

(8) UNFCCC. *The Paris Agreement*:*Paris Climate Change Conference - November 2015*. https://unfccc.int/files/meetings/paris_nov_2015/application/pdf/paris_agreement_english_.pdf (accessed 2021-05-04).

(9) UN DESA. *The Sustainable Development Goals Report 2019*. New York, USA: UN DESA. © UN DESA https://www.un-ilibrary.org/content/books/9789210478878.

(10) Hetemäki, L.; Hanewinkel, M.; Muys, B.; Aho, E. *Leading the way to a european circular bioeconomy strategy*; From Science to Policy, Vol. 5; European Forest Institute, 2017.

(11) Carus, M.; Dammer, L. The Circular Bioeconomy—Concepts, Opportunities, and Limitations. *Industrial Biotechnology* **2018**, *14* (2), 83–91. DOI: 10.1089/ind.2018.29121.mca.

(12) Richardson, B. From a Fossil-Fuel to a Biobased Economy:The Politics of Industrial Biotechnology. *Environment and Planning C: Government and Policy* **2012**, *30* (2), 282–296. DOI: 10.1068/c10209.

(13) Soldal, O. Circular Bricks: Getting the circular construction industry to shore. A scenario analysis of building material streams through the Port of Oslo, Unpublished, 2019.

(14) Stegmann, P.; Londo, M.; Junginger, M. The circular bioeconomy:Its elements and role in European bioeconomy clusters. *Resources, Conservation & Recycling: X* **2020**, *6*, 100029.

(15) Dietz, T.; Börner, J.; Förster, J. J.; Braun, J. von. Governance of the Bioeconomy:A Global Comparative Study of National Bioeconomy Strategies. *Sustainability* **2018**, *10* (9). DOI: 10.3390/su10093190.

(16) Maina, S.; Kachrimanidou, V.; Koutinas, A. A roadmap towards a circular and sustainable bioeconomy through waste valorization. *Current Opinion in Green and Sustainable Chemistry* **2017**, *8*, 18–23. DOI: 10.1016/j.cogsc.2017.07.007.

(17) European Commission. Directorate General for Research and Innovation. *A sustainable bioeconomy for Europe: strengthening the connection between economy, society and the environment : updated bioeconomy strategy*; Publications Office, 2018. DOI: 10.2777/792130.

(18) Ubando, A. T.; Felix, C. B.; Chen, W.-H. Biorefineries in circular bioeconomy:A comprehensive review. *Bioresource Technology* **2020**, *299*, 122585. DOI: 10.1016/j.biortech.2019.122585.

(19) Sovacool, B. K. How long will it take? Conceptualizing the temporal dynamics of energy transitions. *Energy Research & Social Science* **2016**, *13*, 202–215. DOI: 10.1016/j.erss.2015.12.020.

(20) *World Energy Transitions Outlook*. https://www.irena.org/publications/2021/Jun/World-Energy-Transitions-Outlook (accessed 2022-03-16).

(21) Rissman, J. We Will Not Run Out of Fossil Fuels (Op-Ed). *Live Science,* Jun 15, 2013. https://www.livescience.com/37469-fuel-endures.html (accessed 2022-03-16).

(22) Kalair, A.; Abas, N.; Saleem, M. S.; Kalair, A. R.; Khan, N. Role of energy storage systems in energy transition from fossil fuels to renewables. *Energy Storage* **2021**, *3* (1). DOI: 10.1002/est2.135.

(23) ETC. *Global-Hydrogen-Report*. https://energy-transitions.org/wp-content/uploads/2021/04/ETC-Global-Hydrogen-Report.pdf (accessed 2022-03-16).

(24) Dolf Gielen; Francisco Boshell; Deger Saygin; Morgan D. Bazilian; Nicholas Wagner; Ricardo Gorini. The role of renewable energy in the global energy transformation. *Energy Strategy Reviews* **2019**, *24*, 38–50. DOI: 10.1016/j.esr.2019.01.006.

(25) Morais, A. R. C.; Bogel-Lukasik, R. Green chemistry and the biorefinery concept. *Sustainable Chemical Processes* **2013**, *1* (1), 18. DOI: 10.1186/2043-7129-1-18.

(26) Mustafa Balat; Günhan Ayar. Biomass Energy in the World, Use of Biomass and Potential Trends. *Energy Sources* **2005**, *27* (10), 931–940. DOI: 10.1080/00908310490449045.

(27) Shiv Prasad; Avinash P. Ingle. Chapter 12 - Impacts of sustainable biofuels production from biomass. In *Sustainable Bioenergy*; Mahendra Rai, Avinash P. Ingle, Eds.; Elsevier, 2019; pp 327–346. DOI: 10.1016/B978-0-12-817654-2.00012-5.

(28) Yadav, V. G.; Yadav, G. D.; Patankar, S. C. The production of fuels and chemicals in the new world:Critical analysis of the choice between crude oil and biomass vis-à-vis sustainability and the environment. *Clean Technologies and Environmental Policy* **2020**, *22* (9), 1757–1774. DOI: 10.1007/s10098-020-01945-5.

(29) Brandon, N. P.; Kurban, Z. Clean energy and the hydrogen economy. *Philosophical transactions. Series A, Mathematical, physical, and engineering sciences* **2017**, *375* (2098). DOI: 10.1098/rsta.2016.0400.

(30) Shaw, A.; Clark, G. W.; MacLachlan, R.; Bryan, P. ROUNDTABLE: Replacing the whole barrel of oil: Industry perspectives. *Industrial Biotechnology* **2011**, *7* (2), 99–110. DOI: 10.1089/ind.2011.7.099.

(31) Vennestrøm, P. N. R.; Osmundsen, C. M.; Christensen, C. H.; Taarning, E. Beyond petrochemicals: the renewable chemicals industry. *Angewandte Chemie (International ed. in English)* **2011**, *50* (45), 10502–10509. DOI: 10.1002/anie.201102117.

(32) Ślusarczyk, J.; Adamska, E.; Czerwik-Marcinkowska, J. Fungi and Algae as Sources of Medicinal and Other Biologically Active Compounds: A Review. *Nutrients* **2021**, *13* (9). DOI: 10.3390/nu13093178. Published Online: Sep. 12, 2021.

(33) Cherubini, F. The biorefinery concept:Using biomass instead of oil for producing energy and chemicals. *Energy Conversion and Management* **2010**, *51* (7), 1412–1421. DOI: 10.1016/j.enconman.2010.01.015.

(34) Hayder A. Alalwan; Alaa H. Alminshid; Haydar A.S. Aljaafari. Promising evolution of biofuel generations. Subject review. *Renewable Energy Focus* **2019**, *28*, 127–139. DOI: 10.1016/j.ref.2018.12.006.

(35) Hassan, S. S.; Williams, G. A.; Jaiswal, A. K. Moving towards the second generation of lignocellulosic biorefineries in the EU:Drivers, challenges, and opportunities. *Renewable and Sustainable Energy Reviews* **2019**, *101*, 590–599. DOI: 10.1016/j.rser.2018.11.041.

(36) Ghatak, H. R. Biorefineries from the perspective of sustainability:Feedstocks, products, and processes. *Renewable and Sustainable Energy Reviews* **2011**, *15* (8), 4042–4052. DOI: 10.1016/j.rser.2011.07.034.

(37) Maity, S. K. Opportunities, recent trends and challenges of integrated biorefinery:Part I. *Renewable and Sustainable Energy Reviews* **2015**, *43*, 1427–1445. DOI: 10.1016/j.rser.2014.11.092.

(38) Kumar, B.; Bhardwaj, N.; Agrawal, K.; Chaturvedi, V.; Verma, P. Current perspective on pretreatment technologies using lignocellulosic biomass:An emerging biorefinery concept. *Fuel Processing Technology* **2020**, *199*, 106244. DOI: 10.1016/j.fuproc.2019.106244.

(39) Naira, V. R.; Mahesh, R.; Panda, S. K.; Maiti, S. K. Biorefinery Approaches for the Production of Fuels and Chemicals from Lignocellulosic and Algal Feedstocks. *Biorefinery of Alternative Resources: Targeting Green Fuels and Platform Chemicals* **2020**, 141–170.

(40) Johnson, T. J.; Jahandideh, A.; Johnson, M. D.; Fields, K. H.; Richardson, J. W.; Muthukumarappan, K.; Cao, Y.; Gu, Z.; Halfmann, C.; Zhou, R. Producing next-generation

biofuels from filamentous cyanobacteria:An economic feasibility analysis. *Algal Research* **2016**, *20*, 218–228.

(41) Lau, N.-S.; Matsui, M.; Abdullah, A. A.-A. Cyanobacteria: Photoautotrophic Microbial Factories for the Sustainable Synthesis of Industrial Products. *BioMed Research International* **2015**, *2015*, 754934. DOI: 10.1155/2015/754934.

(42) Nurra, C.; Torras, C.; Clavero, E.; Ríos, S.; Rey, M.; Lorente, E.; Farriol, X.; Salvadó, J. Biorefinery concept in a microalgae pilot plant. Culturing, dynamic filtration and steam explosion fractionation. *Bioresource Technology* **2014**, *163*, 136–142.

(43) Case, A. E.; Atsumi, S. Cyanobacterial chemical production. *Journal of Biotechnology* **2016**, *231*, 106–114. DOI: 10.1016/j.jbiotec.2016.05.023.

(44) Chow, T.-J.; Su, H.-Y.; Tsai, T.-Y.; Chou, H.-H.; Lee, T.-M.; Chang, J.-S. Using recombinant cyanobacterium (Synechococcus elongatus) with increased carbohydrate productivity as feedstock for bioethanol production via separate hydrolysis and fermentation process. *Bioresource Technology* **2015**, *184*, 33–41.

(45) Deprá, M. C.; dos Santos, A. M.; Severo, I. A.; Santos, A. B.; Zepka, L. Q.; Jacob-Lopes, E. Microalgal biorefineries for bioenergy production:Can we move from concept to industrial reality? *BioEnergy Research* **2018**, *11* (4), 727–747.

(46) Gerardo, M. L.; van den Hende, S.; Vervaeren, H.; Coward, T.; Skill, S. C. Harvesting of microalgae within a biorefinery approach:A review of the developments and case studies from pilot-plants. *Algal Research* **2015**, *11*, 248–262. DOI: 10.1016/j.algal.2015.06.019.

(47) Lü, J.; Sheahan, C.; Fu, P. Metabolic engineering of algae for fourth generation biofuels production. *Energy Environ. Sci.* **2011**, *4* (7), 2451. DOI: 10.1039/c0ee00593b.

(48) Hossain, G. S.; Liu, L.; Du, G. C. Industrial bioprocesses and the biorefinery concept. In *Current Developments in Biotechnology and Bioengineering*; Elsevier, 2017; pp 3–27.

(49) H Ruohomaa; N Ivanova. From solid waste management towards the circular economy and digital driven symbiosis. *IOP Conference Series: Earth and Environmental Science* **2019**, *337*, 12032. DOI: 10.1088/1755-1315/337/1/012032.

(50) Lopes, T. F.; Bogel-Lukasik, R. Economic, social and environmental impacts attained by the use of the effluents generated within a small-scale biorefinery concept. *Acta Innovations* **2020**, *36*, 57–63.

(51) Jorissen, T.; Oraby, A.; Recke, G.; Zibek, S. A systematic analysis of economic evaluation studies of second-generation biorefineries providing chemicals by applying biotechnological processes. *Biofuels, Bioprod. Bioref.* **2020**, *14* (5), 1028–1045. DOI: 10.1002/bbb.2102.

(52) Balan, V.; Han, C.; Trincone, A.; Sanyal, S.; Garrote, G. Current Challenges in Commercially Producing Biofuels from Lignocellulosic Biomass. *ISRN Biotechnology* **2014**, *2014*, 463074. DOI: 10.1155/2014/463074.

(53) Khawaja, C. *D10.17b_S2Biom_Policy_brief_Vision_to_2030_Final*. https://www.s2biom.eu/images/Publications/D10.17b_S2Biom_Policy_brief_Vision_to_2030_Final.pdf (accessed 2022-03-16).

(54) Hommes, A.; Heeres, H. J.; Yue, J. Catalytic Transformation of Biomass Derivatives to Value-Added Chemicals and Fuels in Continuous Flow Microreactors. *ChemCatChem* **2019**, *11* (19), 4671–4708. DOI: 10.1002/cctc.201900807.

(55) Jonathan Moncada; Johnny A. Tamayo; Carlos A. Cardona. Integrating first, second, and third generation biorefineries: Incorporating microalgae into the sugarcane biorefinery. *Chemical Engineering Science* **2014**, *118*, 126–140. DOI: 10.1016/j.ces.2014.07.035.

(56) Katiyar, R.; Banerjee, S.; Arora, A. Recent advances in the integrated biorefinery concept for the valorization of algal biomass through sustainable routes. *Biofuels, Bioproducts and Biorefining* **2021**.

(57) Kini, S.; Divyashree, M.; Mani, M. K.; Mamatha, B. S. Algae and cyanobacteria as a source of novel bioactive compounds for biomedical applications. In *Advances in cyanobacterial biology*; © 2020 Elsevier Inc, 2020; pp 173–194.

(58) Sydney, E. B.; Neto, C. J. D.; Carvalho, J. C. d.; Vandenberghe, L. P. d. S.; Sydney, A. C. N.; Letti, L. A. J.; Karp, S. G.; Soccol, V. T.; Woiciechowski, A. L.; Medeiros, A. B. P.; Soccol, C. R. Microalgal biorefineries:Integrated use of liquid and gaseous effluents from bioethanol industry for efficient biomass production. *Bioresource Technology* **2019**, *292*, 121955. DOI: 10.1016/j.biortech.2019.121955.

(59) Lam, G. P. 't; Vermuë, M. H.; Eppink, M. H. M.; Wijffels, R. H.; van den Berg, C. Multi-Product Microalgae Biorefineries: From Concept Towards Reality. *Trends in Biotechnology* **2018**, *36* (2), 216–227. DOI: 10.1016/j.tibtech.2017.10.011. Published Online: Nov. 10, 2017.

(60) Kit Wayne, C.; Jing Ying, Y.; Show, P.-L.; Ng, H. S.; Juan, J. C.; Ling, T.; Lee, D.-J.; Chang, J.-S. Microalgae biorefinery:High value products perspectives. *Bioresource Technology* **2017**, *229*, 53–62. DOI: 10.1016/j.biortech.2017.01.006.

(61) Mitra, M.; Mishra, S. Multiproduct biorefinery from Arthrospira spp. towards zero waste:Current status and future trends. *Bioresource Technology* **2019**, *291*, 121928.

(62) Sambusiti, C.; Bellucci, M.; Zabaniotou, A.; Beneduce, L.; Monlau, F. Algae as promising feedstocks for fermentative biohydrogen production according to a biorefinery approach: A comprehensive review. *Renewable and Sustainable Energy Reviews* **2015**, *44*, 20–36. DOI: 10.1016/j.rser.2014.12.013.

(63) Kokossis, A. C.; Tsakalova, M.; Pyrgakis, K. Design of integrated biorefineries. *Computers & Chemical Engineering* **2015**, *81*, 40–56. DOI: 10.1016/j.compchemeng.2015.05.021.

(64) Fasahati, P.; Wu, W.; Maravelias, C. T. Process synthesis and economic analysis of cyanobacteria biorefineries:A superstructure-based approach. *Applied Energy* **2019**, *253*, 113625. DOI: 10.1016/j.apenergy.2019.113625.

(65) Zahra, Z.; Choo, D. H.; Lee, H.; Parveen, A. Cyanobacteria:Review of current potentials and applications. *Environments* **2020**, *7* (2), 13.

(66) Deviram, G.; Mathimani, T.; Anto, S.; Ahamed, T. S.; Ananth, D. A.; Pugazhendhi, A. Applications of microalgal and cyanobacterial biomass on a way to safe, cleaner and a sustainable environment. *Journal of Cleaner Production* **2020**, *253*, 119770. DOI: 10.1016/j.jclepro.2019.119770.

(67) Dixit, R.; Suseela, M. R. Cyanobacteria:Potential candidates for drug discovery. *Antonie van Leeuwenhoek* **2013**, *103.* DOI: 10.1007/s10482-013-9898-0.

(68) *Advances in cyanobacterial biology*; © 2020 Elsevier Inc, 2020. DOI: 10.1016/C2018-0-05196-8.

(69) Demay, J.; Bernard, C.; Reinhardt, A.; Marie, B. Natural Products from Cyanobacteria: Focus on Beneficial Activities. *Marine drugs* **2019**, *17* (6). DOI: 10.3390/md17060320. Published Online: May. 30, 2019.

(70) Ducat, D. C.; Way, J. C.; Silver, P. A. Engineering cyanobacteria to generate high-value products. *Trends in Biotechnology* **2011**, *29* (2), 95–103. DOI: 10.1016/j.tibtech.2010.12.003. Published Online: Jan. 5, 2011.

(71) Rastogi, R. P.; Sinha, R. P. Biotechnological and industrial significance of cyanobacterial secondary metabolites. *Biotechnology Advances* **2009**, *27* (4), 521–539. DOI: 10.1016/j.biotechadv.2009.04.009.

(72) Wijffels, R. H.; Kruse, O.; Hellingwerf, K. J. Potential of industrial biotechnology with cyanobacteria and eukaryotic microalgae. *Current Opinion in Biotechnology* **2013**, *24* (3), 405–413.

(73) Cyano Biotech GmbH. *Cyano Biotech GmbH | Mission*. http://www.cyanobiotech.com/content/mission/index.php (accessed 2022-03-16).

(74) Martínez-Francés, E.; Escudero-Oñate, C. Cyanobacteria and microalgae in the production of valuable bioactive compounds. *Microalgal biotechnology* **2018**, *6*, 104–128.

(75) Wendie Levasseur; Patrick Perré; Victor Pozzobon. A review of high value-added molecules production by microalgae in light of the classification. *Biotechnology Advances* **2020**, *41*, 107545. DOI: 10.1016/j.biotechadv.2020.107545.

(76) Venkata Mohan, S.; Hemalatha, M.; Chakraborty, D.; Chatterjee, S.; Ranadheer, P.; Kona, R. Algal biorefinery models with self-sustainable closed loop approach: Trends and prospective for blue-bioeconomy. *Bioresource Technology* **2020**, *295*, 122128. DOI: 10.1016/j.biortech.2019.122128.

(77) García-Ortega, X.; Cámara, E.; Ferrer, P.; Albiol, J.; Montesinos-Seguí, J. L.; Valero, F. Rational development of bioprocess engineering strategies for recombinant protein production in Pichia pastoris (Komagataella phaffii) using the methanol-free GAP promoter. Where do we stand? *New Biotechnology* **2019**, *53*, 24–34. DOI: 10.1016/j.nbt.2019.06.002. Published Online: Jun. 10, 2019.

(78) Chen, C.-C.; Wu, P.-H.; Huang, C.-T.; Cheng, K.-J. A Pichia pastoris fermentation strategy for enhancing the heterologous expression of an Escherichia coli phytase. *Enzyme and Microbial Technology* **2004**, *35*, 315–320. DOI: 10.1016/j.enzmictec.2004.05.007.

(79) Juturu, V.; Wu, J. C. Heterologous Protein Expression in Pichia pastoris: Latest Research Progress and Applications. *Chembiochem : a European journal of chemical biology* **2018**, *19* (1), 7–21. DOI: 10.1002/cbic.201700460. Published Online: Dec. 13, 2017.

(80) Çalık, P.; Ata, Ö.; Güneş, H.; Massahi, A.; Boy, E.; Keskin, A.; Öztürk, S.; Zerze, G. H.; Özdamar, T. H. Recombinant protein production in Pichia pastoris under glyceraldehyde-3-phosphate dehydrogenase promoter: From carbon source metabolism to bioreactor operation parameters. *Biochemical Engineering Journal* **2015**, *95*, 20–36. DOI: 10.1016/j.bej.2014.12.003.

(81) Looser, V.; Bruhlmann, B.; Bumbak, F.; Stenger, C.; Costa, M.; Camattari, A.; Fotiadis, D.; Kovar, K. Cultivation strategies to enhance productivity of Pichia pastoris:A review. *Biotechnology Advances* **2015**, *33* (6, Part 2), 1177–1193. DOI: 10.1016/j.biotechadv.2015.05.008.

(82) Macauley-Patrick, S.; Fazenda, M. L.; McNeil, B.; Harvey, L. M. Heterologous protein production using the Pichia pastoris expression system. *Yeast (Chichester, England)* **2005**, *22* (4), 249–270.

(83) Nieto-Taype, M. A.; Garcia-Ortega, X.; Albiol, J.; Montesinos-Seguí, J. L.; Valero, F. Continuous Cultivation as a Tool Toward the Rational Bioprocess Development With Pichia Pastoris Cell Factory. *Frontiers in Bioengineering and Biotechnology* **2020**, *8*, 632. DOI: 10.3389/fbioe.2020.00632.

(84) Li, C.; Lin, Y.; Zheng, X.; Pang, N.; Liao, X.; Liu, X.; Huang, Y.; Liang, S. Combined strategies for improving expression of Citrobacter amalonaticus phytase in Pichia pastoris. *BMC Biotechnol* **2015**, *15*, 88. DOI: 10.1186/s12896-015-0204-2.

(85) Bhavsar, K.; Khire, J. M. Current research and future perspectives of phytase bioprocessing. *RSC Adv* **2014**, *4* (51), 26677–26691. DOI: 10.1039/C4RA03445G.

(86) Tang, S.; Potvin, G.; Reiche, A.; Zhang, Z. Modeling of Phytase Production by Cultivation of Pichia pastoris Under the Control of the GAP Promoter. *International Journal of Chemical Reactor Engineering* **2010**, *8.* DOI: 10.2202/1542-6580.2144.

(87) Vasudevan, U. M.; Jaiswal, A. K.; Krishna, S.; Pandey, A. Thermostable phytase in feed and fuel industries. *Bioresource Technology* **2019**, *278*, 400–407.

(88) Yao, M.-Z.; Zhang, Y.-H.; Lu, W.-L.; Hu, M.-Q.; Wang, W.; Liang, A.-H. Phytases:Crystal structures, protein engineering and potential biotechnological applications. *Journal of Applied Microbiology* **2012**, *112* (1), 1–14. DOI: 10.1111/j.1365-2672.2011.05181.x.

(89) Herrmann, K. R.; Ruff, A. J.; Infanzón, B.; Schwaneberg, U. Engineered phytases for emerging biotechnological applications beyond animal feeding. *Applied Microbiology and Biotechnology* **2019**, *103* (16), 6435–6448. DOI: 10.1007/s00253-019-09962-1.

(90) Lei, X. G.; Weaver, J. D.; Mullaney, E.; Ullah, A. H.; Azain, M. J. Phytase, a New Life for an "Old" Enzyme. *Annual Review of Animal Biosciences* **2013**, *1* (1), 283–309. DOI: 10.1146/annurev-animal-031412-103717.

(91) Jose G. Ortiz-Tena; Broder Rühmann; Doris Schieder; Volker Sieber. Revealing the diversity of algal monosaccharides: Fast carbohydrate fingerprinting of microalgae using crude biomass and showcasing sugar distribution in Chlorella vulgaris by biomass fractionation. *Algal Research* **2016**, *17*, 227–235. DOI: 10.1016/j.algal.2016.05.008.

(92) Mareš, J.; Hájek, J.; Urajová, P.; Kopecký, J.; Hrouzek, P. A hybrid non-ribosomal peptide/polyketide synthetase containing fatty-acyl ligase (FAAL) synthesizes the β-amino fatty acid lipopeptides puwainaphycins in the Cyanobacterium Cylindrospermum alatosporum. *PloS one* **2014**, *9* (11), e111904. DOI: 10.1371/journal.pone.0111904.

(93) Kumar, A. K.; Sharma, S.; Dixit, G.; Shah, E.; Patel, A. Techno-economic analysis of microalgae production with simultaneous dairy effluent treatment using a pilot-scale High Volume V-shape pond system. *Renewable Energy* **2020**, *145*, 1620–1632. DOI: 10.1016/j.renene.2019.07.087.

(94) Fasaei, F.; Bitter, J. H.; Slegers, P. M.; van Boxtel, A. Techno-economic evaluation of microalgae harvesting and dewatering systems. *Algal Research* **2018**, *31*, 347–362. DOI: 10.1016/j.algal.2017.11.038.

(95) SUDHANYA BANERJEE. Techno-economic and Sensitivity Analysis of Microalgae-based Biorefinery **2019**, Retrieved from the University Digital Conservancy, https://hdl.handle.net/11299/211752.

(96) Tredici, M. R.; Rodolfi, L.; Biondi, N.; Bassi, N.; Sampietro, G. Techno-economic analysis of microalgal biomass production in a 1-ha Green Wall Panel (GWP®) plant. *Algal Research* **2016**, *19*, 253–263. DOI: 10.1016/j.algal.2016.09.005.

(97) Thomassen, G.; Egiguren Vila, U.; van Dael, M.; Lemmens, B.; van Passel, S. A techno-economic assessment of an algal-based biorefinery. *Clean Techn Environ Policy* **2016**, *18* (6), 1849–1862. DOI: 10.1007/s10098-016-1159-2.

(98) Rizwan, M.; Lee, J. H.; Gani, R. Optimal design of microalgae-based biorefinery: Economics, opportunities and challenges. *Applied Energy* **2015**, *150*, 69–79. DOI: 10.1016/j.apenergy.2015.04.018.

(99) Prabha, S.; Vijay, A. K.; Paul, R. R.; George, B. Cyanobacterial biorefinery: Towards economic feasibility through the maximum valorization of biomass. *The Science of the total environment* **2022**, *814*, 152795. DOI: 10.1016/j.scitotenv.2021.152795.

(100) Chia, S. R.; Chew, K. W.; Show, P. L.; Yap, Y. J.; Ong, H. C.; Ling, T. C.; Chang, J.-S. Analysis of Economic and Environmental Aspects of Microalgae Biorefinery for Biofuels Production: A Review. *Biotechnology Journal* **2018**, *13* (6), e1700618. DOI: 10.1002/biot.201700618. Published Online: Feb. 9, 2018.

(101) Finkbeiner, M.; Schau, E. M.; Lehmann, A.; Traverso, M. Towards Life Cycle Sustainability Assessment. *Sustainability* **2010**, *2* (10), 3309–3322. DOI: 10.3390/su2103309.

(102) Bhambhani, A.; van der Hoek, J. P.; Kapelan, Z. Life cycle sustainability assessment framework for water sector resource recovery solutions: Strengths and weaknesses. *Resources, Conservation and Recycling* **2022**, *180*, 106151. DOI: 10.1016/j.resconrec.2021.106151.

(103) Kua, H. W. On Life Cycle Sustainability Unified Analysis. *Journal of Industrial Ecology* **2017**, *21* (6), 1488–1506. DOI: 10.1111/jiec.12665.

(104) Korbinian Sinzinger; Sebastian Bieringer; Doris Schieder; Herbert Riepl; Volker Sieber. Biorefinery concept for Cylindrospermum alatosporum CCALA 988 extracting multiple high-value compounds and residue utilization by P. pastoris fermentation producing phytase. *Algal Research* **2023**, *76*, 103302. DOI: 10.1016/j.algal.2023.103302.

(105) Fasahati, P.; Wu, W.; Maravelias, C. T. Process synthesis and economic analysis of cyanobacteria biorefineries: A superstructure-based approach. *Applied Energy* **2019**, *253*, 113625. DOI: 10.1016/j.apenergy.2019.113625.

(106) SUBITEC. *Produkt - SUBITEC*. https://www.subitec.com/industrie/kultivierungsmodul/ (accessed 2022-03-15).

(107) Cheel, J.; Urajová, P.; Hájek, J.; Hrouzek, P.; Kuzma, M.; Bouju, E.; Faure, K.; Kopecký, J. Separation of cyclic lipopeptide puwainaphycins from cyanobacteria by countercurrent chromatography combined with polymeric resins and HPLC. *Analytical and bioanalytical chemistry* **2017**, *409* (4), 917–930. DOI: 10.1007/s00216-016-0066-z. Published Online: Nov. 30, 2016.

(108) Helian, Y.; Gai, Y.; Fang, H.; Sun, Y.; Zhang, D. A multistrategy approach for improving the expression of E. coli phytase in Pichia pastoris. *Journal of industrial microbiology & biotechnology* **2020**, *47* (12), 1161–1172. DOI: 10.1007/s10295-020-02311-6. Published Online: Sep. 15, 2020.

(109) Bayarjargal, M.; Munkhbat, E.; Ariunsaikhan, T.; Odonchimeg, M.; Uurzaikh, T.; Gan-Erdene, T.; Regdel, D. Utilization of spent brewer's yeast Saccharomyces cerevisiae for the production of yeast enzymatic hydrolysate. *Mong. J. Chem.* **2014**, *12*, 88–91. DOI: 10.5564/mjc.v12i0.179.

(110) Guo, M.; Wu, K.; Zhuang, Y.; Chu, J.; Zhang, S. Studies on characteristics of kinetics and metabolic shift of genetically engineered yeast Pichia pastoris in high-density chemostat cultivation. *Wei sheng wu xue bao = Acta microbiologica Sinica* **2001**, *41* (5), 617–623.

(111) Kannaujiya, V. K.; Sinha, R. P. An Efficient Method for the Separation and Purification of Phycobiliproteins from a Rice-Field Cyanobacterium Nostoc sp. Strain HKAR-11. *Chromatographia* **2016**, *79* (5-6), 335–343. DOI: 10.1007/s10337-016-3025-0.

(112) Bhavsar, K.; Ravi Kumar, V.; Khire, J. M. Downstream processing of extracellular phytase from Aspergillus niger: Chromatography process vs. aqueous two phase extraction for its simultaneous partitioning and purification. *Process biochemistry* **2012**, *47* (7), 1066–1072. DOI: 10.1016/j.procbio.2012.03.012.

(113) *LCIA: the ReCiPe model | RIVM*. https://www.rivm.nl/en/life-cycle-assessment-lca/recipe (accessed 2022-03-15).

(114) *Labour cost, wages and salaries, direct remuneration (excluding apprentices) by NACE Rev. 2 activity) - LCS surveys 2008, 2012 and 2016 - Products Datasets - Eurostat*. https://ec.europa.eu/eurostat/web/products-datasets/-/lc_ncost_r2 (accessed 2022-03-15).

(115) Institute, Corporate Finance. Net Present Value (NPV). *Corporate Finance Institute,* Jan 22, 2018. https://corporatefinanceinstitute.com/resources/knowledge/valuation/net-present-value-npv/ (accessed 2022-03-15).

(116) Fool, T. M. Advantages and Disadvantages of Net Present Value Method. *Nasdaq,* Sat, Nov 14, 2015. https://www.nasdaq.com/articles/advantages-and-disadvantages-net-present-value-method-2015-11-14 (accessed 2022-03-15).

(117) Rahpeyma, S. S.; Raheb, J. Microalgae Biodiesel as a Valuable Alternative to Fossil Fuels. *BioEnergy Research* **2019**, *12* (4), 958–965. DOI: 10.1007/s12155-019-10033-6.

(118) Palmer, J. S.; Lawton, L. A.; Kindt, R.; Edwards, C. Rapid analytical methods for the microalgal and cyanobacterial biorefinery: Application on strains of industrial importance. *MicrobiologyOpen* **2021**, *10* (1), e1156. DOI: 10.1002/mbo3.1156.

(119) Audrey Beattie; Wim Vermaas; Al Darzins; Steven C. Holland; Shuqin Li; John McGowen; David Nielsen; Jason C. Quinn. A probabilistic economic and environmental impact assessment of a cyanobacteria-based biorefinery. *Algal Research* **2021**, *59*, 102454. DOI: 10.1016/j.algal.2021.102454.

(120) Korbinian Sinzinger; Ulrike Obst; Samed Güner; Manuel Döring; Magdalena Haslbeck; Doris Schieder; Volker Sieber. The Pichia pastoris enzyme production platform: From combinatorial library screening to bench-top fermentation on residual cyanobacterial biomass. *Journal of Bioresources and Bioproducts* **2024**, *9* (1), 43–57. DOI: 10.1016/j.jobab.2023.12.005.

(121) Picanço-Castro, V.; Swiech, K., Eds. *Recombinant Glycoprotein Production: Methods and Protocols*; Springer New York, 2018.

(122) Liu, W.-C.; Zhu, P. Demonstration-Scale High-Cell-Density Fermentation of Pichia pastoris. In *Recombinant Glycoprotein Production: Methods and Protocols*; Picanço-Castro, V., Swiech, K., Eds.; Springer New York, 2018; pp 109–116. DOI: 10.1007/978-1-4939-7312-5_9.

(123) Liu, W.; Inwood, S.; Gong, T.; Sharma, A.; Yu, L.-Y. Fed-batch high-cell-density fermentation strategies for Pichia pastoris growth and production. *Critical Reviews in Biotechnology* **2019**, *39*, 1–14. DOI: 10.1080/07388551.2018.1554620.

(124) V. Looser; B. Bruhlmann; F. Bumbak; C. Stenger; M. Costa; A. Camattari; D. Fotiadis; K. Kovar. Cultivation strategies to enhance productivity of Pichia pastoris: A review. *Biotechnology Advances* **2015**, *33* (6, Part 2), 1177–1193. DOI: 10.1016/j.biotechadv.2015.05.008.

(125) Akbarzadeh, A.; Dehnavi, E.; Aghaeepoor, M.; Amani, J. Optimization of Recombinant Expression of Synthetic Bacterial Phytase in Pichia pastoris Using Response Surface Methodology. *Jundishapur Journal of Microbiology* **2015**, *8* (12), e27553. DOI: 10.5812/jjm.27553. Published Online: Dec. 26, 2015.

(126) Tang, S. Process engineering of Pichia pastoris cultivation for the production of a phytase with GAP promoter:Process engineering of Pichia pastoris cultivation for the production of a phytase with GAP promoter, Université D'Ottawa / University Of Ottawa, 2009. https://ruor.uottawa.ca/handle/10393/28277.

(127) Tolner, B.; Smith, L.; Begent, R. H. J.; Chester, K. A. Production of recombinant protein in Pichia pastoris by fermentation. *Nature protocols* **2006**, *1* (2), 1006–1021. DOI: 10.1038/nprot.2006.126.

(128) Ahmad, M.; Hirz, M.; Pichler, H.; Schwab, H. Protein expression in Pichia pastoris: recent achievements and perspectives for heterologous protein production. *Applied Microbiology and Biotechnology* **2014**, *98* (12), 5301–5317. DOI: 10.1007/s00253-014-5732-5. Published Online: Apr. 18, 2014.

(129) Ruiz, J.; Olivieri, G.; Vree, J. de; Bosma, R.; Willems, P.; Reith, J. H.; Eppink, M. H. M.; Kleinegris, D. M. M.; Wijffels, R. H.; Barbosa, M. J. Towards industrial products from microalgae. *Energy Environ. Sci.* **2016**, *9* (10), 3036–3043. DOI: 10.1039/C6EE01493C.

(130) Bavatharny Thevarajah; Gannoru Kankanamalage Sanuji Hasara Nishshanka; Malith Premaratne; P.H.V. Nimarshana; Dillirani Nagarajan; Jo-Shu Chang; Thilini U. Ariyadasa. Large-scale production of Spirulina-based proteins and c-phycocyanin: A biorefinery approach. *Biochemical Engineering Journal* **2022**, *185*, 108541. DOI: 10.1016/j.bej.2022.108541.

Table of Figures

Table of Tables

Table of Equations

Abbreviations

%	percent
°C	degree Celsius
µL	microliter
µM	micromolar. micromole per liter
2-d-Glc	2-deoxy-D-glucose
2-d-Rib	2-deoxy-D-ribose
AOX	Alcohol oxidase
Ara	L-arabinose
B	Biotin
BG-11	Blue green medium for cyanobacteria
BMGY	Buffered complex glycerol
Cel	D-cellobiose
CO2	Carbon dioxide
ddH2O	ultra-pure water
DNA	deoxyribonucleic acid
EIC	extracted ion chromatogram
EPS	exopolysaccharide
Fuc	L-fucose
g	gram
Gal	D-galactose
GalN	D-galactosamine
GalNAc	N-acetyl-D-galactosamine
GalUA	D-galacturonic acid
GC	gas chromatography
Gen	D-gentiobiose
Glc	D-glucose
GlcN	D-glucosamine
GlcNAc	N-acetyl-D-glucosamine
GlcUA	D-glucuronic acid
GRAS	Generally recognised as safe
GY	Glycerol
h	hours
HT	high throughput
kDa	Kilo dalton
L	liter
LB	Lysogeny broth
LOD	limit of detection
LOQ	limit of quantification
m/z	mass-to-charge ratio
MALDI/TOF	Matrix-Assisted Laser Desorption/Ionization Time-of-Flight mass spectrometer
Man	D-mannose
mg	milligram
min	minutes
mL	milliliter

mM	millimolar. millimol per liter
MS	mass spectrometer
MTP	96-well micro titer plate
N.A.	Not available / not applicable
NREL	National Renewable Energy Laboratory
OD	Optical density
p.a.	Per annum
PAGE	Polyacrylamide gel electrophoresis
PEG	Polyethylene glycol
PMP	1-Phenyl-3-methyl-5-pyrazolone
Rha	L-rhamnose
Rib	D-ribose
rpm	rpm
RT	room temperature
SDS	Sodium dodecyl sulfate
sec	second
TFA	trifluoroacetic acid
U	Units
UA	uronic acid
UHPLC	Ultra High- Performance Liquid Chromatography
UV	ultra violet
v/v	volume per volume
w/v	weight per volume
w/w	weight per weight
x g	x g-force
Xyl	D-xylose
YE	Yeast extract
YNB	Yeast nitrogen base
YPD	Yeast extract peptone dextrose medium

Curriculum Vitae

Korbinian Sinzinger

Since Jan 2024	Field Sales Specialist UCB Pharma GmbH
Feb 2022 – Dec 2023	Senior Field Sales Manager Ferring Pharmaceuticals GmbH
Oct 2021 – Feb 2022	Scientific Representative Aflofarm Germany GmbH
Oct 2017 – Dec 2020	Research Fellow Chair of Chemistry of Biogenic Resources TUM Campus Straubing
Jan 2017 – Jun 2017	Master`s Thesis Chair of Chemistry of Biogenic Resources TUM Campus Straubing
Aug 2016 – Dec 2016	Intern Semester Chair of Chemistry of Biogenic Resources TUM Campus Straubing
Aug 2015 – Jun 2017	Master of Science M.Sc. Industrial Chemistry (Immunology & Biochemistry) TUM ASIA, Singapore
Aug 2011 – Jun 2015	Bachelor of Science B.Sc. & Bachelor of Arts B.A. Biology & Chemistry (Biomedical Sciences) St. Ambrose University, IA, USA